

storm surge prediction using kalman filtering

3

59

6

rijkswaterstaat communications

storm surge prediction using kalman filtering

by

dr. ir. a.w. heemink

thesis Twente University of Technology, 1986

the hague, 1986

All correspondence and applications should be addressed to

rijkswaterstaat
dienst getijdewateren
hooftskade 1
postbus 20907
2500 ex the hague
netherlands

the views in this article are the author's own

recommended catalogue entry:

Heemink, A.W.

Storm surge prediction using kalman filtering / by A.W. Heemink; Rijkswaterstaat. — The Hague: Rijkswaterstaat, 1986. — 194 p.: ill.; 24 cm. — (Rijkswaterstaat communications; no. 46)
With refer.: p. 185-187
Thesis Twente University of Technology, 1986.
With Dutch summary

Contents

	Page
1 Introduction	8
1.1 Introduction	8
1.2 Tidal prediction methods	13
1.2.1 Introduction	13
1.2.2 Prediction of the astronomical tide	14
1.2.3 Operational methods used in the Netherlands	16
1.2.4 Recent results in tidal prediction	18
1.3 Kalman filter approach to tidal prediction	20
1.4 Scope of the investigation	23
2 The Shallow water equations	24
2.1 Introduction	24
2.2 The two-dimensional equations	24
2.3 The one-dimensional equations	27
3 Discrete filtering theory	30
3.1 Introduction	30
3.2 Linear filtering theory	30
3.2.1 The Kalman filter	30
3.2.2 Stability	30
3.3 Non-linear filtering theory	37
3.3.1 Introduction	37
3.3.2 Linearized and extended Kalman filters	38
3.3.3 Non-linear filters	40
3.3.4 Parameter estimation	44
4 Kalman filters for the linear one-dimensional shallow water equations	46
4.1 Introduction	46
4.2 Numerical approximation of differential equations	46
4.3 Discretisation of the one-dimensional shallow water equations	49
4.4 On the choice of the system noise	55

4.5	Kalman filtering in the wave number domain	57
4.6	General discrete system representation	74
4.7	G-K-observability	75
4.8	Numerical properties of some Kalman filter algorithms	79
4.9	Distributed parameter filters	86
5	A Kalman filter based on a one-dimensional model	88
5.1	Introduction	88
5.2	The deterministic model	88
5.2.1	Introduction	88
5.2.2	The tidal movement in the southern North Sea	89
5.2.3	Meteorological effects in the North Sea	92
5.2.4	The mathematical model	94
5.3	The Kalman filter	98
5.3.1	Introduction	98
5.3.2	The stochastic model	99
5.3.3	The boundary treatment	101
5.4	Experiments using simulated data	102
5.4.1	Introduction	102
5.4.2	The constant gain extended Kalman filter	103
5.4.3	Parameter estimation	107
5.5	A Kalman filter based on an Eastern Scheldt model	111
5.6	Experiments using field data	116
5.7	Discussion	126
6	A Kalman filter based on a two-dimensional model	131
6.1	Introduction	131
6.2	The deterministic model	132
6.3	The Kalman filter	139
6.3.1	Introduction	139
6.3.2	The stochastic model	139
6.3.3	The boundary treatment	143
6.3.4	The steady-state filter	144
6.4	Implementation of the algorithm on a vector processor	149
6.5	Experiments using simulated data	152
6.5.1	Introduction	152
6.5.2	Internal surge	154
6.5.3	External surge	163
6.6	Experiments using field data	163
6.7	Discussion	181

7	Conclusions and recommendations	182
References		185
Notation		188
Summary		190
Samenvatting		191

1. Introduction

1.1. Introduction

The delta area in the south-western part of the Netherlands lies below or just above sea level (see *figure 1.1*). Therefore, special precautions have to be taken with respect to the dikes and the coast-line in general. After the disaster of February 1953, when during a period of severe storm conditions the dikes in this area broke and approximately 1800 people were drowned (see *figure 1.2*), the Dutch government

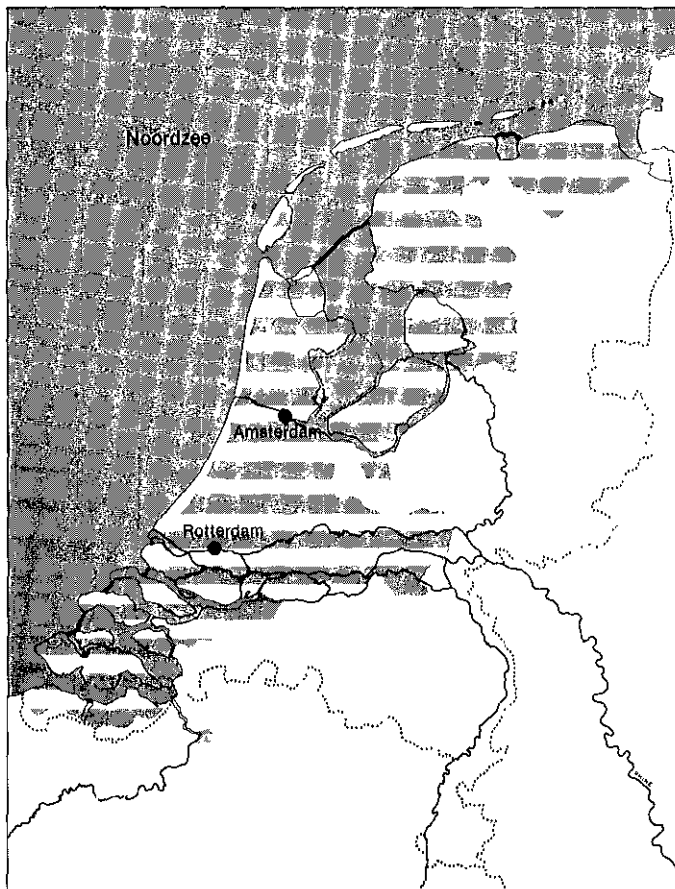


Figure 1.1: The area that would periodically be flooded if the Netherlands would not be protected by dikes.



Figure 1.2: The flooded area during the disaster of February 1953.

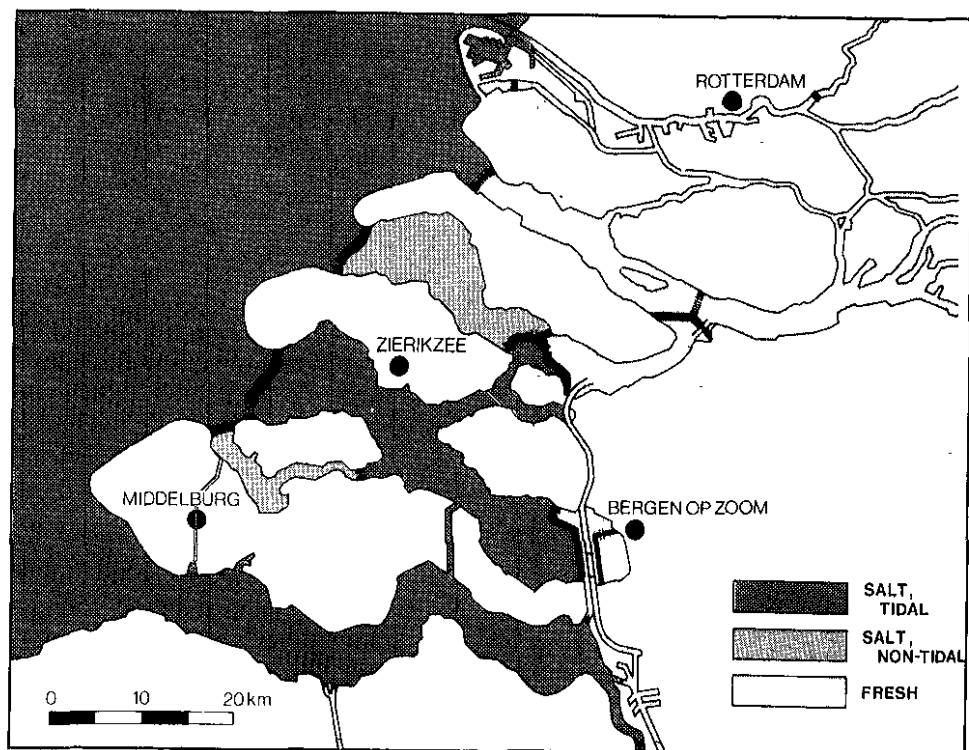


Figure 1.3: The Delta Plan.

decided to solve the problem of the long and vulnerable coast-line of the delta area and planned to close all the estuaries except the free waterway to Antwerp, the Western Scheldt. This massive construction program was called the Delta Plan (see figure 1.3).

Before the start of the project in 1958, little attention was given to the fact that important changes would occur in the estuaries. Since the closed estuaries would cease to be tidal and would be converted into fresh water lakes, the entire flora and fauna of the delta area would change. By 1974, the Delta Plan was nearly completed except for the closing of the largest estuary, the Eastern Scheldt. At that time, work was interrupted as a result of pressure exerted by ecologists and nature protectors, who wanted to preserve the tidal state of the Eastern Scheldt. The very special ecological characteristics of the Eastern Scheldt, such as the great variety of types of environment and the pure and relatively warm water, have brought about an exceptional abundance of flora and fauna (Saeijs 1982). Closure would threaten not only this rich and rare ecology but also the oyster and mussel industries located in the Eastern Scheldt. In 1976, the Dutch government altered the original Delta Plan and decided to insert a storm surge barrier containing many large gates that will be closed

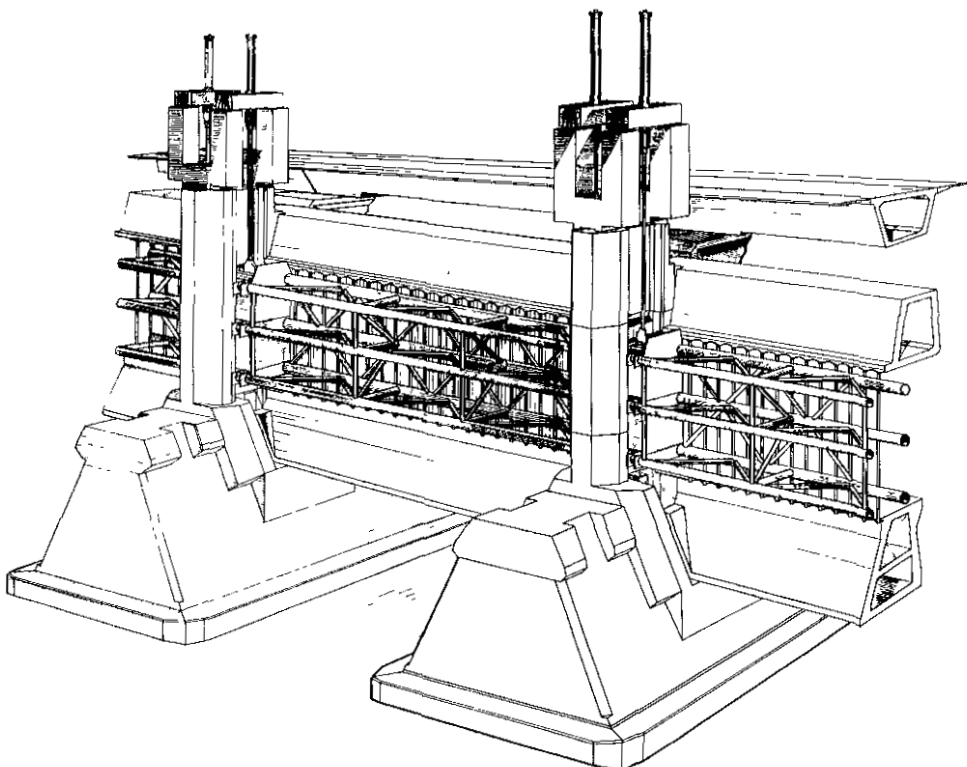


Figure 1.4: The storm surge barrier.

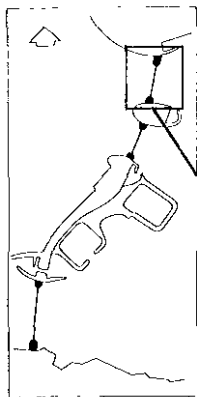


Photo 1.1: The storm surge barrier, February 1986.

only in case of extreme high water (see *figure 1.4* and *photo 1.1*). In normal weather conditions, the gates will be opened to allow a reduced tide to pass into the Eastern Scheldt.

When the building of the storm surge barrier is completed and the barrier is in operational service, the prediction of water-levels in the Eastern Scheldt will be of

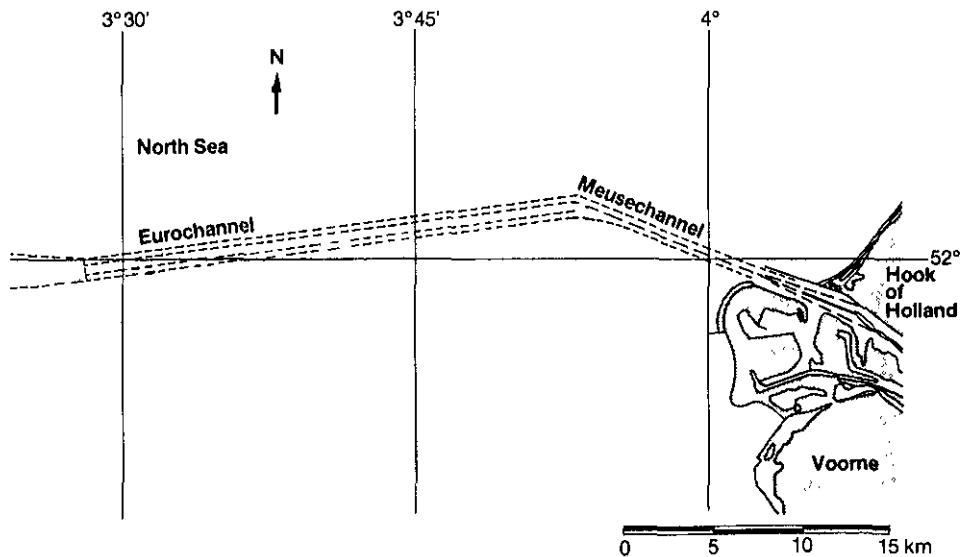


Figure 1.5: The Euro Channel and the Meuse Channel.

great importance. Since the barrier will have to be closed a few hours before the expected occurrence of extreme high water, accurate predictions are required to ensure that the barrier will be closed in time.

Accurate predictions for the entire Dutch coast, approximately six hours ahead, are also necessary to decide what precautionary actions have to be taken to protect the dikes. Furthermore, with the increase in the size of ships using the Euro Channel and the Meuse Channel to Rotterdam harbour (see *figure 1.5*), this port has become inaccessible to many ships except during a short period at high water. Therefore, to allow safe passage, there is a demand for accurate tidal predictions.

Previously, tidal prediction methods have been either statistical or deterministic in nature. Applying statistical methods - i.e. simple empirical or black-box models derived from series of observations - it is possible to use on-line measurements of the water-level. This feature is very important considering the fact that the number of on-line measurement stations in the North Sea is increasing rapidly. Deterministic methods, including the analytical or numerical solutions to the hydrodynamic equations, do not have this possibility. However, they have a more physical basis and provide a more realistic description of the water movement. These facts suggest the use of a method that is a combination of the statistical and the deterministic approach in order to obtain the best features of both. Such a method is the Kalman filter. This stochastic filter is based on a deterministic model and has also the capability of correcting model predictions using on-line information.

In this investigation Kalman filters have been developed for the prediction of the water-level during stormy periods. In the remaining part of this introductory chapter we first summarize in Section 1.2 the tidal prediction methods used up to now. Section 1.3 describes the Kalman filter approach to the prediction of water-levels and finally Section 1.4 gives an exposition of the scope of the entire investigation.

1.2 Tidal prediction methods

1.2.1 Introduction

The astronomical tide of the oceans is created by forces from the sun and moon. The attraction of the moon is approximately twice as strong as that of the sun. Because of their greater distance or smaller size, other celestial bodies have a negligible effect on the tides. In the Atlantic Ocean tidal amplitude are rather small: less than 50 cm. In shallow waters, such as the North Sea, the tide generating force acting directly on the mass of water in these areas can be neglected. However, as the Atlantic tide progresses into the North Sea the tide is amplified and its amplitude can reach values of 1-2 meters along the Dutch coast. Furthermore, when the tide penetrates into shallow coastal waters or into an estuary its propagation is affected by the coast and by the frictional effects caused by the reduced depth.

A surge is defined as the meteorological effect on the tidal propagation. A surge that is generated by severe storms outside the North Sea area is called an external surge when it enters this area. This storm surge propagates through the North Sea approximately like the tide. In the southern part of the North Sea external surges usually have 50 cm or less amplitude. Internal surges are caused by meteorological phenomena inside the North Sea area. During north-westerly storms - owing to the funnel shape of the North Sea - these storm surges can reach values of more than 2 meters along the Dutch coast.

The meteorological effect is created by two physical phenomena. Firstly, the atmospheric pressure profile of a storm affects the water-level lying directly underneath. Secondly, wind blowing over water creates a frictional force on the surface of the water that sets up the water-level in the direction of the wind. In shallow waters, such as the North Sea, the wind effect is, in general, strongly predominant in relation to the pressure effect.

Most tidal prediction techniques are based on the simple superposition of the astronomical tide and the meteorological effect. Since the astronomical tide can be predicted relatively accurately, attention has been concentrated on the prediction of the meteorological effect. In this section we summarize the existing tidal prediction

methods. In Subsection 1.2.2 the culmination method, the harmonic method and the response method for predicting the astronomical tide are briefly described. For a thorough treatment of these methods, involving the description of the movements of the earth, moon and sun, and the development of the tide generating potential, the reader is referred to Hornman (1977) for the culmination method, to Dronkers (1964, 1975) or Godin (1972) for the harmonic method, and to Munk and Cartwright (1966) for the response method. Subsection 1.2.3 is devoted to the operational methods used in the Netherlands for predicting the meteorological effect along the Dutch coast. Finally, some recent results in the development of tidal prediction methods are discussed in Subsection 1.2.4.

1.2.2 Prediction of the astronomical tide

In 1831 Lubbock published an analysis of the relationship between the tides and the motion of the moon and sun in relation to the earth. It has been known for centuries that, of all the factors that describe this motion, the time of culmination of the moon* has the most important influence on the high and low water-levels in the North Sea. To predict the times and heights of low and high water, Lubbock empirically determined the relationship between these tidal data and the time of culmination using observations gathered over a few years. Corrections were derived to take into account some other characteristics of the motions of moon, sun and earth. Lubbock's method was called the culmination method and proved to be quite successful in those days.

Another approach to tidal prediction was developed by Kelvin and Darwin, following the suggestion by Laplace that as a result of periodic variations in the force exerted on the mass of water the water will move with the same periodicity. This approach to the analysis of tides was called the harmonic method and treats the tidal elevation at a single location as the summation of a large number of independent sinusoidal motions:

$$h(t) = h_0 + \sum_{i=1}^N A_i \cos(2\omega_i t + \phi_i) \quad (1.1)$$

where:

$h(t)$ = water-level

h_0 = mean sea level

A_i = amplitude of the i -th harmonic constituent

ϕ_i = phase of the i -th constituent

ω_i = astronomical frequency of the i -th constituent.

* The time at which the path of the moon crosses the meridian of the observer.

In principle, the number of astronomical frequencies is infinite. Using the gravitational tidal potential due to the moon and sun, the most important harmonic constituents can be selected. However, if shallow water effects become significant, constituents that are not found or have been neglected in the original tidal potential can become very important. These frequencies have to be selected empirically for each location. Since the harmonic analysis is usually applied to time series no longer than one year, the estimated amplitude A_i and phases ϕ_i depend on tidal motions with longer periods*. In order to take these effects into account, correction factors $f_i(t)$ and $u_i(t)$ are introduced by rewriting (1.1) as:

$$h(t) = h_0 + \sum_{i=1}^N f_i(t) A_i \cos(2\omega_i t + \phi_i + u_i(t)) \quad (1.2)$$

where:

$f_i(t)$ = correction for the amplitude of the i -th constituent

$u_i(t)$ = correction for the phase of the i -th constituent.

The correction factors are computed using the tidal potential. The unknown amplitude A_i and phase ϕ_i are determined by least squares estimation.

The harmonic method is usually applied using time series of approximately one year. Since the shallow water effects along the Dutch coast are very strong, many tidal constituents (100-150) are required to describe the tide. Most of these constituents have amplitude smaller than 3 cm. To give an example the harmonic analysis has been applied to hourly observations of the water-level registered during 1983 at the measurement station OS IV, located in the mouth of the Eastern Scheldt. The analysis was carried out by Voogt (1984) using 107 constituents. The most important harmonic constituents are summarized in table 1.1.

name	ω (degrees/hour)	A (cm)
SA	0,0410	10,5
O ₁	13,9430	9,9
N ₂	28,4397	21,6
M ₂	28,9841	131,9
S ₂	30,0000	33,7
M ₄	57,9682	11,1
MS ₄	58,9841	7,5
M ₆	86,9523	6,0
2MS ₆	87,9682	5,8

Table 1.1: The most important harmonic constituents at the tide gauge OS IV.

* For a detailed discussion on the resolution of tidal constituents, involving both the record length as well as the underlying noise process, the reader is referred to Munk and Hasselmann (1964).

Another approach to tidal predictions was introduced by Munk and Cartwright (1966). Their response method is physically more realistic than the harmonic method and is based on the response of the sea surface to the tidal potential. The results have proved to be comparable with the harmonic analysis (Cartwright 1978). However, the response method requires approximately 19 years of observations to estimate the response weights. In most locations observations recorded during such a long period are not available and, moreover, at many locations the conditions do not remain constant over a period of 19 years owing to sedimentation, dock construction or changing salinity. Since in addition, harmonic analysis is easier to use and interpret, the response method has seldom been applied to predict the astronomical tide.

In the Netherlands, until 1986 the tide tables* were produced by means of a modified version of the culmination method using five years of observations. In this respect the Netherlands were fairly unique, since almost every other country used harmonic tide analysis. Furthermore, most textbooks on tides or tidal prediction only mention the culmination method as an historical curiosity or do not refer to it at all. Nevertheless, due to the very strong shallow water effects at most locations along the Dutch coast, the harmonic analysis is, surprisingly, not significantly more accurate than the culmination method. However, since the latter only predicts the times and heights of high and low water, it has been replaced by the harmonic analysis in 1986.

1.2.3 Operational methods used in the Netherlands

The operational tidal prediction techniques in the Netherlands are based on the superposition of the astronomical tide and the meteorological effect. While the astronomical tide can be determined by the culmination method or by harmonic analysis, the meteorological effect is predicted on an operational basis by using two approaches simultaneously.

In the first approach predictions are accomplished using a numerical model of the North Sea and parts of the adjoining waters. This model is based on the linearized shallow water equations** :

$$\frac{\partial u}{\partial t} + g \frac{\partial h}{\partial x} - f v + \lambda \frac{u}{D} - \gamma \frac{V^2 \cos \psi}{D} + \frac{1}{Q_w} \frac{\partial p_a}{\partial x} = 0 \quad (1.3)$$

* Tide tables consist of the predicted water-levels (times and heights of high and low water) over a period of one year. These tables are published every year.

** The description of the general non-linear shallow water equations as well as the linearization of these equations can be found in Chapter 2.

$$\frac{\partial v}{\partial t} + g \frac{\partial h}{\partial y} + fu + \lambda \frac{v}{D} - \gamma \frac{V^2 \sin \psi}{D} + \frac{1}{\rho_w} \frac{\partial p_a}{\partial y} = 0 \quad (1.4)$$

$$\frac{\partial h}{\partial t} + \frac{\partial (Du)}{\partial x} + \frac{\partial (Dv)}{\partial y} = 0 \quad (1.5)$$

where:

- h = water-level
- u, v = water velocities in respectively the x and y -directions
- D = depth of the water
- f = Coriolis parameter
- λ = linear bottom friction coefficient
- γ = wind friction coefficient
- V = wind speed
- ψ = wind direction
- ρ_w = density of water
- p_a = atmospheric pressure
- g = acceleration of gravity.

Equations (1.3)-(1.5) are discretised on a staggered grid using the Fischer scheme (Van der Houwen 1968). The mesh length in the southern part of the North Sea has been chosen at 42 km, while for reasons of stability in more remote parts of the North Sea and of the Channel it has been increased to 84 km in one of the directions. The time step has been chosen at 7.5 min. At the boundaries the meteorological effect is neglected and assumed to be zero.

Based on the work of Lauwerier and Damsté (1963) and of Van der Houwen (1966), the model was implemented by Timmerman on the computer at the K.N.M.I. (Royal Netherlands Meteorological Institute) and has been used since 1971. A detailed description of the model can be found in Timmerman (1975, 1977). The model provides predictions of the meteorological effect along the Dutch coast over a 24 hour period. Unfortunately, it takes approximately six hours to compute these predictions. This delay is mainly due to the time required to collect the meteorological data and to run the atmospheric model for predicting the meteorological conditions which are the inputs for the North Sea model.

The second approach to storm surge predictions has been developed particularly for predicting the meteorological effect at the time of the next high water. This is of great importance for taking precautionary actions to protect the dikes. The method is based on the early work of Schalkwijk (1947). On the basis of theoretical considerations, Schalkwijk assumed a quadratic relationship between the wind speed and the wind effect during stationary weather conditions. He divided the North Sea

and the Channel into three areas and used a stationary model to write the wind effect at Hook of Holland as the sum of the contributions of the districts North, South and Channel, assuming for each of these districts a homogeneous wind field to occur:

$$s = a_N V_N^2 \cos(\psi_N - \chi_N) + a_S(\psi_S) V_S^2 + a_C V_C^2 \cos(\psi_C - \chi_C) \quad (1.6)$$

where:

s	= wind effect or set up
V_N, V_S, V_C	= wind speed in the district North, South and Channel
χ_N, χ_C	= direction of the maximum wind effect in the districts North and Channel
ψ_N, ψ_S, ψ_C	= wind direction in the districts North, South and Channel
$a_N, a_C, a_S(\psi_S)$	= coefficients.

The coefficients a_N , a_C , $a_S(\psi_S)$, χ_N and χ_C were computed with the aid of 14 storm surges that occurred in the period 1920-1940.

Weenink (1958) improved the method by subdividing the district South into three areas. Furthermore, to give the method a more physical basis he determined the wind effect of these three areas by solving the shallow water equations (1.3)-(1.5). Since Weenink in those days was obliged to use analytical solutions it was necessary to introduce simplifications and to consider the stationary equations. He compiled the results into tables of the wind effect for various wind speeds and directions. For the districts North and Channel Weenink accepted Schalkwijk's results. In 1971, Timmerman again improved the method by dividing the North Sea and the Channel into six areas. The stationary wind effect of each area was computed using the just described numerical model of the North Sea and the results were compiled into tables, like Weenink did.

The main advantage of using the tables instead of the North Sea model is that it takes less than three hours for the predictions to be available. The reason for this is due to the fact that the wind velocities, used as input for the tables, are predicted by the meteorologist and not by running the atmospheric model. It should be noted that when using the tables, the external surges and the internal pressure effect are not taken into account. The North Sea model only neglects surges generated outside the model.

1.2.4 Recent results in tidal prediction

Tidal prediction techniques can roughly be divided into deterministic methods which include the analytical or numerical solutions to the hydrodynamic equations

and statistical methods which are based on empirical or black-box models. The parameters of these models are estimated by using long series of observations. As pointed out in Subsection 1.2.3, Schalkwijk used a statistical approach to predict the meteorological effect at Hook of Holland.

The most important characteristic of statistical methods is the possibility to make use of the on-line measurements of the water-level. Furthermore, these methods are very easy to employ and can be implemented on very small computers. Simple linear regression models (based on wind, pressure and water-level data) have been derived by Rossiter (1959) among others, to predict the meteorological effect at various locations along the eastern coast of England. Christianssen and Sieferd (1978) presented a similar approach to predict the meteorological effect at the German Bight. To predict the water height in inland waters such as Lake St. Clair, where the tide can be neglected, Budgell and El-Shaarawi (1978) applied a Box and Jenkins (1970) transfer function model using measurements of the water height, atmospheric pressure, wind and temperature. Unfortunately, the applications of the statistical methods just described were not always satisfactory. This is mainly caused by the fact that the parameters of the models were estimated by using long series of observations, assuming stationarity of the observed processes. During storm surge periods when conditions can change rapidly, this is not a very realistic assumption. Therefore, attention has been more and more concentrated on the deterministic methods which have a more physical basis.

The early deterministic methods were based on analytical solutions of the hydrodynamic equations. In order to obtain these solutions simplifications had to be imposed, e.g. a linear bottom friction term and a constant or linearly varying depth. As described in Subsection 1.2.3, this approach was used by Weenink to predict the meteorological effect along the Dutch coast. Other analytical methods for storm surge prediction are reviewed by Bretscheider (1966, 1967).

Within the last decennia, increasing computer capacity has permitted the computation of numerical solutions to the hydrodynamic equations. In the countries around the North Sea two-dimensional numerical models of the North Sea and adjacent waters have been developed. Linear models, neglecting the tide and only describing the meteorological effect, were implemented by Heaps (1969) and Timmerman (1975, 1977) among others. Non-linear tidal models were developed for example by Flather (1976) and recently by Voogt (1985). Unfortunately, non-linear models tend to be too large to be used on an operational basis. This is caused by the fact that at the open boundaries of the models the wind effect is not known and has to be neglected. This is only a reasonable assumption when these boundaries are located on the Atlantic Ocean. In addition, for a sufficient description of the tidal movement in the North Sea the grid size has to be rather small, yielding very large

models. Therefore, as described in Subsection 1.2.3, the operational model used in the Netherlands does not consider the tidal movement and describes the meteorological effect only. As a consequence, the grid size can be larger yielding a much smaller model. However, in this case the interaction between tide and meteorological effect is neglected.

In seeking prediction techniques that are not based on the simple superposition of the astronomical tide and meteorological effect, small non-linear models have been developed. To avoid that the model becomes too large, a rather coarse grid size has to be used. Since the tide cannot accurately be represented on this grid, the model is used to predict the meteorological effect by carrying out two computations, one for tide and surge together, the other with meteorological input removed and for the tide only. The difference of the two computations gives the required meteorological effect including the important non-linear interaction between tide and surge, assuming that the errors caused by the crude discretisation can be eliminated to a large extent in this way. In England (Flatcher and Proctor 1983), Germany (Soetje and Brockmann 1983) and Denmark (Duun-Christensen 1983), this approach has been in routine operation since the late seventies. In the Netherlands, plans have been made to replace the linear North Sea model described in Subsection 1.2.3 by a non-linear model within a year or two.

During the last few years, at a number of research institutes three-dimensional numerical models have been developed. Recently, Davies (of his numerous publications we mention Davies (1980)) has implemented a three-dimensional model of the North Sea. Although the results look very encouraging, especially in the case of storm surges, three-dimensional models are not likely to be used on an operational basis in the near future. These models are very large and, furthermore, the development of these models is far from complete.

1.3. Kalman filter approach to tidal prediction

As described in Subsection 1.2.4, tidal prediction techniques have been either statistical or deterministic in nature. Employing a statistical method it is possible to use on-line measurements of the water-level, while the deterministic approach provides a more realistic picture of the tidal dynamics. When a numerical tidal model is combined with a Kalman filter one obtains the best features of both the deterministic and the statistical methods. Furthermore, in modelling the water movement the various parameters that represent the influence of the physical phenomena on these movements, such as the bottom friction coefficient and wind friction coefficient, are inserted in deterministic models as constants. However, since the knowledge available about these phenomena is far from complete and they are modelled by empiri-

cal parametrizations, the parameters are sensitive to changing conditions. Employing a Kalman filter approach it is possible to correct the predictions of the water-level and to adapt the model to changing physical circumstances using on-line information. This property of the Kalman filter becomes increasingly important during storm surge periods, when conditions usually change rapidly.

Considering the fact that the number of on-line measurement stations is increasing rapidly and that in future it will be possible to obtain information of the water movement in the North Sea by means of satellites, the Kalman filter approach promises to become very important.

Since the original work of Kalman and Bucy (1960, 1961), Kalman filters have been successfully used in numerous applications. Most of these filters were developed for the determination of satellite orbits and for the navigation of submarines, aircraft and spaceships. In the last decennium Kalman filter techniques have also gained acceptance in meteorology (Ghil et al 1981), oceanography (Miller 1986) and in several areas of hydraulics and water resources (Chao-lin Chiu 1978). Desalu, Gould and Scheppe (1974), Koda and Seinfeld (1978) and Fronza, Spirito and Tonielli (1979) have all developed Kalman filters for the prediction of air pollution, while Chao-lin Chiu and Isu (1978) have employed a Kalman filter to estimate the friction coefficient in the shallow water equations. However, these techniques have seldom been applied to tidal prediction problems. Budgell and Unny (1980, 1981) have developed a Kalman filter to predict tides in branched estuaries. This filter is based on the one-dimensional shallow water equations and is used to estimate and predict water-levels at spacially distributed measurement locations as well as between these locations. Although this application is a valuable contribution to the use of Kalman filters in tidal prediction problems, the practical usefulness of the filter is limited because the time interval over which predictions are produced, is only 30 minutes. Furthermore, the filter has only been employed during a period when the meteorological effect was very small and could be neglected. Therefore, the Kalman filter approach has yet to be applied to storm surge prediction problems.

The combination of the Kalman filter with a non-linear tidal model of the entire North Sea is, from a computational point of view, not (yet) feasible. Therefore, in this investigation two different approaches have been developed. The first is based on the approximation of the tidal movement in the Dutch coastal area by a one-dimensional model. The two-dimensional effects due to the wind and the Coriolis force are taken into account by introducing some additional, empirical, equations. Water-levels and velocities as well as the parameters in the model are estimated on-line by the Kalman filter. Since the model is continuously being adapted to the changing conditions even this simple conceptual model gives satisfactory predictions

at a low computational cost. However, the time interval over which accurate predictions can be produced is limited because the one-dimensional approximation is only realistic for a small part of the southern North Sea.

To increase the prediction interval the second Kalman filter approach that is developed in this investigation is based on a two-dimensional model of the entire North Sea and the Channel. The extension of the one-dimensional filter to two space dimensions does not give rise to conceptual problems, but as noted before, impose an unacceptably greater computational burden. In order to obtain a computationally efficient Kalman filter, the filter is approximated by a time-invariant one. In this case the time-consuming filter equations do not have to be computed over again as new measurements become available, but need only be solved once. As a consequence, these computations can be carried out off-line on a large computer. Furthermore, for the computation of a time-invariant filter special algorithms have been developed to reduce the amount of computations drastically. Unfortunately, in the case of a time-invariant filter it is not possible to estimate the parameters in the model on-line. However, using a large two-dimensional model this feature is less important than in the one-dimensional approach. Moreover, the amount of data available for the North Sea is too small to produce reliable estimates of both the tidal movement and the large number of parameters.

Summarizing, the first Kalman filter approach is based on the simplification of the model while employing the second approach the filter equations are simplified to obtain a computationally efficient filter. By using a small conceptual model, it is possible to exploit all the capabilities of Kalman filtering, such as the possibility to estimate uncertain parameters in the model. However, by employing the second approach it becomes possible to use a detailed two-dimensional model.

Although in this investigation attention is concentrated on the application of Kalman filters to predict storm surges, these filters can also be used to design and optimize water-level monitoring networks. Since the filter provides estimates of water-levels and velocities based on the measured water-levels as well as the accuracy of these estimates, it is possible to optimize the location of the measurement stations.

Finally, Kalman filters can be used to improve empirical parametrizations in the mathematical model. Employing the filter based on the one-dimensional model, estimates of the uncertain parameters in the model are produced. Studying these estimates may increase the insight into the performance of the model and suggest improvements of the underlying deterministic model.

1.4 Scope of the investigation

As described in Section 1.3, in this investigation two Kalman filters have been developed to predict the water-level in the mouth of the Eastern Scheldt. First in Chapter 2 a short description of the shallow water equations is given. Chapter 3 contains an introduction to the theory of Kalman filters, linear and non-linear. In Chapter 4 we apply the theory to the linear one-dimensional shallow water equations to study some theoretical aspects of the filtering problem. Furthermore, we develop analytical methods to investigate the performance of the filter and to increase the insight into the complex filtering problem. Finally, in this chapter the numerical aspects of some Kalman filter algorithms are discussed. Chapter 5 deals with the one-dimensional approach to predict water-levels in the Eastern Scheldt. Attention is concentrated on the development of the model equations. To examine filter performance both simulated data and field data have been used. In Chapter 6, using the insight gained from the one-dimensional approach, the filter based on a two-dimensional model is developed. Again, this filter has been tested using simulated data and field data. The investigation is concluded in Chapter 7 with a discussion of the results and recommendations for further study.

2 The shallow water equations

2.1 Introduction

To make this study more self-contained, in this chapter a short description of the shallow water equations is given. We do not intend to present a detailed treatment, but describe some aspects of the shallow water equations that are relevant to the filtering problems dealt with in this study. For a more complete treatment the reader is referred to Abbott (1966, 1979) or Gerritsen (1982) among others.

In Section 2.2 the general non-linear two-dimensional equations are derived to recall the basic assumptions of the theory of long waves. Section 2.3 deals with the one-dimensional equations. For this case, the characteristic formulation of the equations is given. This formulation increases the insight into the wave motion and can be used to derive boundary conditions.

2.2 The two-dimensional equations

Consider an Eulerian system of coordinates x, y, z with the z -axis vertically upward. Neglecting effects of viscosity the general dynamic equations describing the motion of a fluid may be written:

$$\frac{\partial u}{\partial t} + u \frac{\partial u}{\partial x} + v \frac{\partial u}{\partial y} + w \frac{\partial u}{\partial z} + \frac{1}{\rho} \frac{\partial p}{\partial x} = F_x \quad (2.1)$$

$$\frac{\partial v}{\partial t} + u \frac{\partial v}{\partial x} + v \frac{\partial v}{\partial y} + w \frac{\partial v}{\partial z} + \frac{1}{\rho} \frac{\partial p}{\partial y} = F_y \quad (2.2)$$

$$\frac{\partial w}{\partial t} + u \frac{\partial w}{\partial x} + v \frac{\partial w}{\partial y} + w \frac{\partial w}{\partial z} + \frac{1}{\rho} \frac{\partial p}{\partial z} = -g + F_z \quad (2.3)$$

where:

u, v, w = velocities in respectively the x, y and z -directions

ρ = density of the fluid

p = pressure

F_x, F_y, F_z = components of extraneous forces

g = acceleration of gravity

The general equation of continuity for an incompressible fluid is:

$$\frac{\partial u}{\partial x} + \frac{\partial v}{\partial y} + \frac{\partial w}{\partial z} = 0 \quad (2.4)$$

The equations (2.1) - (2.3) describe the conservation of momentum, while equation (2.4) describes the conservation of mass. The derivation of these equations can be found in most textbooks on fluid dynamics (Batchelor 1970).

We now derive the shallow water equations describing the propagation of long water waves, i.e. waves with a length that is very great compared to the depth of the water. In the classical theory of long waves, the vertical accelerations are neglected in comparison with the acceleration of gravity. Furthermore, it is assumed that the external forces in the vertical direction can also be neglected with respect to gravity. Consequently, it follows from equation (2.3) that the pressure is assumed to be hydrostatic and is a linear function of the water-level:

$$p(z) = \rho_w g(h-z) + p_a \quad (2.5)$$

where:

h = water-level with respect to the undisturbed water surface

p_a = atmospheric pressure

ρ_w = density of water.

To obtain the equations for the depth averaged flow the vertically integrated velocity components are introduced according to:

$$\bar{u} = \frac{1}{h} \int_{-D}^h \frac{u}{D+h} dz \quad (2.6)$$

$$\bar{v} = \frac{1}{h} \int_{-D}^h \frac{v}{D+h} dz \quad (2.7)$$

where D is the distance between the undisturbed water surface and the bottom.

Substituting equation (2.5) into the equations (2.1) and (2.2) and integrating the resulting equations over the region $z=-D$ to $z=h$ yields:

$$\frac{\partial \bar{u}}{\partial t} + \bar{u} \frac{\partial \bar{u}}{\partial x} + \bar{v} \frac{\partial \bar{u}}{\partial y} + g \frac{\partial h}{\partial x} = - \frac{1}{\rho_w} \frac{\partial p_a}{\partial x} + F_x \quad (2.8)$$

$$\frac{\partial \bar{v}}{\partial t} + \bar{u} \frac{\partial \bar{v}}{\partial x} + \bar{v} \frac{\partial \bar{v}}{\partial y} + g \frac{\partial h}{\partial y} = - \frac{1}{\rho_w} \frac{\partial p_a}{\partial y} + F_y \quad (2.9)$$

Other terms introduced by the integration have been omitted. However, in this case it is necessary that the velocity distributions over the vertical are fairly constant (Dronkers 1964, 1975).

Including the effect of the earth's rotation and introducing empirical formulas describing the bottom friction and the wind stress into the equations (2.8) and (2.9) results in:

$$\frac{\partial \bar{u}}{\partial t} + \bar{u} \frac{\partial \bar{u}}{\partial x} + \bar{v} \frac{\partial \bar{u}}{\partial y} + g \frac{\partial h}{\partial x} = f \bar{v} - \mu \frac{\bar{u} \sqrt{\bar{u}^2 + \bar{v}^2}}{D + h} + \gamma \frac{V^2 \cos \psi}{D + h} - \frac{1}{\rho_w} \frac{\partial p_a}{\partial x} \quad (2.10)$$

$$\frac{\partial \bar{v}}{\partial t} + \bar{u} \frac{\partial \bar{v}}{\partial x} + \bar{v} \frac{\partial \bar{v}}{\partial y} + g \frac{\partial h}{\partial y} = -f \bar{u} - \mu \frac{\bar{v} \sqrt{\bar{u}^2 + \bar{v}^2}}{D + h} + \gamma \frac{V^2 \sin \psi}{D + h} - \frac{1}{\rho_w} \frac{\partial p_a}{\partial y} \quad (2.11)$$

where:

f = Coriolis parameter

μ = bottom friction coefficient

γ = wind friction coefficient

V = wind velocity

ψ = direction of the wind with respect to the positive x-axis.

In a similar way the equation of continuity (2.4) can be integrated over the vertical. The boundary conditions required can easily be established. If the equation of a boundary surface is $F(x,y,z,t)=0$ then, since a particle that is on the surface will remain on it*, we have:

$$\frac{dF}{dt} = \frac{\partial F}{\partial t} + u \frac{\partial F}{\partial x} + v \frac{\partial F}{\partial y} + w \frac{\partial F}{\partial z} = 0 \quad (2.12)$$

At the free surface $z=h$:

$$w(h) = \frac{\partial h}{\partial t} + u \frac{\partial h}{\partial x} + v \frac{\partial h}{\partial y} \quad (2.13)$$

while at the bottom $z=-D$:

* This is a fundamental consequence of the continuum hypothesis (Batchelor 1970).

$$w(-D) + u \frac{\partial D}{\partial x} + v \frac{\partial D}{\partial y} = 0 \quad (2.14)$$

With these boundaries, integration of equation (2.4) over the region $z=-D$ to $z=h$ yields:

$$\frac{\partial h}{\partial t} + \frac{\partial((D+h)\bar{u})}{\partial x} + \frac{\partial((D+h)\bar{v})}{\partial y} = 0 \quad (2.15)$$

The momentum equations (2.10) and (2.11) and the continuity equation (2.15) are the basis for the study of the tides in shallow water such as the North Sea.

In practice the non-linear shallow water equations are often linearized, yielding the equation (1.3)-(1.5) that have been shown in Subsection 1.2.3. As described in this subsection, the complex astronomical tide can in this case be described separately by means of an harmonic analysis (Godin 1972). Consequently, a model based on the linearized equations needs only be used to describe the meteorological effects that are superimposed on the astronomical tide.

The wave motion is not completely described without boundary conditions. In general two types of boundary conditions are to be distinguished: closed and open ones. Closed boundaries are physical land-water boundaries, whereas open boundaries are artificial ones that have been chosen arbitrarily to restrict the domain of the problem. Using the characteristic formulation of the equations (2.10), (2.11) and (2.15) it is possible to determine the number of boundary conditions that is necessary for the problem to be well posed, i.e. the solution exists, is unique and depends continuously on initial and boundary conditions. At a closed boundary where the normal velocity is equal to zero, no additional condition is required. At an open boundary one condition is required in case of outflow and two conditions in case of inflow. Here, it is assumed that the flow is subcritical:

$$\bar{u}^2 + \bar{v}^2 < g(D + h)$$

For the linearized equations (1.3) - (1.5) only one condition is required at an open boundary. The derivation of the characteristic formulation of the two-dimensional shallow water equations can be found in Gerritsen (1982).

2.3. The one-dimensional equations

Along a coast or in a river the flow of the water is predominantly in one direction so that the water motion is considered to be one-dimensional. If the x -axis is chosen

along the flow direction, the velocity component v perpendicular to the flow can be neglected. In this case the equations of motion (2.10) and (2.11) become (leaving the bars off again):

$$\frac{\partial u}{\partial t} + u \frac{\partial u}{\partial x} + g \frac{\partial h}{\partial x} = -\mu \frac{u|u|}{D+h} + \gamma \frac{V^2 \cos \psi}{D+h} - \frac{\partial p_a}{\rho_w \partial x} \quad (2.16)$$

$$g \frac{\partial h}{\partial y} = -f u + \gamma \frac{V^2 \sin \psi}{D+h} - \frac{\partial p_a}{\rho_w \partial y} \quad (2.17)$$

and the continuity equation (2.15) becomes:

$$\frac{\partial h}{\partial t} + \frac{\partial((D+h)u)}{\partial x} = 0 \quad (2.18)$$

If these equations are used to describe the flow in a channel with very small width, the Coriolis force and the meteorological effect across the width can be neglected and equation (2.17) can be left out of consideration.

We now give the characteristic formulation of the equations (2.16) and (2.18). This formulation is important to gain insight into the tidal motion and to determine whether the number of boundary conditions is correct and the problem is well posed. If the equations (2.16) and (2.18) are generalized by introducing the functions E_1 and E_2 :

$$\frac{\partial u}{\partial t} + u \frac{\partial u}{\partial x} + g \frac{\partial h}{\partial x} = E_1 \quad (2.19)$$

$$\frac{\partial h}{\partial t} + \frac{\partial((D+h)u)}{\partial x} = E_2 \quad (2.20)$$

the characteristic form of these equations becomes:

$$\left(\frac{\partial}{\partial t} + (u + \sqrt{g(D+h)}) \frac{\partial}{\partial x} \right) (u + 2\sqrt{g(D+h)}) = E_1 + \sqrt{\frac{g}{D+h}} E_2 + g \frac{dD}{dx} \quad (2.21)$$

$$\left(\frac{\partial}{\partial t} + (u - \sqrt{g(D+h)}) \frac{\partial}{\partial x} \right) (u - 2\sqrt{g(D+h)}) = E_1 - \sqrt{\frac{g}{D+h}} E_2 + g \frac{dD}{dx} \quad (2.22)$$

These equations can be interpreted as equations that describe the propagation (left hand side terms) and the deformation (right hand side terms) of the (quasi) Riemann invariants

$$u \pm 2\sqrt{g(D+h)} \quad (2.23)$$

along the characteristic lines determined by:

$$\frac{dx}{dt} = u \pm \sqrt{g(D+h)} \quad (2.24)$$

Using this characteristic formulation, the number of boundary conditions required, i.e. the number of characteristic lines pointing outside the domain of the problem, can be established easily.

On the basis of the physical interpretation of the equations (2.21)-(2.24) it is easy to formulate boundary conditions that correspond with a physical configuration of the boundary. Neglecting frictional forces and meteorological effects, we consider the following boundary conditions:

- total reflection at closed boundaries:

$$u - 2\sqrt{g(D+h)} = -(u + 2\sqrt{g(D+h)})$$

or

$$u = 0 \quad (2.25)$$

- free outflow:

$$u - 2\sqrt{g(D+h)} \text{ is constant}$$

or

$$u - 2\sqrt{g(D+h)} + 2\sqrt{gD} = 0 \quad (2.26)$$

- partial reflection:

$$u - 2\sqrt{g(D+h)} + 2\sqrt{gD} = -\eta(u + 2\sqrt{g(D+h)} - 2\sqrt{gD}) \quad (2.27)$$

where η is the reflection coefficient. Note that for $\eta = 1$ this boundary condition reduces to relation (2.25) while for $\eta = 0$ the condition (2.26) is obtained.

Here we assumed that the flow is subcritical ($u^2 < g(D+h)$) and consequently the (quasi) Riemann invariants propagate in opposite directions. Introducing friction and meteorological effects the boundary treatment becomes more complicated. The interested reader is referred to Verboom, Stelling and Officier (1982) or Ten Brummelhuis, De Jong and Heemink (1985).

3 Discrete filtering theory

3.1 Introduction

Since the original papers by Kalman and Bucy (1960, 1961) a considerable amount of literature has become available on the theory and applications of Kalman filters. In this chapter we give a short review of the filtering theory. We by no means attempt to give a complete treatment. We have concentrated our attention on the aspects of discrete filtering theory that are of major relevance to the problems dealt with in this study. Rather than strive for the mathematical precision of a theorem-proof structure, we merely recall the basic assumptions and characteristics of filtering theory. For a thorough treatment that is still accessible to most practical engineers, the reader is referred to the excellent textbooks of Jazwinski (1979), Maybeck (1979, 1982) or Anderson and Moore (1979).

In Section 3.2 we introduce the Kalman filter for linear discrete systems. Considerable attention is paid to the stability of the filter. Section 3.3 is devoted to some aspects of non-linear filtering theory. Some non-linear filters that have proved to be successful in practical applications are summarized. In this chapter we do not pay attention to the important numerical aspects of the filtering problem. These are discussed in detail in Chapter 4 in connection with the problems dealt with in this study.

3.2 Linear filtering theory

3.2.1 The Kalman filter

Assume that modelling techniques have produced an adequate description in the form of a linear stochastic system to describe the propagation in time of a state vector \underline{X}_{t_k} :

$$\begin{aligned}\underline{X}_{t_k} &= \Phi(t_k, t_{k-1}) \underline{X}_{t_{k-1}} + B(t_k) \underline{u}_{t_k} + G(t_k) \underline{W}_{t_k}, \quad k = 1, 2, \dots \\ \underline{X}_{t_0} &= \underline{X}_0\end{aligned}\tag{3.1}$$

Here \underline{X}_{t_k} is an n-vector state process, $\Phi(t_k, t_{k-1})$ is the non-singular n-by-n system dynamics matrix, $B(t_k)$ is an n-by-r input matrix, \underline{u}_{t_k} is an r-vector deterministic

input, $G(t_k)$ is an n -by- p noise input matrix and \underline{W}_{t_k} is a p -vector white Gaussian noise process. The statistics of this noise process are assumed to be:

$$\begin{aligned} E\{\underline{W}_{t_k}\} &= 0 \\ E\{\underline{W}_{t_k} \underline{W}_{t_l}^T\} &= R(k) , k = 1 \\ &\quad 0 , k \neq l \end{aligned} \tag{3.2}$$

with $R(k)$ being a p -by- p symmetric positive-semidefinite matrix. The system noise \underline{W}_{t_k} includes the effects of variability in the natural system as well as model structure errors. The initial condition \underline{X}_0 is also assumed to be Gaussian with statistics:

$$\begin{aligned} E\{\underline{X}_0\} &= \hat{\underline{X}}_0 \\ E\{[\underline{X}_0 - \hat{\underline{X}}_0] [\underline{X}_0 - \hat{\underline{X}}_0]^T\} &= P_0 \end{aligned} \tag{3.3}$$

where P_0 is an n -by- n symmetric positive-definite matrix.

Measurements are available at discrete time points t_1, t_2, \dots and are modelled by the relation:

$$\underline{Z}_{t_k} = M(t_k) \underline{X}_{t_k} + \underline{V}_{t_k} \tag{3.4}$$

Here \underline{Z}_{t_k} is the m -vector measurement process, $M(t_k)$ is the m -by- n measurement matrix and \underline{V}_{t_k} is an m -vector white Gaussian noise process with statistics:

$$\begin{aligned} E\{\underline{V}_{t_k} \underline{V}_{t_l}^T\} &= 0 \\ E\{\underline{V}_{t_k} \underline{V}_{t_l}^T\} &= R(k) , k = 1 \\ &\quad 0 , k \neq l \end{aligned} \tag{3.5}$$

The measurement noise \underline{V}_{t_k} represents the uncertainty associated with the measurement process. It is further assumed that $R(k)$ is a symmetric positive-definite matrix and that the initial state \underline{X}_0 , the system noise \underline{W}_{t_k} and the measurement noise \underline{V}_{t_k} are mutually independent.

It is desired to combine the measurements \underline{Z}_{t_k} , taken from the actual system, with the information provided by the system model in order to obtain an estimate of the system state \underline{X}_{t_k} . To solve this filtering problem we adopt the Bayesian approach and determine the conditional probability density of the state \underline{X}_{t_k} , conditioned on the entire history of the measurements taken: $\underline{Z}_{t_1}, \underline{Z}_{t_2}, \dots, \underline{Z}_{t_l}, l \leq k$. Once this density is explicitly described an optimal estimate of the state \underline{X}_{t_k} can be defined.

Under the assumptions of the model described above it can easily be proved that the conditional density is Gaussian. As a result it is completely characterized by its mean and covariance matrix. Therefore, the mean, mode, median or any other logical choice of estimate of \underline{X}_{t_k} based on the conditional density will result in the same estimated value $\hat{X}(k|l)$ and the same covariance matrix of the estimation error $P(k|l)$. Recursive filter equations to obtain these quantities can be summarized as follows. The optimal state estimate is propagated from measurement time t_{k-1} to measurement time t_k by the equations:

$$\hat{X}(k|k-1) = \Phi(t_k, t_{k-1}) \hat{X}(k-1|k-1) + B(t_k) u_{t_k} \quad (3.6)$$

$$P(k|k-1) = \Phi(t_k, t_{k-1}) P(k-1|k-1) \Phi(t_k, t_{k-1})^T + \\ G(t_k) Q(k) G(t_k)^T \quad (3.7)$$

At measurement time t_k , the measurement Z_{t_k} becomes available. The estimate is updated by the equations:

$$\hat{X}(k|k) = \hat{X}(k|k-1) + K(k) [Z_{t_k} - M(t_k) \hat{X}(k|k-1)] \quad (3.8)$$

$$P(k|k) = P(k|k-1) - K(k) M(t_k) P(k|k-1) \quad (3.9)$$

where:

$$K(k) = P(k|k-1) M(t_k)^T [M(t_k) P(k|k-1) M(t_k)^T + R(k)]^{-1} \quad (3.10)$$

is the filter gain. The initial condition for the recursion is given by:

$$\begin{aligned} \hat{X}(0|0) &= \hat{X}_0 \\ P(0|0) &= P_0 \end{aligned} \quad (3.11)$$

The filter just described is the celebrated Kalman filter for a discrete problem formulation. The derivation of these filter equations can be found for instance in Maybeck's work (1979). Maybeck uses a probabilistic approach to the filtering problem: The state vector is considered to be a stochastic process evolving in time, whose probability law is to be determined by using observations of another, related stochastic process. Since any logical choice of estimate of the state \underline{X}_{t_k} will result in the same filter equations, the Kalman filter can also be derived using classical statistical methods such as maximum likelihood or least squares estimation (Jazwinski, 1970). However, these methods tend to mask the fundamental probabilistic structure of the filtering problem which is very important when dealing with non-linear problems.

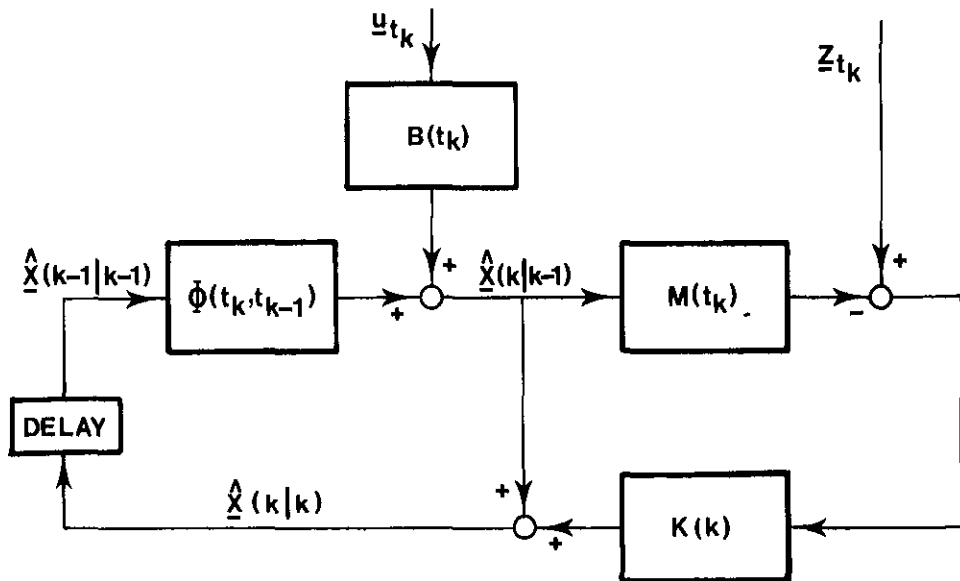


Figure 3.1: Block diagram representation of the Kalman filter.

The Kalman filter has a predictor-corrector structure. Based on all previous information, a prediction of the state vector at time t_k is made by means of the equations (3.6) and (3.7). Once this prediction is known it is possible to predict the next measurement by means of the equation (3.4). When this measurement has become available the difference between this measurement and its predicted value is used to update the prediction of the state vector by means of the equations (3.8)-(3.10). *Figure 3.1* is a block diagram representation of the algorithm. Note that the filter gain $K(k)$ does not depend on the measurements and therefore may be precomputed.

The performance of the filter can be judged by monitoring the residuals \underline{R}_{t_k} , defined as the difference between the measurements and the prediction of these measurements based on all previous information:

$$\underline{R}_{t_k} = \underline{z}_{t_k} - M(t_k) \hat{x}_{(k|k-1)} \quad (3.12)$$

It is easy to verify that:

$$E\{\underline{R}_{t_k}\} = 0 \quad (3.13)$$

$$E\{\underline{R}_{t_k} \underline{R}_{t_k}^T\} = M(t_k) P(k|k-1) M(t_k)^T + R(k) \quad (3.14)$$

Since the theoretical statistics of the residuals \underline{R}_{t_k} are known, the actual residuals can be monitored and compared with this description. By checking whether the residuals indeed possess their theoretical statistical properties we are able to judge whether or not the mathematical model satisfactorily describes the real system behaviour.

The model described in this section is not the most general one. It is possible to allow both P_0 and $R(k)$ to be positive-semidefinite instead of positive-definite. Furthermore, the system and measurement noise may be correlated. However, these generalizations have been omitted here since they are not relevant to the problem considered in this study. The interested reader is referred to Jazwinski (1970) or Maybeck (1979).

Finally, we note that if the initial condition X_0 , the system noise W_{t_k} and the measurement noise V_{t_k} are not assumed to be Gaussian but only described by their mean and covariance, the Kalman filter equations (3.6) - (3.10) are still optimal in least squares sense. However in this case, unlike the Gaussian one, knowledge of the mean $\hat{X}(k | k)$ and covariance $P(k | k)$ does not provide complete information about the probability density function of X_{t_k} , conditioned on the measurement: $Z_{t_1}, Z_{t_2}, \dots, Z_{t_k}$.

3.2.2 Stability

Optimality of the filter does not imply stability. In order to define the stability of the filter it is useful to rewrite the Kalman filter as:

$$\hat{X}(k | k) = \Psi(t_k, t_{k-1})\hat{X}(k-1 | k-1) + B(t_k)u_{t_k} + K(k)Z_{t_k} \quad (3.15)$$

where $K(k)$ is determined by the equations (3.7), (3.9) and (3.10) and

$$\Psi(t_k, t_{k-1}) = [I - K(k)M(t_k)]\Phi(t_k, t_{k-1}) \quad (3.16)$$

is the state transition matrix of the filter. The filter just described is said to be stable if there exists a constant $c_1 > 0$ so that:

$$\|\Psi(t_k, t_0)\| < c_1, \text{ for all } t_k \geq t_0^* \quad (3.17)$$

Here $\| . \|$ denotes a matrix norm.

* This stability definition is not the only possible one. For the definitions of various types of stability the reader is referred to Hahn (1963) among others.

The filter is uniformly exponentially stable if there exist constants $c_2 > 0$ and $c_3 > 0$ so that:

$$\|\Psi(t_k, t_0)\| < c_2 e^{-c_3(t_k - t_0)} \quad (3.18)$$

Exponential stability of the filter implies that bounded inputs \underline{u}_{t_k} and \underline{Z}_{t_k} produce bounded outputs $\hat{X}(k | k)$.

An immediate consequence of the exponential stability of a filter is that if $P^1(k | k)$ and $P^2(k | k)$ are two solutions to the filter equations for different initial conditions $P^1_{t_0}$ and $P^2_{t_0}$ respectively, then:

$$\|P^1(k | k) - P^2(k | k)\| < c_2^2 e^{-2c_3(t_k - t_0)} \|P^1_{t_0} - P^2_{t_0}\| \quad (3.19)$$

This essentially means that the effect of the initial condition P_{t_0} vanishes as more and more measurements are incorporated. This is important since P_{t_0} is often poorly known. Furthermore, equation (3.19) also indicates that the computation of $P(k | k)$ is stable and that numerical errors in $P(k | k)$ similarly vanish. This is a very favourable property since in case the Kalman filter algorithm (3.6)-(3.10) is employed for ill-conditional problems, these numerical errors can become large. In Chapter 4 this problem is discussed in more detail.

In order to obtain stability results we introduce some system theoretical concepts. We begin by considering the controllability of the system model (3.1). Suppose that no measurements are available. The equations to obtain the covariance matrix reduce to:

$$P(k | k) = \Phi(t_k, t_0)P_0\Phi(t_k, t_0)^T + \sum_{i=1}^k \Phi(t_k, t_i)G(t_i)Q(i)G(t_i)^T\Phi(t_k, t_i)^T \quad (3.20)$$

Defining the controllability gramian as:

$$C(k, k-N_1) = \sum_{i=k-N_1}^k \Phi(t_k, t_i)G(t_i)Q(i)G(t_i)^T\Phi(t_k, t_i)^T, \quad 0 \leq N_1 < k \quad (3.21)$$

equation (3.20) can be rewritten as:

$$P(k | k) = \Phi(t_k, t_{k-N_1-1})P(k-N_1-1 | k-N_1-1)\Phi(t_k, t_{k-N_1-1})^T + C(k, k-N_1) \quad (3.22)$$

The system model (3.1) is said to be uniformly completely controllable if there exist an N_1 and positive constants c_4 and c_5 so that:

$$c_4 I < C(k, k-N_1) < c_5 I, \text{ for all } k > N_1 \quad (3.23)$$

As can be seen from equation (3.22) this implies that the system noise sequence $\underline{W}_{t_{k-N_1}}, \underline{W}_{t_{k-N_1+1}}, \dots, \underline{W}_{t_k}$, affects all the components of the state \underline{X}_{t_k} . Furthermore, this effect is bounded from below as well as from above. Controllability prevents certain components of the state to be determined almost exactly in which case new observations would have very little effect on the estimates of these components and the estimates and measurements could easily diverge. This problem is known as filter divergence. If a filter is not controllable numerical difficulties also are very likely to occur. Since in case some state components (or linear combination of state components) can be estimated very accurately, some eigenvalues of the covariance matrix become almost zero. Due to the finite wordlength on the computer, these eigenvalues can easily become negative, a condition that is theoretically impossible and usually leads to a total failure of the recursion. This important aspect of Kalman filtering as well as the problem of filter divergence are discussed in Chapter 4.

A concept dual to that of controllability is observability. Suppose the system model (3.1) is noise-free, i.e. $\underline{W}_{t_k} = 0$ for all k . In that case, applying some clever matrix algebra (Maybeck 1979), the equations to obtain the covariance matrix can be rewritten as:

$$P(k|k)^{-1} = \Phi(t_k, t_0)^{-T} P_0^{-1} \Phi(t_k, t_0)^{-1} + \sum_{i=1}^k \Phi(t_k, t_i)^{-T} M(t_i)^T R(i)^{-1} M(t_i) \Phi(t_k, t_i)^{-1} \quad (3.24)$$

Defining the observability gramian as:

$$O(k, k-N_2) = \sum_{i=k-N_2}^k \Phi(t_k, t_i)^{-T} M(t_i)^T R(i)^{-1} M(t_i) \Phi(t_k, t_i)^{-1}, \quad 0 \leq N_2 < k \quad (3.25)$$

equation (3.24) can be rewritten as:

$$P(k|k)^{-1} = \Phi(t_k, t_{k-N_2-1})^{-T} P(k-N_2-1|k-N_2-1)^{-1} \Phi(t_k, t_{k-N_2-1})^{-1} + O(k, k-N_2) \quad (3.26)$$

The system model (3.1) and (3.4) is now said to be uniformly completely observable if there exist an N_2 and positive constants c_6 and c_7 so that:

$$c_6 I < O(k, k-N_2) < c_7 I, \quad \text{for all } k > N_2 \quad (3.27)$$

As can easily be deduced from equation (3.26) this implies that incorporating the measurements $\underline{Z}_{t_{k-N_2}}, \underline{Z}_{t_{k-N_2+1}}, \dots, \underline{Z}_{t_k}$, improve the estimates of all the components of the state \underline{X}_{t_k} ^{*}. Furthermore, this improvement is bounded from below and from

* In fact this property is defined as reconstructibility (Kwakernaak and Sivan 1972). Observability is defined such that incorporating the measurements $\underline{Z}_{t_{k-N_2}}, \underline{Z}_{t_{k-N_2+1}}, \dots, \underline{Z}_{t_k}$ improve the estimates of all the components of the state $\underline{X}_{t_{k-N_2}}$. However, for the problem described in Subsection 3.2.1 observability and reconstructibility are not significantly distinct issues.

above. Observability guarantees that the entire state can be determined from the data and prevents that certain eigenvalues of the covariance matrix can grow without bounds. It also implies that the effects of changes in any component of the state can be observed in the measurements.

Having defined the concepts of observability and controllability, both introduced by Kalman, Lyapunov stability theory can be applied to establish exponentially stability results. Through the explicit generation of an appropriate Lyapunov function, it can be proved that if a system model is both uniformly completely observable and controllable, the Kalman filter is uniformly exponentially stable (Kalman 1963).

Another approach to the stability of the filter can be obtained from the filter equations (3.6)-(3.10). It is easy to show that for the model described in Subsection 3.2.1:

$$\| [I - K(k)M(t_k)] \| \leq 1, \text{ for all } k \quad (3.28)$$

so that:

$$\| \Psi(t_k, t_0) \| \leq \| \Phi(t_k, t_0) \| \quad (3.29)$$

This implies that if the original system (3.1) is (exponentially) stable the Kalman filter is also (exponentially) stable (Kwakernaak and Sivan 1972). From equation (3.29) it can be seen that the filter is always more stable than the original system. This stability improvement property of the filter is a very favourable property. Note that if the filter is uniformly completely observable and controllable the stability of the original system is not required for filter stability. A system model can be unstable while the Kalman filter is stable.

3.3 Non-linear filtering theory

3.3.1 Introduction

Using the probabilistic approach to non-linear filtering problems we seek, as in the linear case, the conditional probability density of the state conditioned on the measurements taken. This density is, unlike that of the linear case, usually non-Gaussian and, therefore, generally cannot be characterized completely by a finite set of parameters. Since propagating and updating an entire density (or an infinite number of describing parameters for this density) is not implementable, simplifying assumptions have to be imposed. In this section attention is concentrated on the parametrization of the conditional density via central moments, since the resulting

approximate non-linear filters – from the computational point of view – are very attractive and have proved to be successful in numerous applications.

As in linear filtering problems, the main interest is to compute the conditional mean and covariance matrix since the mean is always the minimum variance estimate and the covariance matrix measures the uncertainty in the estimate. Note that, unlike the linear case, the mode, median or another estimate of the state do not, in general, result in the same estimated value of the mean. Propagating and updating the conditional mean and the covariance matrix in non-linear problems usually requires all the central moments of the conditional probability density. By making certain assumptions about these moments approximate estimators can be generated. One might assume for instance that the conditional density is nearly symmetric, so that third and higher-order odd central moments are negligible, and that in addition it is concentrated near its mean, so that fourth and higher-order even central moments can be neglected as well. The resulting approximate filter is called the truncated second-order filter. In another approximation the fourth-order central moment is not neglected but, assuming that the conditional density is nearly Gaussian, expressed in terms of the covariance. This additional assumption gives rise to the so-called Gaussian second-order filter. Computational considerations lead to first-order filters, such as the celebrated extended Kalman filter.

In Subsection 3.3.2 we first derive the extended Kalman filter as a rather straightforward extension of the linear filter since the results from the linear theory can be exploited easily for this non-linear problem. Furthermore, this subsection can serve as an introduction to the more general non-linear filters. Subsection 3.3.3 is devoted to the non-linear filters described in this introduction and to some filters that are not based on the parametrization of the conditional probability density via central moments. Finally, in Subsection 3.3.4 the use of the non-linear filters to estimate uncertain parameters in a model is discussed.

3.3.2 Linearized and extended Kalman filters

Suppose that a linear model does not provide a valid description of the problem. Assume that the system state can be presented by the non-linear stochastic system:

$$\begin{aligned} \underline{X}_{t_k} &= \underline{\Phi}(\underline{X}_{t_{k-1}}, t_{k-1}, t_k) + B(t_k) \underline{u}_{t_k} + G(t_k) \underline{W}_{t_k}, \quad k=1, 2, 3\dots \\ \underline{X}_{t_0} &= \underline{X}_0 \end{aligned} \tag{3.30}$$

where $\underline{\Phi}(\underline{X}_{t_{k-1}}, t_{k-1}, t_k)$ is an n-vector describing the system dynamics. Let the measurements be modelled by the non-linear equation:

$$\underline{Z}_{t_k} = \underline{m}(\underline{X}_{t_k}, t_k) + \underline{V}_{t_k} \quad (3.31)$$

where $\underline{m}(\underline{X}_{t_k}, t_k)$ is an m-vector describing the relation between the state and the measurements. The other model assumptions are completely similar to the linear case described in Subsection 3.2.1. Note that the system as well as the measurement noise are still assumed to enter in an additive fashion. Therefore the linear theory can be extended to the non-linear problem just described.

Suppose that it is possible to generate a discrete reference state trajectory $\bar{\underline{x}}_{t_k}$. The state equation (3.30) may be rewritten as:

$$\underline{X}_{t_k} = [\underline{\Phi}(\underline{X}_{t_{k-1}}, t_{k-1}, t_k) - \underline{\Phi}(\bar{\underline{x}}_{t_{k-1}}, t_{k-1}, t_k)] + \underline{\Phi}(\bar{\underline{x}}_{t_{k-1}}, t_{k-1}, t_k) + B(t_k) \underline{u}_{t_k} + G(t_k) \underline{W}_{t_k} \quad (3.32)$$

and the observation equation (3.31) as:

$$\underline{Z}_{t_k} = [\underline{m}(\underline{X}_{t_k}) - \underline{m}(\bar{\underline{x}}_{t_k}, t_k)] + \underline{m}(\bar{\underline{x}}_{t_k}, t_k) + \underline{V}_{t_k} \quad (3.33)$$

If the deviation $\underline{X}_{t_k} - \bar{\underline{x}}_{t_k}$ from the reference trajectory is small, a Taylor's series expansion yields:

$$\underline{\Phi}(\underline{X}_{t_{k-1}}, t_{k-1}, t_k) - \underline{\Phi}(\bar{\underline{x}}_{t_{k-1}}, t_{k-1}, t_k) \approx \underline{\Phi}(\bar{\underline{x}}_{t_{k-1}}, t_{k-1}, t_k) (\underline{X}_{t_{k-1}} - \bar{\underline{x}}_{t_{k-1}}) \quad (3.34)$$

$$\underline{m}(\underline{X}_{t_k}, t_k) - \underline{m}(\bar{\underline{x}}_{t_k}, t_k) \approx M(\bar{\underline{x}}_{t_k}, t_k) (\underline{X}_{t_k} - \bar{\underline{x}}_{t_k}) \quad (3.35)$$

where:

$$(\underline{\Phi}(\bar{\underline{x}}_{t_{k-1}}, t_{k-1}, t_k))_{ij} = \frac{\partial(\underline{\Phi}(\bar{\underline{x}}_{t_{k-1}}, t_{k-1}, t_k))_i}{\partial(\bar{\underline{x}}_{t_{k-1}})_j} \quad (3.36)$$

$$(M(\bar{\underline{x}}_{t_k}, t_k))_{ij} = \frac{\partial(\underline{m}(\bar{\underline{x}}_{t_k}, t_k))_i}{\partial(\bar{\underline{x}}_{t_k})_j} \quad (3.37)$$

are the matrices of partial derivatives along the reference trajectory. The equations (3.34) and (3.35) can be used to obtain the approximate linear system:

$$\begin{aligned} \underline{X}_{t_k} &= \underline{\Phi}(\bar{\underline{x}}_{t_{k-1}}, t_{k-1}, t_k) \underline{X}_{t_{k-1}} - \underline{\Phi}(\bar{\underline{x}}_{t_{k-1}}, t_{k-1}, t_k) \bar{\underline{x}}_{t_{k-1}} + \\ &\quad \underline{\Phi}(\bar{\underline{x}}_{t_{k-1}}, t_{k-1}, t_k) + B(t_k) \underline{u}_{t_k} + G(t_k) \underline{W}_{t_k} \end{aligned} \quad (3.38)$$

and the approximate linear observation equation:

$$\underline{Z}_{t_k} = M(\bar{\underline{x}}_{t_k}, t_k) \underline{X}_{t_k} - M(\bar{\underline{x}}_{t_k}, t_k) \bar{\underline{x}}_{t_k} + \underline{m}(\bar{\underline{x}}_{t_k}, t_k) + \underline{V}_{t_k} \quad (3.39)$$

Given the linearized model described by the equations (3.38) and (3.39) the standard Kalman filter can be employed to obtain the estimate of the state \underline{X}_{t_k} and its covariance matrix.

The remaining problem is the choice of the reference trajectory. An obvious choice is to take:

$$\bar{x}_{t_k} = \Phi(\bar{x}_{t_{k-1}}, t_{k-1}, t_k) + B(t_k) u_{t_k} \quad (3.40)$$

$$\bar{x}_{t_0} = \dot{\underline{X}}_0$$

so that the reference trajectory is completely determined by the prior estimate of the state. This estimator is called the linearized Kalman filter.

The basic idea of the extended Kalman filter is to relinearize about each estimate $\dot{\underline{X}}(k|k)$:

$$\begin{aligned} \bar{x}_{t_p} &= \Phi(\bar{x}_{t_{p-1}}, t_{p-1}, t_p) + B(t_p) u_{t_p}, \quad p = k+1, k+2, \dots \\ \bar{x}_{t_k} &= \dot{\underline{X}}(k|k) \end{aligned} \quad (3.41)$$

As soon as a new measurement is available and a new state estimate has been obtained, a new and better reference trajectory is incorporated into the estimation process. With this choice of reference trajectory large initial estimation errors are not allowed to propagate through time and therefore, the linearity assumption is less likely to be violated. Note that the extended Kalman filter gain, unlike the linearized Kalman filter gain, depends on the measurements and therefore, cannot be precomputed.

3.3.3 Non-linear filters

Consider a model described by the non-linear stochastic system equation:

$$\begin{aligned} \underline{X}_{t_k} &= \Phi(\underline{X}_{t_{k-1}}, t_{k-1}, t_k) + B(t_k) u_{t_k} + G(\underline{X}_{t_k}, t_k) \underline{W}_{t_k}, \quad k=1,2,3, \dots \\ \underline{X}_{t_0} &= \underline{X}_0 \end{aligned} \quad (3.42)$$

where $G(\underline{X}_{t_k}, t_k)$ is an n-by-p noise input matrix. The measurement relation is given by equation (3.31). The other assumptions are completely similar to the model described in Subsection 3.3.2. As we have done in the linear case we seek the conditional mean and covariance matrix. Propagating and updating these quantities

generally require the knowledge of the entire conditional density. Take for example the propagation of the conditional mean:

$$\begin{aligned}\hat{X}(k|k-1) &= E\{\underline{X}_{t_k} | \underline{Z}_{t_1}, \underline{Z}_{t_2}, \dots, \underline{Z}_{t_{k-1}}\} \\ &= \int_{-\infty}^{\infty} \Phi(\underline{x}, t_{k-1}, t_k) P_{\underline{X}_{t_{k-1}} | \underline{Z}_{t_1}, \underline{Z}_{t_2}, \dots, \underline{Z}_{t_{k-1}}}(\underline{x} | \underline{z}_{t_1}, \underline{z}_{t_2}, \dots, \underline{z}_{t_{k-1}}) d\underline{x}\end{aligned}\quad (3.43)$$

where:

$$P_{\underline{X}_{t_{k-1}} | \underline{Z}_{t_1}, \underline{Z}_{t_2}, \dots, \underline{Z}_{t_{k-1}}}(\underline{x} | \underline{z}_{t_1}, \underline{z}_{t_2}, \dots, \underline{z}_{t_{k-1}})$$

is the conditional probability density of the state $\underline{X}_{t_{k-1}}$ based on the measurements $\underline{Z}_{t_1}, \underline{Z}_{t_2}, \dots, \underline{Z}_{t_{k-1}}$. In this subsection attention is concentrated on parametrization of this density via central moments.

We first consider the truncated second-order filter. In deriving this filter the third and higher-order central moments are neglected. This is appropriate if the conditional density is almost symmetric and concentrated near its mean. This filter has been derived by Henriksen (1980), correcting an error made in previous derivations and yielding the following filter equations:

$$\begin{aligned}\hat{X}(k|k-1) &= \Phi(\hat{X}(k-1|k-1), t_{k-1}, t_k) + \\ &\quad \frac{1}{2} P(k-1|k-1) \Phi_{xx}(\hat{X}(k-1|k-1), t_{k-1}, t_k)\end{aligned}\quad (3.44)$$

with:

$$\begin{aligned}(P(k-1|k-1) \Phi_{xx}(\hat{X}(k-1|k-1), t_{k-1}, t_k))_i &= \\ \sum_{j,l=1}^n (P(k-1|k-1))_{jl} & \frac{\partial^2 (\Phi(\hat{X}(k-1|k-1), t_{k-1}, t_k))_i}{\partial (\hat{X}(k-1|k-1))_j \partial (\hat{X}(k-1|k-1))_l} \\ P(k|k-1) &= \Phi(\hat{X}(k-1|k-1), t_{k-1}, t_k) P(k-1|k-1) \Phi(\hat{X}(k-1|k-1), t_{k-1}, t_k)^T + \\ G(\hat{X}(k-1|k-1), t_{k-1}) Q(k-1) G(\hat{X}(k-1|k-1), t_{k-1})^T &+ \\ P(k-1|k-1) Q(k-1) G_x(\hat{X}(k-1|k-1), t_{k-1})^2 &+ \\ \frac{1}{2} P(k-1|k-1) Q(k-1) G_{xx}(\hat{X}(k-1|k-1), t_{k-1}) G(\hat{X}(k-1|k-1), t_{k-1}) &+ \\ \frac{1}{2} (P(k-1|k-1) Q(k-1) G_{xx}(\hat{X}(k-1|k-1), t_{k-1}) G(\hat{X}(k-1|k-1), t_{k-1}))^T &\quad (3.45)\end{aligned}$$

Here $\Phi(\hat{X}(k-1 | k-1), t_{k-1}, t_k)$ is defined by equation (3.36) and

$$\begin{aligned}
 & (P(k-1 | k-1)Q(k-1)G_x(\hat{X}(k-1 | k-1), t_{k-1})^2)_{ij} = \\
 & \sum_{j,l=1}^p \sum_{s,t=1}^n (P(k-1 | k-1))_{st} (Q(k-1))_{jl} \frac{\partial(G(\hat{X}(k-1 | k-1), t_{k-1}))_{ij}}{\partial(\hat{X}(k-1 | k-1))_s} \\
 & \frac{\partial(G(\hat{X}(k-1 | k-1), t_{k-1}))_{ql}}{\partial(\hat{X}(k-1 | k-1))_t} \\
 & (P(k-1 | k-1)Q(k-1)G_{xx}(\hat{X}(k-1 | k-1), t_{k-1})G(\hat{X}(k-1 | k-1), t_{k-1}))_{iq} = \\
 & \sum_{j,l=1}^p \sum_{s,t=1}^n (P(k-1 | k-1))_{st} (Q(k-1))_{jl} \frac{\partial^2(G(\hat{X}(k-1 | k-1), t_{k-1}))_{ij}}{\partial(\hat{X}(k-1 | k-1))_s \partial(\hat{X}(k-1 | k-1))_t} \\
 & (G(\hat{X}(k-1 | k-1), t_{k-1}))_{ql} \\
 & \hat{X}(k | k) = \hat{X}(k | k-1) + K(k) [Z_{t_k} - m(\hat{X}(k | k-1), t_k) - \\
 & \quad \frac{1}{2} P(k | k-1) m_{xx}(\hat{X}(k | k-1), t_k)] \tag{3.46}
 \end{aligned}$$

with:

$$\begin{aligned}
 & (P(k | k-1)m_{xx}(\hat{X}(k | k-1), t_k))_i = \sum_{j,l=1}^m (P(k | k-1))_{jl} \\
 & \frac{\partial^2(m(\hat{X}(k | k-1), t_k))_i}{\partial(\hat{X}(k | k-1))_j \partial(\hat{X}(k | k-1))_l}
 \end{aligned}$$

$$\begin{aligned}
 K(k) &= P(k | k-1)M(\hat{X}(k | k-1), t_k)^T [M(\hat{X}(k | k-1), t_k)P(k | k-1) \\
 &\quad M(\hat{X}(k | k-1), t_k)^T + R(k)]^{-1} \tag{3.47}
 \end{aligned}$$

Here $M(\hat{X}(k | k-1), t_k)$ is defined by equation (3.37).

$$P(k | k) = [I - K(k)M(\hat{X}(k | k-1), t_k)] P(k | k-1) \tag{3.48}$$

The vectors

$$\underline{b}_\Phi(k-1) = \frac{1}{2} P(k-1 | k-1) \underline{\Phi}_{xx}(\hat{X}(k-1 | k-1), t_{k-1}, t_k) \tag{3.49}$$

$$\underline{b}_m(k) = \frac{1}{2} P(k | k) \underline{m}_{xx}(\hat{X}(k | k-1), t_k) \tag{3.50}$$

respectively appearing in equation (3.44) and (3.46), are called the bias correction terms. Note that when using the second-order truncated filter just described the model is relinearized about each new estimate $\hat{X}(k | k)$ when it becomes available, as is the case with the extended Kalman filter.

Now consider the Gaussian second-order filter. Whereas the truncated second-order filter ignores all the central moments above second-order, the Gaussian second-order filter accounts for the fourth moment as well by assuming that the conditional density is nearly Gaussian and by expressing the fourth central moment in terms of the covariance. In addition, the third and fourth-order non-linearities that in this case appear in the equations are also neglected in the Gaussian second-order filter approximation. The resulting equations of this filter may be found in Jazwinski (1970). Compared to the truncated second-order filter additional terms appear in the equations for the conditional covariance, while the equations for the conditional mean are exactly the same.

In cases where the dimension of the state is large, the calculation of the second-order filter equations to obtain the covariance matrix are very time-consuming. However, the primary benefit is usually due to the bias correction terms (3.49) and (3.50). Therefore, in deriving a first-order filter with bias correction terms, the second-order non-linearities appearing in the equations for the covariance matrix are neglected. The equations for the conditional mean are identical to the second-order filter equations (3.44) and (3.46) including the bias correction terms. When these terms can be neglected too, the approximate filter is called a truncated first-order filter. Finally, if G is only a function of t_k and not of X_{t_k} , the truncated first-order filter reduces to the extended Kalman filter which has been derived in Subsection 3.3.2.

The non-linear filters just described are all based on the parametrization of the conditional probability density via central moments. Representing the non-linear functions, Φ , G and m by a Taylor series expanded about the state estimate and neglecting higher-order central moments and if necessary, higher-order model nonlinearities, approximate filters can be derived. These filters have been successfully applied to numerous non-linear filtering problems.

Filters that are not based on the parametrization of the conditional density and therefore, do not require a representation of the non-linear functions by Taylor series, have also been reported in literature. Among these the so-called assumed density filters assume the conditional probability density to be Gaussian with mean and covariance as computed within the algorithm itself (Maybeck 1982). Propagating and updating the conditional mean and covariance are generally carried out by numerical integration of these expectations. Take for example the equation (3.43)

describing the propagation of the conditional mean. Assuming

$$\underline{P} \underline{X}_{t_{k-1}} | \underline{Z}_{t_1}, \underline{Z}_{t_2}, \dots, \underline{Z}_{t_{k-1}} (x | z_{t_1}, z_{t_2}, \dots, z_{t_{k-1}})$$

to be Gaussian with mean $\hat{X}(k-1 | k-1)$ and covariance matrix $P(k-1 | k-1)$, equation (3.43) can be integrated numerically. Note that this assumption implies that these filters, unlike the other filters described in this section, do not neglect higher-order central moments.

For the special case that G is not a function of the state, a statistically linearized filter may be employed (Maybeck 1982). Structurally the filter equations are the same as those for the extended Kalman filter, but instead of neglecting second and higher-order non-linearities, the non-linear functions $\underline{\Phi}$ and \underline{m} are approximated as follows:

$$\underline{\Phi}(\underline{X}_{t_{k-1}}, t_{k-1}, t_k) = \underline{\phi}_0(t_{k-1}) + \Phi(t_{k-1})\underline{X}_{t_{k-1}} + \underline{e}_1 \quad (3.51)$$

$$\underline{m}(\underline{X}_{t_k}, t_k) = \underline{m}_0(t_k) + M(t_k)\underline{X}_{t_k} + \underline{e}_2 \quad (3.52)$$

where the vectors $\underline{\phi}_0(t_{k-1})$ and $\underline{m}_0(t_k)$ and the matrices $\Phi(t_{k-1})$ and $M(t_k)$ are determined by the minimization of respectively \underline{e}_1 and \underline{e}_2 in (generalized) least squares sense. Similarly to the assumed density filters, the expectations involved are calculated by numerical integration, assuming the conditional densities to be Gaussian.

In some applications, assumed density filters (Maybeck 1982) and statistically linearized filters (Kikkawa and Iwase 1980) have shown to be more accurate than the extended Kalman filter. However, this advantage was gained at the expense of severely time-consuming computations. Therefore, when the dimension of the state is very large the use of these filters from a computational point of view is not attractive.

3.3.4 Parameter estimation

A particular application of non-linear filters is the estimation of an uncertain parameter P in the model (Eykhoff 1974). This parameter can be treated as additional state variable with system equation:

$$P_{t_k} = P_{t_{k-1}} + W_{P_{t_k}} \quad (3.53)$$

By adding the system noise $W_{P_{t_k}}$ to this equation the random character of the parameter can be taken into account. Note that in general even a linear model in this

case becomes a highly non-linear one. By employing a non-linear filter to estimate both the state and the uncertain parameters, it is possible to adapt the model to changing physical conditions. Compared to other methods for combined state and parameter estimation this procedure is attractive from the computational point of view. However, it also has a shortcoming. Owing to the neglected higher-order non-linearities bias errors may appear in the parameter estimate. The more pronounced the non-linearities are, the more the filter performance is degraded by this effect. Therefore, in a given application the capability of the filter to estimate uncertain parameters has to be verified by employing the filter using simulated data. In this case the true value of the parameter is known and, consequently, the performance of the filter can be evaluated under a variety of circumstances.

4. Kalman filters for the linear one-dimensional shallow water equations

4.1 Introduction

In this chapter some aspects of Kalman filters for the shallow water equations are discussed. To gain insight into the filtering problem, filters are derived on the basis of the linear one-dimensional equations. Moreover, using these linear equations, it becomes possible to employ analytical methods to investigate the performance of the filters.

In Section 4.2 we recall some basic aspects of the numerical approximation of differential equations. Section 4.3 and 4.4 are respectively devoted to the discretisation of the shallow water equations and to the choice of the noise statistics. To gain insight into the complex filtering problem, a special problem is solved analytically in Section 4.5. For this case, the sensitivity of the filter performance is studied with respect to the choice of the finite difference scheme and modelling errors. In Section 4.6 the discrete system representation of the general model is derived. Observability of the filter is discussed in Section 4.7, while Section 4.8 deals with the numerical properties of various Kalman filter algorithms. Finally, Section 4.9 briefly discusses the distributed parameter filtering problem in a more general context.

4.2 Numerical approximation of differential equations

This section recalls in a tutorial way the basic aspects of the numerical approximation of differential equations, such as consistency, convergence and stability. The treatment is based on the linear homogeneous partial-differential equations. However, to illustrate the relevant concepts this is not a real limitation. For a thorough treatment the reader is referred to Van der Houwen (1968), among others.

The partial-differential equation is written as:

$$Lf(x,t) = 0, \quad x \in \Omega, \quad t \in [t_0, T] \quad (4.1)$$

with initial condition:

$$f(x, t_0) = f_0(x), \quad x \in \Omega \quad (4.2)$$

and boundary condition:

$$L_b f(x, t) = \phi_b(x, t), \quad x \in \Gamma, \quad t \in [t_0, T] \quad (4.3)$$

where L and L_b are linear differential operators and Γ is the boundary of Ω .

The problem described above is assumed to be well posed so that it has a unique solution $f(x, t)$. In order to approximate the differential equation a grid is defined: a set of points with coordinates $(i\Delta x, k\Delta t)$. It is assumed that:

$$\Delta t = \Delta t(\Delta x),$$

$$\lim_{\Delta x \rightarrow 0} \Delta t(\Delta x) = 0$$

Denote by Ω_Δ the set of grid points that result when Ω is covered with the grid and let Γ_Δ denote the boundary of Ω_Δ . Using a finite difference scheme equations (4.1) - (4.3) can be converted into a set of difference equations:

$$L_\Delta f_i^k = 0 \quad (4.4)$$

$$f_i^0 = f_0(i\Delta x) \quad (4.5)$$

$$L_{b\Delta} f_i^k = \phi_b(i\Delta x, k\Delta t) \quad (4.6)$$

where f_i^k is the approximation of $f(i\Delta x, k\Delta t)$ and L_Δ and $L_{b\Delta}$ are the finite difference operators approximating L and L_b respectively.

The finite difference scheme (4.4) is a consistent approximation of order n of (4.1) if:

$$\| L_\Delta f(i\Delta x, k\Delta t) \| \leq c_g(\Delta x)^n \quad (4.7)$$

where c_g is a constant. Consistency of the approximation of the boundary condition can be defined in a similar way. The quantity under the norm here is called the truncation error and measures how accurately the solution of the original differential equation satisfies the finite difference equations.

To show the analogy with the discrete system theory described in Section 3.2, we define:

$$\underline{x}_{t_k} = [\dots f_i^k \ f_{i+1}^k \dots]^T \quad (4.8)$$

and write the difference equations (4.4) – (4.6) as* :

$$\underline{A}\underline{x}_{t_{k+1}} = \underline{B}\underline{x}_{t_k} + \underline{u}_{t_{k+1}} \quad (4.9)$$

where A and B are coefficient matrices and \underline{u}_{t_k} depends on the boundary condition. Symbolically we write:

$$\underline{x}_{t_{k+1}} = \Phi \underline{x}_{t_k} + A^{-1} \underline{u}_{t_{k+1}} \quad (4.10)$$

where $\Phi = A^{-1}B$. Defining:

$$\underline{x}(k) = [\dots f(i\Delta x, k\Delta t) \ f((i+1)\Delta t, k\Delta t) \dots]^T \quad (4.11)$$

the finite difference scheme (4.10) is said to be convergent of order n if:

$$\| \underline{x}_{t_k} - \underline{x}(k) \| \leq c_9 (\Delta x)^n \quad (4.12)$$

where c_9 is a constant. If a scheme is convergent the solution of the difference equations converges for $\Delta x \rightarrow 0$ and thereby $\Delta t \rightarrow 0$ to the solution of the original differential equation.

The finite difference scheme (4.10) is said to be stable if there exists a $c_{10} > 0$ such that:

$$\| \Phi^k \| \leq c_{10}, \quad k = 1, 2, \dots, T/\Delta t, \text{ for all } \Delta t \quad (4.13)$$

where c_{10} is a constant. Stability implies that numerical errors in f_i^k are bounded if $\Delta x \rightarrow 0$ and thereby $\Delta t \rightarrow 0$, with T constant. Note that stability is a property of the finite difference scheme and is not related to the original differential equations.

Direct proofs of convergence are often hard to give. However, for a consistent finite difference approximation to a linear problem, stability is a necessary and sufficient condition for convergence (Lax's equivalence theorem).

Another important aspect of the behaviour of finite difference schemes is O'Brien-Hyman-Kaplan stability, as treated by Van der Houwen (1968). The finite difference scheme (4.10) is said to be O'B-H-K stable if:

$$\| \Phi^k \| \leq c_{11}, \text{ for all } k \quad (4.14)$$

* Not all approximation problems can be written in this form. However, as pointed out in Section 4.6, this is not a real limitation for the problems dealt with in this study.

where c_{11} is a constant. O'B-H-K stability implies that the numerical errors in f_i^k are bounded if $T \rightarrow \infty$ with Δx and Δt constant. Note that for the same problem O'B-H-K stability is equivalent with the stability of a filter as defined in Subsection 3.2.2.

From a practical point of view it is convenient that a finite differential scheme is stable in the sense of both stability definitions described in this section (Stelling 1983).

4.3 Discretisation of the one-dimensional shallow water equations

The linear one-dimensional equations used throughout this chapter are (see Chapter 2):

$$\frac{\partial \underline{f}}{\partial t} + C_1 \frac{\partial \underline{f}}{\partial x} + C_2 \underline{f} = 0 \quad (4.15)$$

where:

$$\underline{f} = [u \quad h]^T$$

$$C_1 = \begin{bmatrix} 0 & g \\ D & 0 \end{bmatrix}$$

$$C_2 = \begin{bmatrix} \lambda & 0 \\ 0 & 0 \end{bmatrix}$$

Here we recall that:

h = water-level

u = water velocity

D = depth of the water

g = acceleration of gravity

λ = linear bottom friction coefficient ($\lambda = \lambda/D$)

The water movement is completely described by these equations, provided that initial and boundary conditions are given.

To develop a discrete system representation for the description of the water movement, the equation (4.15) is discretised. Defining a grid (see figure 4.1), we consider two different finite difference schemes to accomplish this task. Firstly, we employ the implicit four-point Preissmann scheme (Liggett and Cunge 1975):

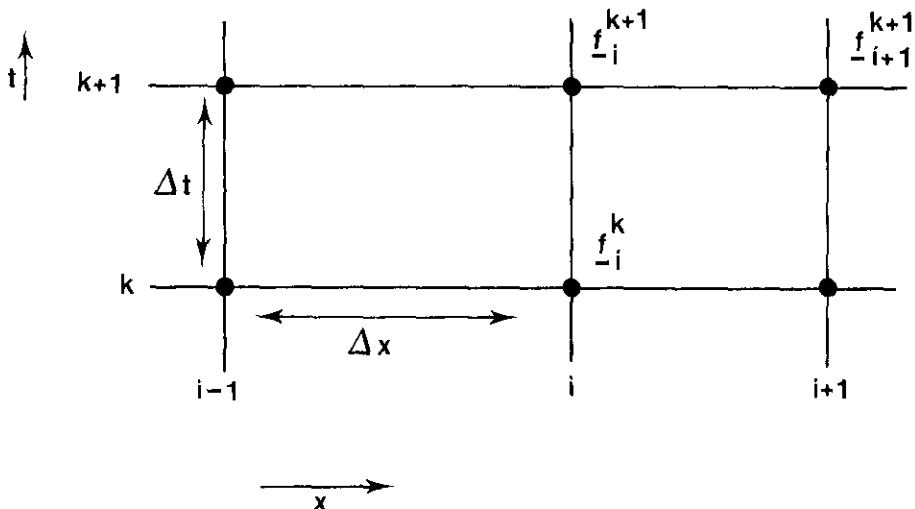


Figure 4.1: The grid.

$$\frac{1}{\Delta t} (f_{i+\frac{1}{2}}^{k+1} - f_{i+\frac{1}{2}}^k) + \frac{1}{\Delta x} C_1 (f_{i+1}^{k+\theta} - f_i^{k+\theta}) + C_2 f_{i+\frac{1}{2}}^{k+\frac{\theta}{2}} = 0 \quad (4.16)$$

where f_i^k is the approximation of $f(i \Delta x, k \Delta t)$ and

$$f_{i+\frac{1}{2}}^k = \gamma_2 (f_{i+1}^k + f_i^k)$$

$$f_i^{k+\theta} = \theta f_i^{k+1} + (1-\theta) f_i^k$$

and θ is a weighting factor. For the special case $\lambda=0$ it is easy to show that the finite difference scheme (4.16) is a consistent approximation of second-order of the partial-differential equation:

$$\frac{\partial f}{\partial t} + C_1 \frac{\partial f}{\partial x} - (\theta-0.5) \Delta t C_1^2 \frac{\partial^2 f}{\partial x^2} = 0 \quad (4.17)$$

Comparing equation (4.17) with (4.15) we see that only for $\theta = 0.5$ the original equation (4.15) is solved with second-order accuracy. By choosing $0.5 < \theta \leq 1.0$ one introduces numerical diffusion.

The second finite difference scheme that is considered is the well-known explicit Lax-Wendroff scheme (Richtmyer and Morton 1967):

$$\begin{aligned} \underline{f}_i^k &= \underline{f}_i^k - \frac{\Delta t}{2\Delta x} C_1 (\underline{f}_{i+1}^k - \underline{f}_{i-1}^k) + \gamma_2 \left(\frac{\Delta t}{\Delta x} C_1 \right)^2 (\underline{f}_{i+1}^k - 2\underline{f}_i^k + \underline{f}_{i-1}^k) \\ &\quad - \gamma_2 \Delta t C_2 (\underline{f}_{i-1}^k + \underline{f}_{i+1}^k) \end{aligned} \quad (4.18)$$

The scheme is of second-order accuracy.

To analyse the stability and to gain insight into the dissipative properties of the schemes for initial value problems, a Von Neumann stability analysis can be employed. Consider the behaviour of the Fourier integral:

$$\underline{f}_i^k = \int_{-1/2\Delta x}^{1/2\Delta x} \xi^k(l) e^{j2\pi l i \Delta x} dl \quad (4.19)$$

under the operation given by equation (4.16). Here j is the imaginary unit, l is the wave number and $1/2\Delta x$ is the highest wave number that can be resolved. Substituting the Fourier integral (4.19) into the Preissmann scheme (4.16) yields:

$$A(l) \xi^{k+1}(l) = B(l) \xi^k(l) \quad (4.20)$$

where:

$$A(l) = I + \gamma_2 \Delta t C_2 + 2j \frac{\Delta t}{\Delta x} \theta \tan(\pi l \Delta x) C_1$$

$$B(l) = I - \gamma_2 \Delta t C_2 - 2j \frac{\Delta t}{\Delta x} (1-\theta) \tan(\pi l \Delta x) C_1$$

Equation (4.20) can be rewritten as:

$$\xi^{k+1}(l) = G(l) \xi^k(l) \quad (4.21)$$

where $G(l) = A(l)^{-1}B(l)$ is the amplification matrix of the finite difference scheme. This matrix amplifies the value of $\xi^k(l)$ over a time step Δt . The eigenvalues of $G(l)$ can be shown to be:

$$g_{1,2}(l) = \frac{1 - v^2 \theta (1-\theta) \pm \sqrt{v^2 - \frac{1}{4}\Delta t^2 \lambda^2 + \frac{1}{2}\Delta t \lambda v^2 ((1-\theta)^2 - \theta^2)}}{1 + v^2 \theta^2 + \frac{1}{2}\Delta t \bar{\lambda}} j \quad (4.22)$$

where:

$$v = \sqrt{gD} \frac{\Delta t}{\Delta x} \tan(\pi l \Delta x) = Cr \tan(\pi l \Delta x) \quad (4.23)$$

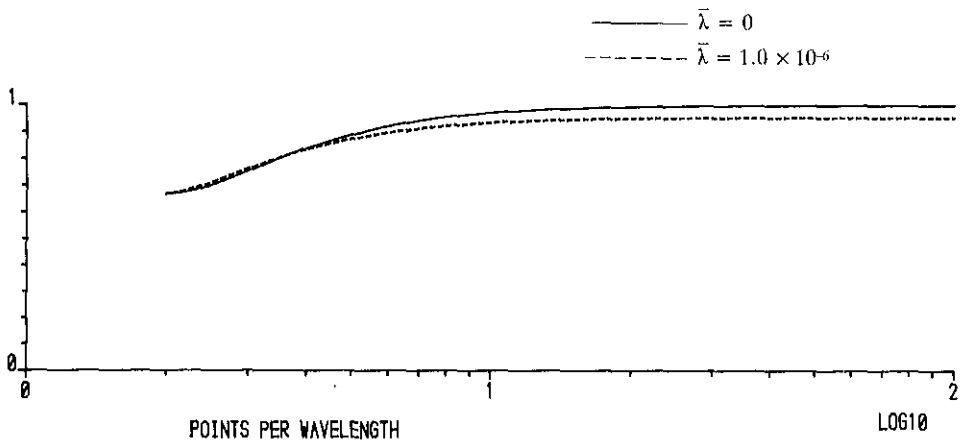


Figure 4.2: The modulus of the eigenvalues of the amplification matrix using the Preissmann scheme

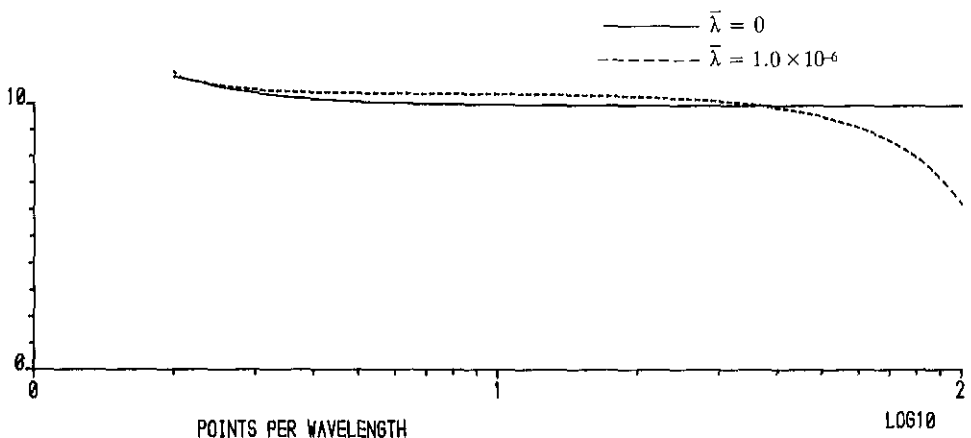


Figure 4.3: The celerity of the numerically computed wave using the Preissmann scheme.

with C_r as the Courant number. In figures 4.2 and 4.3 respectively the modulus of the eigenvalues of the amplification matrix and the celerity of the numerically computed wave C_c given by* :

$$C_c(l) = -\frac{1}{2\pi l \Delta t} \arctan [\operatorname{Im}(g_{1,2}(l)) / \operatorname{Re}(g_{1,2}(l))] \quad (4.24)$$

* The derivation of the expression for the celerity can be found in Abbott (1979).

are shown for some values of $\bar{\lambda}$ in case $Cr = 0.75$. Here, following Leendertse (1967), we introduce the number of grid points per wave length $N = 1/l\Delta x$ as the independent variable. Furthermore we note that if:

$$v^2 - \frac{1}{4} \Delta t^2 \bar{\lambda}^2 + \frac{1}{2} \Delta t \bar{\lambda} v^2 ((1-\theta)^2 - \theta^2) > 0 \quad (4.25)$$

or approximately if the wave length $1/l$ satisfies:

$$1/l < 2\pi\sqrt{gD/\bar{\lambda}} \quad (4.26)$$

the eigenvalues $g_{1,2}(l)$ have imaginary parts and

$$|g_1(l)| = |g_2(l)| \quad (4.27)$$

However, for very long waves the eigenvalues of $G(l)$ are real and positive with different moduli and therefore these waves do not advance. This is a physical effect and is not caused by the finite difference approximation. For the very short waves a similar behaviour can be noticed. However, this effect is introduced by the discretisation.

The Von Neumann necessary condition for stability results from the fact that the matrix:

$$G(l)^k, k = 1, 2, \dots, T/\Delta t \quad (4.28)$$

has to be uniformly bounded. Hence, we have the necessary condition:

$$g_a(l) \leq 1 \quad (4.29)$$

where:

$$g_a(l) = \max_m \{|g_m(l)|\} \quad (4.30)$$

is the amplification factor of the finite difference scheme. If the eigenvalues of $G(l)$ satisfy:

$$|g_m(l)| < 1 \quad (4.31)$$

with the possible exception of one, the condition (4.29) is sufficient as well as necessary for stability. For the Preissmann scheme we have in case $\bar{\lambda} = 0$ and $0 \leq \theta < 0.5$ that $g_a(l) > 1$ for some l and consequently the scheme is unstable. In case

* This condition has to be generalized in case $\xi^k(l)$ is amplified by physical influences.

$0.5 < \theta \leq 1$ the amplification factor $g_a(l) < 1$ and the scheme is unconditionally stable.

Analogously the amplification matrix of the Lax-Wendroff scheme is given by:

$$G(l) = I - j \frac{\Delta t}{\Delta x} C_1 \sin(2\pi l \Delta x)$$

$$- \left(\frac{\Delta t}{\Delta x} C_1 \right)^2 (1 - \cos(2\pi l \Delta x)) - \Delta t C_2 \cos(2\pi l \Delta x) \quad (4.32)$$

yielding a sufficient condition for stability:

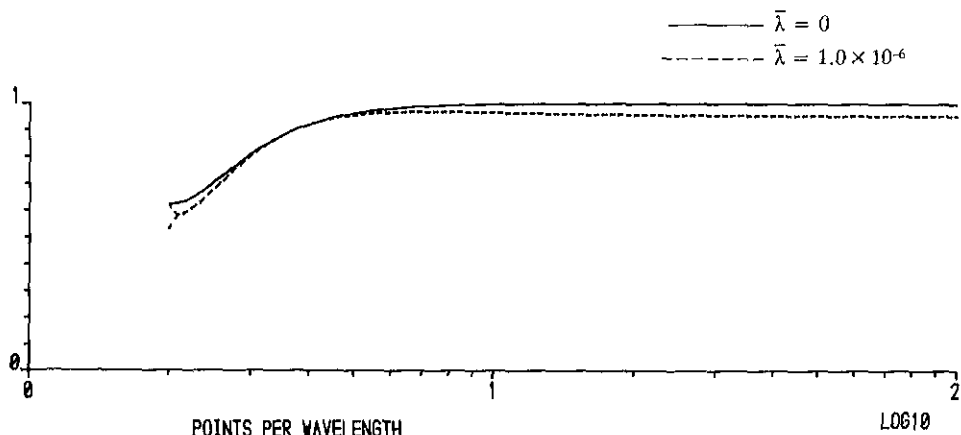


Figure 4.4: The modulus of the eigenvalues of the amplification matrix using the Lax-Wendroff scheme.

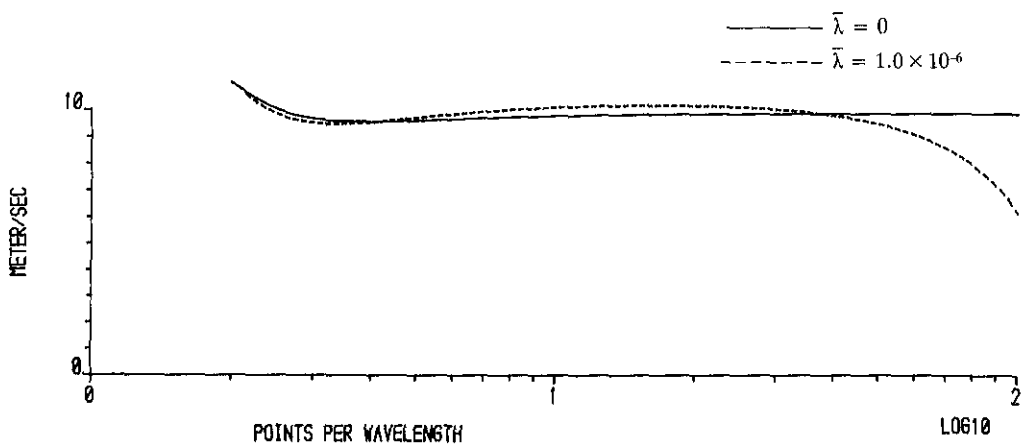


Figure 4.5: The celerity of the numerically computed wave using the Lax-Wendroff scheme.

$$\sqrt{\gamma_2 \lambda \Delta t} < Cr < \sqrt{1 + \gamma_2 \lambda \Delta t} \quad (4.33)$$

In figure 4.4 the modulus of the eigenvalues of the amplification matrix for the Lax-Wendroff scheme are shown for some values of λ in case $Cr = 0.75$. The celerity of the computed wave can be found in figure 4.5.

4.4 On the choice of the system noise

The tidal movement is not perfectly described by the finite difference equations. Therefore, we embed these equations into a stochastic environment by adding system noise. For the Preissmann scheme we obtain:

$$\frac{1}{\Delta t} (F_{i+\frac{1}{2}}^{k+1} - F_{i-\frac{1}{2}}^{k+1}) + \frac{1}{\Delta x} C_1 (F_{i+1}^{k+\theta} - F_i^{k+\theta}) + C_2 F_{i+\frac{1}{2}}^{k+\frac{1}{2}} + \underline{W}_i^k = 0 \quad (4.34)$$

where:

$$\underline{W}_i^k = [W_m_i^k \ W_c_i^k]^T$$

is the system noise. $W_m_i^k$ and $W_c_i^k$ are the noise processes associated with the uncertainty of respectively the momentum equation and the continuity equation. The covariance of \underline{W}_i^k is chosen to be:

$$E \left\{ \underline{W}_{i_1}^{k_1} \underline{W}_{i_2}^{k_2} \right\} = Q_{i_1, i_2}(k_1), \quad k_1 = k_2$$

$$0 \quad , \quad k_1 \neq k_2$$

F_i^k is the stochastic generalization of the deterministic process f_i^k . By introducing the system noise as just described, we associate this random process with the discretised momentum and continuity equations. However, when employing an implicit scheme it is also possible to introduce the system noise process after the finite difference equations have been solved and F_i^{k+1} is known explicitly. In this case the system noise process is associated with the uncertainty of the computed water-levels and velocities. From the physical point of view we prefer the first possibility since the errors concerned with the continuity equation are usually very small and assumed to be zero*. This assumption also guarantees that if the finite difference scheme conserves mass, the filter conserves mass too. A perfect con-

* Unfortunately, in some cases this approach introduces numerical difficulties (see Section 4.5).

tinuity equation can only be modelled by associating the system noise with the uncertainty of the equations and not with the uncertainty of the components of the state vector. Note that for most explicit schemes this discussion is not relevant.

For the Lax-Wendroff scheme we introduce the system noise as follows:

$$\begin{aligned} \underline{E}_i^{k+1} = & \underline{E}_i^k - \frac{\Delta t}{2\Delta x} C_1 (\underline{E}_{i+1}^k - \underline{E}_{i-1}^k) + \gamma_2 \left(\frac{\Delta t}{\Delta x} C_1 \right)^2 (\underline{E}_{i+1}^k - 2\underline{E}_i^k + \underline{E}_{i-1}^k) \\ & - \gamma_2 \Delta t C_2 (\underline{F}_{i-1}^k + \underline{F}_{i+1}^k) + \Delta t \underline{W}_i^k \end{aligned} \quad (4.35)$$

The system noise represents the errors of the corresponding deterministic model. It includes the variability in the natural system, e.g. due to turbulent effects and model structure errors such as neglected non-linearities or wrong parameter values, as well as errors caused by the discretisation of the partial-differential equations. Unfortunately, in practice very little is known about the statistics of the system noise. In some cases (Jazwinski 1970) it is possible to use a systematic approach to determine the covariance $Q_{i_1, i_2}(k)$. However, usually it has to be established by means of "trial and error", i.e. the filter is employed for various values of $Q_{i_1, i_2}(k)$, until one gets satisfactory filter performance. In fact, the determination of the covariance matrix of the system noise is the calibration of the filter.

In choosing a suitable value for $Q_{i_1, i_1}(k)$, it has to be taken into account that finite difference schemes are not able to accurately represent short waves, i.e. waves with a wavelength of the order of $2\Delta x$. Therefore, in order to obtain meaningful solutions when solving the time propagation of the covariance of the estimation error, the energy of these short noise waves should be limited.

Assuming the system noise is location invariant it can be described by the spatial covariance functions:

$$E \{ Wm_{i_1}^k \ Wm_{i_2}^k \} = Q_m(|i_1 - i_2|, k) \quad (4.36)$$

$$E \{ Wc_{i_1}^k \ Wc_{i_2}^k \} = Q_c(|i_1 - i_2|, k) \quad (4.37)$$

where Wm_i^k and Wc_i^k are supposed to be mutually independent. Neglecting boundary effects the distribution of the system noise as function of the wave number i is given by:

$$Sm(l, k) = \Delta x \sum_{i=-\infty}^{\infty} Q_m(|i|, k) e^{-j2\pi li\Delta x} \quad (4.38)$$

$$Sc(l, k) = \Delta x \sum_{i=-\infty}^{\infty} Q_c(|i|, k) e^{-j2\pi li\Delta x} \quad (4.39)$$

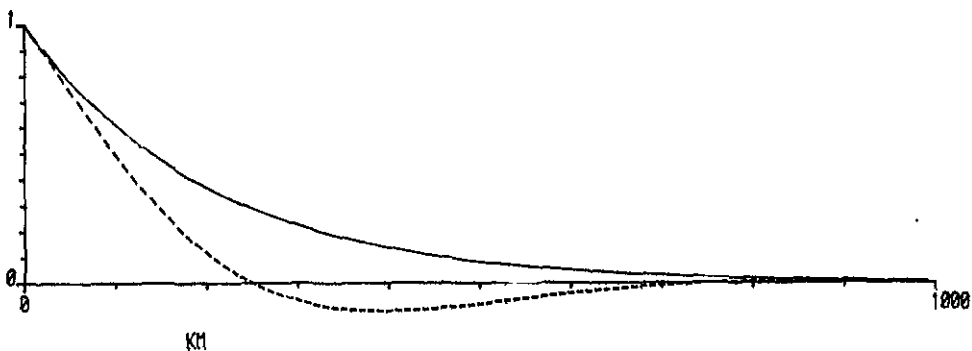


Figure 4.6: Some spatial covariances.

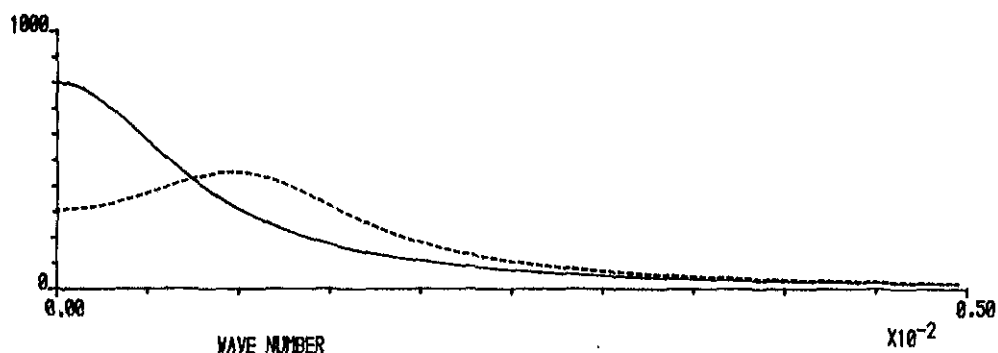


Figure 4.7: Spectra of the covariances shown in figure 4.6.

Some spatial covariance functions and their spectra are given in figure 4.6 and 4.7 respectively. Here $\Delta x = 100$ km and consequently the highest wave number that can be resolved is 0.005 km^{-1} .

As noted before, the energy of the short waves has to be limited. However, this energy is not allowed to be too small to avoid that the filtering problem is ill-conditioned and that numerical difficulties are likely to occur. A detailed discussion on this subject can be found in Section 4.8. Finally, we note that in practice the time-varying behaviour of the statistics of the noise processes is poorly known. Therefore, these processes are usually assumed to be stationary.

4.5 Kalman filtering in the wave number domain

As described in Section 4.2, a finite difference scheme can be transformed into the wave number domain by deriving the amplification matrix $G(l)$ of the scheme.

Although this procedure can only be employed for linear equations and does not include the influence of the boundary conditions, it increases the insight into the properties of a finite difference scheme. In some special cases, this approach can be generalized to study the properties of the Kalman filter.

Suppose the propagation in time of the process \underline{F}_i^k is described by equation (4.34) or (4.35), where the noise processes Wm_i^k and Wc_i^k are supposed to be location invariant, stationary and mutually independent (see Section 4.4). Observations of the water-level are assumed to be available in all the grid points:

$$Z_i^k = [0 \quad 1] \underline{F}_i^k + V_i^k \quad (4.40)$$

where V_i^k is the measurement noise with covariance:

$$\begin{aligned} E\{V_{i_1}^{k_1} V_{i_2}^{k_2}\} &= r^2, k_1 = k_2, i_1 = i_2 \\ &0, k_1 \neq k_2 \\ &0, i_1 \neq i_2 \end{aligned}$$

Analogously to the approach described in Section 4.3 we consider the Fourier integrals:

$$\underline{F}_i^k = \int_{-1/2\Delta x}^{1/2\Delta x} F^k(l) e^{j2\pi li\Delta x} dl \quad (4.41)$$

$$Wm_i^k = \int_{-1/2\Delta x}^{1/2\Delta x} Wm^k(l) e^{j2\pi li\Delta x} dl \quad (4.42)$$

$$Wc_i^k = \int_{-1/2\Delta x}^{1/2\Delta x} Wc^k(l) e^{j2\pi li\Delta x} dl \quad (4.43)$$

$$Z_i^k = \int_{-1/2\Delta x}^{1/2\Delta x} Z^k(l) e^{j2\pi li\Delta x} dl \quad (4.44)$$

$$V_i^k = \int_{-1/2\Delta x}^{1/2\Delta x} V^k(l) e^{j2\pi li\Delta x} dl \quad (4.45)$$

where l is the wave number. Substituting these integrals into equation (4.34) or (4.35) and into equation (4.40) yields:

$$\underline{F}^{k+1}(l) = G(l) \underline{F}^k(l) + A(l)^{-1} \begin{bmatrix} W_m^k(l) \\ W_c^k(l) \end{bmatrix} \quad (4.46)$$

$$Z^k(l) = [0 \ 1] \underline{F}^k(l) + V^k(l) \quad (4.47)$$

where $G(l)$ is the amplification matrix of the finite difference scheme and, for the Preissmann scheme, $A(l)$ is defined by equation (4.20). For the Lax-Wendroff scheme we have $A(l) = I$. The covariance of the system and measurement noise are respectively:

$$Q(l) = \begin{bmatrix} Sm(l) & 0 \\ 0 & Sc(l) \end{bmatrix} \quad (4.48)$$

$$R(l) = Sr \quad (4.49)$$

Here $Sm(l,k) = Sm(l)$ and $Sc(l,k) = Sc(l)$ are defined by respectively the equations (4.38) and (4.39).

In this section we first consider the Lax-Wendroff scheme and the Preissmann scheme in case the system noise is introduced after the implicit finite difference equations have been solved (see Section 4.4). In both cases the matrix $A(l)^{-1}$ does not appear in equation (4.46). Given the model (4.46) - (4.49) and an initial condition, the original Kalman filter equations (3.6) - (3.10) can be employed to solve the filtering problem for each wave number separately. Of course the system is controllable if $Sm(l) > 0$ and $Sc(l) > 0$. It is easy to verify from the definitions shown in Subsection 3.2.2 that also for $Sm(l) > 0$ and $G(l)$ not lower triangular the system is controllable. The system is observable if $G(l)$ is not upper triangular. If the filter is both controllable and observable, the filter is exponentially stable (see Subsection 3.2.2). Since in addition the model (4.46) - (4.49) is time-invariant, the filter equations converge to a steady-state condition in which the covariance of the estimation error and the filter gain are time-invariant (Anderson and Moore 1979).

Employing the Preissmann scheme we have for waves with a length of $2\Delta x$

$$G(1/2\Delta x) = \begin{bmatrix} -\frac{1-\theta}{\theta} & 0 \\ 0 & -\frac{1-\theta}{\theta} \end{bmatrix} \quad (4.50)$$

and as a consequence the water velocity is not observable. In this case the stability of the original system, introduced by choosing $1 \geq \theta > 0.5$ has to guarantee the stability of the filter.

Analogously, employing the Lax-Wendroff scheme we have for waves with a wave length of $2\Delta x$:

$$G(1/2\Delta x) = \begin{bmatrix} 1-2Cr^2 + \lambda\Delta t & 0 \\ 0 & 1-2Cr^2 \end{bmatrix} \quad (4.51)$$

and again the velocity component is not observable. However, in this case the sufficient condition for stability (4.33) guarantees the stability of the filter. Finally, for both the Preissmann and the Lax-Wendroff schemes, the amplification matrix for very long waves approaches:

$$G(0) = \begin{bmatrix} 1-\lambda\Delta t & 0 \\ 0 & 1 \end{bmatrix} \quad (4.52)$$

Again, the velocity component is not observable. In this case bottom friction has to guarantee the stability of the filter.

To eliminate the effect of the initial condition we study the steady-state behaviour of the filter. We define:

$$P^+(l) = \begin{bmatrix} P_u^+(l) & P_{uh}^+(l) \\ P_{uh}^+(l) & P_h^+(l) \end{bmatrix} \quad (4.53)$$

where $P_u^+(l)$ and $P_h^+(l)$ are the steady-state distributions of the estimation error of respectively the water velocity and water-level just after a measurement has been incorporated. $P_{uh}^+(l)$ is the cross spectrum between these processes. Analogously we define:

$$P^-(l) = \begin{bmatrix} P_u^-(l) & P_{uh}^-(l) \\ P_{uh}^-(l) & P_h^-(l) \end{bmatrix} \quad (4.54)$$

as the steady-state distribution of the prediction error just before a new measurement becomes available. The equations to obtain the steady-state solution can be derived easily:

$$P^-(l) = G(l) P^+(l) G(l)^T + Q(l) \quad (4.55)$$

$$P^+(l) = [I - \underline{K}(l) [0 \quad 1]] P^-(l) [I - \underline{K}(l) [0 \quad 1]]^T + \underline{K}(l) S_r \underline{K}(l)^T \quad (4.56)$$

with:

$$\underline{K}(l) = \frac{1}{P_h^-(l) + S_r} \begin{bmatrix} P_{uh}^-(l) & P_h^-(l) \end{bmatrix}^T \quad (4.57)$$

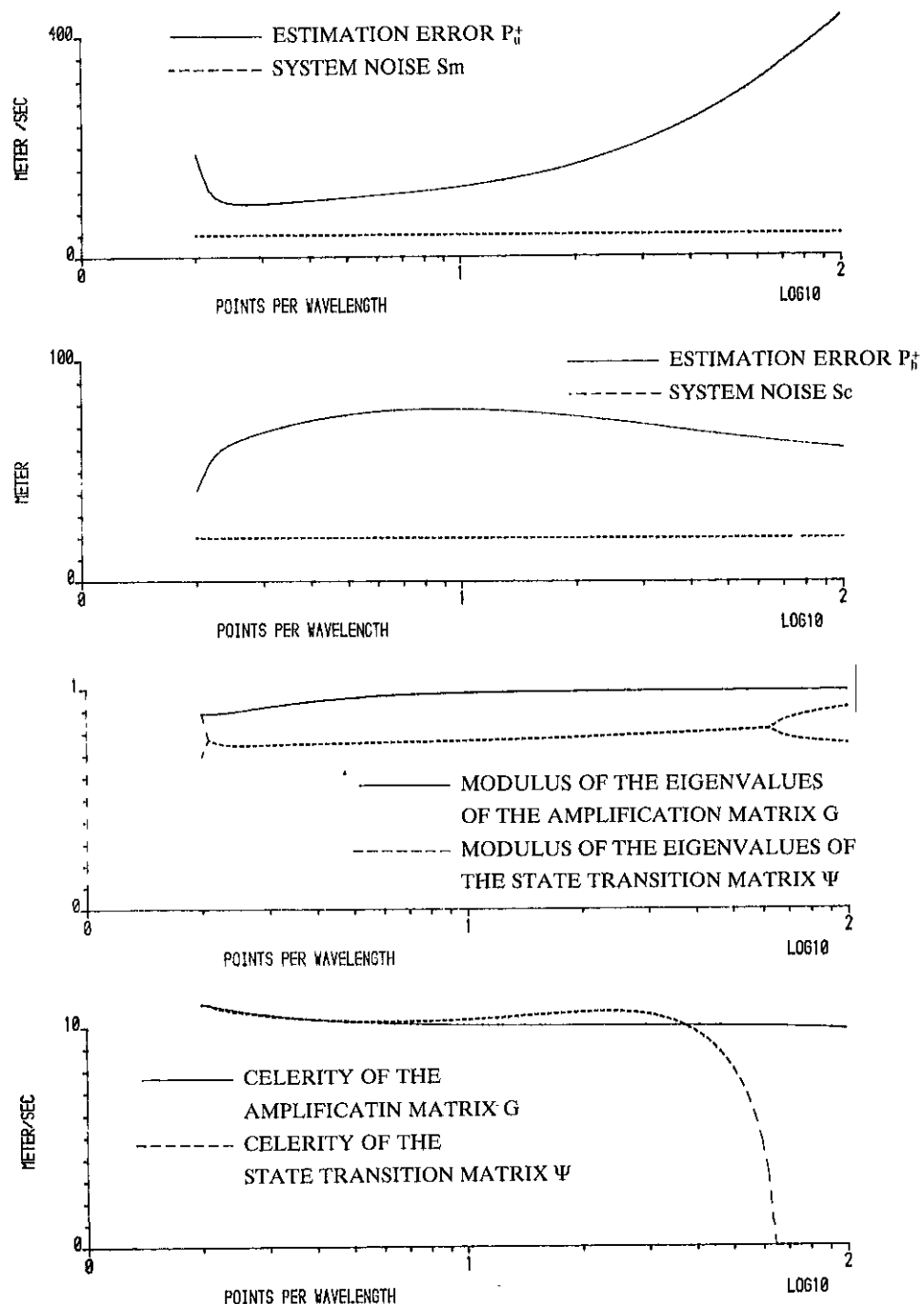


Figure 4.8: Steady-state filter performance using the Preissmann scheme with $\theta = 0.53$ and with a bottom friction coefficient $\bar{\lambda} = 0.25 \times 10^{-6}$.

The equations (4.55) - (4.57) can be easily solved for various values of the wave number l . To gain insight into the stability of the filter we compute the state transition matrix of the steady-state filter (see Subsection 3.2.2):

$$\Psi(l) = [I - \underline{K}(l) [0 \quad 1]] G(l) \quad (4.58)$$

and its eigenvalues $h_{1,2}(l)$.

In figure 4.8 the steady-state distributions $P_u^+(l)$ and $P_h^+(l)$ are shown as a function of the number of grid points per wave length $N = 1/l\Delta x$ if the Preissmann scheme is used. The system noise has been chosen to be uncorrelated in space, yielding $Sm(l) = Sm$ and $Sc(l) = Sc$. These values are also shown in figure 4.8. The depth was chosen to be 10 meters while the effects of bottom friction ($\bar{\lambda} = 0.25 \times 10^{-6}$) and numerical viscosity ($\theta = 0.53$) were taken into account in order to obtain an exponentially stable filter. It can be seen from figure 4.8 that the uncertainty P_u^+ for the number of grid points per wave length $N = 2$ is rather large. As described above this is caused by the fact that this velocity component is not observable and P_u^+ for $N = 2$ is only bounded because of the numerical viscosity. The fact that P_h^+ for $N = 2$ is relatively small is caused by the same effect. Since the water velocity component does not affect the water-level, the appearance of the system noise Sm for $N = 2$ does not increase the uncertainty P_h^+ of this water-level component. Similar effects occur for the very long wave lengths. In this case bottom friction has to guarantee that P_u^+ for large N is bounded.

In figure 4.8 the modulus of the eigenvalues $g_{1,2}$ of the amplification matrix and $h_{1,2}$ of the state transition matrix are shown too. Studying the behaviour of $h_{1,2}$ is important regarding the stability of the filter. It can be seen from figure 4.8 that the filter is more stable than the original system. This stability improvement property of the filter has already been discussed in Subsection 3.2.2. Unfortunately, this stability improvement turns out to be the least for very short waves. In figure 4.8 we also compare the wave celerity of the wave motion described by the amplification matrix and the state transition matrix.

In figure 4.9 we increase the bottom friction coefficient ($\bar{\lambda} = 1.0 \times 10^{-6}$) and the numerical viscosity ($\theta = 0.60$). As a consequence, P_u^+ is decreased both for the long wave lengths as for the very short waves. Decreasing the uncertainty for the very short waves is essential since finite difference schemes are not able to represent short waves accurately. The existence of these short waves can cause unsatisfactory filter performance or may, in the non-linear case, introduce instabilities. By choosing in figure 4.10 a system noise which is correlated in space, P_u^+ and P_h^+ for these short waves can be further reduced to an acceptable level (see Section 4.4).

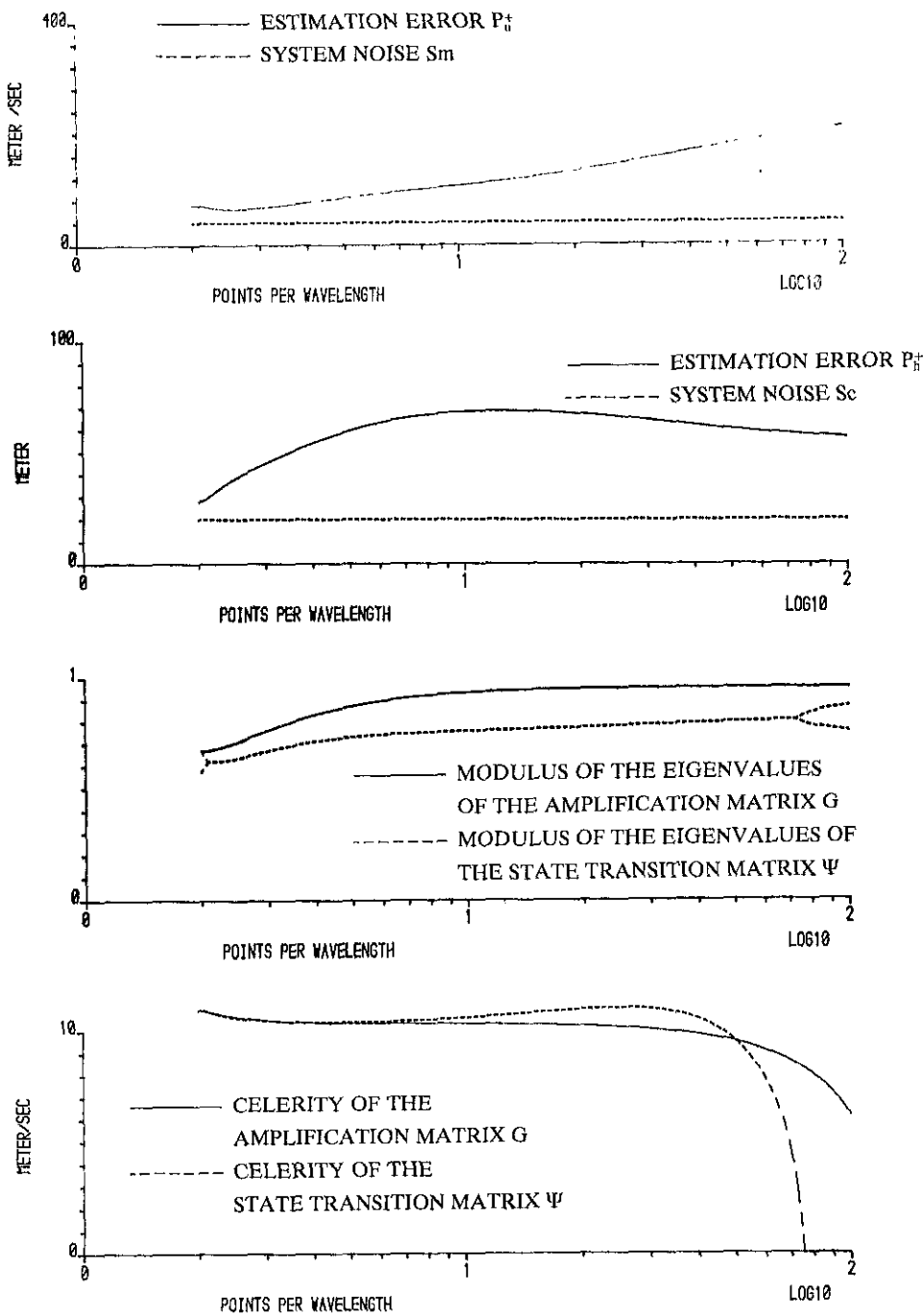


Figure 4.9: Steady-state filter performance using the Preissmann scheme with $\theta = 0.60$ and with a bottom friction coefficient $\bar{\lambda} = 1.0 \times 10^{-6}$.

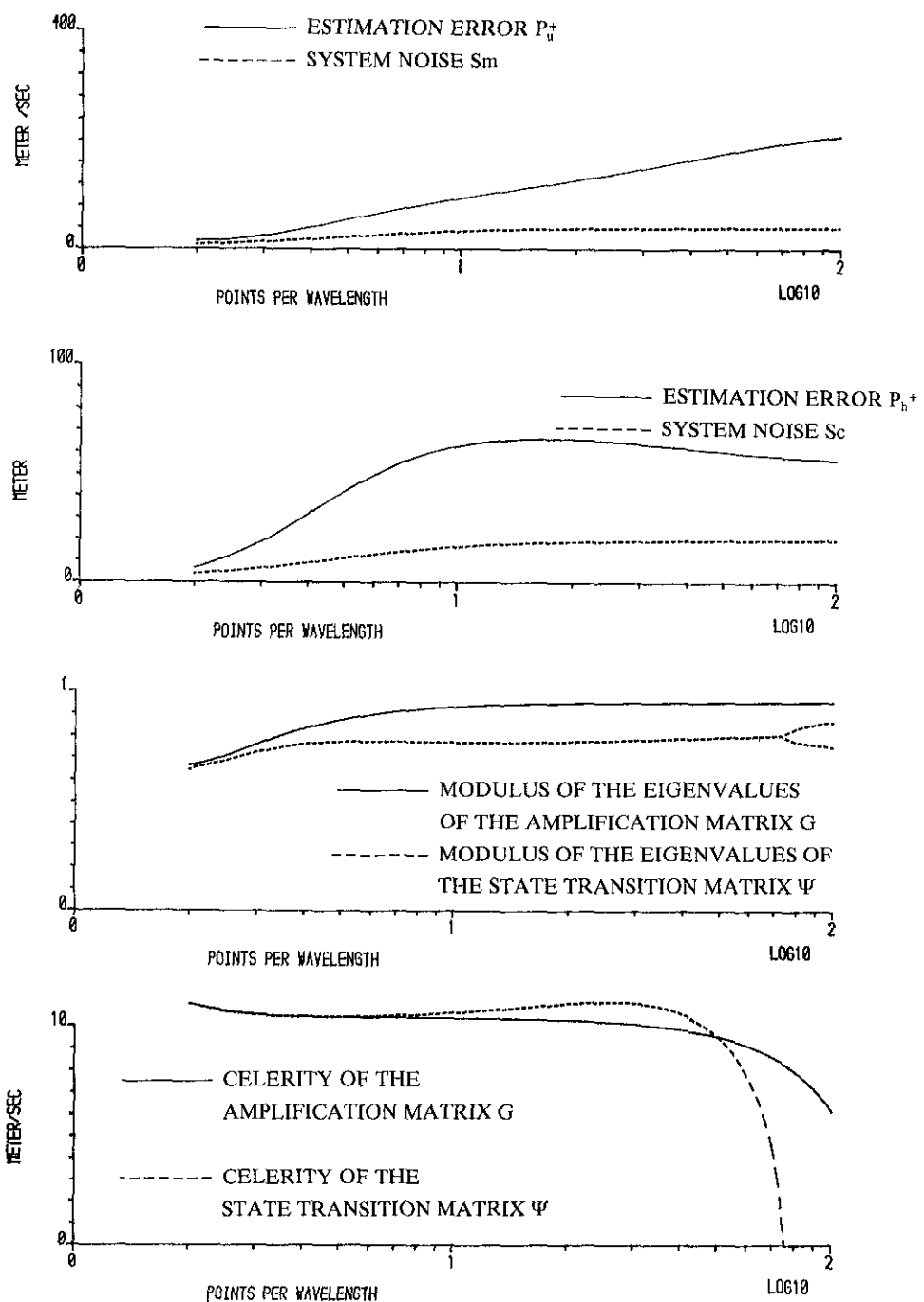


Figure 4.10: Steady-state filter performance using the Preissmann scheme with $\theta = 0.60$, bottom friction coefficient $\bar{\lambda} = 1.0 \times 10^{-6}$ and spatially correlated system noise.

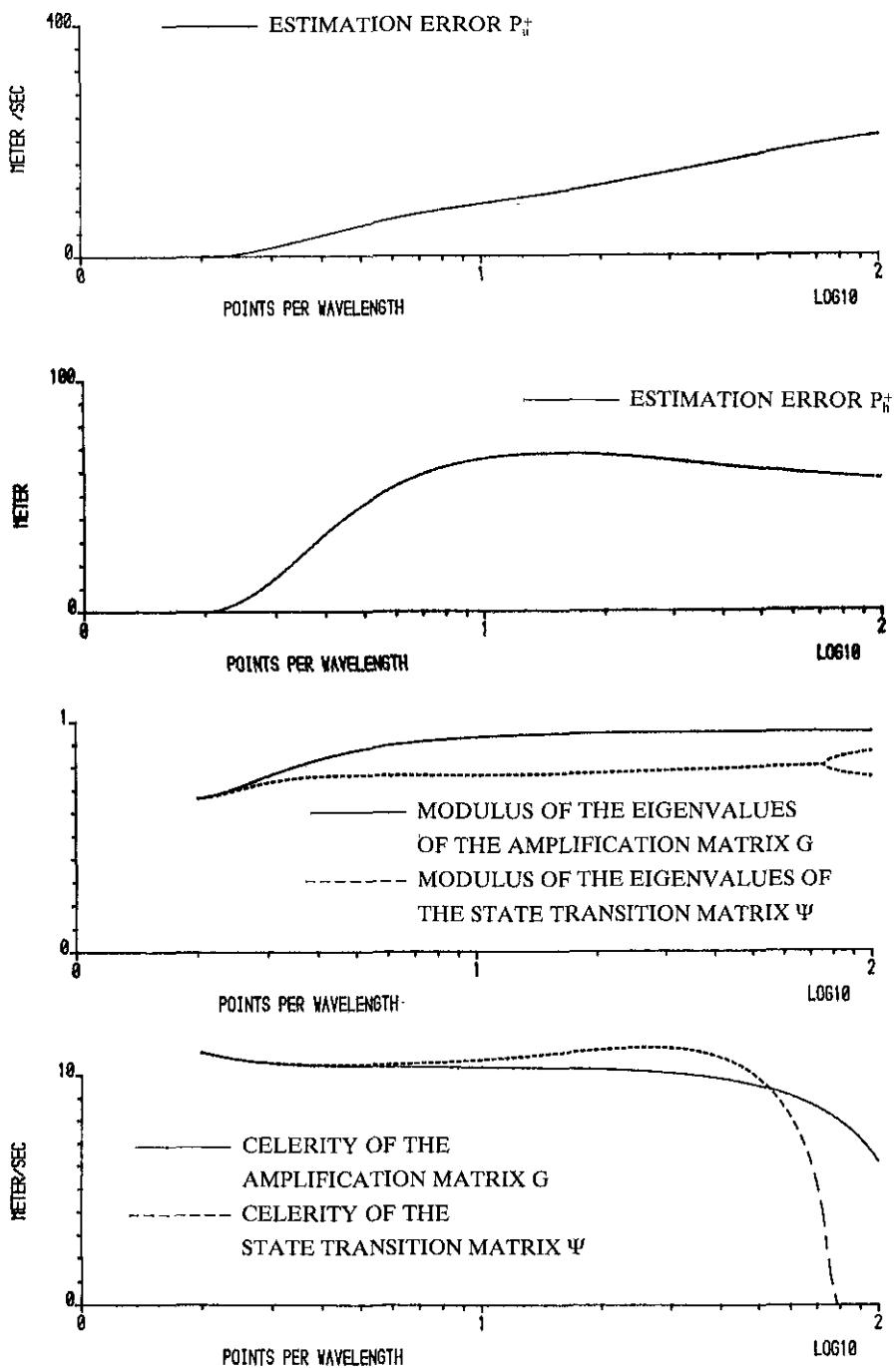


Figure 4.11: Steady-state filter performance using the Preissmann scheme with $\theta = 0.60$, bottom friction coefficient $\lambda = 1.0 \times 10^{-6}$ and system noise introduced implicitly.

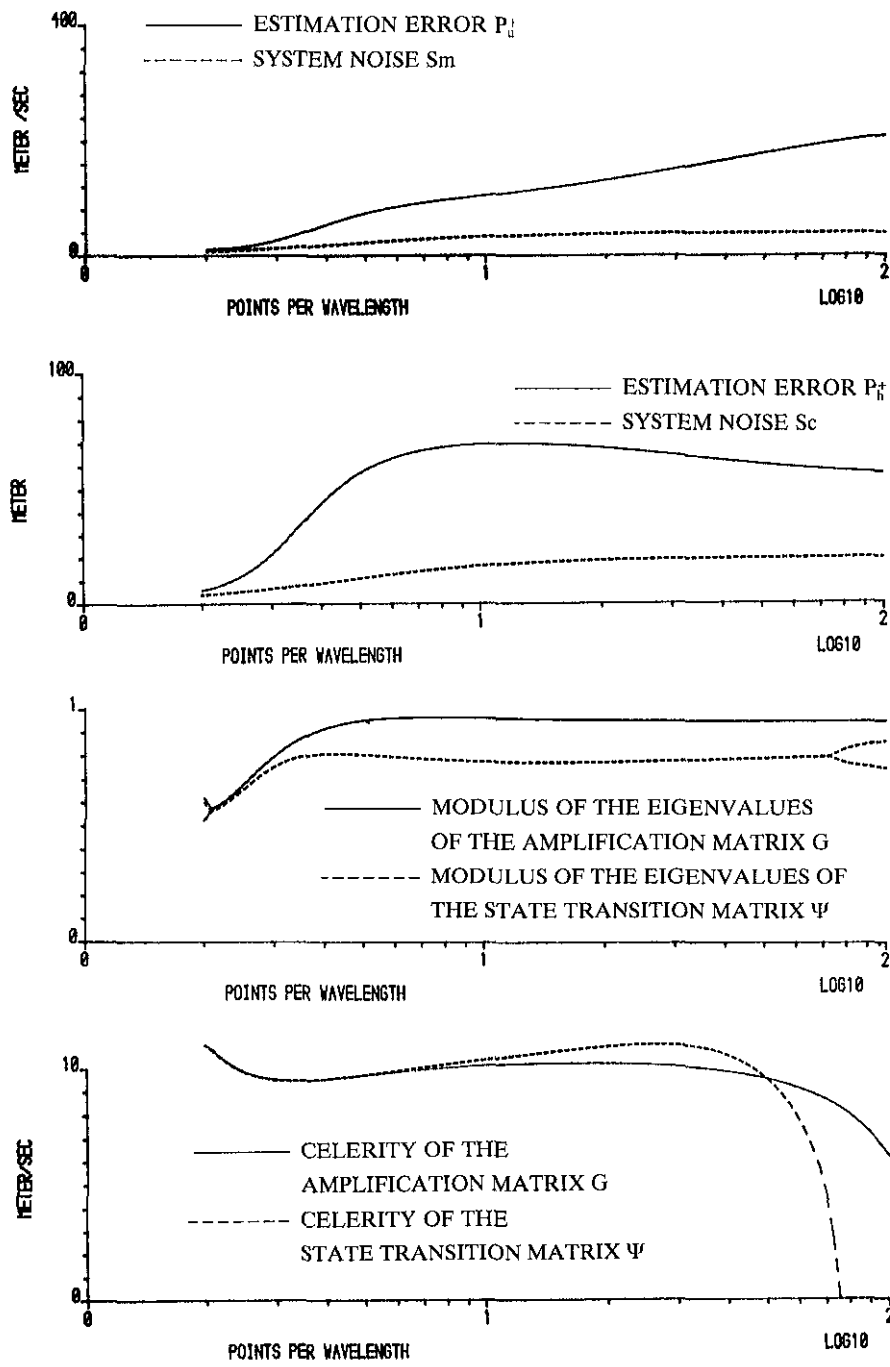


Figure 4.12: Steady-state filter performance using the Lax-Wendroff scheme with bottom friction coefficient $\lambda = 1.0 \times 10^{-6}$.

In figure 4.11 we consider the Preissmann scheme in which the system noise is introduced implicitly as described by equation (4.46) and not, as in the case of figures 4.8 - 4.10, after the implicit finite difference equations have been solved. The system noise has been chosen to be uncorrelated in space. As can be seen from figure 4.11, P_u^+ and P_h^+ behave in a similar way as in figure 4.10 and in this case, it is not necessary to assume that the system noise is spatially correlated. However, the filter is not controllable for the very short waves. Despite the fact that Q is positive definite, all the elements of A^{-1} and consequently of the noise covariance $A^{-1}QA^{-1}$ are zero for the short waves. Therefore, also the eigenvalues of P^+ for these waves become zero. In practical situations this may easily cause numerical difficulties. This aspect of Kalman filtering is discussed in detail in Section 4.8.

Finally, figure 4.12 demonstrates that similar results as in the case of figure 4.10 can be obtained by using the Lax-Wendroff scheme.

In applying the filter to the system (4.46)-(4.49) the bottom friction coefficient as well as the noise statistics must be specified. However, these parameters are not known exactly. That is, the system model used in constructing the filter differs from the real system that generates the observations. It is clear that an inexact filter model degrades the performance of the filter. For the special case described in this subsection, we study this effect quantitatively. Suppose that the real system is described by:

$$\underline{F}^{k+1}(l) = G_r(l) \underline{F}^k(l) + A_r(l)^{-1} \begin{bmatrix} Wm^k(l) \\ Wc^k(l) \end{bmatrix} \quad (4.59)$$

$$Z^k(l) = [0 \quad 1] \underline{F}^k(l) + V^k(l) \quad (4.60)$$

where the covariance of the system and measurement noise are:

$$Q_r(l) = \begin{bmatrix} Sm_r(l) & 0 \\ 0 & Sc_r(l) \end{bmatrix} \quad (4.61)$$

$$R_r(l) = S_r \quad (4.62)$$

A measure of filter performance is provided by the estimation error covariance. The best performance of the filter is obtained when we model the real system by the correct equations (4.59) - (4.62). Solving the filter equations results in the steady-state filter gain $K_r(l)$ and estimation error:

$$P_r^+(l) = \begin{bmatrix} P_{u_r}^+(l) & P_{uh_r}^+(l) \\ \frac{P_{uh_r}^+(l)}{P_{uh_r}^+(l)} & P_{h_r}^+(l) \end{bmatrix} \quad (4.63)$$

However, in practice, we model the system by the equations (4.46) - (4.49) that differs from the real system described by the equations (4.59) - (4.62). Solving the filter equations (4.55) - (4.57) using this erroneous model yields the steady-state filter gain $\underline{K}(l)$ and estimation error $P^+(l)$.

Now the computed covariance matrix $P^+(l)$ is not the actual estimation error since the filter model differs from the real model. Neither does this filter produce the optimal estimation error $P_r^+(l)$. The actual estimation error:

$$P_a^+(l) = \begin{bmatrix} P_{u_a}^+(l) & P_{u_h a}^+(l) \\ \overline{P_{u_h a}^+(l)} & P_{h_a}^+(l) \end{bmatrix}$$

can be obtained by solving the equations:

$$P_a^-(l) = G_r(l) P_a^+(l) G_r(l)^T + A_r(l)^{-1} Q_r(l) A_r(l)^{-1} \quad (4.64)$$

$$P_a^+(l) = [I - \underline{K}(l) [0 \quad 1]] P_a^-(l) [I - \underline{K}(l) [0 \quad 1]]^T + \\ \underline{K}(l) S_r \underline{K}(l)^T \quad (4.65)$$

Of course, $P_a^+(l)$ only exists if the filter is exponentially stable (see Subsection 3.2.2). However, this is the case in most practical applications, where the system (4.46) - (4.49) is a “reasonable” approximation of the real system (4.59) - (4.62). In fact, from the exponential stability condition it is possible to derive, for a given filter gain $\underline{K}(l)$, a set of real systems for which $P_a^+(l)$ exists.

In figures 4.13 - 4.16 the solutions of the equations (4.64) and (4.65) are shown for some cases to study the effect of erroneous noise statistics. Here we employ the Lax-Wendroff scheme and assume that the real system behaviour is described by figure 4.12. The bottom friction coefficient $\bar{\lambda}$ is again chosen to be 1.0×10^{-6} . The following situations are considered:

- (figure 4.13)

$$\begin{aligned} Sm(l) &= 0.1 Sm_r(l) \\ Sc(l) &= 0.1 Sc_r(l) \\ Sr &= Sr_r \end{aligned}$$
- (figure 4.14)

$$\begin{aligned} Sm(l) &= 10 Sm_r(l) \\ Sc(l) &= 10 Sc_r(l) \\ Sr &= Sr_r \end{aligned}$$

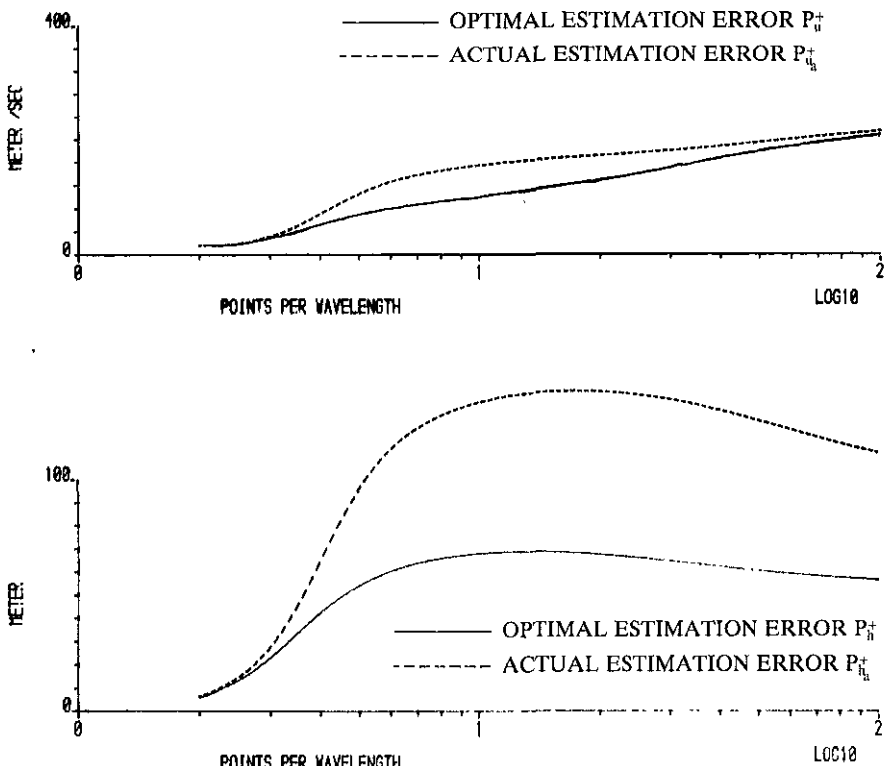


Figure 4.13: Steady-state filter performance in case of an erroneous system noise.

- (figure 4.15)

$$Sm(l) = Sm_r(l)$$

$$Sc(l) = 10 Sc_r(l)$$

$$Sr = 10 Sr_r$$

- (figure 4.16)

$$Sm(l) = 10 Sm_r(l)$$

$$Sc(l) = Sc_r(l)$$

$$Sr = 10 Sr_r$$

The main conclusions that can be drawn from these figures are:

- The effect of choosing a large incorrect system noise variance is small with respect to the large error that was introduced. This is of practical importance since the statistics of the system noise are often poorly known.

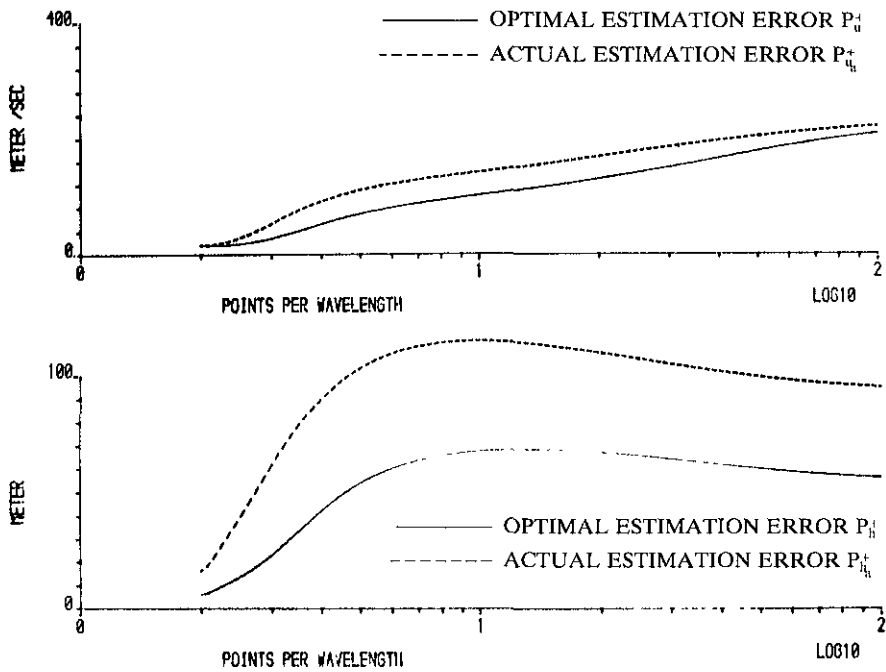


Figure 4.14: Steady-state filter performance in case of an erroneous system noise.

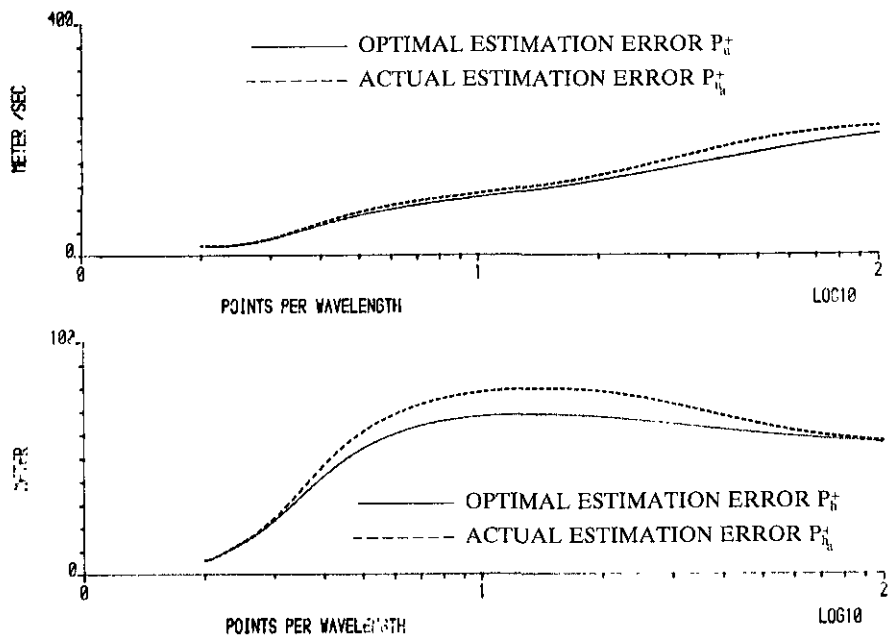


Figure 4.15: Steady-state filter performance in case of an erroneous system noise.

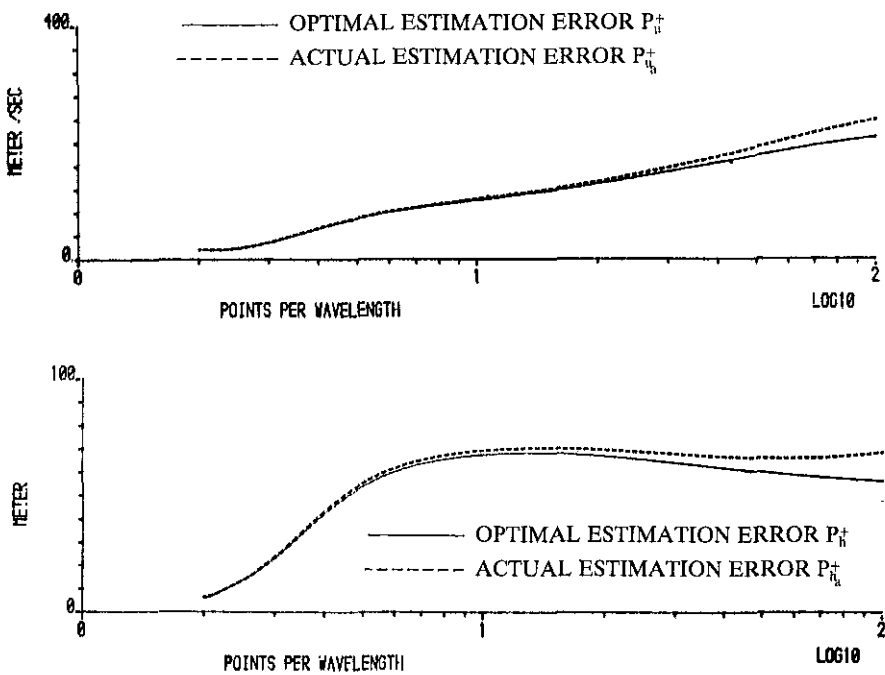


Figure 4.16: Steady-state filter performance in case of an erroneous system noise.

- Over-estimation of the system noise variance is less serious than under-estimation.
- If both the system noise and the measurement noise variance are over-estimated, the degradation of the filter performance is small. This is of practical importance since in situations when the actual system noise is very small, e.g. when the wind velocities are negligible, the measurements are in general very accurate. Here we note that if:

$$S_m(l) = c_{12} S_{m_r}(l)$$

$$S_c(l) = c_{12} S_{c_r}(l)$$

$$S_r = c_{12} S_{r_r}$$

for some $c_{12} > 0$, the filter results are still optimal. This can easily be deduced from the filter equations.

In *figure 4.17* we consider the case of choosing an erroneous bottom friction parameter:

$$\bar{\lambda} = 2\bar{\lambda}_r = 2.0 \times 10^{-6}$$

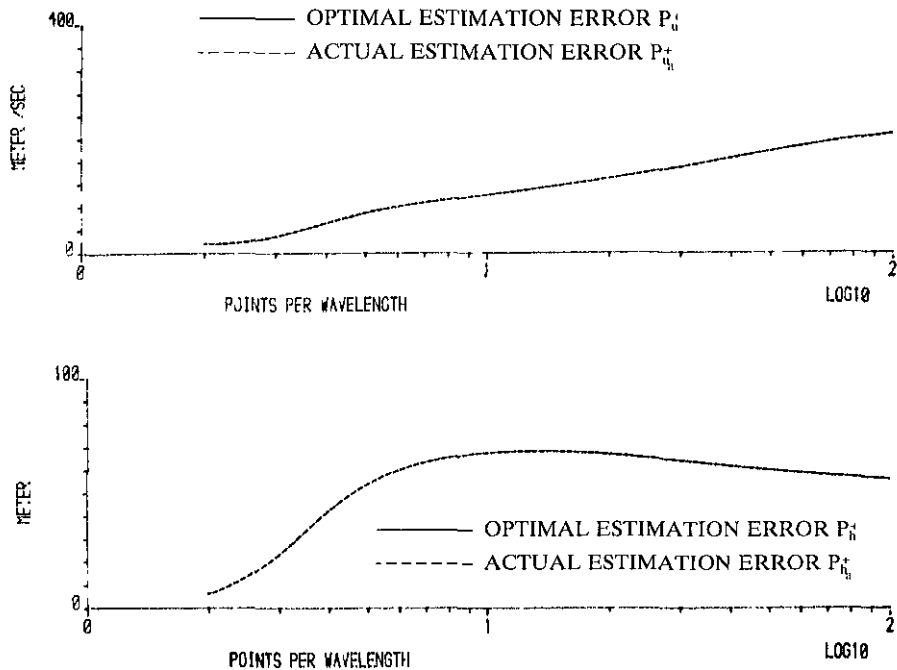


Figure 4.17: Steady-state filter performance in case of an erroneous bottom friction coefficient.

where $\bar{\lambda}_r$ is the bottom friction in the real system. The noise statistics are assumed to be perfectly known. The results of this experiment shows that the influence of an erroneous bottom friction coefficient on the filter performance is very small in comparison with the effects caused by an incorrect noise variance. This is of practical use if the friction parameter is varying in time, e.g. due to non-linearities. In this case, the optimal time-varying filter can be approximated accurately by the steady-state filter that is obtained by setting the bottom friction coefficient to its mean value. Note that this does not imply that the time-varying property of this coefficient can be neglected in the original deterministic system (4.15), but only in the equation describing the propagation of the covariance matrix. This important aspect of the Kalman filter is discussed in more detail in Chapters 5 and 6.

Finally, we study the influence of the use of a finite difference scheme that possesses first-order accuracy. The scheme that is considered is the Lax scheme (Richtmyer and Morton 1967):

$$\begin{aligned} \underline{F}_i^{k+1} = & \gamma_2 (\underline{F}_{i-1}^k + \underline{F}_{i+1}^k) - \frac{\Delta t}{2\Delta x} C_1 (\underline{F}_{i+1}^k - \underline{F}_{i-1}^k) \\ & - \gamma_2 \Delta t C_2 (\underline{F}_{i-1}^k + \underline{F}_{i+1}^k) \end{aligned} \quad (4.66)$$

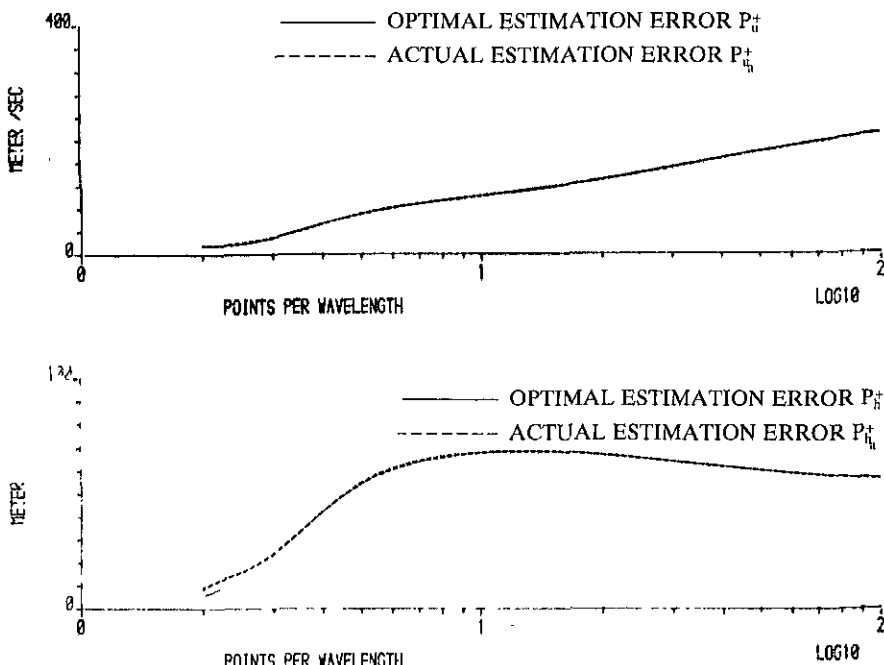


Figure 4.18: Steady-state filter performance using the first-order Lax scheme instead of the second-order Lax-Wendroff scheme.

with amplification matrix:

$$G(l) = \cos(2\pi l \Delta x) I - j \frac{\Delta t}{\Delta x} C_1 \sin(2\pi l \Delta x) - \Delta t C_2 \cos(2\pi l \Delta x) \quad (4.67)$$

Again we assume that the real system employs the Lax-Wendroff scheme with second-order accuracy and that it behaves as described in figure 4.12. Both the noise statistics as the bottom friction coefficient ($\bar{\lambda} = 1.0 \times 10^{-6}$) are assumed to be known perfectly. However, we model the system using the scheme of Lax. The results shown in figure 4.18 indicate that the influence of the second-order terms of the finite difference equations is - except for very short waves - small compared to the effect of the choice of an incorrect system noise.

In this section, the filtering problem has been solved analytically for a special case. The importance of such an exercise is that it increases the insight into the complex filtering problem. It becomes possible to study questions of observability, controllability and stability of the filter. This is especially of importance for the very short waves which, both in the deterministic model as in the Kalman filter approach, often cause numerical difficulties. Here we note that finite difference schemes cannot describe the propagation of the very short waves accurately and produce

results which mutually may differ very much. Therefore, filter performance is for these waves very sensitive with respect to the choice of finite difference scheme. The results described in this section also provide information about the effect of the noise statistics and the finite difference approximation on the distribution of the estimation error as a function of the wave length. To avoid unsatisfactory filter performance, the estimation error has to be small for the very short waves.

The idea of Kalman filtering in the wave number domain can also be employed to increase the insight into the degradation of the performance of the filter in case an erroneous filter model is used. In view of the results of the sensitivity analysis described in this section, we claim that in solving the second moment equations and computing the filter gain the poorly known noise statistics are, in general, the most important cause for a degradation of filter performance. The effects of an erroneous bottom friction coefficient and the influence of the finite difference scheme are relatively small.

Finally we note that in practical problems Kalman filtering is more complex. However, the main object of the analysis performed in this section is to expose the potential difficulties of the Kalman filter application. From the insights thus obtained one is able to compare different implementations with respect to the expected filter performance.

4.6 General discrete system representation

In Sections 4.3 - 4.5 we have discussed the filtering problem for initial value problems and have not considered boundary effects. However, in practice we have to restrict the domain of the problem. As a consequence, at the boundary of this domain additional relations must be prescribed in order to be able to solve the problem. As described in Section 4.2, a finite difference approximation to the continuous problem (4.15) including boundary conditions can be written as a discrete system:

$$\underline{A}\underline{x}_{t_{k+1}} = \underline{B}\underline{x}_{t_k} + \underline{u}_{t_{k+1}} \quad (4.68)$$

where the state vector is defined as:

$$\underline{x}_{t_k} = [\dots u_i^k \quad u_{i+1}^k \dots \dots h_{i+1}^k \dots]^T$$

Symbolically we write:

$$\underline{x}_{t_{k+1}} = \Phi \underline{x}_{t_k} + A^{-1} \underline{u}_{t_{k+1}} \quad (4.69)$$

Here, the matrices $\Phi = A^{-1}B$ and A^{-1} are neither computed or stored, they serve to represent a sequence of linear operations defined by the finite difference scheme. Introducing system noise yields (see Section 4.4):

$$\underline{X}_{t_{k+1}} = \Phi \underline{X}_{t_k} + A^{-1} \underline{u}_{t_{k+1}} + A^{-1} \underline{W}_{t_{k+1}} \quad (4.70)$$

or

$$\underline{X}_{t_{k+1}} = \Phi \underline{X}_{t_k} + A^{-1} \underline{u}_{t_{k+1}} + \underline{W}_{t_{k+1}} \quad (4.71)$$

where the covariance matrix $Q(k)$ of \underline{W}_{t_k} can be derived easily from equations (4.36) and (4.37). To model the uncertainty associated with the boundary conditions some additional assumptions have to be imposed depending on the particular physical configuration of the boundary.

Note that the discrete system (4.68) only represents two time level schemes. This restriction is imposed to ensure that \underline{X}_{t_k} is a Markov process and that the discrete Kalman filter described in Chapter 3 can be employed. Although using three time level schemes this Markov property can be restored by augmenting the state vector, this possibility is not attractive from the computational point of view and therefore omitted.

By assuming that water-levels are available in some of the gridpoints at $t = t_k$, $k = 1, 2, \dots$, the observation equation becomes:

$$\underline{Z}_{t_k} = M \underline{X}_{t_k} + \underline{V}_{t_k} \quad (4.72)$$

where \underline{Z}_{t_k} is the m-vector measurement process, \underline{V}_{t_k} is the measurement noise with covariance matrix $R(k)$ and M is a sparse n-by-m matrix, containing at each row one non-zero element. In practice, measurements are not available exactly at gridpoints. Furthermore, in general, measurements are not taken at each time t_k , but at each time lt_k , where l is an integer constant. However, the model described in this section can easily be modified to account for these facts. In practice, we may assume that the measurement errors at different locations are independent and as a consequence $R(k)$ is diagonal.

4.7 G-K-Observability

Resolving the question of the observability of a system is important in choosing measurement locations in the spatial domain and to get insight into the predictive capabilities of the Kalman filter. As was stated in Subsection 3.2.2 observability of a

filter is defined as the possibility of recovering the entire state X_{t_k} using the measurements $Z_{t_k}, Z_{t_{k+1}}, \dots, Z_{t_{k+N_2}}$, for some integer constant N_2 . Solving equation (3.27) the question of the observability of the discrete system model described by equations (4.70) and (4.72) can be answered*. However, we adopt the definition of observability of a distributed parameter system proposed by Goodson and Klein (1970) who have investigated the observability from a continuum physics viewpoint. Their definition is based on the theory of the existence and uniqueness of a solution of a partial-differential equation.

Consider the continuous equation (4.15) and assume measurements to be available for all $t > t_o$ at some locations. This system is said to be G-K-observable in the domain $\Omega_o(x, t)$ if and only if a unique solution $u(x, t), h(x, t)$ in $\Omega_o(x, t)$ is established by the measurements taken and the boundary conditions. G-K-observability may be established by the measurements alone without knowledge of the boundary conditions. It can be shown that for linear ordinary differential equations G-K-observability reduces to observability as defined by Kalman (1960) (Goodson and Klein 1970).

We prefer the concept of G-K-observability since, as is clearly demonstrated by Goodson and Klein (1970, 1971), observability definitions based on initial state recovery are not satisfactory for distributed systems. Most hyperbolic type systems are not observable in the sense of Kalman. Another reason to prefer the concept of G-K-observability is that the domain $\Omega_o(x, t)$ of the system (4.15) can be constructed easily using the characteristic lines of the system. Moreover, establishing the G-K-observability increases the insight into the predictive capabilities of the filter. Establishing controllability and G-K-observability, however, does not imply the stability of the filter. In most practical situations the exponential stability of the original system has to guarantee the exponential stability of the filter (see Subsection 3.2.2).

The concept of the G-K-observability domain $\Omega_o(x, t)$ can also be used to define a prediction horizon at time t . If $\Omega_o(x, t, t_p)$ is the G-K-observability domain using the measurements up to and including time t_p , the prediction horizon $\Gamma_o(x, t_p) \geq t_p$ is determined by:

$$t \in [t_p, \Gamma_o(x, t_p)] \rightarrow (x, t) \in \Omega_o(x, t, t_p),$$

$$(x, \Gamma_o(x, t_p) + \varepsilon) \notin \Omega_o(x, t, t_p) \text{ for all } \varepsilon > 0.$$

* For some special cases, observability can be verified by analysing the behaviour of the filter for each wave number separately (see Section 4.5).

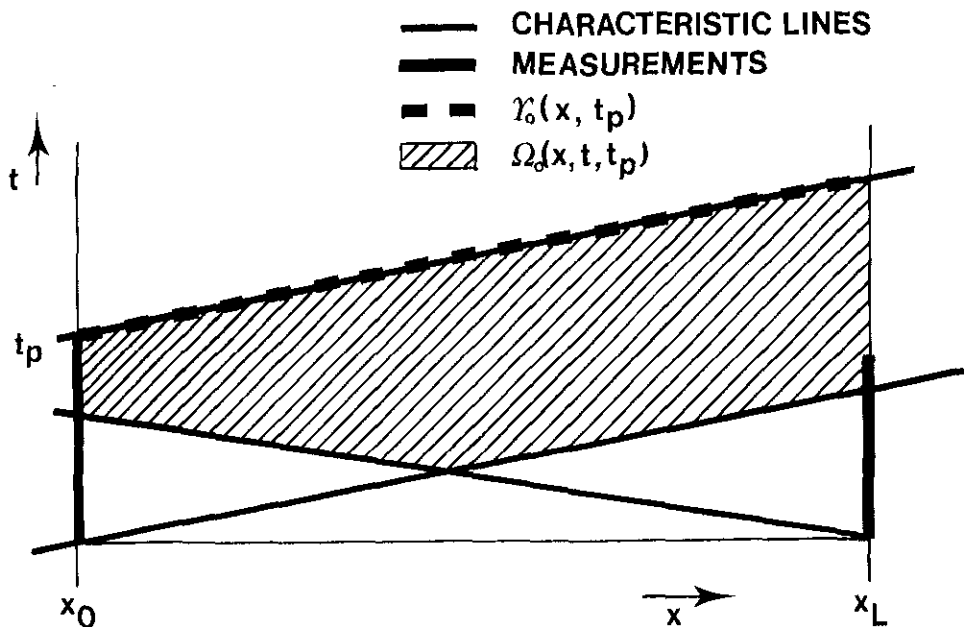


Figure 4.19: Construction of the observability domain and the prediction horizon.

The prediction horizon of the filter establishes in each point of the spatial domain the period over which predictions are uniquely determined by the measurement taken up to time t and, if known, the boundary conditions. In figure 4.19 an example of the G-K-observability domain $\Omega_o(x, t, t_p)$ and the prediction horizon $\Gamma_o(x, t_p)$ is given. Here we consider the model (4.15) without friction and prescribe at $x=x_0$ the water-level and at $x=x_L$ the condition $u=0$.

Now we consider again the system (4.15) without bottom friction and with boundary conditions as just described and we construct the set of characteristic lines that intersect the line $t = t_p$, $x \in [x_0, x_L]$. This domain can be considered as the memory of the filter (see figure 4.20). Since the water-levels and velocities outside the memory domain do not affect $u(x, t_p)$ and $h(x, t_p)$, $x \in [x_0, x_L]$, only measurements taken inside this domain may be useful to estimate $u(x, t_p)$ and $h(x, t_p)$, $x \in [x_0, x_L]$. From figure 4.20 it can be seen that only the most recent observations are used to determine these estimates.

Constructing the memory domain is important with respect to the problem of filter divergence. This problem is caused by the fact that the stochastic model that is used by the filter is never perfect. When the filter operates over a great amount of data, it may learn the state "too well". The error covariance as well as the filter gain become

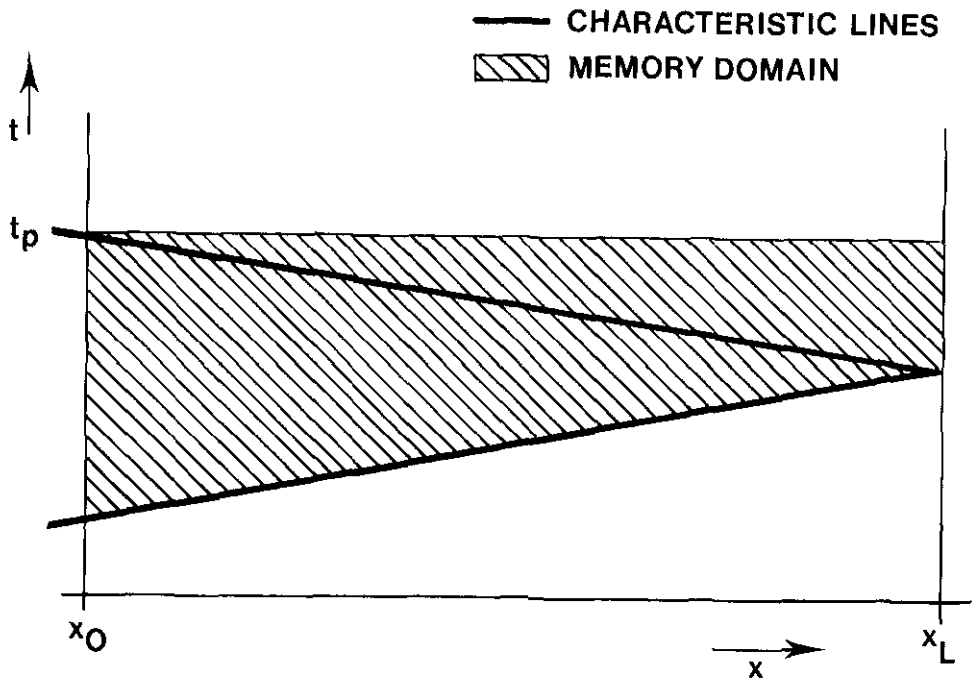


Figure 4.20: Construction of the memory domain.

very small and subsequent observations have little effect on the estimate. In essence, filter divergence is due to the fact that old observations are weighted too heavily, although when predicted over long periods of time through an erroneous model they can be valueless. Numerous ad hoc remedies to the problem of filter divergence have been developed (Jazwinski 1970). A well-known approach which has a sound theoretical basis is the limited memory filter. This filter produces estimates of the state \underline{X}_{t_k} only based on the most recent observations $\underline{Z}_{t_{k-N}}, \dots, \underline{Z}_{t_k}$. N should be chosen such that the model is an adequate approximation to the real system over the time interval $[t_{k-N}, t_k]$. By constructing the memory domain of the system (4.15) without bottom friction (see figure 4.20), it can be shown that the memory of this filter is limited in nature. Therefore, filter divergence is not likely to occur*. Furthermore, the limited memory also guarantees that the effect of the initial condition P_0 which is often poorly known, vanishes after a limited period of time. These important conclusions hold for a large class of problems of the hyperbolic type.

* Of course, filter divergence might still occur due to the numerical computation of the filter equations using finite wordlength. This problem is discussed in detail in Section 4.8.

The concept of the memory domain can also be employed to determine whether or not the application of the Kalman filter may be useful for a given prediction horizon $t_p + T$, when measurements are available up to and including the present time t_p . If the memory domain of the state $u(x, t_p + T)$, $h(x, t_p + T)$, $x \in [x_0, x_L]$, does not contain any measurement, the prediction of this state computed at time t_p is completely established by the boundary conditions. As a consequence, this filter prediction is identical with the prediction produced by the underlying deterministic model without using the measurements available. Obviously, for such a prediction interval the use of a Kalman filter is meaningless.

4.8 Numerical properties of some Kalman filter algorithms

In Section 3.2 the conventional Kalman filter algorithm to solve the discrete filtering problem is given. However, in some applications this algorithm was shown to be prone to numerical difficulties (Bierman 1977). Although it is theoretically impossible for the covariance matrix to have negative eigenvalues this can happen due to numerical computation using finite wordlength. This condition can lead to filter divergence or a total failure of the recursion. To circumvent these numerical problems alternative recursion relationships have been developed. Although algebraically equivalent to the conventional Kalman filter these algorithms exhibit improved precision at the cost however of additional computations and memory storage requirements.

The basic idea of the square root and related filters is to factorize the covariance matrix P as:

$$P = S S^T$$

where S is chosen to be triangular or:

$$P = U D U^T$$

where U is triangular and unitary, and D is diagonal. Square root and related filters have been reviewed by Maybeck (1979). Van Dooren and Verhaegen (1983) propose an implementation of the square root filters that is based on the choice of an initial state transformation that condenses the model. This preliminary transformation can be done without loss of numerical precision and may lead to substantial savings in computing time.

* Since P is positive definite these factorizations exist.

The square root filter implementations as well as the approach suggested by Van Dooren and Verheagen have shown in many applications to be numerically robust. With respect to the original algorithm square root filters are less sensitive to ill-conditionality of a problem while using these filters the covariance matrix always remains positive-semidefinite. However, they are in our case not attractive from the computational point of view. This is due to the fact that the problem described in this study is characterized by a large dimension of the state vector and by matrices A and B that are very sparse. Using a square root filter implementation the sparseness of these matrices can be exploited only in a very limited way. It can be shown that by using these algorithms the number of computations to go from time k to time k+1 is, in general, $O(n^3)$ (n is the dimension of the state vector). Employing the conventional Kalman filter algorithm the special structure of the matrices A and B can be exploited more efficiently to reduce this number to $O(n^2)$. The square root algorithm of Van Dooren and Verheagen is more efficient than the other square root implementations. However, it is still not competitive with the conventional algorithm.

Since the system equations (4.70) and (4.72) are time-invariant and we are only interested in obtaining the steady-state filter, it is possible to use a discrete form of the Chandrasekhar-type algorithm. This algorithm was first proposed by Morf, Sidhu and Kailath (1974) and makes use of the fact that for certain initial conditions the incremental covariance has rank p (p is the dimension of the system noise process) and can be factorized as follows:

$$P(k|k) - P(k-1|k-1) = S(k)L(k)S(k)^T \quad (4.73)$$

where $S(k)$ is an n -by- p matrix and $L(k)$ is a p -by- p matrix. For the model (4.70) and (4.72) the equations to obtain the steady-state of an exponentially stable filter are:

$$Y(k+1) = \Phi S(k) \quad (4.74)$$

$$G(k+1) = G(k) + Y(k+1)L(k)Y(k+1)^TM^T \quad (4.75)$$

$$R^e(k) = R^e(k) + MY(k+1)L(k)Y(k+1)^TM^T \quad (4.76)$$

$$K(k+1) = G(k+1)R^e(k+1)^{-1} \quad (4.77)$$

$$S(k+1) = Y(k+1) - K(k+1)MY(k+1) \quad (4.78)$$

$$L(k+1) = L(k) + L(k)Y(k+1)^TM^TR^e(k)^{-1}MY(k+1)L(k) \quad (4.79)$$

where the initial condition for the recursion is given by:

$$\begin{aligned}
Y(1) &= A^{-1} \\
G(0) &= 0 \\
R^e(0) &= R \\
L(0) &= Q
\end{aligned} \tag{4.80}$$

Note that since the filter is assumed to be exponentially stable it can be shown by using equations (4.74) and (4.78) that:

$$\|S(k)\| \leq \|\Psi(k, 1)\| \|S(1)\| \leq c_2 e^{-c_3(t_k - t_1)} \|S(1)\| \tag{4.81}$$

where c_2 and c_3 are positive constants (see Subsection 3.2.2). The number of computations to go from time k to time $k+1$ can be seen to be $O(np)$. There will be a computational advantage in comparison with the conventional algorithm if $p \ll n$. The covariance matrix $P(k | k)$ does not enter the equations (4.74) - (4.79). If desired it can be computed by means of:

$$P(k | k) = \sum_{i=1}^k S(i)L(i)S(i)^T \tag{4.82}$$

However, this is not attractive since it requires a large additional computational effort.

With respect to both the conventional algorithm as the Chandrasekhar-type implementation we note that the equations have been written in a form in which it is clear that several combinations, like $Y(k+1)^T M^T$ and $L(k) Y(k+1)^T M^T$, will be computed first and then reused so as to reduce the number of operations. Furthermore, to reduce the storage requirements of the filter, the matrices A , B and M are not stored but only represent a sequence of linear operations. In this case the number of variables which has to be stored is approximately n^2 for the conventional algorithm and $np + p^2$ for the Chandrasekhar-type implementation. Finally, we note that to reduce the number of computations as well as to improve the numerical properties of the algorithms (see Van Dooren and Verheagen 1986) only the lower triangular form of the symmetric matrices are computed.

To gain insight into the numerical performance of the original Kalman filter equations and the Chandrasekhar-type implementation we analyse the effect of rounding errors. The analysis which is a modification of the very recent work of Van Dooren and Verheagen (1986), is split into two parts:

- The derivation of upper bounds for the errors performed in one iteration.
- The propagation and accumulation of these errors.

In deriving upper bounds for the errors performed in one time step Van Dooren and Verheagen assume that no serious errors occur in the products of matrices. They demonstrate that in this case for the original equations the condition number of the matrix $MP(k+1|k)M^T + R$ plays an important role in the cause of numerical errors*. Clearly, this number is dependent on the choice of the system noise processes W_m and W_c (see Section 4.4) and on the resulting condition number of the noise covariance matrix Q . Using the Chandrasekhar-type equations similar results can be derived for the condition number of the matrix $R^\epsilon(k+1)$. If the system noise process is chosen carefully the condition numbers described above are rather small for the problems dealt with in this investigation. Therefore, in our case, unlike the cases discussed by Van Dooren and Verheagen, numerical errors are often mainly caused by the simple accumulation of rounding errors in computing the products of large matrices. In order to obtain upper bounds for the numerical errors performed in one iteration we neglect the errors caused by the above mentioned ill-conditionality of the problem. Since the matrices A , B and M are very sparse we in addition assume that no serious cancellations occur in the products involving these matrices.

Using the conventional implementation we can derive for the error $\delta P(k+1|k+1)$ in $P(k+1|k+1)$, assuming the computations up to iteration k are exact:

$$\|\delta P(k+1|k+1)\| \leq \epsilon O(m^2) \|P(k+1|k)\|^2 \| [MP(k+1|k)M^T + R]^{-1} \| \quad (4.83)$$

Here ϵ is a constant close to machine precision.

Similar results can be obtained for the Chandrasekhar-type equations, assuming that the errors are $O(\Delta)$, $\Delta^2 \ll \Delta$:

$$\|\delta G(k+1)\| \leq \epsilon O(p^2) \|Y(k+1)\|^2 \|L(k)\| \quad (4.84)$$

$$\|\delta R(k+1)\| \leq \epsilon O(p^2) \|Y(k+1)\|^2 \|L(k)\| \quad (4.85)$$

$$\begin{aligned} \|\delta S(k+1)\| &\leq \epsilon O(m^2) \|G(k+1)\| \|R^\epsilon(k+1)^{-1}\| \|Y(k+1)\| \\ &+ \|\delta G(k+1)\| \|R^\epsilon(k+1)^{-1}\| \|Y(k+1)\| \\ &+ \|G(k+1)\| \|R^\epsilon(k+1)^{-1}\| \|\delta R^\epsilon(k+1)\| \|R^\epsilon(k+1)^{-1}\| \|Y(k+1)\| \\ &+ O(\Delta^2) \end{aligned} \quad (4.86)$$

* The condition number $K(M)$ of a matrix M is defined as:

$$K(M) = \lambda_{\max}/\lambda_{\min},$$

where λ_{\max} and λ_{\min} are the maximum and minimum eigenvalues of $M^T M$ respectively.

$$\|\delta L(k+1)\| \leq \epsilon O(m^2 p) \|Y(k+1)\| \|L(k)\| \|Y(k+1)L(k)\| \|R^\epsilon(k)^{-1}\| \quad (4.87)$$

Here we have used the relation (Van Dooren and Verheagen 1986):

$$\delta(M^{-1}) = M^{-1} \delta M M^{-1} + O(\Delta^2)$$

for a nonsingular matrix M and a δM satisfying:

$$\frac{\|\delta M\|}{\|M\|} = O(\Delta), \Delta^2 \ll \Delta$$

The upper bounds just derived do not provide information about the relative errors in the matrices involved. These errors may be large if e.g. Q is ill-conditioned or if some eigenvalues of the matrix $K(k)M$ are close to unity. In the last case equation (3.9) for the original algorithm and equation (4.78) for the Chandrasekhar-type implementation can involve the typical numerical problem of computing the small difference of large numbers. For the conventional implementation these numerical difficulties can become serious in the case of large eigenvalues of P and very accurate measurements.

The upper bounds are derived under the assumption that the computations up to step k are exact. However, if at step k the accumulated errors are $O(\Delta)$, it can easily be shown that the upper bounds for the errors performed in step k is $O(\Delta^2)$ -close to the bounds (4.84) - (4.87) (Van Dooren and Verheagen 1986). Furthermore, we note that the upper bounds just derived are very pessimistic and do not take into account the statistical distribution of rounding errors. However, as Wilkinson (1961) points out the main object of such an analysis is to expose the potential instabilities of the algorithms. From the insight thus obtained we are able to compare different implementations with respect to the expected numerical performance.

From the upper bounds just derived two important differences between the algorithms can be noted:

- While in general the upper bound (4.83) is of the same order of magnitude for each k , the upper bounds (4.84) - (4.87) as a consequence of relation (4.81) decrease exponentially with k .
- Upper bound (4.83) is $O(m^2)$ while the upper bounds (4.84) - (4.87) are $O(p^2)$ or $O(m^2 p)$. Since in general $p \gg m \gg 1$ we may expect that for small k , the errors performed in one iteration using the Chandrasekhar-type algorithm are an order of magnitude larger than in the case of the original algorithm.

Note that increasing the domain of our problem without changing the number of measurement locations does not cause - for the conventional algorithm - an increase

in the errors performed in one iteration. This is a very favourable property resulting in small errors even in the case of very large models*.

To study the propagation of errors for the conventional Kalman filter algorithm, let $\delta P(k|k)$ be the symmetric error in $P(k|k)$. Using equation (3.19) it is easy to show that, if the filter is exponentially stable, for all 1:

$$\|\delta P(k+1|k+1)\| \leq c_2 e^{-2c_3(t_{k+1}-t_k)} \|\delta P(k|k)\| \quad (4.88)$$

This relation shows that numerical errors in $P(k|k)$ vanish as new measurements are incorporated and as a consequence we may expect the original algorithm to be stable.

To study the propagation of errors for the Chandrasekhar-type implementation we start with errors $\delta G(k)$, $\delta S(k)$, $\delta R^\epsilon(k)$ and $\delta L(k)$. Since it is assumed that no serious cancellations occur in the products involving the matrices M and Φ we have $\delta R^\epsilon(k) = M\delta G(k)$ and $\delta Y(k+1) = \Phi\delta S(k)$. Using the equation (4.81) and assuming $G(k)$, $R^\epsilon(k)$ and $L(k)$ are bounded from above, one can derive:

$$\begin{aligned} \delta G(k+1) &= \delta G(k) + \Phi\delta S(k)L(k)^T S(k)^T \Phi^T M^T \\ &\quad + \Phi S(k) \delta L(k) S(k)^T \Phi^T M^T + \Phi S(k) L(k) \delta S(k)^T \Phi^T M^T + O(\Delta^2) \\ &\leq \delta G(k) + c_{13} e^{-c_3 t_k} \delta S(k) + c_{13} e^{-c_3 t_k} \delta L(k) + O(\Delta^2) \end{aligned} \quad (4.89)$$

$$\delta R^\epsilon(k+1) = M\delta G(k+1) \leq c_{14} \delta G(k+1) \quad (4.90)$$

$$\begin{aligned} \delta K(k+1) &= \delta G(k+1) R^\epsilon(k+1)^{-1} - G(k+1) R^\epsilon(k+1)^{-1} \delta R^\epsilon(k+1) R^\epsilon(k+1)^{-1} \\ &\quad + O(\Delta^2) \end{aligned} \quad (4.91)$$

$$\leq c_{15} \delta G(k+1) + O(\Delta^2) \quad (4.92)$$

$$\begin{aligned} \delta S(k+1) &= [I - K(k+1)M] \Phi \delta S(k) - \delta K(k+1) M S(k) + O(\Delta^2) \\ &\leq \delta S(k) + c_{16} e^{-c_3 t_k} \delta G(k+1) + O(\Delta^2) \end{aligned} \quad (4.93)$$

* Most square root filters do not have this property and as a consequence using these filters the errors performed in one iteration may become significant in case of very large models.

$$\begin{aligned}
\delta L(k+1) = & \delta L(k) + \delta L(k) S(k)^T \Phi^T M^T R^e(k)^{-1} M \Phi S(k) L(k) \\
& + L(k) S(k)^T \Phi^T M^T R^e(k)^{-1} M \Phi S(k) \delta L(k) \\
& + L(k) \delta S(k)^T \Phi^T M^T R^e(k)^{-1} M \Phi S(k) L(k) \\
& + L(k) S(k)^T \Phi^T M^T R^e(k)^{-1} M \Phi \delta S(k) L(k) \\
& + L(k) S(k)^T M^T R^e(k)^{-1} \delta R^e(k) R^e(k)^{-1} M \Phi S(k) L(k) + O(\Delta^2) \\
\leq & (1 + c_{17} e^{-c_3 t_k}) \delta L(k) + c_{18} e^{-c_3 t_k} \delta Y(k) + c_{19} e^{-c_3 t_k} \delta G(k) + O(\Delta^2) \quad (4.94)
\end{aligned}$$

Here $c_i >$ are constants. Defining:

$$\underline{n}(k+1) = [\|G(k+1)\| \quad \|S(k+1)\| \quad \|L(k+1)\|]^T \quad (4.95)$$

it is easy to show that:

$$\underline{n}(k+1) \leq N(k+1, k) \underline{n}(k) + O(\Delta^2) \quad (4.96)$$

where:

$$N(k+1, k) = \begin{bmatrix} 1 & c_{20} e^{-c_{21} t_k} & c_{20} e^{-c_{21} t_k} \\ c_{20} e^{-c_{21} t_k} & 1 & c_{20} e^{-c_{21} t_k} \\ c_{20} e^{-c_{21} t_k} & c_{20} e^{-c_{21} t_k} & 1 + c_{20} e^{-c_{21} t_k} \end{bmatrix}$$

and the inequality is meant elementwise. Since $N(k+1, k)$ is normal we have:

$$\|N(k+1, k)\| = \max_m \{\lambda_m(k+1, k)\} \quad (4.97)$$

where $\lambda_m(k+1, k)$ are the eigenvalues of $N(k+1, k)$.

Since (Gerschgorin's theorem):

$$\max_m \{\lambda_m(k+1)\} \leq 1 + 3c_{20} e^{-c_{21} t_k} \quad (4.98)$$

we have:

$$\begin{aligned}
\left\| \prod_{i=k}^{k+1} N(i+1, i) \right\| &\leq \left\| \prod_{i=k}^{k+1} N(i+1, i) \right\| \\
&= \prod_{i=k}^{k+1} (1 + 3c_{20} e^{-c_{21} t_i})
\end{aligned}$$

$$\begin{aligned}
&\leq e^{\left(\prod_{i=k}^{k+1} \ln(1+3c_{20}e^{-c_{21}t_i})\right)} \\
&\leq e^{\left(\sum_{i=k}^{k+1} 3c_{20}e^{-c_{21}t_i}\right)} \\
&\leq e^{\left(\sum_{i=k}^{k+\infty} 3c_{20}e^{-c_{21}t_i}\right)} \\
&\leq c_{22}
\end{aligned} \tag{4.99}$$

Hence:

$$\|\underline{n}(k+l)\| \leq c_{22} \|\underline{n}(k)\| + O(\Delta^2) \tag{4.100}$$

where c_{22} does not depend on l . Equation (4.100) shows that numerical errors in $G(k)$, $S(k)$ and $L(k)$ grow in time. However, the growth decreases in time and upper bounds of the errors can be obtained.

From the inequality (4.100) we see that, as for the conventional Kalman filter algorithm, we may expect that the accumulated numerical errors are bounded from above. However, the structure of the accumulation of errors is fundamentally different. For the conventional algorithm the numerical errors performed at each iteration are of the same order of magnitude and the stability of the algorithm is due to the fact that numerical errors vanish. For the Chandrasekhar-type equations numerical errors do not vanish and stability is due to the fact that the errors performed at the iterations decrease with the number of iterations. In Chapter 6 some numerical results of the error accumulation of the two algorithms are described in detail.

4.9 Distributed parameter filters

The shallow water equations are distributed in nature. In developing methods for the identification of the water-levels and velocities in this distributed parameter system, one is faced sooner or later with the necessity of approximating the solution to a set of algebraic equations. Thus, an important problem is to decide at what point in the solution procedure the approximation is introduced. In this study we first approximate the partial-differential equation by a discrete system after which the discrete filter theory can be employed. Another approach is to retain the distributed

nature of the equations as long as possible and to derive the continuous filter equations for the distributed parameter system. In order to obtain the solution, these equations have to be approximated numerically. Thus, the problem is whether the numerical approximation is carried out before or after the optimization. On this problem numerous discussions have appeared in literature (Polis and Goodson 1976, Chavant 1979, Polis 1982, among others). However, for the problems dealt with in this study this discussion is a rather academic one.

Consider for example, the noise-free distributed model (4.15). In this case the equations to describe the propagation in time of the covariance $P(x_1, x_2, t)$ can be shown to be (Koda and Seinfeld 1978):

$$\frac{\partial P}{\partial t} + C_1 \frac{\partial P}{\partial x_1} + C_2 P + \frac{\partial P}{\partial x_2} C_1^T + P C_2^T = 0 \quad (4.101)$$

To obtain a solution, a first-order finite difference approximation can be employed.

However, if we first approximate the model (4.15) using a first-order finite difference scheme and then employ the discrete filter theory it can be shown that the filter gains resulting from the two different approaches are $O(\Delta t)$ -close to each other. Of course, this is not very surprising. Since both approaches are different numerical approximations to the same problem, we may expect that for $\Delta t \rightarrow 0$ the results will become identical.

As is demonstrated in Section 4.5, solving the filter equations the influence of the finite difference approximation is, except for the very short waves, very small compared to the uncertainty associated with the system noise statistics. Therefore, we may expect that in general the results of the two different approaches do not differ significantly.

From the theoretical point of view we agree with Polis (1982) who prefers to approximate the continuous problem early. Of his arguments we recall that the discrete filter based on the discretised model involves no approximations other than those that are introduced to obtain the discrete model. The discretisation of a continuous filter is only an approximation to this optimal discrete filter.

5 A Kalman filter based on a one-dimensional model

5.1 Introduction

Using the insights gained in Chapter 4, a Kalman filter based on the non-linear one-dimensional shallow water equations is developed in this chapter. Attention is concentrated on the modelling of the water movement in the southern part of the North Sea by means of a relatively simple one-dimensional model. Of course, this conceptual model is *not* perfect. Consequently, it is essential in this approach that the uncertain parameters introduced into the model are estimated on-line by the Kalman filter to adapt the conceptual model to changing circumstances.

The model describing the water movement along the coasts of Belgium and the south-western part of the Netherlands is described in Section 5.2. Section 5.3 deals with the Kalman filter based on this model. The filter has been tested using simulated data in Section 5.4. To improve the filter and to be able to predict the water-level in the Eastern Scheldt, Ten Brummelhuis and De Jong have developed a Kalman filter based on a one-dimensional Eastern Scheldt model (Ten Brummelhuis, De Jong and Heemink 1984, 1985). This filter is described briefly in Section 5.5. After linking this filter to the filter describing the water movement along the coast, field data is used to examine the performance of the combined filter. The results of these tests are described in Section 5.6. This chapter concludes in Section 5.7 with a discussion of the results of the one-dimensional approach.

5.2 The deterministic model

5.2.1 Introduction

In this section the deterministic model for the description of the water movement in the southern part of the North Sea is developed. Based on this model the Kalman filter is derived in Section 5.3. Firstly, the main characteristics of the tidal movement and the meteorological effects in the southern part of the North Sea are qualitatively described in the Subsections 5.2.2 and 5.2.3 respectively. In Subsection 5.2.4 the conceptual model is derived taking into account most of these characteristics.

5.2.2 Tidal movement in the southern part of the North Sea

The Coriolis force, induced by the earth's rotation, greatly affects the tidal motion in seas and estuaries. It is responsible for the occurrence of the amphidromic points, where the water-level is constant while, in general, water velocities at these points are time-varying. In this subsection we employ the theory of Kelvin waves, i.e. the tidal waves subject to the Coriolis force, to obtain a general insight into the tidal motion in the southern part of the North Sea and to give an explanation of the location of the amphidromic point in this part of the North Sea.

The Kelvin wave is a particular analytical solution of the linear two-dimensional shallow water equations in the neighbourhood of a straight coastal line. It is assumed that the velocity component perpendicular to the coast can be neglected and that the depth is constant. Although a linear bottom friction term may be taken into account, it is omitted in this subsection since it complicates the formulas considerably and does not increase the general insight into the tidal motion. The interested reader is referred to Dronkers (1964, 1975). The assumptions just described yield the following equations for the Kelvin wave* :

$$\frac{\partial u}{\partial t} + g \frac{\partial h}{\partial x} = 0 \quad (5.1)$$

$$fu + g \frac{\partial h}{\partial y} = 0 \quad (5.2)$$

$$D \frac{\partial u}{\partial x} + \frac{\partial h}{\partial t} = 0 \quad (5.3)$$

where the x-axis coincide with the coastal line. Here we recall that:

h = water-level

u = water velocity

g = acceleration of gravity

f = Coriolis parameter

D = water depth.

The equations (5.1) - (5.3) can be solved by the method of separation of variables. In the case of a tidal wave with frequency ω the solution can be written as:

$$h(x,y,t) = Ae^{-\frac{fy}{\sqrt{gD}}} \cos(\omega t - \frac{\omega}{\sqrt{gD}}x + \phi) \quad (5.4)$$

$$u(x,y,t) = \sqrt{\frac{g}{D}} h(x,y,t) \quad (5.5)$$

* These equations can be derived easily from the equations (1.3)-(1.5).

where A and ϕ are constants. From these equations it can be seen that the tidal amplitude decreases on the line perpendicular to the coastline which is to the left of the line of propagation of the Kelvin wave (see figure 5.1).

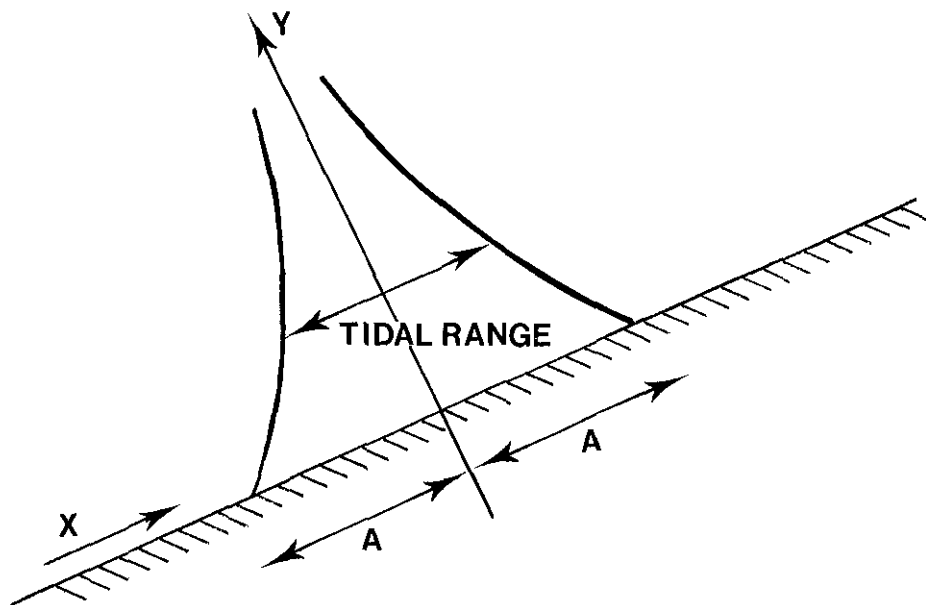


Figure 5.1: Propagation of a Kelvin wave along a straight coastal line.

We now consider the case of two Kelvin waves with the same frequency, propagating in opposite directions in a channel between two parallel coastal lines. In this case, amphidromic points occur in the channel. The locations of these points can be easily determined from the constants A and ϕ of the two Kelvin waves. The phase of the waves varies around the amphidromic points and decreases in the clockwise sense* (see figure 5.2). Note that in essence this tidal motion is one-dimensional.

The concept of the Kelvin wave can be used to describe in a qualitative way the tidal propagation in the southern part of the North Sea, since even for this wide channel the velocity perpendicular to the coast is rather small and Kelvin waves are predominant with respect to the cross-sectional motions. In the North Sea the M_2 tide with a period of approximately 12.5 hours strongly predominates. From the

* This is only true in the northern hemisphere where $f > 0$. At the equator the Coriolis force does not occur ($f = 0$), while in the southern hemisphere $f < 0$ and the phase of the waves varies around the amphidromic points decreasing in the counter-clockwise sense.

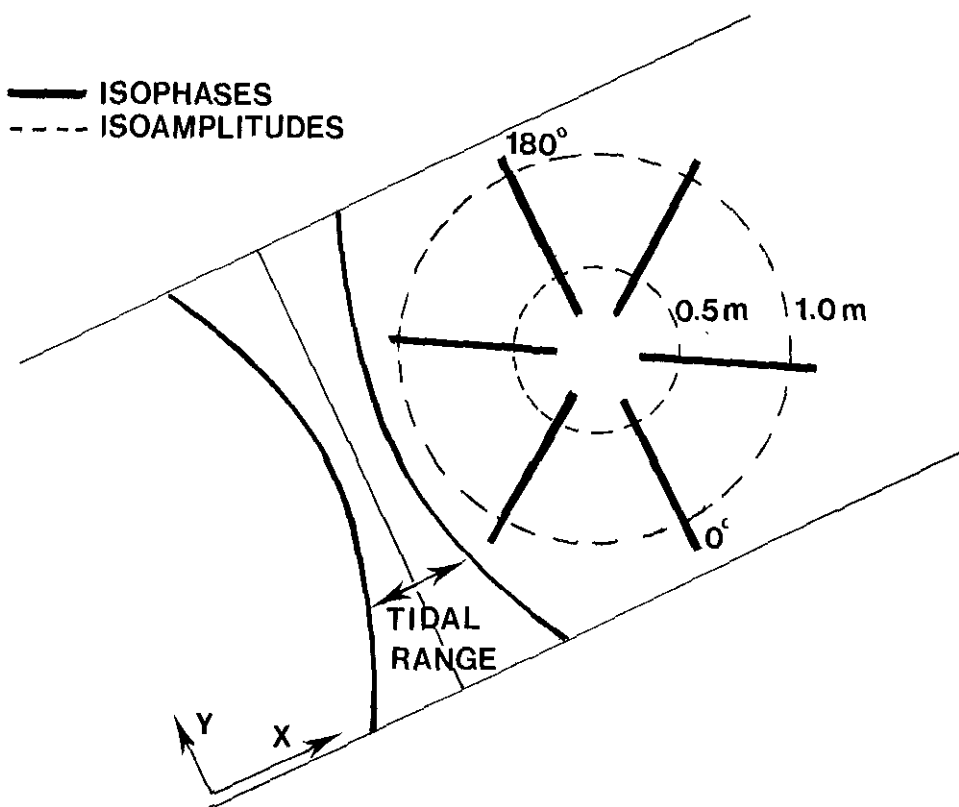


Figure 5.2: Two Kelvin waves propagating in opposite directions between two parallel coastal lines.

north, this tidal wave enters the southern part of the North Sea along the English coast. Since the Strait of Dover is very narrow, much of the wave is reflected and propagates together with the M_2 tide entering the North Sea at Dover along the coasts of Belgium and the Netherlands toward the north. Therefore, the tidal motion in this part of the North Sea can be described by two Kelvin waves propagating in opposite directions (see figure 5.3). In this way, the presence of the amphidromic point can be explained.

External surges and surges created in the northern part of the North Sea propagate in the southern part of the North Sea approximately like Kelvin waves along with the tide. As a consequence, these surges often enter the Dutch coastal waters from the south.

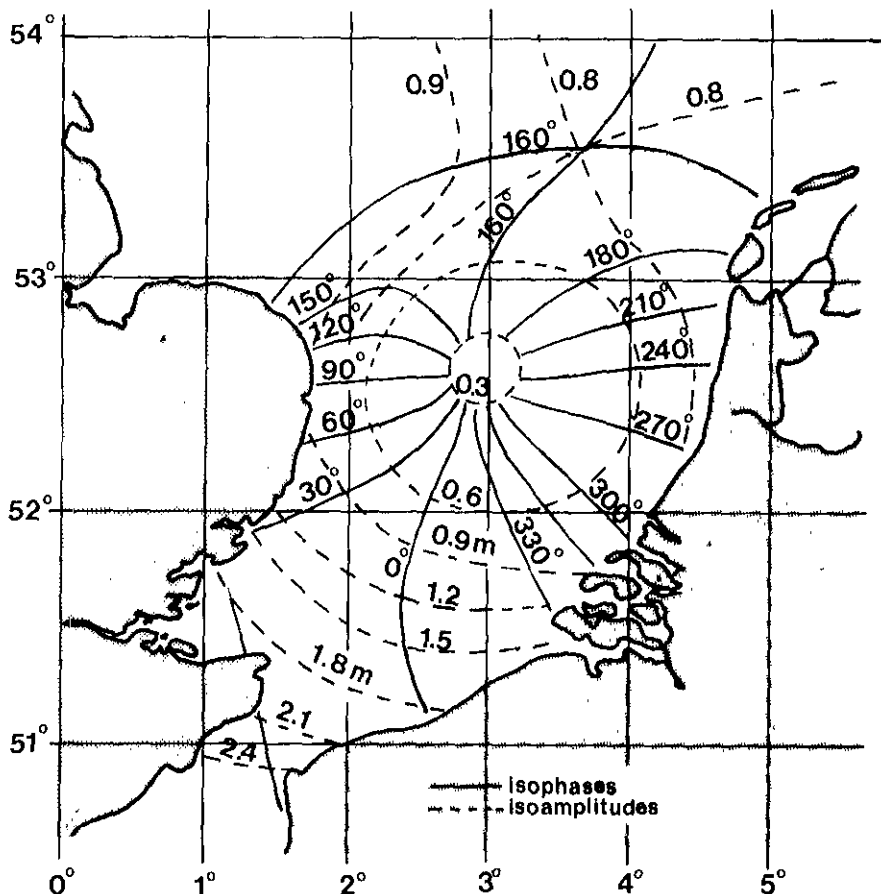


Figure 5.3: The M_2 tide in the southern North Sea.

5.2.3 Meteorological effects in the North Sea

The weather conditions have two different effects on the water movement in the North Sea. Firstly, the atmospheric pressure profile p of a storm directly affects the water-level underneath.

Secondly, wind blowing over water creates a frictional force F_w on the surface of the water. This force sets up the surface of the water in the direction of the wind until the surface gradient is sufficient to create a counteractive force equal to the frictional wind force on the surface and a steady-state condition is reached.

Under stationary conditions an empirical relation has been developed (Bretschneider 1966, 1967)*:

$$\frac{ds}{dy} = \gamma \frac{V^2}{g(D+s)} \quad (5.6)$$

where γ is the wind friction coefficient, V is the wind velocity and s is the set up. The y -axis is chosen parallel to the direction of the wind (see *figure 5.4*).

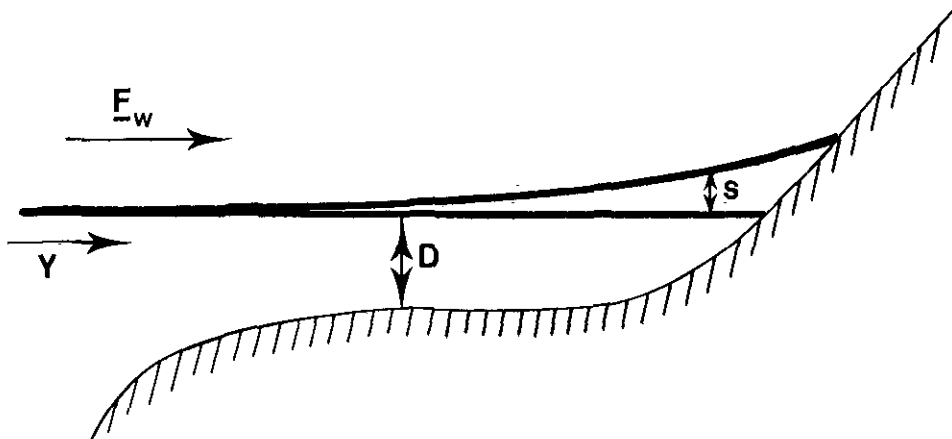


Figure 5.4: Set up perpendicular to the coast.

Note that when the steady-state condition is reached this does not mean that the water is calm. On the surface the wind blows the water in the direction of the wind while at the bottom a return flow occurs.

As can be seen from equation (5.6) the set up created by the wind depends (unlike the pressure force) on the water depth. As a consequence, this depth is important to determine whether or not the pressure term may be neglected with regards to the wind term. Following Timmerman (1977), we introduce *figure 5.5*, in which the relative importance of the wind effect to the pressure effect is shown as a function of the wind velocity and water depth.

Since in the southern part of the North Sea the depth is approximately 20-30 m, the pressure effect has been left out of consideration in the derivation of the conceptual model.

* Note that this empirical formula is also used to model the frictional wind force in the shallow water equations.

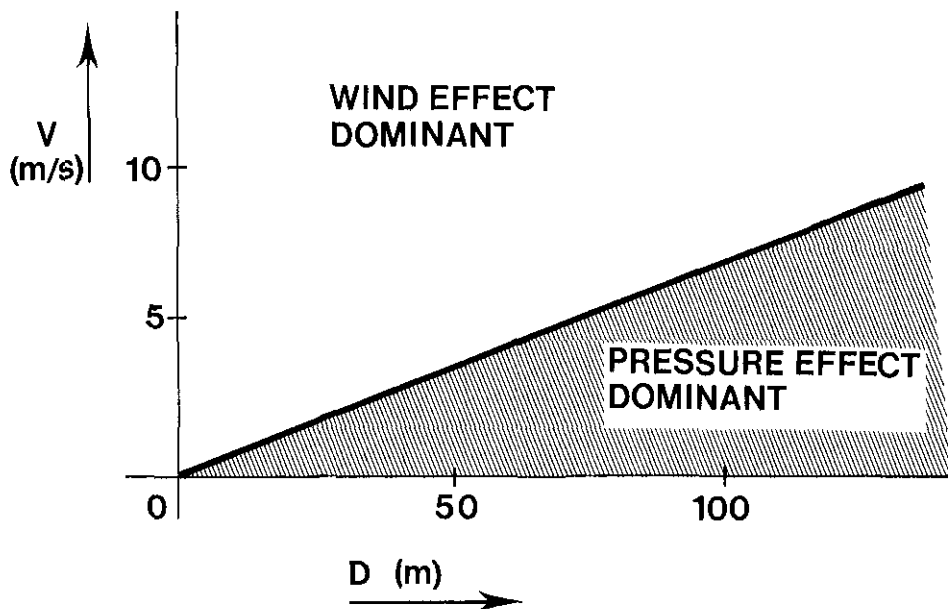


Figure 5.5: Relative importance of the wind effect and the pressure effect.

5.2.4 The mathematical model

In this subsection the conceptual model is derived, taking into account the main characteristics of the water movement in the southern North Sea that have been discussed in Subsections 5.2.2 and 5.2.3. At first, we adopt the concept of the Kelvin wave to describe the tidal motion along the coasts of Belgium and the south-western part of the Netherlands. In the neighbourhood of these coastal lines the velocity component v perpendicular to the coastal line can be neglected. Furthermore, if we assume the depth to be independent of y , the coordinate perpendicular to the coast, the tidal movement becomes essentially one-dimensional and can be described by (see Section 2.3):

$$\frac{\partial u}{\partial t} + u \frac{\partial u}{\partial x} + g \frac{\partial h}{\partial x} + \mu \frac{u|u|}{D+h} - \gamma \frac{V^2 \cos \psi}{D+h} = 0 \quad (5.7)$$

$$g \frac{\partial h}{\partial y} + fu - \gamma \frac{V^2 \sin \psi}{D+h} = 0 \quad (5.8)$$

$$\frac{\partial h}{\partial t} + \frac{\partial}{\partial x} (u(D+h)) = 0 \quad (5.9)$$

where the x -axis is parallel to the coastal line.

Since we are only interested in the water-level along the coast, equations (5.7) and (5.9) are used to describe the water motion in a narrow strip parallel with the coast. In this case, equation (5.8) can be approximated by:

$$h(y) \approx h(y_0) + \frac{1}{g} [-fu(y_0) + \gamma \frac{V^2 \sin \psi}{D+h(y_0)}] (y-y_0) \quad (5.10)$$

By means of this equation it is possible to describe the water-level variations perpendicular to the x-axis ($y=y_0$). This possibility is important since the measurement stations available are generally not located exactly on this axis. As a consequence, the water-level observations taken at these stations have to be corrected to obtain information about the water-level along the x-axis. Along this axis the water-level can be computed by solving equations (5.7) and (5.9). Thus, the model becomes essentially one-dimensional.

As described in the Subsections 5.2.2 and 5.2.3 the tidal waves as well as the external surges mainly propagate from the south along the coast toward the north. Consequently, we propose to use as boundary condition at a Belgian measurement station ($x=x_0$) a prescribed water-level and at the mouth of the Eastern Scheldt ($x=x_L$) a free outflow condition (see Chapter 2).

The simple one-dimensional model just described can be used to predict water-levels in the Dutch coastal waters. Here it is essential that observations of the water-levels are used to adapt the conceptual model to changing conditions. By introducing uncertainty to the boundary condition at $x=x_0$ the measurements at this location are used to correct the predictions if an external wave enters the model. Analogously, by associating uncertainty with the continuity equation the model is adapted if a wind effect perpendicular to the coast occurs. In this last case, however, only accurate estimates of this wind effect can be made. Predictions have to be computed assuming this effect will remain constant. To improve the model and to be able to predict variations of a wind effect perpendicular to the coast, we make use of the empirical relation (5.6) between the wind and the set-up along the coast. Defining $s(t)$ as the set-up at the coast ($y=y_0$) created by the component of the wind perpendicular to the coast, we follow Schalkwijk (1947) and propose the simple empirical relation:

$$s(t) = a V(t-\tau)^2 \cos(\psi(t-\tau) - \chi_0) \quad (5.11)$$

to predict the variations of the wind effect along the Dutch coast. Here a is a constant, τ is a time delay, ψ is the direction of the wind and χ_0 is the direction of the maximum wind effect. The relation has been derived using equation (5.6).

Combining equations (5.11) with the model described by equations (5.7) and (5.9) yields:

$$\frac{\partial u}{\partial t} + u \frac{\partial u}{\partial x} + g \frac{\partial h}{\partial x} + \mu \frac{u |u|}{D+h+s} - \gamma \frac{V^2 \cos \psi}{D+h+s} = 0 \quad (5.12)$$

$$\frac{\partial h}{\partial t} + \frac{\partial}{\partial x} (u(D+h+s)) + \frac{ds}{dt} = 0 \quad (5.13)$$

while in this case, the relation:

$$h(y) = h(y_0) + \frac{1}{g} [-fu(y_0) + \gamma \frac{V^2 \sin \psi}{D+h(y_0)+s}] (y-y_0) \quad (5.14)$$

can be used to correct the water-level perpendicular to the x-axis. In the equations (5.12) - (5.14) h is considered to be the water-level with respect to the reference $D+s$.

Following the approach described in Chapter 4, equations (5.12) and (5.13) are discretised in order to obtain a system representation. As shown in this chapter the Lax-Wendroff scheme is a suitable finite difference method. Since we want the x-coordinate of the locations of the measurement stations to coincide with grid points, the grid is chosen to be non-equidistant*. If equations (5.12) and (5.13) are written in conservation-law form:

$$\frac{\partial f}{\partial t} + \frac{\partial F(f)}{\partial x} = G(f) \quad (5.15)$$

where:

$$\underline{f} = \begin{bmatrix} u \\ h+s \end{bmatrix}$$

$$\underline{F}(f) = \begin{bmatrix} F_1(u, h) \\ F_2(u, h) \end{bmatrix} = \begin{bmatrix} u^2/2 + gh \\ u(D+h+s) \end{bmatrix}$$

$$\underline{G}(f) = \begin{bmatrix} G_1(u, h) \\ G_2(u, h) \end{bmatrix} = \begin{bmatrix} -\mu \frac{u |u|}{D+h+s} + \gamma \frac{V^2 \cos \psi}{D+h+s} \\ 0 \end{bmatrix}$$

the finite difference equations can be written as:

$$\begin{aligned} \underline{f}_m^{k+1} &= \underline{f}_m^k - \frac{\Delta t}{\Delta x_{m-1} + \Delta x_m} (\underline{F}(\underline{f}_{m+1}^k) - \underline{F}(\underline{f}_{m-1}^k)) + \\ &\quad \frac{2\Delta t^2}{(\Delta x_{m-1} + \Delta x_m)^2} [A_{m+1/2}^k (\underline{f}_{m+1}^k - \underline{f}_m^k) - A_{m-1/2}^k (\underline{f}_m^k - \underline{f}_{m-1}^k)] \\ &\quad - \frac{\Delta t}{(\Delta x_{m-1} + \Delta x_m)} [\Delta x_m \underline{G}(\underline{f}_{m-1}^k) + \Delta x_{m-1} \underline{G}(\underline{f}_{m+1}^k)] \end{aligned} \quad (5.16)$$

* It is also possible to use an equidistant grid and to use interpolation to find the measurements of the water-level from the water-levels at the grid points.

where:

$$(A(\underline{f}))_{ij} = \left[-\frac{\partial(F)_i}{\partial(f)_j} \right] \quad (5.17)$$

and

$$\begin{aligned} A_{m-\frac{1}{2}}^k &= A\left(\frac{1}{2}(f_m^k + f_{m-1}^k)\right) \\ A_{m+\frac{1}{2}}^k &= A\left(\frac{1}{2}(f_{m+1}^k + f_m^k)\right) \end{aligned} \quad (5.18)$$

Furthermore, $x_m, m=0,1,\dots,L$ are the grid points and $\Delta x_m = x_{m+1} - x_m$ are the distance steps. In practice Richtmyer's modification of the Lax-Wendroff scheme is often used (Richtmyer and Morton 1967). This scheme is slightly simpler to implement since it does not require the matrix A to be known explicitly. However, since the Kalman filter algorithm in any case requires this knowledge, in our approach we prefer to use the original Lax-Wendroff scheme.

Having defined the boundaries, the wave motion is, physically, completely described. However, the Lax-Wendroff scheme requires both u and h to be known at the boundaries. Therefore, using the characteristic formulation of the shallow water equations (see Chapter 2) we derive additional boundary equations. Consider the boundary at $x=x_0$ where the water-level is known. Along the characteristic C^- (see figure 5.6) we have:

$$[u - 2 \sqrt{g(D+h+s)}]_{x=x_0, t=t_{k+1}} = [u - 2 \sqrt{g(D+h+s)} + \Delta t G_1(u, h) + \Delta t g \frac{dD}{dx}]_{x=x^-, t=t_k} \quad (5.19)$$

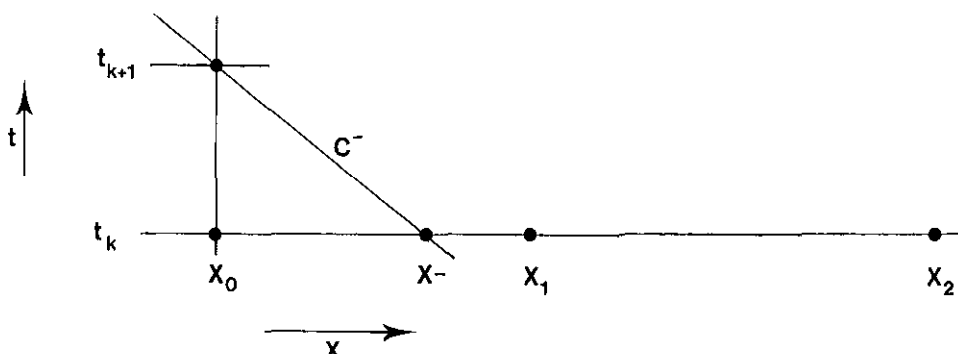


Figure 5.6: Boundary treatment at $x = x_0$.

where x^- can be determined using the equation of C⁻:

$$x^- = x_0 + \Delta t [u - \sqrt{g(D+h+s)}]_{x=x_0, t=t_{k+1}} + O(\Delta t^2) \quad (5.20)$$

and u_{x^-} and h_{x^-} are computed by means of a second-order interpolation using the water velocities and water-levels at x_0, x_1 and x_2 . In order to determine u_0^{k+1} equations (5.19) and (5.20) have to be solved iteratively starting with $u_0^{k+1} = u_0^k$. For second-order accuracy two iterations are required. The equations for the free outflow boundary at $x=x_L$ can be derived similarly.

The difference equations can be rewritten as:

$$\underline{x}_{t_{k+1}} = \underline{\Phi}(\underline{x}_{t_k}) + \underline{u}_{t_{k+1}} \quad (5.21)$$

where $\underline{x}_{t_{k+1}}$ consists of the water-levels and velocities in the grid points:

$$\underline{x}_{t_k} = [u_0^k \ u_1^k \ \dots \ h_1^k \ h_2^k \ \dots] \quad (5.22)$$

and \underline{u}_{t_k} represents the prescribed water-level at $x=x_0$.

The model (5.21) describes the water movement along the coasts of Belgium and the southern part of the Netherlands. Extending the model to the coast of France is not attractive since in the neighbourhood of the Street of Dover the tidal movement is very complex and we expect that it can only be described accurately by using a two-dimensional model.

In the model the depth $D(x)$ has to be specified. Of course, we cannot use the measured depth along the x-axis. It has to be smoothed along the y-axis in order that $D(x)$ is representative for the depth in the neighbourhood of the x-axis.

5.3 The Kalman filter

5.3.1 Introduction

In analogy with the approach presented in Chapter 4, in this section the Kalman filter based on the non-linear one-dimensional model described in Section 5.2 is derived. In Subsection 5.3.2 this discrete deterministic model is embedded in a stochastic environment which is a rather straightforward procedure. Before predictions of the state vector can be made the boundary conditions have to be predicted first. Subsection 5.3.3 is devoted to this problem.

5.3.2 The stochastic model

Based on the system representation (5.21) of the deterministic model derived in Subsection 5.2.4, the stochastic model to describe the propagation in time of the stochastic process \underline{X}_{t_k} is:

$$\underline{X}_{t_{k+1}} = \Phi(\underline{X}_{t_k}) + \underline{u}_{t_{k+1}} + \underline{W}_{t_{k+1}} \quad (5.23)$$

where \underline{W}_{t_k} is the system noise with statistics as described in Section 4.4. In deriving the measurement equation we need to consider that the measurement stations or tide gauges where the water-level is observed, are generally not located exactly on the x-axis. However, by means of equation (5.14) derived in Subsection 5.2.4, it is possible to correct the water-level perpendicular to the x-direction taking into account the effects of the wind in the y-direction and more important, the Coriolis force. Using this equation we can express the measured water-level as a function of the state \underline{X}_{t_k} , containing the water-levels and velocities at the grid points. Suppose Z_{t_k} is a scalar measurement taken at t_k on the line $x=x_m$ (see figure 5.7). In this case the measurement equation can be written as:

$$Z_{t_k} = m^i(\underline{X}_{t_k}) + V_{t_k} \quad (5.24)$$

where V_{t_k} is the scalar measurement noise with covariance r_i^2 and:

$$m^i(\underline{X}_{t_k}) = (1+a_i) H(x_m, t_k) + \frac{\Delta y}{g} \left[-f U(x_m, t_k) + \gamma \frac{V^2 \sin \psi}{D(x_m) + H(x_m, t_k) + s(t_k)} \right] \quad (5.25)$$

- MEASUREMENT STATION
- GRID POINT

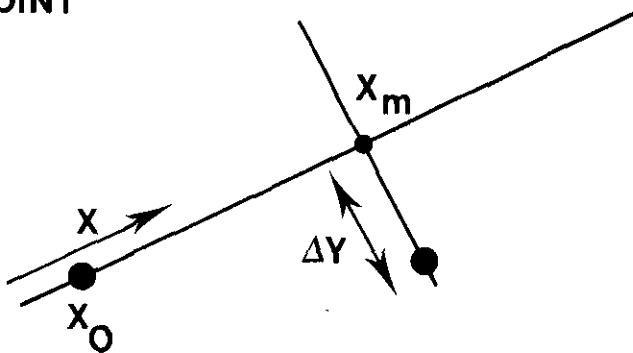


Figure 5.7: A measurement station not located on the x-axis.

Here Δy is the distance between the measurement station and the x-axis (see figure 5.7). H and U are the stochastic water-level and velocity respectively. The parameter $a_i \ll 1$ is introduced to account for local, slowly varying effects.

Generalizing the scalar case just described yields the observation equation:

$$\underline{Z}_{t_k} = \underline{m}(\underline{X}_{t_k}) + \underline{V}_{t_k} \quad (5.26)$$

where:

$$\underline{m}(\underline{X}_{t_k}) = \begin{bmatrix} m^1(\underline{X}_{t_k}) \\ m^m(\underline{X}_{t_k}) \end{bmatrix}$$

and $m^i(\underline{X}_{t_k})$ is given by equation (5.25). The covariance matrix $R(k)$ of the measurement noise \underline{V}_{t_k} is diagonal with element r_i^2 on the diagonal. The x-axis is chosen so that the measurement stations at $x=x_0$ and $x=x_L$ are located exactly on the x-axis:

$$m^1(\underline{X}_{t_k}) = H(x_0, t_k) \quad (5.27)$$

$$m^m(\underline{X}_{t_k}) = H(x_L, t_k) \quad (5.28)$$

The bottom friction parameter μ , the wind friction parameter γ and the parameters a_i in the model are not constant but are sensitive to changing conditions. Therefore, these parameters are estimated together with the water-levels and velocities by augmenting the state vector as described in Section 3.4. Based on the system representation of the model just described, the Kalman filter theory for non-linear systems can be employed to estimate the water-levels and velocities as well as the uncertain parameters in the model.

An important question with respect to the approach just described is which parameters are to be estimated by the filter. If the number of these parameters is small, then the filter may not be able to adapt the model to the changing circumstances. However, if this number is too large, filter divergence may occur. This is, e.g., the case if the same water-level variations can be described by different combinations of parameter values. In other words, the parameters cannot be determined uniquely from the data. Theoretically, it is very difficult to attack this problem, since the question is not only whether the parameters are observable, but also how observable they are. Therefore we have verified the capability of the filter to estimate the uncertain parameters using simulated data. In this case the true values of the parameters are known and consequently, the performance of the filter can be evaluated under a variety of circumstances. Some of these experiments are described in Section 5.4.

These kinds of tests have shown that the problem of filter divergence due to parameters that cannot be observed sufficiently accurately, is very likely to occur. Therefore, based on this experience the Kalman filter is only used to estimate the coefficients μ , γ and a_i . Since the parameters of the empirical relation (5.11) cannot be estimated sufficiently accurately using the measurements available, these parameters are chosen approximately as Schalkwijk (1947) did:

$$\begin{aligned} a &= 4.0 \times 10^{-3} \text{ s}^2/\text{m} \\ \chi_0 &= 340^\circ \text{ (North} = 0^\circ\text{)} \\ \tau &= 2 \text{ hours} \end{aligned}$$

Here we note that intuitively we may expect that if a parameter cannot be identified from the water-level data accurately, an erroneous value of this parameter usually does not degrade the performance of the filter very much.

5.3.3 The boundary treatment

If starting at $t=t_k$ predictions of the water-levels and velocities are required, the non-linear system equation (5.21) has to be solved without system noise whereas initial condition the estimate of the state \underline{X}_{t_k} is used. However, at $x=x_0$ the water-level $h_0(t)$ is prescribed and, consequently, has to be predicted too. This can be established by a harmonic analysis of the water-level at this location as described in Section 1.2.2:

$$h_0^a(t) = \sum_{i=1}^N f_i(t) A_i \cos(2\omega_i t + \phi_i + u_i(t)) \quad (5.29)$$

Here $h_0^a(t)$ is the astronomical tide at $x=x_0$. If the water-level is considered to be the superposition of the astronomical tide $h_0^a(t)$ and the internal wind effect $s(t)$, the prediction of $h_0(t)$, $t \geq t_k$, is given by:

$$\begin{aligned} h_0(t) &= h_0^a(t) + s(t) \\ &= h_0(t_k) + h_0^a(t) - h_0^a(t_k) + s(t) - s(t_k) \\ &= h_0(t_k) + u_t \end{aligned} \quad (5.30)$$

where u_t is defined by:

$$u_t = h_0^a(t) - h_0^a(t_k) + s(t) - s(t_k)$$

and $s(t)$ is given by equation (5.11).

We now consider the water-level $h_0(t)$ as an additional component of the state vector and introduce the system noise into the equation (5.30) by defining:

$$H_0(t_{k+1}) = H_0(t_k) + u_{t_{k+1}} + Wb_{t_{k+1}} \quad (5.31)$$

Here Wb_{t_k} represents the uncertainty of the boundary condition (5.30). By introducing this uncertainty the filter is able to correct this boundary if an external surge enters the model. Of course, there are other ways to model an uncertain boundary condition. A general discussion on the stochastic boundary treatment which is much more important in the two-dimensional case, can be found in Chapter 6.

5.4 Experiments using simulated data

5.4.1 Introduction

Before the filter can be employed using field data, it is necessary to investigate its performance when the conditions are known. In Section 4.5 filter performance has been studied in detail for a special linear problem. The results have increased the insight into the influence of the noise statistics and the finite difference approximation on the filter performance. Moreover, we have been able to investigate the effects of modelling errors, such as incorrect noise statistics or an erroneous bottom friction parameter. However, the influence of non-linearities and the capability of the filter to estimate uncertain parameters cannot be studied analogously.

The approach followed here is to construct a set of data using a "truth-model". By means of a random generator it is possible to simulate the noise processes. Having generated the measurements, the filter is applied to study whether it is able to reconstruct the tidal motion and the values of the unknown parameters using the simulated data. Furthermore, if the "filter-model" is chosen different from the truth-model it is possible to investigate whether the filter is still performing satisfactorily. The importance of these numerical experiments is that the true water-levels, velocities and parameters are known and consequently, filter performance can be evaluated quantitatively under a variety of circumstances.

In two publications a large number of these experiments have been described (Heemink 1980, Ten Brummelhuis 1984). The extended Kalman filter is shown to be capable of compensating inaccuracies in the model by adjusting the uncertain parameters. In this way the predictions are adapted to changing circumstances.

In this section we concentrate on some experiments that have not been published previously. First, in Subsection 5.4.2 we study the performance of the extended Kalman filter in case the parameters of the model are assumed to be known. It is demonstrated that in this case the variation in time of the Kalman gain caused by the

linearization is very small and if necessary, can be neglected. Of course, this conclusion only holds when the non-linearities of the model are relatively small. This important observation is exploited in the two-dimensional case described in Chapter 6 to obtain a computationally efficient filter. In Section 5.4.3 we investigate the capability of the filter to estimate the uncertain parameters in the model.

We have also studied the numerical errors caused by the finite wordlength of the computer. As can be expected from the analysis in Section 4.8 of the conventional algorithm, we have found that if the noise processes are chosen carefully these errors are very small and close to machine precision. Here we note that the study of these numerical errors is much more important if we use large two-dimensional models and if the Chandrasekhar-type implementation is employed. This case is discussed in Chapter 6.

5.4.2 The constant gain extended Kalman filter

The linearized or extended Kalman filter can be summarized as follows (see Section 3.3.2):

$$\underline{\dot{X}}(k|k-1) = \underline{\Phi}(\underline{\dot{X}}(k-1|k-1), t_{k-1}, t_k) + \underline{B}(t_k) \underline{u}_{t_k} \quad (5.32)$$

$$\underline{\dot{X}}(k|k) = \underline{\dot{X}}(k|k-1) + K(k) [\underline{Z}_{t_k} - \underline{m}(\underline{\dot{X}}(k|k-1), t_k)] \quad (5.33)$$

where the time-varying Kalman gain $K(k)$ is determined by linearizing the vectors $\underline{\Phi}$ and \underline{m} about a reference trajectory. If the parameters in the model are not considered to be components of the state vector, the time-variations of $K(k)$ are only caused by the non-linearities of the model (5.21). However, in our application these non-linear terms are relatively small. As a consequence, the time-variations of $K(k)$ are small with respect to $K(k)$. Moreover, since deterministic tidal models usually give a reasonable description of the tidal movement, the correction produced by the Kalman filter to obtain the estimates is small in relation to the deterministic results. Therefore, a relatively small error in $K(k)$ hardly affects these estimates and we may expect that a constant gain extended Kalman filter which is based on the linearization of $\underline{\Phi}$ and \underline{m} about an equilibrium state, produces estimates that are nearly optimal. Here we note that optimality itself is questionable in a physical system, because the reality always deviates from the assumptions of the filter.

This suggestion has also been raised in Section 4.5, where we have showed that the influence of choosing an incorrect bottom friction coefficient on the filter performance is very small compared to the effects caused by specifying incorrect noise statistics. Therefore, we expect that if the bottom friction coefficient is time-varying, e.g. due to a non-linear bottom friction term, the optimal time-varying filter can be

approximated accurately by setting the bottom friction coefficient to its mean value. Here we refer to the work of Safonov and Athans (1978) who show that for many non-linear applications one can obtain satisfactory performance using a constant gain extended Kalman filter. Furthermore, they give sufficient conditions for the non-divergence of state estimates generated by such non-linear estimators. Unfortunately, in our case it turns out to be very difficult – if at all possible – to verify these conditions and therefore, this exercise has been omitted.

Finally, we emphasize that a time-invariant filter approximation can only be employed if the parameters in the model are constant. If these parameters are considered to be components of the state vector, a significant non-linearity which cannot be neglected, is introduced.

In the experiments 5.1 and 5.2 we illustrate the discussion just described.

Experiment 5.1

We consider the non-linear model (5.21) described in Subsection 5.2.4 with zero wind input and constant parameters:

$$\begin{aligned}\mu &= 2.0 \times 10^{-3} \\ \gamma &= 3.0 \times 10^{-6} \\ a_1 &= -0.10 \\ a_2 &= -0.05 \\ a_3 &= 0.05 \\ a_4 &= -0.05 \\ a_5 &= 0.10 \\ a_6 &= -0.05\end{aligned}$$

At $x=x_0$ we prescribe an astronomical tide and add an external surge effect. The length of the channel considered is chosen to be 72 km, while the depth is assumed to be 10 m. Furthermore, $\Delta x=8$ km and $\Delta t=10$ min. By means of this truth-model measurements of the water-level are generated in some of the gridpoints with standard deviation $r=0.1$ m (see figure 5.8).

Using the generated observations, the extended Kalman filter is employed to identify the water-levels and velocities. The statistics of the system noise processes are chosen to be (see Section 4.4):

$$\begin{aligned}Q_m(|i_1-i_2|) &= 4.0 \times 10^{-4} e^{-0.9|i_1-i_2|} \\ Q_c(|i_1-i_2|) &= 1.0 \times 10^{-4} e^{-0.9|i_1-i_2|}\end{aligned}$$

The system noise is introduced each time step.

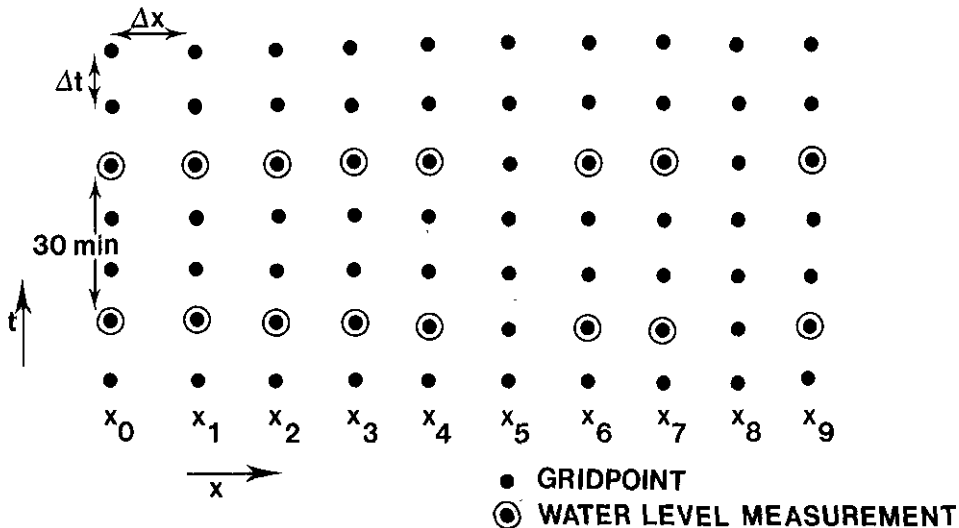


Figure 5.8: The observations available in the x-t-domain.

At the boundary $x=x_0$ we prescribe in the filter model the astronomical tide and have neglected the external surge effect. However, by introducing a large uncertainty to the boundary equation at $x=x_0$, the effects of an erroneous boundary condition can be taken into account:

$$E \{ Wb^2 \} = 0.0025$$

In figure 5.9 the simulated and filtered velocity at $x=x_0+40$ km are shown. Also the deterministic prediction produced by the filter model without using the generated data can be found in this figure. Without using the generated data the predictions computed by the filter model are quite bad. However, by filtering this data, the water-level and velocity can be reconstructed accurately:

Experiment 5.2

In this experiment the measurements that have been generated to perform experiment 5.1, are filtered by employing a constant gain extended Kalman filter. Here, to compute the time-invariant filter gain, a linear model is employed. In figure 5.10 the simulated as well as the filtered velocity at $x=x_0+40$ km are presented, showing a remarkable resemblance with figure 5.9. The largest difference between the extended Kalman filter estimates and the results of the constant gain filter is in this case less than 0.01 m/s. Of course, these results depend very much on the non-linearities in the model. In case of very shallow water the non-linear effects may be too significant for the constant gain filter to be an accurate approximation of the extended Kalman filter.

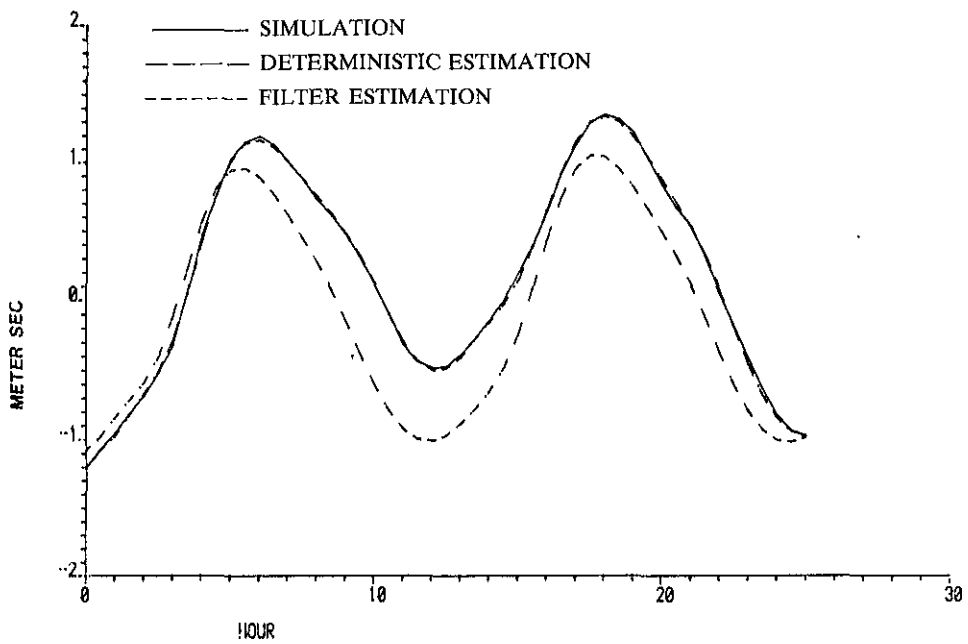


Figure 5.9: Estimation of the water velocity using the extended Kalman filter.

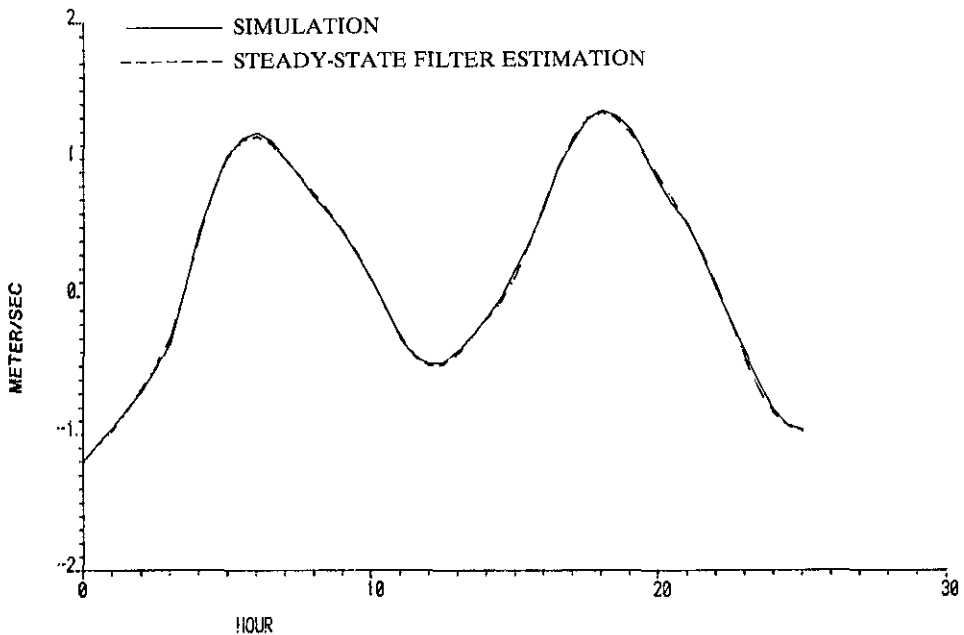


Figure 5.10: Estimation of the water velocity using the constant gain extended Kalman filter.

5.4.3 Parameter estimation

Experiment 5.3

In this experiment we investigate the capability of the filter to estimate the bottom friction coefficient. Again, the generated data of experiment 5.1 are used by the filter to estimate the water-levels and velocities as well as the bottom friction coefficient. The initial estimation of this parameter is chosen to be:

$$\hat{\mu}_0 = 0.0, E\{(\mu_0 - \hat{\mu}_0)^2\} = 4.0 \times 10^{-6}$$

In the figures 5.11 - 5.13 the parameter estimates produced by the filter are shown, respectively choosing the variance of the corresponding system noise component:

- (figure 5.11)

$$E\{W_\mu^2\} = 10^{-6}$$

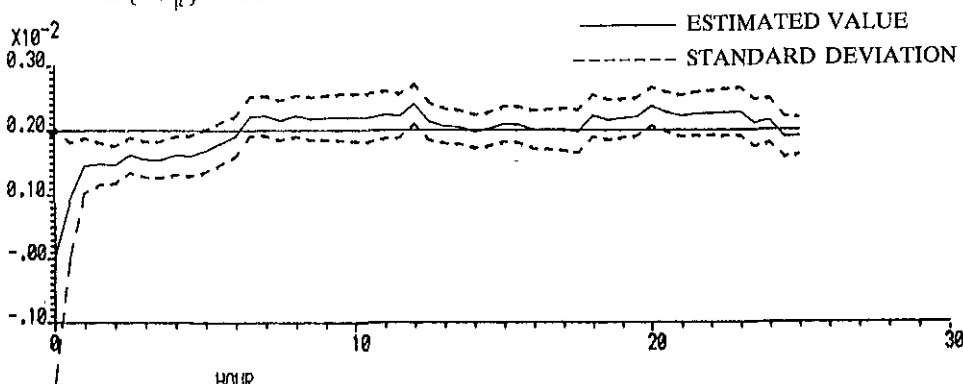


Figure 5.11: Estimation of the bottom friction coefficient in case of a system noise variance of 1.0×10^{-6} .

- (figure 5.12)

$$E\{W_\mu^2\} = 10^{-7}$$

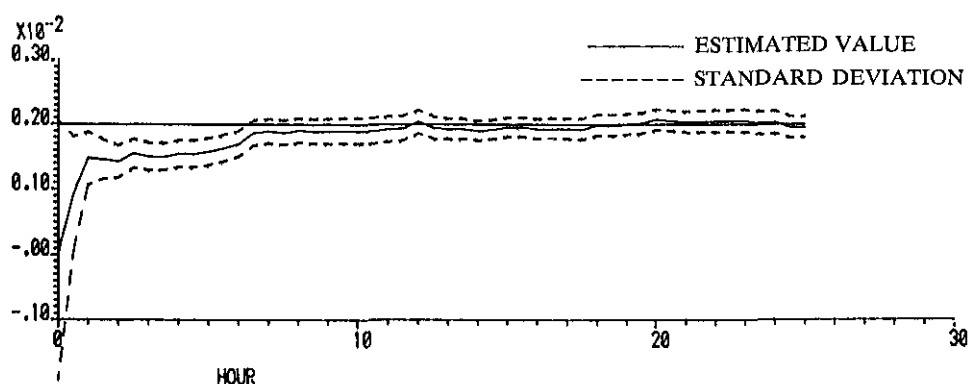


Figure 5.12: Estimation of the bottom friction coefficient in case of a system noise variance of 1.0×10^{-7} .

- (figure 5.13)

$$E \{ W_\mu^2 \} = 10^{-8}$$

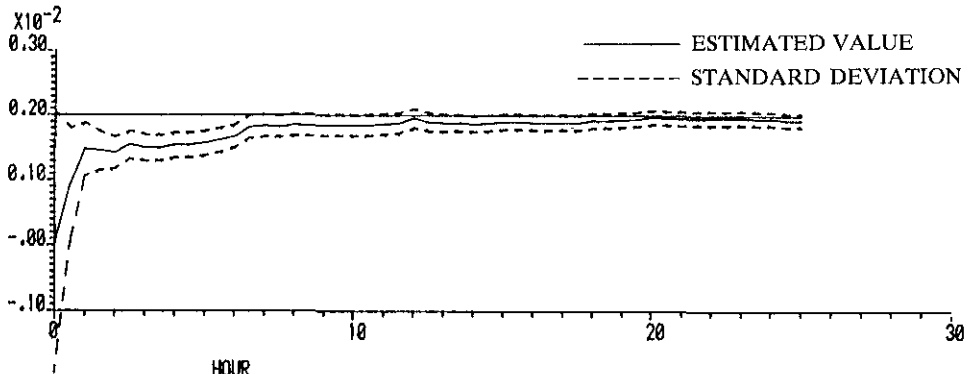


Figure 5.13: Estimation of the bottom friction coefficient in case of a system noise variance of 1.0×10^{-8} .

The system noise processes associated with the momentum and continuity equations are chosen as in experiment 5.1, independent of the other noise components.

The results show a satisfactory performance of the filter. Only in case of a system noise variance of 10^{-8} a small bias error in the parameter estimate can be noticed (figure 5.13).

Experiment 5.4

As was shown in experiment 5.2 the non-linearities of the model are relatively small and a constant gain filter is often an accurate approximation of the extended Kalman filter. Therefore, we may expect that the effect of the bias correction terms on the estimates of the water-level and velocity is usually very small. However, in case also the uncertain parameters in the model are estimated by the filter, significant non-linearities are introduced and consequently, the correction produced by these terms is more important.

To study the influence of the bias correction terms on the parameter estimates, in this experiment the filter is employed with and without these terms. The truth-model and the filter-model are both chosen as in experiment 5.3. The results are shown in, respectively, figures 5.14 and 5.15. To eliminate the effect of the random generator this experiment is also performed using measurements without generated measure-

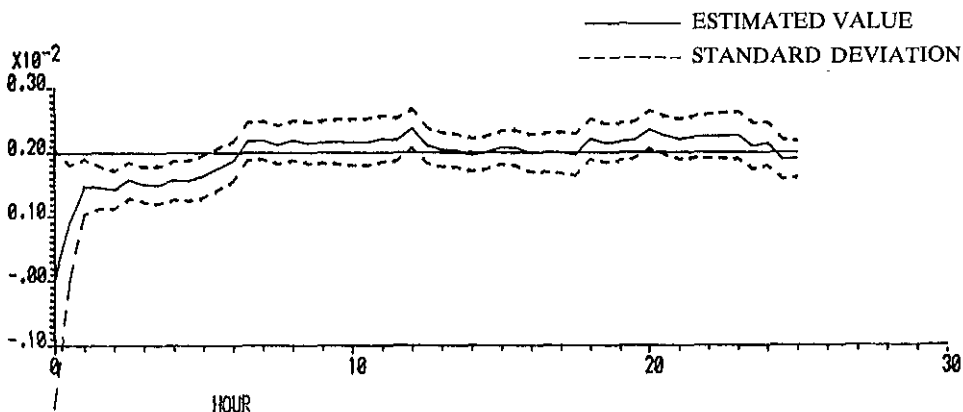


Figure 5.14: Estimation of the bottom friction coefficient without bias correction terms.

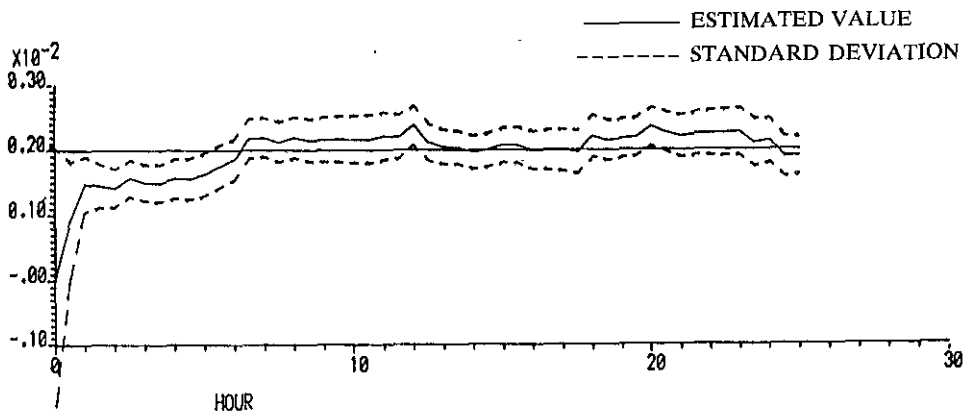


Figure 5.15: Estimation of the bottom friction coefficient with bias correction terms.

ment noise. In the filter-model it is still assumed that $r=0.1$ m. In this case the results are not masked by the noise component of the observations and it becomes possible to notice some details. These results are shown in *figures 5.16 and 5.17*. It is clear from these figures that the effect of the bias correction terms is very small. However, a small improvement can be noticed. Here we note that this effect depends very much on the non-linearities in the model. In very shallow water the improvement is more important. Note from *figures 5.16 and 5.17* the periodic behaviour of the parameter estimates. This is caused by the fact that the bottom friction can be identified more accurately during ebb and flood tides and less accurately during the turn of the tide.

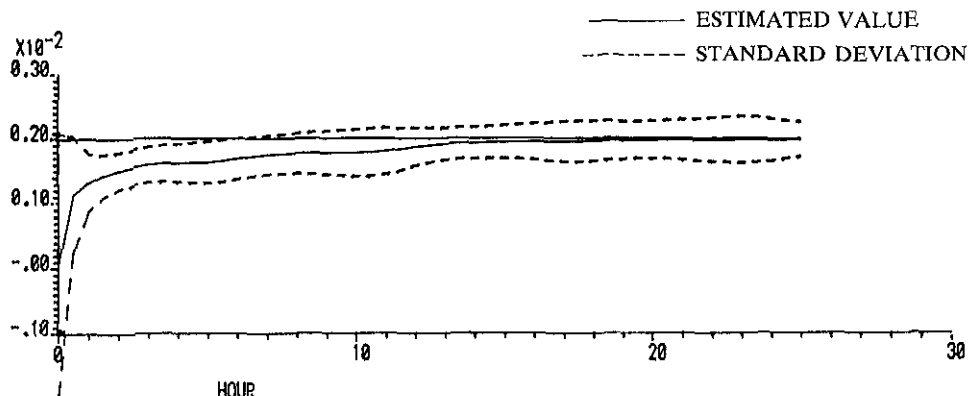


Figure 5.16: Estimation of the bottom friction coefficient without bias correction terms using noise-free observations.

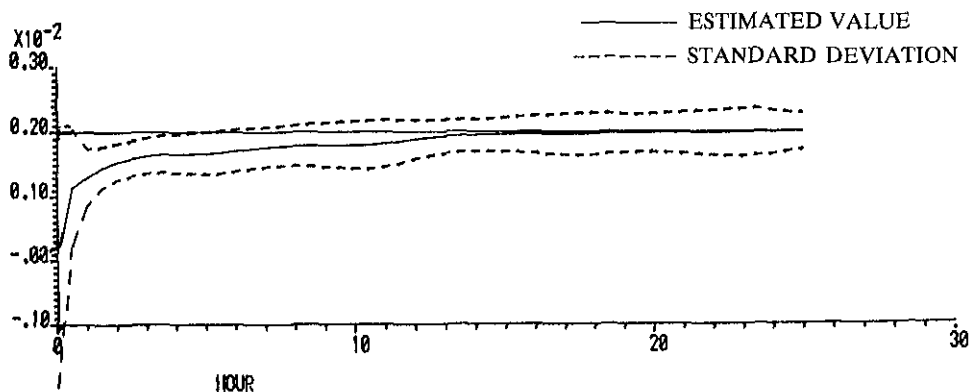


Figure 5.17: Estimation of the bottom friction coefficient with bias correction terms using noise-free observations.

Experiment 5.5

In order to verify that the filter is able to identify all the uncertain parameters simultaneously we employ the filter to estimate the water-level and velocities as well as the parameters μ , γ , a_1 , a_2 , a_3 , a_4 , a_5 and a_6 . As in experiment 5.1 we generate measurements with $r=0.1$ m. However, now we assume a constant wind of 15 m/s to occur along the x-axis. The initial estimation of the parameters are chosen to be:

$$\begin{aligned}\hat{\mu}_0 &= 0.0 & E\{(\mu_0 - \hat{\mu}_0)^2\} &= 4.0 \times 10^{-6} \\ \hat{\gamma}_0 &= 1.0 \times 10^{-6}, & E\{(\gamma_0 - \hat{\gamma}_0)^2\} &= 4.0 \times 10^{-12}\end{aligned}$$

$$\begin{aligned}
 \hat{a}_{1_0} &= 0.10, & E\{(a_{1_0} - \hat{a}_{1_0})^2\} &= 0.04 \\
 \hat{a}_{2_0} &= 0.15, & E\{(a_{2_0} - \hat{a}_{2_0})^2\} &= 0.04 \\
 \hat{a}_{3_0} &= -0.15, & E\{(a_{3_0} - \hat{a}_{3_0})^2\} &= 0.04 \\
 \hat{a}_{4_0} &= 0.15, & E\{(a_{4_0} - \hat{a}_{4_0})^2\} &= 0.04 \\
 \hat{a}_{5_0} &= -0.10, & E\{(a_{5_0} - \hat{a}_{5_0})^2\} &= 0.04 \\
 \hat{a}_{6_0} &= 0.15, & E\{(a_{6_0} - \hat{a}_{6_0})^2\} &= 0.04
 \end{aligned}$$

The corresponding system noise components are assumed to be:

$$\begin{aligned}
 E\{W_\mu^2\} &= 10^{-6} \\
 E\{W_\gamma^2\} &= 10^{-12} \\
 E\{W_{a_1^2}\} &= 0.001 \\
 E\{W_{a_2^2}\} &= 0.001 \\
 E\{W_{a_3^2}\} &= 0.001 \\
 E\{W_{a_4^2}\} &= 0.001 \\
 E\{W_{a_5^2}\} &= 0.001 \\
 E\{W_{a_6^2}\} &= 0.001
 \end{aligned}$$

The other noise processes are chosen as in experiment 5.3.

The results that are presented in figures 5.18 and 5.19 indicate that the filter is able to identify all the parameters simultaneously. Here we note that since the length of the channel that has been considered is quite short, the wind effect is small compared to the measurement noise. As a consequence, the wind friction parameter cannot be identified very accurately. Of course, the observability of this parameter not only depends on the length of the channel but also very much on the wind velocity.

5.5 A Kalman filter based on an Eastern Scheldt model

The filter described in the Sections 5.2 and 5.3 has been applied to field data recorded during a stormy period (September 11-13, 1975). Predictions of the water-level at the mouth of the Eastern Scheldt are made 1.5 hours ahead. The results can be found in Heemink and de Jong (1982). The filter is shown to be capable of adapting the model to varying circumstances while the inaccuracies in the bottom geometry are easily compensated by adjusting the bottom friction coefficient and the parameters a_i introduced in the observation equation (5.26). However, at the mouth of the estuary systematic differences between measurements and predictions are observed. These errors are mainly due to the interaction of the tidal wave along the coast and the water movement in the Eastern Scheldt. To improve the filter Ten

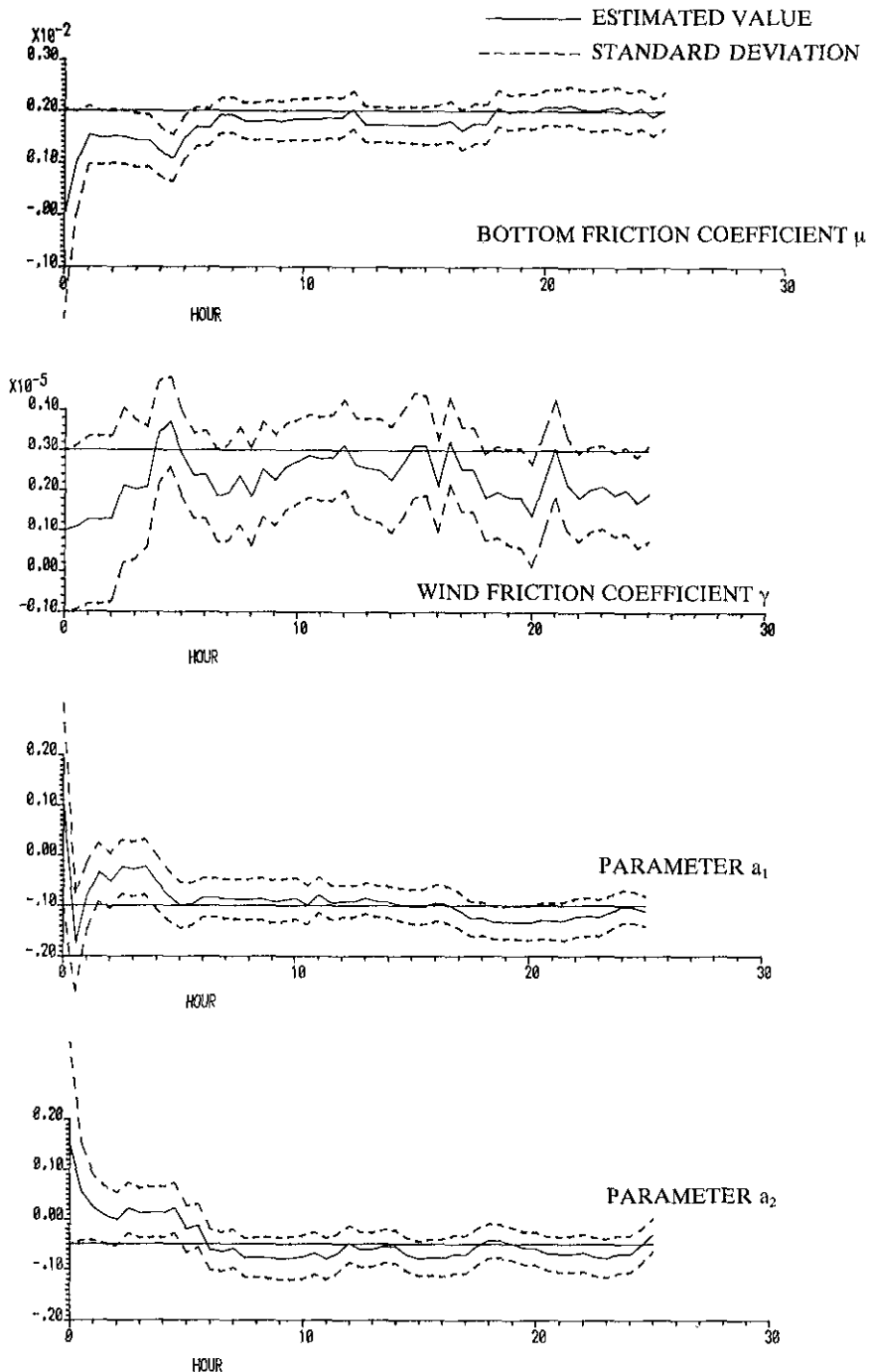


Figure 5.18: Simultaneous estimation of the parameters.

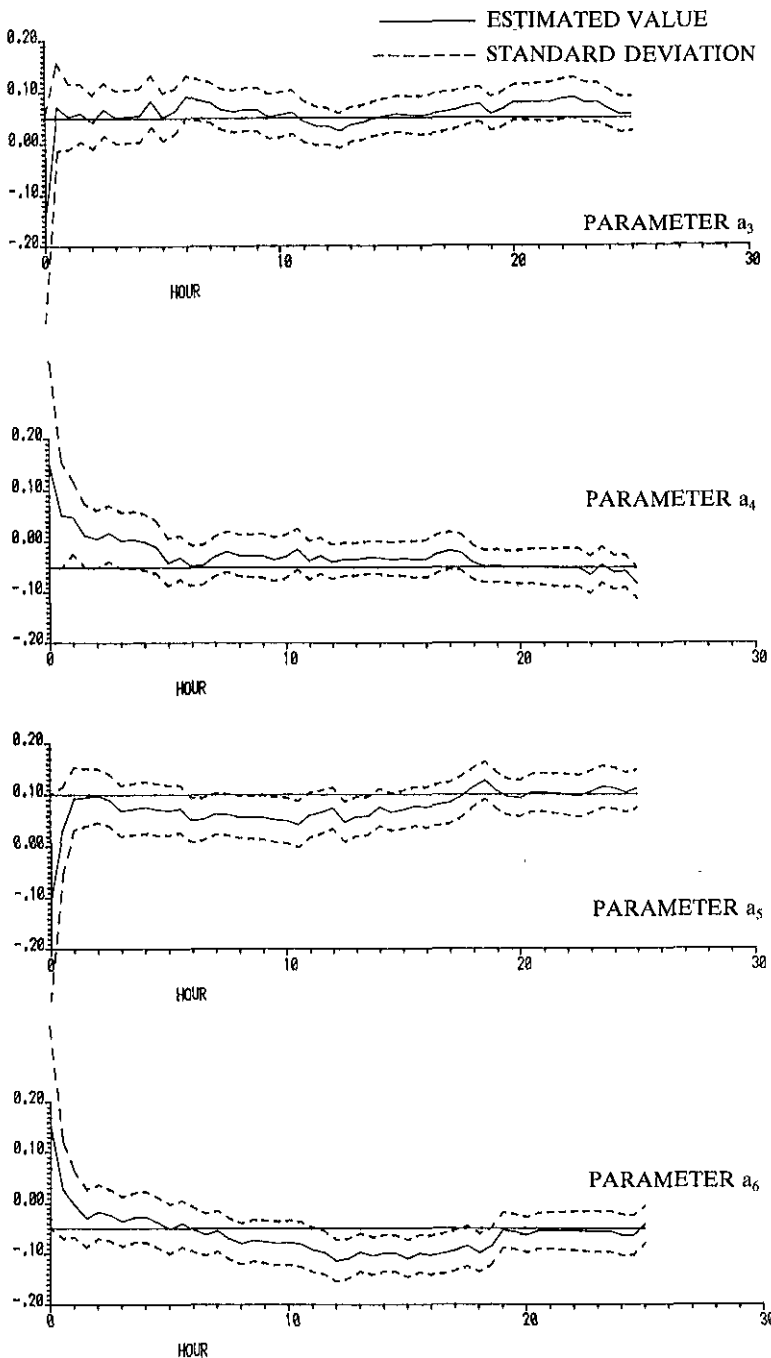


Figure 5.19: Simultaneous estimation of the parameters.

Brummelhuis and de Jong have developed a Kalman filter based on an Eastern Scheldt model which has been linked to the filter described in the Sections 5.2 and 5.3 (Ten Brummelhuis, de Jong and Heemink 1984). The filter is derived and tested in a similar way as the filter based on the model along the coast (Ten Brummelhuis, 1984). However, a few important differences can be noted. In this section we briefly describe the filter of Ten Brummelhuis and de Jong and discuss the differences mentioned. A more thorough description can be found in Ten Brummelhuis, de Jong and Heemink (1984, 1985).

The basis of the model consists of the St. Venant equations describing the tidal motion in a channel with a specific geometrical configuration*:

$$\frac{\partial u}{\partial t} + u \frac{\partial u}{\partial x} + g \frac{\partial u}{\partial x} + \mu \frac{u|u|P}{A} - \gamma \frac{bV^2 \cos \psi}{A} = 0 \quad (5.34)$$

$$\frac{\partial h}{\partial t} + \frac{1}{b} \frac{\partial(uA)}{\partial x} = 0 \quad (5.35)$$

where:

$A(x, h)$ = cross sectional area

$b(x, h)$ = width of the channel

$P(x, h)$ = wetted perimeter

$u(x, t)$ = velocity averaged over $A(x, h)$

In figure 5.20 the main stream sections in the Eastern Scheldt are shown.

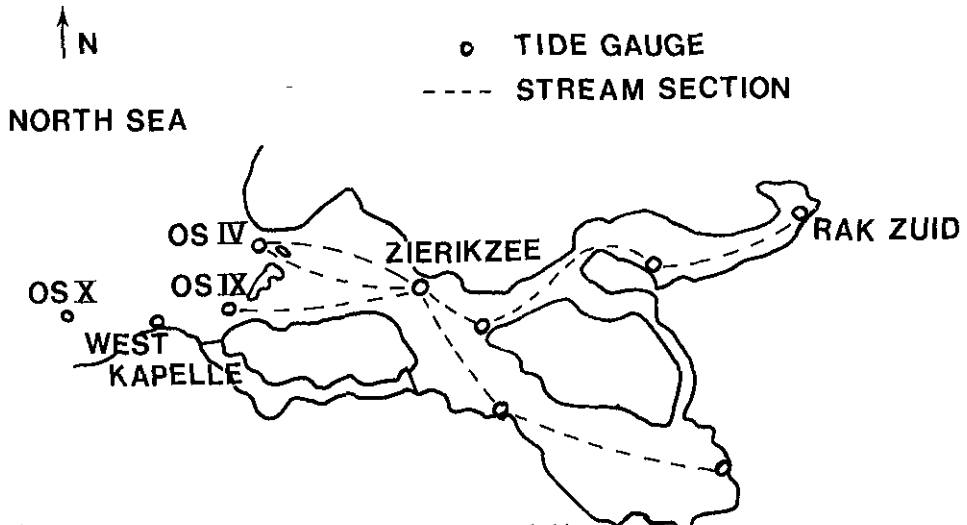


Figure 5.20: The main stream sections in the Eastern Scheldt.

* These equations can be derived similarly as the one-dimensional shallow water equations described in Chapter 2 (Cunge, Holly and Verwey 1978).

At a network junction the total inflow is constrained to equal the total outflow (see figure 5.21):

$$\sum_{i=1}^3 u_i A_i(x, h_i) = 0 \quad (5.36)$$

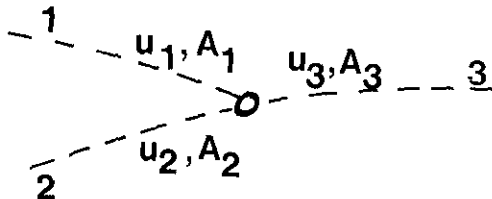


Figure 5.21: A network junction.

In addition, continuity of the quantity $h + \alpha(u^2/2g)^*$ is assumed:

$$h_1 + \alpha_1 \frac{u_1^2}{2g} = h_2 + \alpha_2 \frac{u_2^2}{2g} = h_3 + \alpha_3 \frac{u_3^2}{2g} \quad (5.37)$$

where $\alpha_i, 0 \leq \alpha_i \leq 1$ have to be specified (Dronkers 1964). At both closed ends of the estuary a boundary condition allowing for a certain amount of reflection is prescribed by the introduction of a reflection coefficient (see Chapter 2).

In estuarine problems implicit finite difference methods are recommended to discretise the partial-differential equations involved since these schemes are unconditionally (linearly) stable (Cunge, Holly and Verwey 1980). Therefore, the Preissmann four points scheme is chosen to approximate the equations (5.34) and (5.35). An additional advantage of this scheme is the relatively simple implementation of the boundary conditions and of the equations (5.36) and (5.37). Furthermore, using the Preissmann scheme it is very easy to deal with non-equidistant grids.

In a similar way as described in Sections 5.2 and 5.3 the Kalman filter is employed to produce estimates of the water-levels and velocities as well as the uncertain parameters in the model: bottom friction coefficients, the wind stress coefficient and the reflection coefficients. At the measurement stations OS X or West Kapelle the

* The factor α is introduced to account for local effects. Note that for $\alpha = 1$ this quantity is the energy head.

model along the coast is linked to the model of the Eastern Scheldt (see figure 5.20). Here the estimates and predictions of the water-level together with their accuracy as predicted by the model along the coast serve as the boundary condition for the Eastern Scheldt model.

5.6 Experiments using field data

In this section we describe some experiments with the combined Kalman filter using data gathered in the southern part of the North Sea. During September 12-13, 1975, water-level measurements were taken at the locations indicated in figure 5.22. Observations of the wind were available from the station BG II (see figure 5.23). To get insight into the predictive capability of the filter, in figure 5.24 we construct the observability domain and the prediction horizon as described in Section 4.7. In predicting the water-levels and velocities the boundary at KNIKPUNT I has to be extrapolated. In general, this extrapolation is relatively inaccurate. In this case the prediction horizon indicates the maximum length of the time interval during which the predictions are not affected by this extrapolated boundary condition.

The space steps Δx_i are chosen so that the x-coordinate of the measurement stations coincide with grid points, yielding $8000 \leq \Delta x_i \leq 10.000$. In view of the relation (4.33) $\Delta t = 7.5$ min.

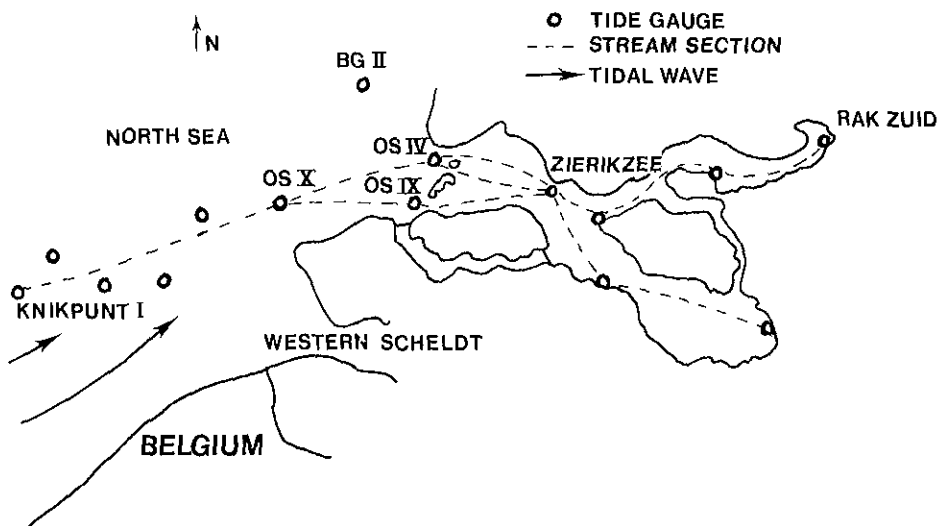


Figure 5.22: Tide gauges available during September 1975.

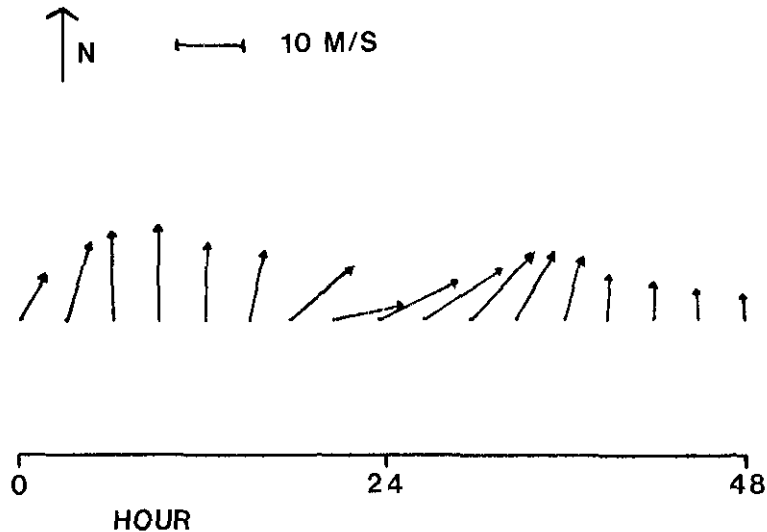


Figure 5.23: Observations of the wind at the measurement station BG II during September 12 1975, 00:00 – September 14 1975, 00:00.

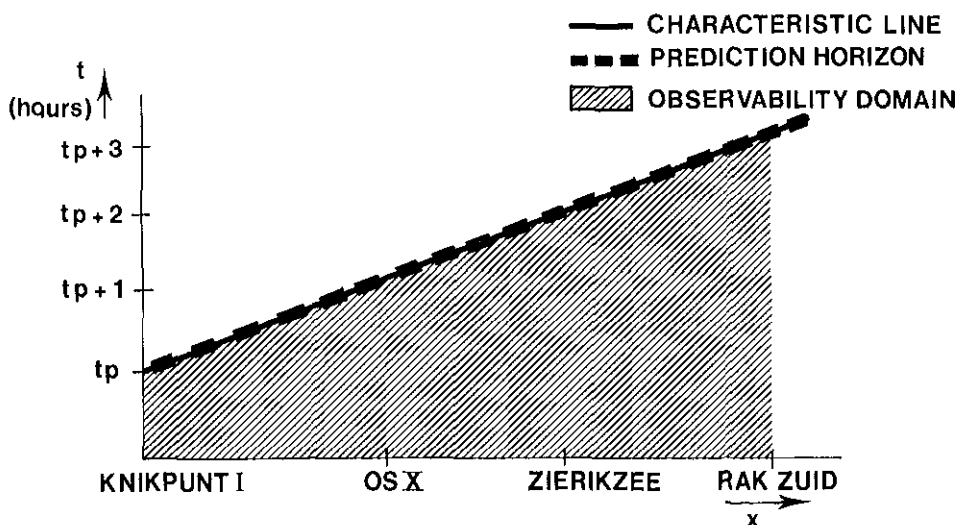


Figure 5.24: Observability domain and prediction horizon.

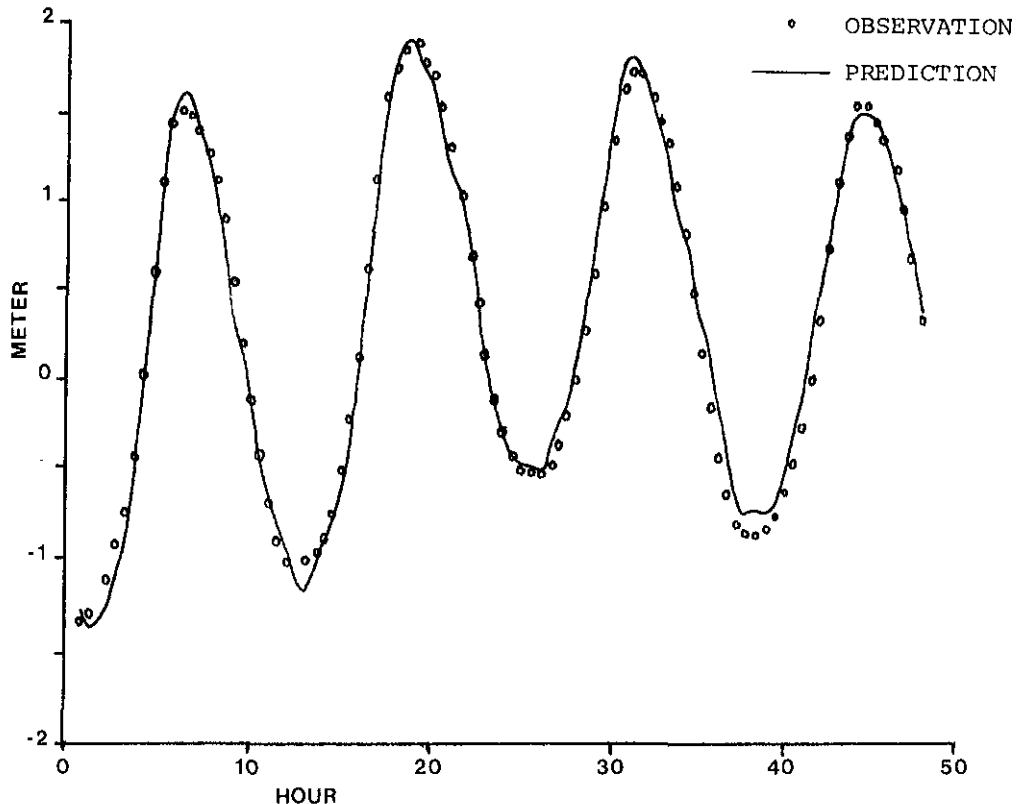


Figure 5.25: One and a half hours ahead predictions at OS IV.

We choose the statistics of the system noise processes associated with the momentum and continuity equation to be:

$$Q_m(|x_{i_1} - x_{i_2}|) = 4.0 \times 10^{-4} e^{-0.9 |(x_{i_1} - x_{i_2})/10000|}$$

$$Q_c(|x_{i_1} - x_{i_2}|) = 4.0 \times 10^{-4} e^{-0.9 |(x_{i_1} - x_{i_2})/10000|}$$

The system noise is introduced each time step. The system noise components of the boundary condition at $x = x_0$ and of the parameters are assumed to be independent of the noise processes described above with statistics:

$$E\{Wb^2\} = 0.0016$$

$$E\{W_\mu^2\} = 10^{-7}$$

$$E\{W_\gamma^2\} = 10^{-12}$$

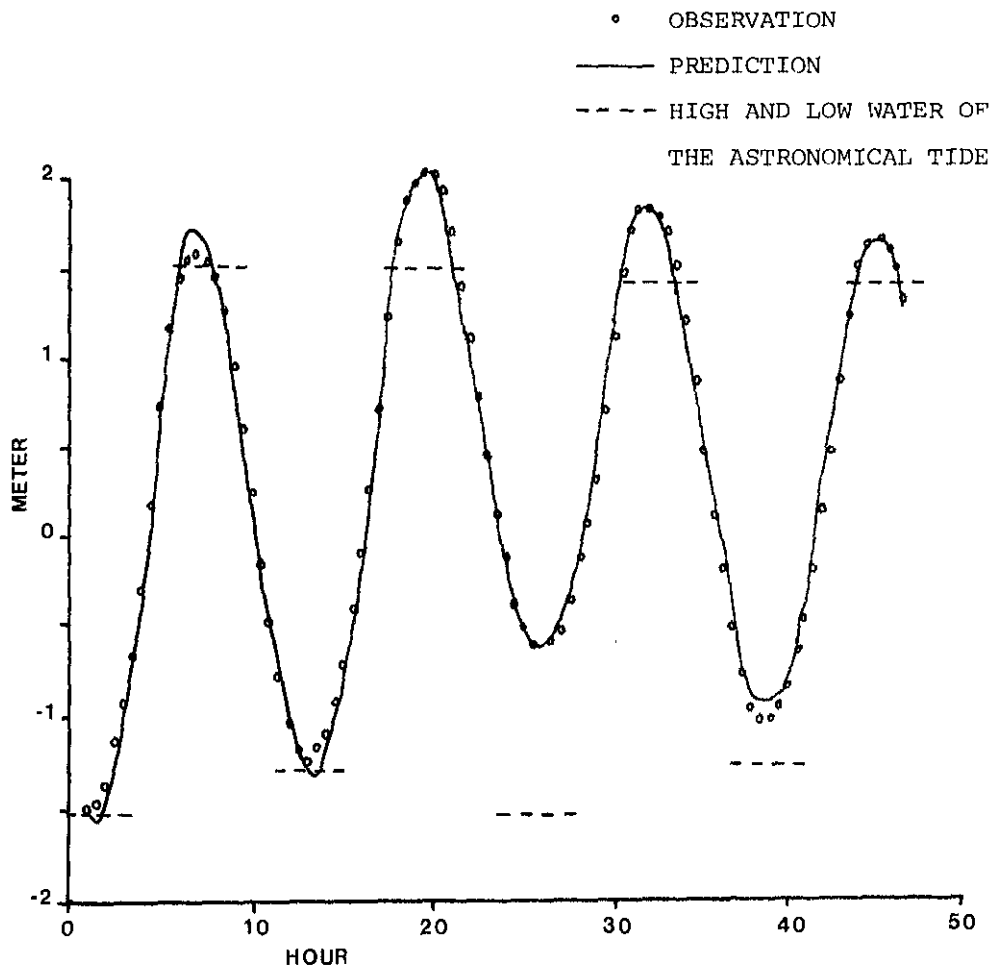


Figure 5.26: Two hours ahead predictions at Zierikzee,

$$E\{W_{a_1}^2\} = 0.001$$

$$E\{W_{a_2}^2\} = 0.001$$

$$E\{W_{a_3}^2\} = 0.001$$

$$E\{W_{a_4}^2\} = 0.001$$

$$E\{W_{a_5}^2\} = 0.001$$

$$E\{W_{a_6}^2\} = 0.001$$

Finally the measurement noise is chosen to be:

$$r = 0.03 \text{ m}$$

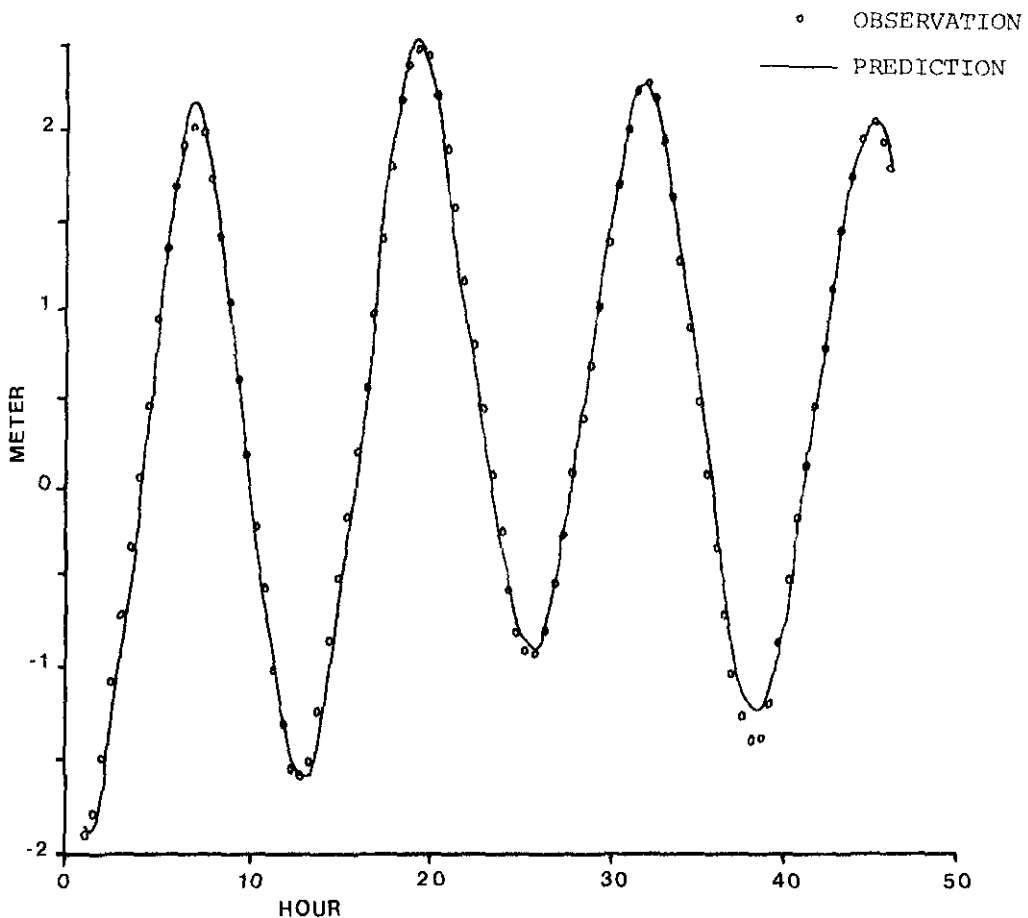


Figure 5.27: Three hours ahead predictions at Rak Zuid.

The specification of these noise statistics is established by a combination of "physical intuition" and "trial and error".

As described in Section 4.7 physically the choice of the initial value of the water-levels and velocities as well as their uncertainty is not relevant. However, since these uncertainties are very poorly known and in addition the difference between the first measurements available and the model predictions can be very large, numerical difficulties are likely to occur. Filtering the first observations often yield unrealistic estimates of water-levels and velocities and, as a consequence, can introduce instabilities. To avoid these problems the first tidal period is estimated without filtering the data available. After this period the initial uncertainties have vanished.

Furthermore, since deterministic models usually give a reasonable description of the tidal movement we may expect that the differences between the first measurements and the results of the model are now limited.

In the *figures 5.25 - 5.27* representative examples are shown of the predictions of the water-level in some of the measurement locations.

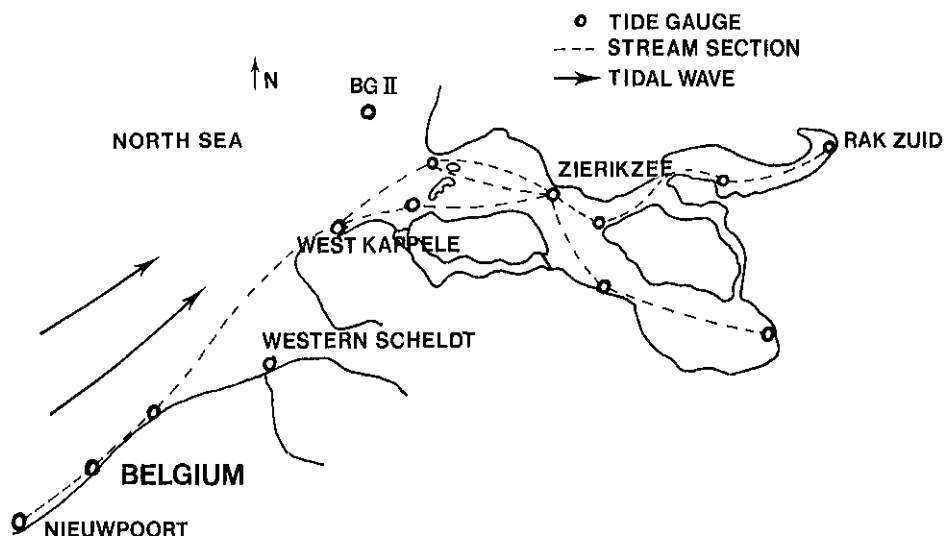


Figure 5.28: Tide gauges available during January-February 1983.

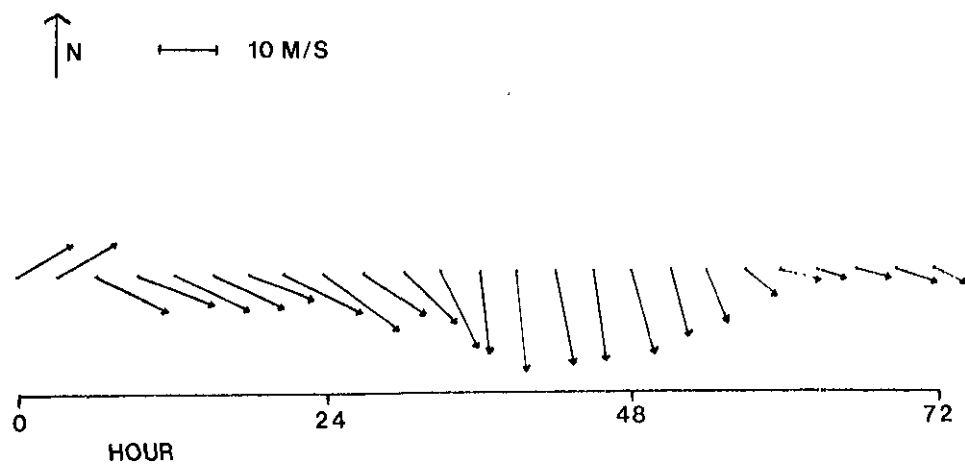


Figure 5.29 Observations of the wind at the measurement station BG II during January 18 1983,00:00 -- January 21 1983, 00:00.

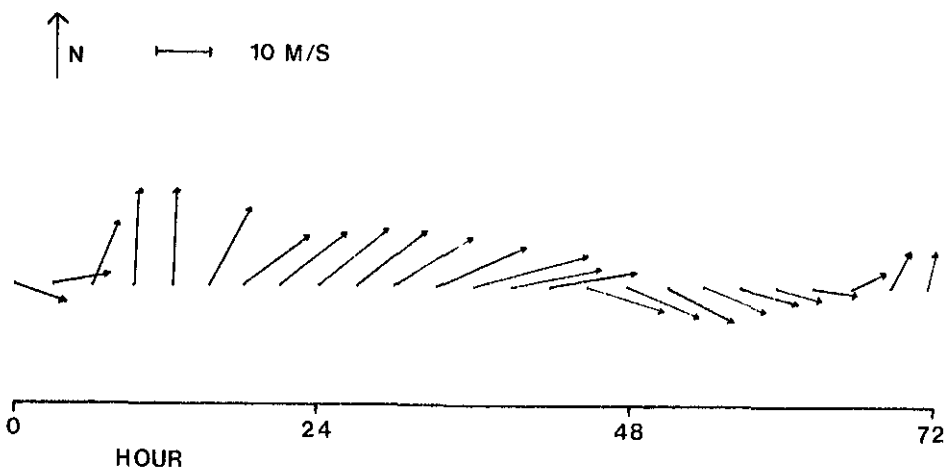


Figure 5.30: Observations of the wind at the measurement station BG II during January 31 1983, 00:00–February 3 1983, 00:00.

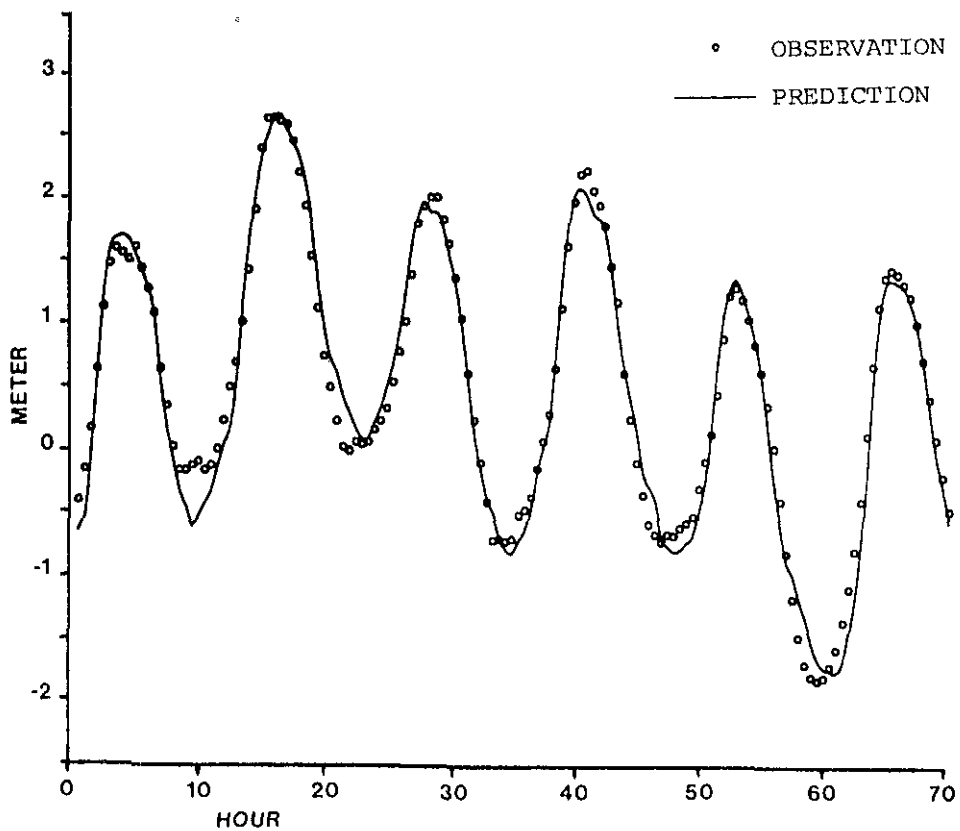


Figure 5.31: One and a half hours ahead predictions at OS IX.

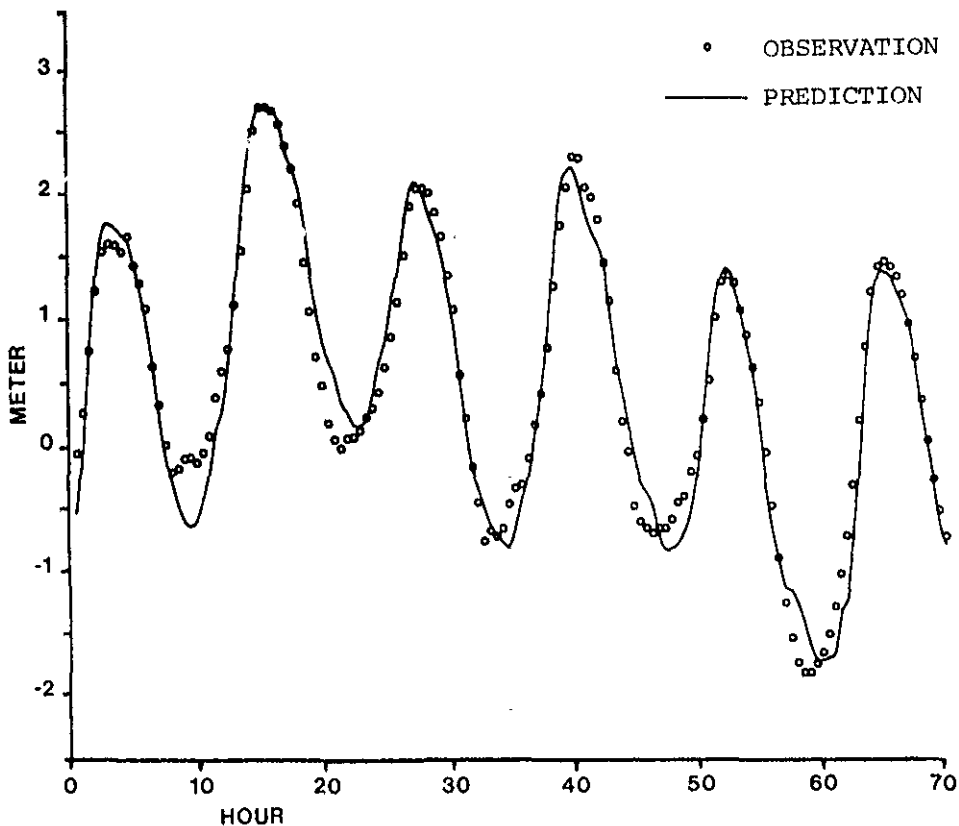


Figure 5.32: Two hours ahead predictions at OS IV.

During two very stormy periods, January 18-20, 1983 and January 31 - February 2, 1983, water-level measurements were available at the stations shown in figure 5.28. The wind velocities measured during these periods at BG II can be found in the figures 5.29 and 5.30. Constructing the observability domain and the prediction horizon yields similar results as shown in figure 5.24. However, using these observations the prediction horizon at the Eastern Scheldt is increased with half an hour. In the figures 5.31 - 5.38 the water-level predictions are shown. The results show that the filter is able to produce accurate predictions. However, in some cases significant errors can be noticed. These errors are mainly caused by:

- The meteorological input (or, which amounts to the same thing, by the simple empirical parametrizations describing the influence of the wind on the water movement).

During the periods that have been considered, wind data were available only from a single measurement station. These observations of the wind have to be

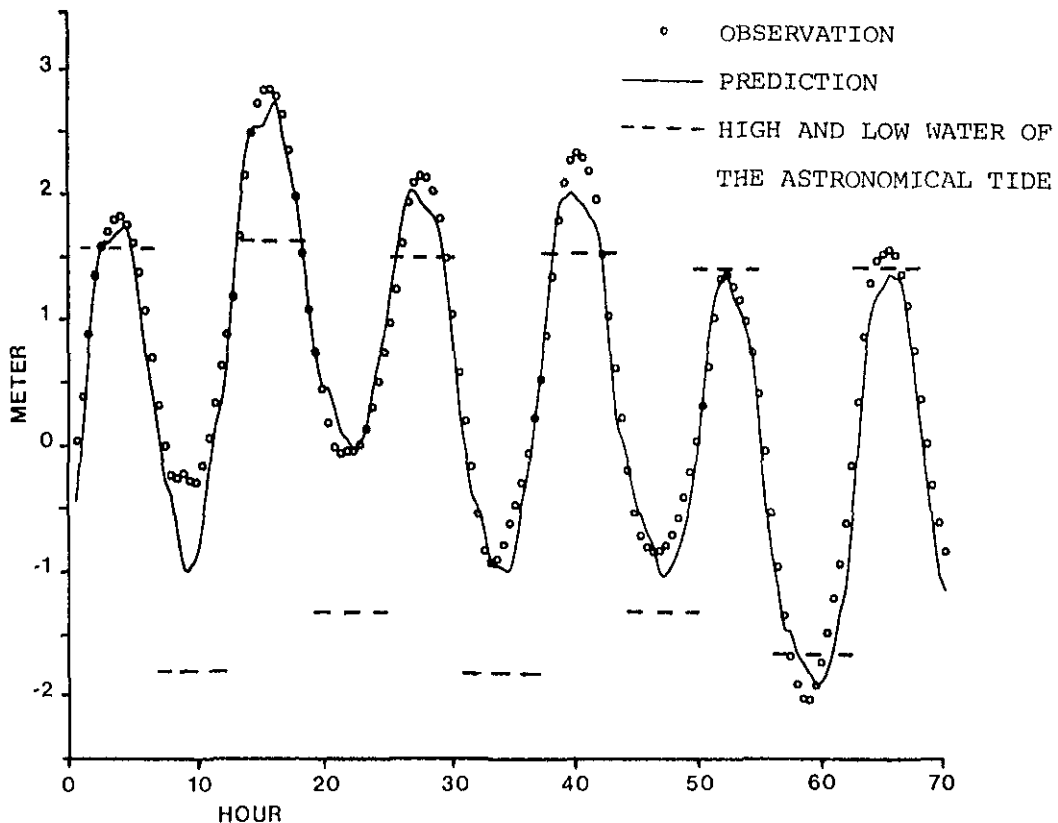


Figure 5.33: Two and a half hours ahead predictions at Zierikzee.

assumed to be valid for the entire domain of the model neglecting the spatial variability of the wind. Of course, this assumption is questionable. During September 12-13, 1975, the wind velocities were relatively small and therefore, the influence of the meteorological input is small too. As a consequence, during this period the water-level predictions are accurate. However, during the two very stormy periods the incorrect meteorological input introduces important errors (see figure 5.38 at $t = 22$ hours).

If the meteorological conditions strongly vary in space a two-dimensional model has to be employed. In this case it is possible to use the wind fields as computed by a numerical model of the atmosphere. A filter based on a two-dimensional model is described in Chapter 6.

- The free outflow condition at $x = x_L$ (BG II).

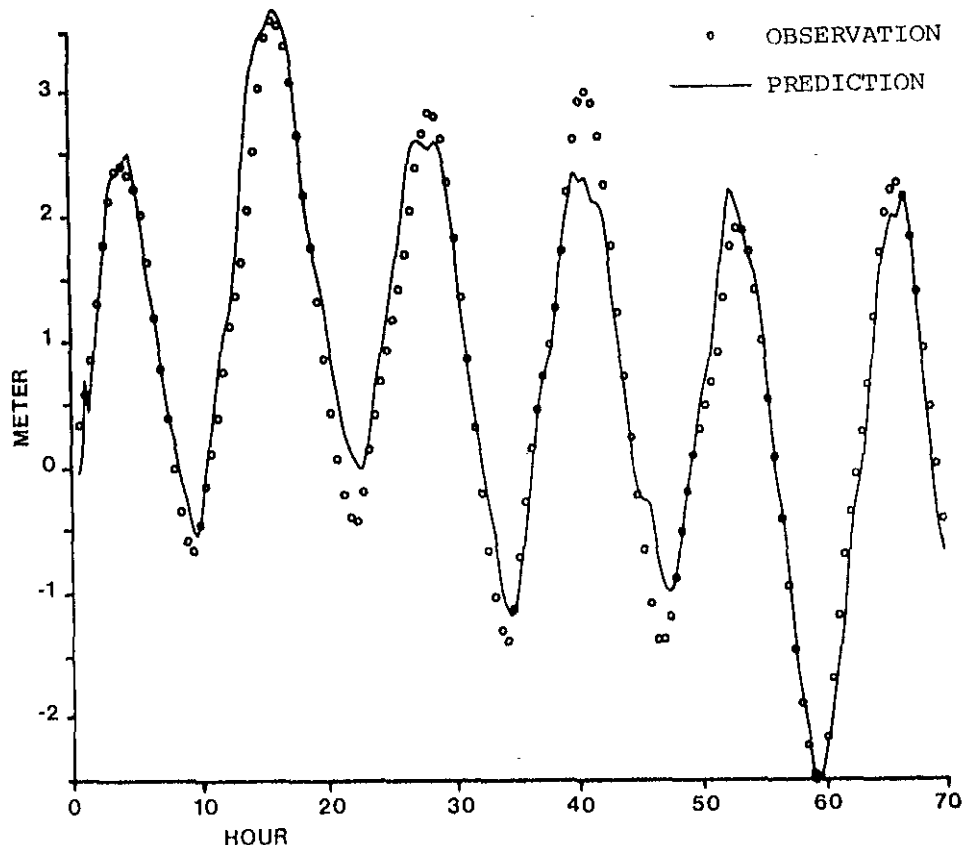


Figure 5.34: Three hours ahead predictions at Rak Zuid.

As described in the Subsection 5.2.2 the tidal waves and surges often propagate from the south, along the coast, toward the north. Therefore, a free outflow condition is prescribed at $x = x_L$. This procedure is of course not correct for all cases (see figure 5.31 at $t = 11$ hours).

- The relatively crude grid of the Eastern Scheldt model. This is due to storage restrictions occurring when using the programming language ALGOL on the UNIVAC 1100/60 of the Rijkswaterstaat.

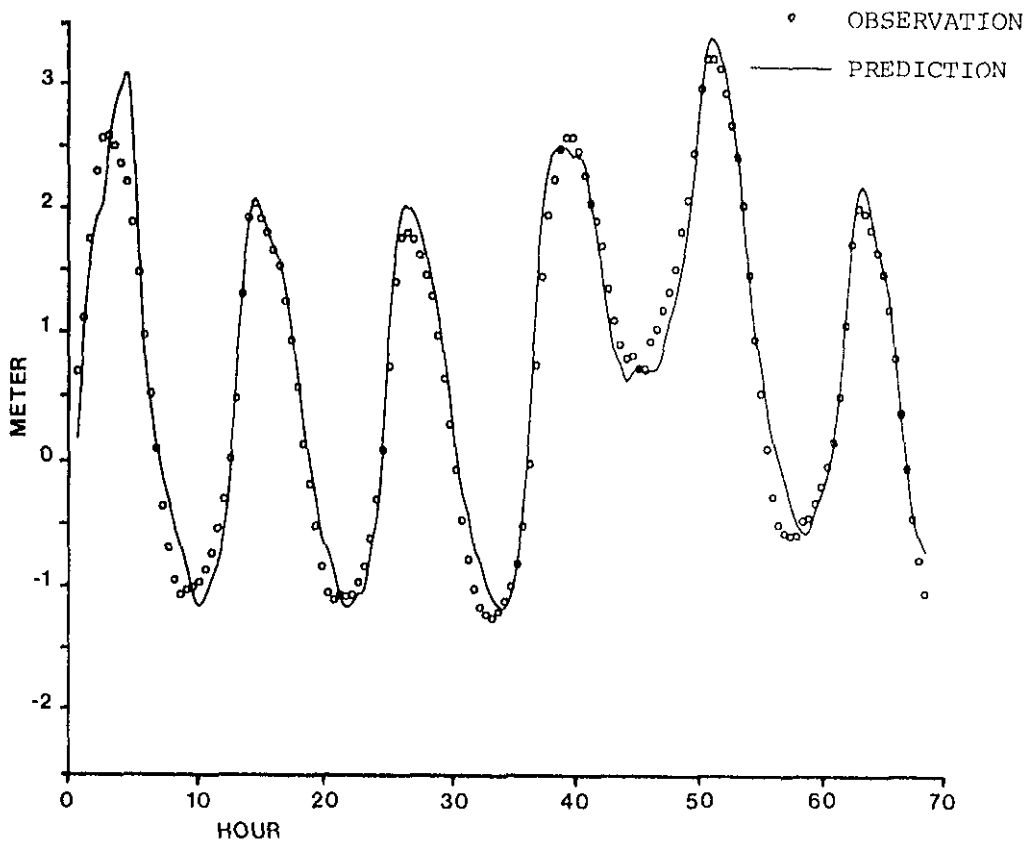


Figure 5.35: One and a half hours ahead predictions at OS IX.

5.7 Discussion

In this chapter a Kalman filter based on a conceptual one-dimensional model has been developed and tested using simulated data as well as field data. After discussing the main characteristics of the tidal movement and the meteorological effects in the southern part of the North Sea qualitatively, a model describing the water movement along the coast is derived. Using the results of Chapter 4 the finite difference scheme and the system noise processes are chosen such that numerical difficulties are avoided. Experiments with the simulated data reveal that the filter is successful in

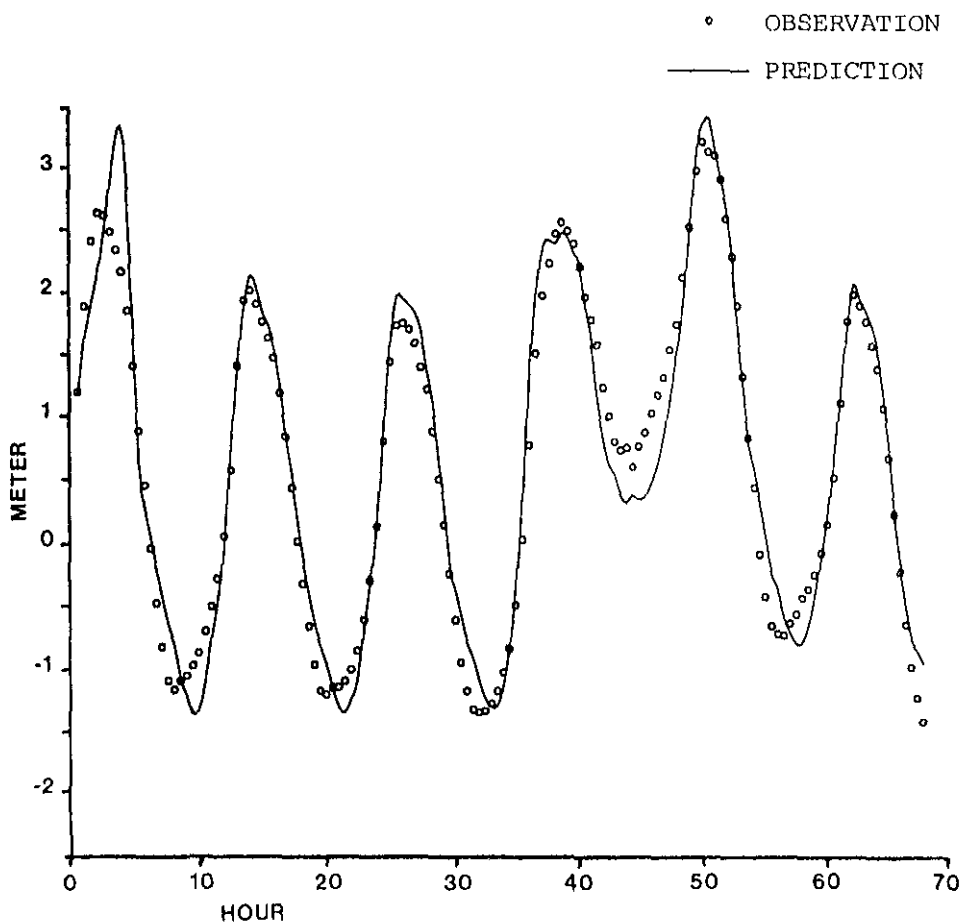


Figure 5.36: Two hours ahead predictions at OS IV.

estimating uncertain parameters in the model. Here we note that both the number of parameters to be estimated as well as the statistics of the system noise components representing the uncertainty of these parameters, have to be chosen with care to avoid filter divergence.

To be able to predict the water-level in the Eastern Scheldt the filter is combined with a similar Kalman filter approach which has been developed by Ten Brummelhuis and de Jong to estimate water-levels, velocities and uncertain parameters in the model of this estuary.

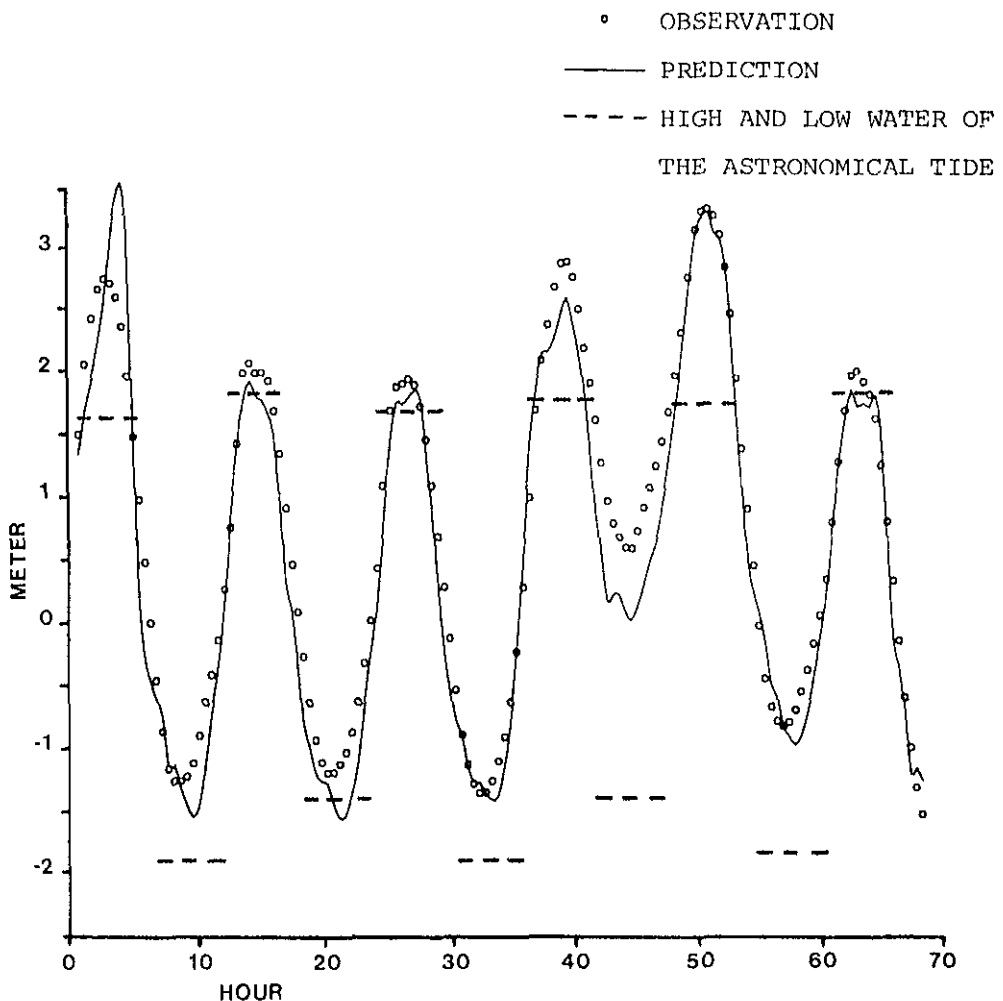


Figure 5.37: Two and a half hours ahead predictions at Zierikzee.

The combined filter has been tested extensively using field data gathered during a number of stormy periods. The results show satisfactory filter performance, although in some cases significant errors have occurred. These errors are mainly caused by the simple modelling of the two-dimensional phenomena. Furthermore, the one-dimensional approximation of the tidal movement being only realistic for a small part of the southern North Sea, the time interval over which accurate predictions can be produced is limited. To overcome these difficulties we have developed a Kalman filter that is based on a two-dimensional model of the entire North Sea. This filter is described in Chapter 6.

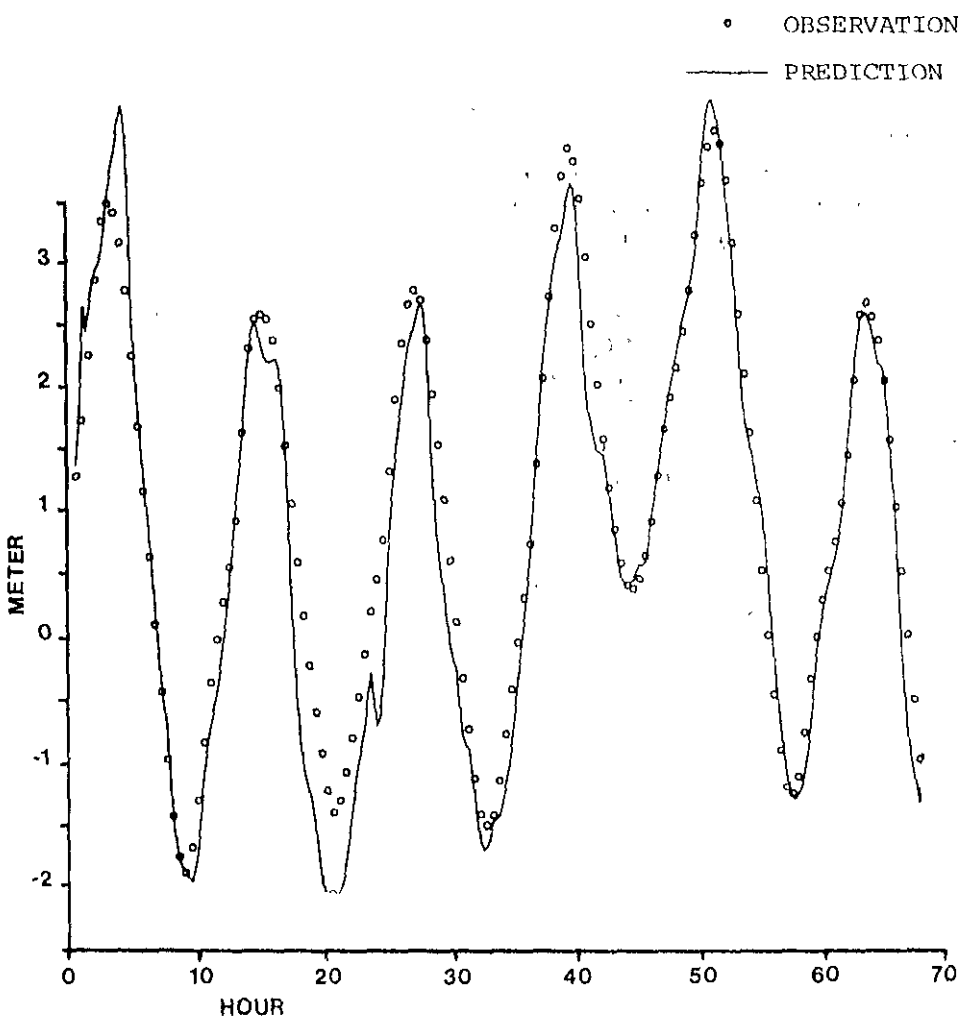


Figure 5.38: Three hours ahead predictions at Rak Zuid.

Using the insight gained from the experiments with the one-dimensional approach, WAKFIL, a general software package for one-dimensional tidal filtering, has been developed in cooperation with the Hydraulics Laboratory. It is based on the IMPLIC system developed by Rijkswaterstaat for the deterministic description of the tidal movement in branched estuaries or rivers. Since IMPLIC uses the Preissmann scheme to discretise the St. Venant equations (Dronkers 1969), the filter also makes use of this finite difference scheme. With WAKFIL it becomes possible to combine the Kalman filter procedure with any existing IMPLIC model with approximately less than 150 sections.

Applying the WAKFIL system it is intended to improve the one-dimensional approach described in this chapter by using an existing more detailed deterministic model of the Eastern Scheldt. In Chapter 7 we briefly discuss another possible improvement of the approach by combining the one-dimensional Kalman filter with the filter based on a two-dimensional model described in Chapter 6. In this way the sensitivity with respect to the erroneous meteorological input and the incorrect free outflow condition can be reduced.

In one experiment we demonstrate that the results of the constant gain extended Kalman filter are often nearly optimal. Since the filter is used to estimate uncertain parameters in the model this observation cannot be exploited in the one-dimensional approach. Moreover, since the computational effort of this extended Kalman filter is limited it is not necessary to use a time-invariant approximation. Of course, in developing a two-dimensional non-linear filter it is inevitable to use a suboptimal filter.

Finally we note that in this study attention has been concentrated on the use of Kalman filters to predict water-levels. As described in Chapter 1 these filters can also be used for optimized water-level monitoring networks and for improving the empirical parametrization in the mathematical model. A detailed discussion of these applications, together with a number of experiments using field data, can be found in Ten Brummelhuis, de Jong and Heemink (1985).

6 A Kalman filter based on a two-dimensional model

6.1 Introduction

The extension of the one-dimensional Kalman filter described in Chapter 5 to two space dimensions does not give rise to conceptual problems, but would impose a much greater computational burden. In order to obtain a computationally efficient filter, simplifications have to be introduced. However, there are serious problems with the more obvious simplifications one may consider.

One possibility may be to divide the domain of interest into a number of sub-regions and apply the filter to each sub-region individually. The main difficulty associated with this approach is that only the measurement stations located inside a sub-region are used by the filter to correct the estimates in this sub-region. The information available in other sub-regions cannot be incorporated to improve these estimates. As a consequence, strong variations may result between the components corresponding to sub-region boundaries and components corresponding to grid points immediately outside. Hence at the boundaries of the sub-regions artificial, high gradients are likely to be introduced. Although this Kalman filter approach has been successfully applied to predict diffusion processes (Fronza, Spirito and Tonielli 1979) we may expect serious difficulties if it is employed to predict the tidal movement. Since the system of the shallow water equations describing this movement is hyperbolic, the distortions introduced by the partial filtering would propagate through the entire domain of the problem probably causing unsatisfactory filter performance or instabilities.

Another approach would be to calculate the covariance matrix on a coarser grid than that used for the computation of the estimates. As a consequence, the correction produced by the filter is also available on the coarser grid and has to be extended to the finer grid to obtain the estimates. In case of a complicated boundary, this procedure is very complex and prone to numerical difficulties. Moreover, a covariance matrix calculated on the basis of a coarser mesh would be the covariance matrix for a model with different geometry. As Miller (1986) pointed out: it would be the right solution to the wrong problem. Still, this approach is worth exploring.

Another possibility for simplification would be to make an assumption about the structure of the covariance matrix. If it is assumed that errors at large distant points are not correlated, the covariance matrix is banded down its diagonal. The sparse-

ness of the covariance matrix can easily be exploited to reduce the computation time and the storage requirements. In our case however, the assumption just mentioned is not realistic since the errors are highly correlated in space.

Probably due to the difficulties described above, a realistic application of Kalman filtering to two-dimensional tidal prediction problems has not yet appeared in literature. Therefore, in this study we have developed a Kalman filter approach that can be combined with large deterministic tidal models.

The filter is based on a linear two-dimensional numerical model. The main advantage of using a linear model is that if the noise statistics are time-invariant the filter is time-invariant as well. Here we note that this assumption concerning the noise statistics is not very restrictive since very little is known (yet) about the time-varying behaviour of the noise processes and as a consequence, these processes are usually assumed to be stationary. In case the filter is time-invariant the time-consuming second moment calculations can be performed off-line on a large computer. Furthermore, by defining the system noise on a coarser grid than that used for the computation of the estimates, high dimensionality of the filter equations is avoided by using the Chandrasekhar-type algorithm.

In Section 6.2 the system representation of the model is derived. Based on this system the steady-state filter is developed in Section 6.3. Section 6.4 is devoted to an efficient implementation of the algorithm on a vector processor. To examine filter performance, it has been applied to simulated data as well as field data in Sections 6.5 and 6.6 respectively. Finally, the results are discussed in Section 6.7. Here, using the insights gained in Section 4.5 and 5.4, we propose to use a constant gain extended Kalman filter in the non-linear case.

6.2 The deterministic model

The model is based on the linearized shallow water equations (1.3) - (1.5). To obtain a discrete system representation of the model, the equations are discretised. Defining a space-staggered grid G_1 (see figure 6.1) and using the scheme proposed by Sielecki (Van der Houwen 1968) the difference equations become:

$$u_{i,j}^{k+1} = u_{i,j}^k - g \frac{\Delta t}{2\Delta x} (h_{i,j}^k - h_{i-1,j}^k) + \\ f \frac{\Delta t}{4} (v_{i-1,j}^k + v_{i-1,j+1}^k + v_{i,j}^k + v_{i,j+1}^k) - 2\Delta t \frac{\lambda u_{i,j}^k - V^2 \cos \psi}{D_{i,j} + D_{i,j+1}} \quad (6.1)$$

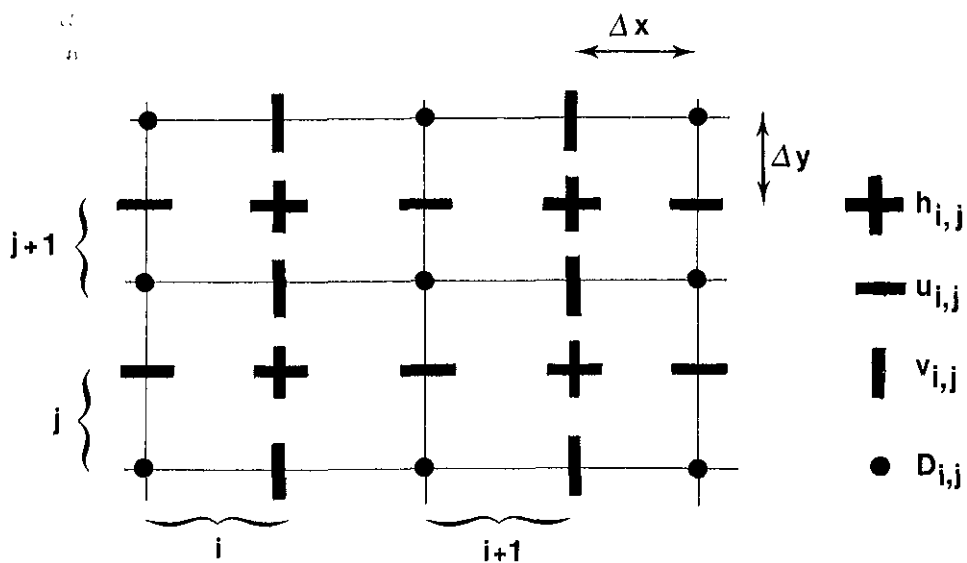


Figure 6.1: The space-staggered grid G_v .

$$v_{i,j}^{k+1} = v_{i,j}^k - g \frac{\Delta t}{2\Delta y} (h_{i,j}^k - h_{i,j-1}^k) - f \frac{\Delta t}{4} (u_{i,j-1}^{k+1} + u_{i+1,j-1}^{k+1} + u_{i+1,j}^{k+1} + u_{i,j}^{k+1}) - 2\Delta t \frac{\lambda v_{i,j}^k - V^2 \sin \psi}{D_{i,j} + D_{i+1,j}} \quad (6.2)$$

$$h_{i,j}^{k+1} = h_{i,j}^k - \frac{\Delta t}{4\Delta x} \left[(D_{i+1,j} + D_{i+1,j+1}) u_{i+1,j}^{k+1} - (D_{i,j} + D_{i,j+1}) u_{i,j}^{k+1} \right] - \frac{\Delta t}{4\Delta y} \left[(D_{i,j+1} + D_{i+1,j+1}) v_{i,j+1}^{k+1} - (D_{i,j} + D_{i+1,j}) v_{i,j}^{k+1} \right] \quad (6.3)$$

Here Δx and Δy are the distance steps, Δt is the time step and i, j, k are integer indices such that $u_{i,j}^k$, $v_{i,j}^k$ and $h_{i,j}^k$ are the finite difference approximations of $u((2i-1)\Delta x, 2j\Delta y, k\Delta t)$, $v(2i\Delta x, (2j-1)\Delta y, k\Delta t)$ and $h(2i\Delta x, 2j\Delta y, k\Delta t)$ respectively, and $D_{i,j} = D((2i-1)\Delta x, (2j-1)\Delta y)$. The wind speed and direction as a function of space and time are computed by means of a numerical model of the atmosphere. The grid of this model is much coarser than the grid G_v and therefore, interpolation is necessary to obtain the wind speed and direction in the grid points of G_v .

The finite difference approximation possesses second-order accuracy in space and first-order accuracy in time. It is a modification of the well-known Fischer scheme

(Van der Houwen 1968) that was used in developing the North Sea model described in Section 1.2.3. While the Fischer scheme is unstable for small bottom friction ($\lambda/D < f$), the scheme proposed by Sielecki does not have this shortcoming.

The amplification matrix of the Sielecki scheme can be shown to be (assuming the depth to be constant):

$$G(l_1, l_2) = A(l_1, l_2)^{-1} B(l_1, l_2) \quad (6.4)$$

where:

$$A(l_1, l_2) = \begin{bmatrix} 1 & 0 & 0 \\ \frac{f}{\Delta t} \cos(2\pi l_1 \Delta x) \cos(2\pi l_2 \Delta y) & 1 & 0 \\ D \frac{\Delta t}{\Delta x} \sin(2\pi l_1 \Delta x) & D \frac{\Delta t}{\Delta y} \sin(2\pi l_2 \Delta y) & 1 \end{bmatrix}$$

and

$$B(l_1, l_2) = \begin{bmatrix} 1 - \frac{\lambda \Delta t}{D} & \frac{f}{\Delta t} \cos(2\pi l_1 \Delta x) \cos(2\pi l_2 \Delta y) & g \frac{\Delta t}{\Delta x} \sin(2\pi l_1 \Delta x) \\ 0 & 1 - \frac{\lambda \Delta t}{D} & g \frac{\Delta t}{\Delta y} \sin(2\pi l_2 \Delta y) \\ 0 & 0 & 1 \end{bmatrix}$$

Here l_1 and l_2 are the wave numbers in respectively the x and y-directions.

If $g_m(l_1, l_2)$, $m = 1, 2, 3$, are the eigenvalues of $G(l_1, l_2)$ it can be shown that for $\lambda \ll D/\Delta t$, $f \ll 1/\Delta t$ and

$$\Delta t < \frac{2 \Delta x \Delta y}{\sqrt{gD(\Delta x^2 + \Delta y^2)}} \quad (6.5)$$

we have:

$$|g_m(l_1, l_2)| < 1, \quad m = 1, 2, 3 \quad (6.6)$$

with the exception of one eigenvalue with modulus one in case $l_1 = 1/2\Delta x$ and $l_2 = 1/2\Delta y$. Consequently, the scheme is stable. If the bottom friction parameter $\lambda = 0$, relation (6.5) is only necessary for stability since in this case:

$$|g_m(l_1, l_2)| = 1, \quad m = 1, 2, 3 \quad (6.7)$$

Equation (6.7) implies that without bottom friction the scheme is not dissipative. By analysing the wave-celerity as given by the amplification matrix it can be shown that for very short waves the computed wave-celerity is considerably less than the true wave-celerity (see Section 4.3).

If the difference scheme (6.1) - (6.3) is embedded in a Kalman filter, it is important that the very short waves are eliminated (see Section 4.5). Therefore, to improve stability we introduce a smoothing operator. At each time step the velocities are smoothed according to:

$$u_{i,j}^{k*} = (1 - (2 + 2(\frac{\Delta x}{\Delta y})^2)c) u_{i,j}^k + c((\frac{\Delta x}{\Delta y})^2 u_{i,j-1}^k + u_{i-1,j}^k + u_{i+1,j}^k + (\frac{\Delta x}{\Delta y})^2 u_{i,j+1}^k) \quad (6.8)$$

$$v_{i,j}^{k*} = (1 - (2 + 2(\frac{\Delta x}{\Delta y})^2)c) v_{i,j}^k + c((\frac{\Delta x}{\Delta y})^2 v_{i,j-1}^k + v_{i-1,j}^k + v_{i+1,j}^k + (\frac{\Delta x}{\Delta y})^2 v_{i,j+1}^k) \quad (6.9)$$

where $u_{i,j}^{k*}$ and $v_{i,j}^{k*}$ are the smoothed values of $u_{i,j}^k$ and $v_{i,j}^k$ respectively and $c < \frac{1}{2} \Delta y^2 / (\Delta x^2 + \Delta y^2)$ is a positive constant that is chosen as small as possible to guarantee that the finite difference scheme is still an accurate approximation of the equations (1.3) - (1.5). By defining the equations (6.8) and (6.9) we introduce numerical viscosity. It is easy to show that the smoothing operators (6.8) and (6.9) are the second-order approximations of respectively the diffusion terms:

$$\frac{4c\Delta x^2}{\Delta t} (\frac{\partial^2 u}{\partial x^2} + \frac{\partial^2 u}{\partial y^2}) \quad (6.10)$$

and

$$\frac{4c\Delta x^2}{\Delta t} (\frac{\partial^2 v}{\partial x^2} + \frac{\partial^2 v}{\partial y^2}) \quad (6.11)$$

The very short waves which cannot be represented by the finite difference approximations (6.1) - (6.3) in any case are now dissipated.

Wave motion is not completely described without boundary conditions. At a closed boundary where the velocity normal to the boundary is zero, no special boundary scheme is required. At an open boundary usually the water-level is prescribed:

$$h = f_H(t) \quad (6.12)$$

In addition it is assumed that along the open boundary the velocity parallel to the boundary is zero. This assumption is necessary only because of the discretised Coriolis terms.

From the numerical point of view, the boundary condition (6.12) is not very attractive since it is often prone to numerical reflections. A more stable condition would be obtained by prescribing a Riemann invariant at the open boundary (Stelling 1983):

$$v_{\perp} \pm \sqrt{\frac{g}{D}} h = f_R(t) \quad (6.13)$$

where v_{\perp} denotes the velocity normal to the boundary. However, Riemann invariants are quantities that are not measured in nature. As a consequence, the condition (6.13) cannot be used in general. In case we may neglect the in-going waves, $f_R(t)$ is approximately constant (see Chapter 2) and (6.13) reduces to the weakly reflective condition:

$$v_{\perp} \pm \sqrt{\frac{g}{D}} h = f_R(t_0) \quad (6.14)$$

or equivalently:

$$\frac{\partial}{\partial t} (v_{\perp} \pm \sqrt{\frac{g}{D}} h) = 0 \quad (6.15)$$

In order to profit from the stabilizing effect of Riemann invariants while water-levels are still prescribed as boundary conditions, Stelling (1983) proposed the following boundary condition:

$$h \pm \beta \left[\frac{\partial}{\partial t} (v_{\perp} \pm \sqrt{\frac{g}{D}} h) \right] = f_H(t) \quad (6.16)$$

For sufficiently small values of $\beta > 0$ the condition (6.16) is an accurate approximation of (6.12) while for very short wave lengths (6.16) acts as a weakly reflective boundary condition (Verboom and Slob 1984). For very large values of β the boundary condition reduces to (6.15).

The discretised open boundary conditions (6.12), (6.13) and (6.16) are, respectively (see figure 6.2):

$$h_{i,j}^{k+1} = f_{H,i}^{k,j}(t_{k+1}) \quad (6.17)$$

$$v_{i,j}^{k+1} \pm \sqrt{\frac{g}{D}} h_{i,j}^{k+1} = f_{R,i}^{k,j}(t_{k+1}) \quad (6.18)$$

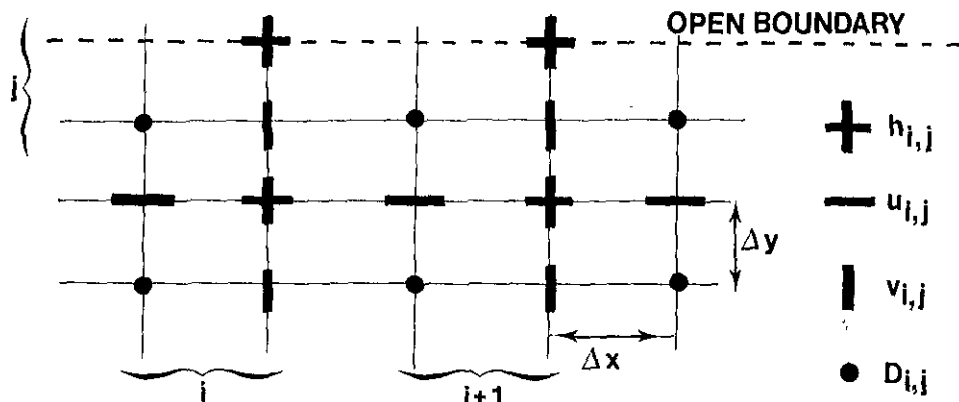


Figure 6.2: The open boundary.

$$h_{i,j}^{k+1} = f_{H,i}^j(t_{k+1}) \mp \beta \left[v_{i,j}^{k+1} - v_{i,j}^k \pm \sqrt{\frac{g}{D}} (h_{i,j}^{k+1} - h_{i,j}^k) \right] \quad (6.19)$$

Note that (6.18) and (6.19) are no second-order approximations.

The approach described above has been used to develop a numerical model describing the water movement in the entire North Sea and the Channel. In figure 6.3 the grid G_1 covering this area is shown. Here $\Delta x = 18.5$ km and $\Delta y = 19$ km and as a consequence of condition (6.5) $\Delta t = 10$ min. Furthermore, the parameters in the model are chosen to be: the linear bottom friction coefficient $\lambda = 2.4 \times 10^{-3}$, the Coriolis parameter $f = 1.25 \times 10^{-4}$ and the wind friction coefficient $\gamma = 3.2 \times 10^{-6}$. The smoothing operators (6.8) and (6.9) are not necessary for deterministic computations but are introduced if the model is embedded in a Kalman filter.

In this study we have chosen an explicit finite difference scheme since the restriction of the timestep given by equation (6.5) is for the model just described not a real limitation. Of course, if the approach should be applicable to a wide range of practical two-dimensional flow identification problems, implicit schemes are recommendable (Stelling 1983). Analogously to Stelling (1983) we use a space-staggered grid for the discretisation of the equations. Of his arguments we recall that this choice simplifies the implementation of the boundary conditions considerably.

As described in Chapter 4 the finite difference equations (6.1) - (6.3) and the smoothing operators (6.8) and (6.9) can be rewritten as:

$$\underline{A}x_{t_{k+1}} = \underline{B}x_{t_k} + \underline{u}_{t_{k+1}} \quad (6.20)$$

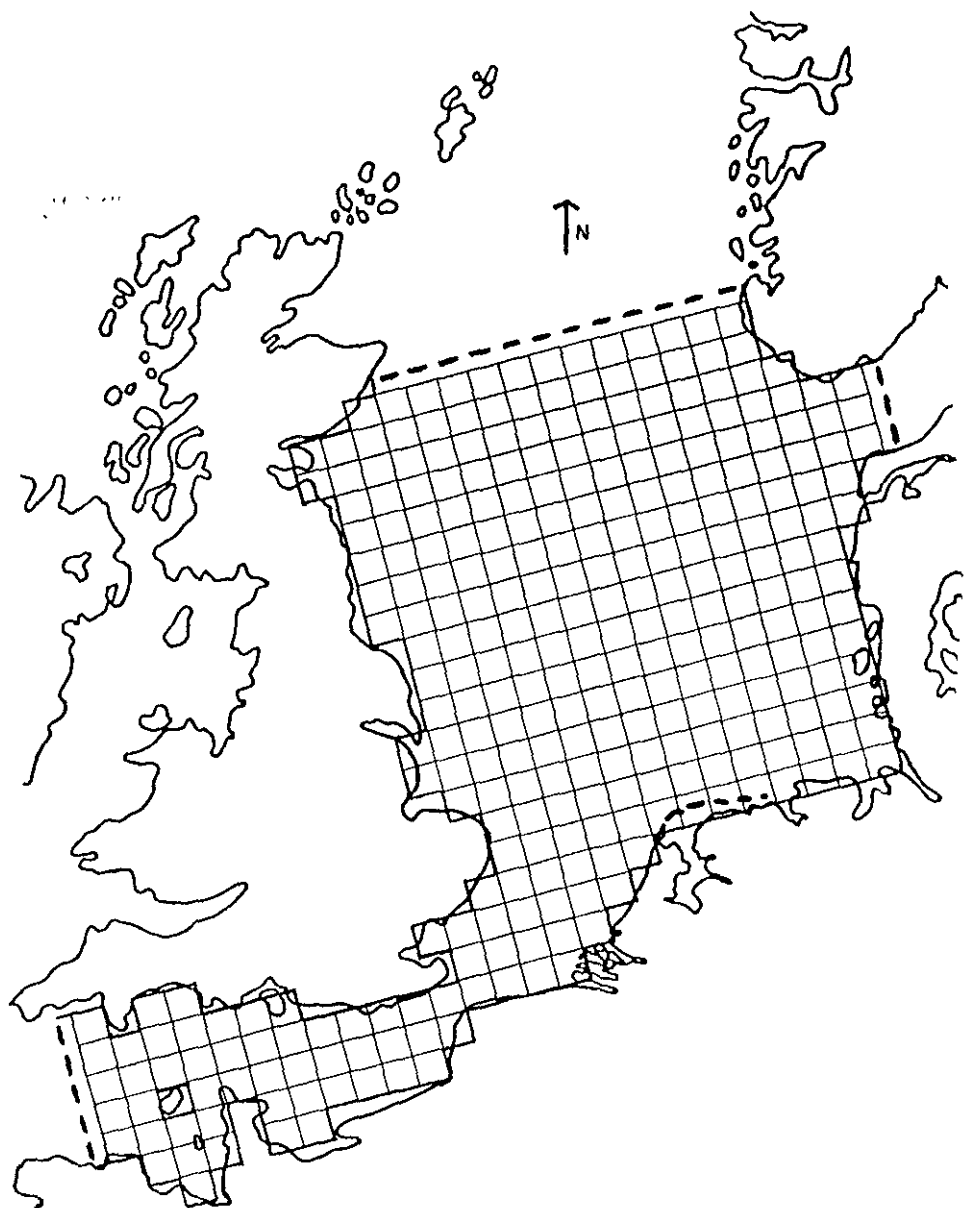


Figure 6.3: The grid of the North Sea model.

or symbolically as:

$$\underline{x}_{t_{k+1}} = \Phi \underline{x}_{t_k} + A^{-1} \underline{u}_{t_{k+1}} \quad (6.21)$$

where \underline{u}_{t_k} represents the boundary conditions and the meteorological input.

6.3 The Kalman filter

6.3.1 Introduction

In this section a Kalman filter based on the deterministic model (6.21) is described. Analogously to the one-dimensional case we first embed the model in a stochastic environment in Subsection 6.3.2. Subsection 6.3.3 is devoted to the boundary treatment. The important capability of the filter to correct an erroneous open boundary condition is shown. Finally, in Subsection 6.3.4 we derive the steady-state filter using the Chandrasekhar-type equations. Attention is concentrated on the numerical properties of the algorithm.

6.3.2 The stochastic model

The model (6.21) derived in Section 6.2 is not perfect. The most important errors are introduced by fluctuations in the meteorological input (or, which amounts to the same thing, by the poorly known influence of the wind on the water movement described by the wind friction coefficient) and by the open boundary conditions that have to be specified. To account for these errors we embed the discrete system in a stochastic environment by adding system noise.

Most errors not introduced by the poorly known open boundary are concerned with uncertainty in the momentum equations and are often caused by an erroneous wind input. Since in addition the water velocities created by the wind are inversely proportional to the depth of the water, we suppose that the quantities uD and vD are corrupted by the system noise processes Wu and Wv respectively. Generalizing the approach described in Section 4.4, these processes are assumed to be location invariant with statistics*:

$$E \{ Wu(x, y) \} = 0 \quad (6.22)$$

$$E \{ Wu(x_1, y_1) Wu(x_2, y_2) \} = \sigma^2 e^{-\alpha \sqrt{(x_1-x_2)^2 + (y_1-y_2)^2}} \quad (6.23)$$

* Note that we implicitly assume the medium to be isotropic.

$$E \{ Wv(x, y) \} = 0 \quad . \quad (6.24)$$

$$E \{ Wv(x_1, y_1) Wv(x_2, y_2) \} = \sigma^2 e^{-\alpha \sqrt{(x_1-x_2)^2 + (y_1-y_2)^2}} \quad (6.25)$$

$$E \{ Wu(x_1, y_1) Wu(x_2, y_2) \} = 0 \quad (6.26)$$

Here the parameters σ^2 and α have to be specified. The covariances are parameterized rather simply. However, as long as our knowledge of the system noise processes is very poor, it is not useful to improve these parametrizations.

The noise processes Wu and Wv are introduced to model the uncertainty associated with the momentum equations. The continuity equation is assumed to be perfect.

The parameter α in the equations (6.23) and (6.25) can be interpreted as a measure of the spatial variability of the errors concerned with the momentum equations. As with the one-dimensional approach (see Section 4.4) this parameter has to be chosen such that the energy of the short waves is limited so as to avoid numerical problems. When employing a Kalman filter based on a two-dimensional model these problems are much more likely to occur than in the one-dimensional case.

If the system noise is defined on a grid G_2 which need not be space-staggered, the system model can be described by:

$$\underline{X}_{t_{k+1}} = \Phi \underline{X}_{t_k} + A^{-1} \underline{u}_{t_{k+1}} + A^{-1} \Lambda \underline{W}_{t_{k+1}} \quad (6.27)$$

where \underline{W}_{t_k} is a p-vector consisting of the noise components at the grid points of G_2 , with covariance matrix Q that can be derived from the equations (6.22) - (6.26). The matrix Λ represents the sequence of linear operations required to interpolate the system noise at the grid points of G_1 .

In deriving the formulas for the interpolation, we make use of the statistics (6.22) - (6.26) of the system noise. It is easy to show that (see figure 6.4):

$$\widehat{Wu}(x, y) = [Wu(x_1, y_1) \ Wu(x_2, y_2) \ Wu(x_3, y_3) \ Wu(x_4, y_4)] \underline{v} \quad (6.28)$$

where:

$$\underline{v} = C^{-1} \underline{d}$$

$$(C)_{ij} = E \{ Wu(x_i, y_i) Wu(x_j, y_j) \}$$

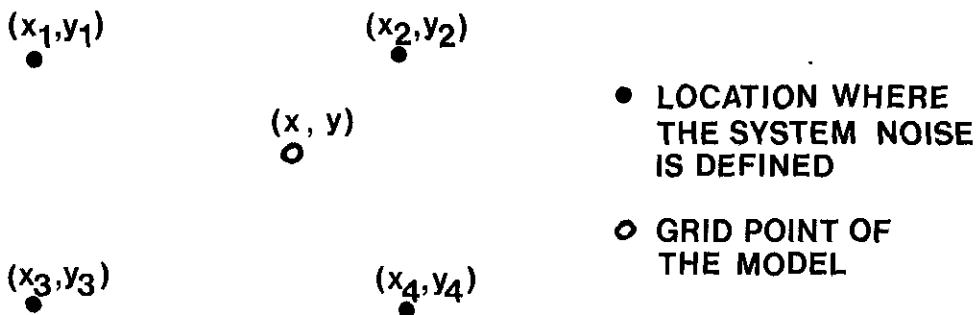


Figure 6.4: Interpolation at a grid point (x, y) of G_1 using four grid points of G_2 .

and

$$(d)_i = E \{ W_u(x_i, y_i) W_u(x, y) \}$$

is the least squares interpolation of $W_u(x, y)$ given the system noise components at (x_i, y_i) , $i = 1, 2, 3, 4$ (Schagen 1979). Of course, similar results can be obtained for $W_v(x, y)$. If necessary, the formulas derived above can be generalized easily if more grid points of G_2 are used for the interpolation. However, in our filter procedure we do not consider this case.

Since the most important model errors are caused by fluctuations in the meteorological input, G_2 is chosen to coincide approximately with the grid of the atmospheric model, yielding $p \ll n$. An important advantage of the fact that the grid G_2 of the system noise is coarser than the grid G_1 is that the energy of the short waves introduced on G_1 by the filter, is limited. Moreover, in case the grid G_2 is very coarse with respect to G_1 and if in addition the bottom friction is sufficiently strong, the introduction of the numerical viscosity to eliminate the short waves may not be necessary.

Assuming that measurements of the water-level are available at m grid points of G_1 , the observation equation can be derived easily:

$$\underline{Z}_{t_k} = M \underline{X}_{t_k} + \underline{V}_{t_k} \quad (6.29)$$

where the m -vector \underline{Z}_{t_k} contains the measurements taken at time k and \underline{V}_{t_k} is the measurement noise with covariance matrix R . If necessary, it is easy to modify equation (6.29) to account for the fact that not all measurements are available exactly at grid points.

The grid G_2 and some measurement locations available in the North Sea are shown in figure 6.5.

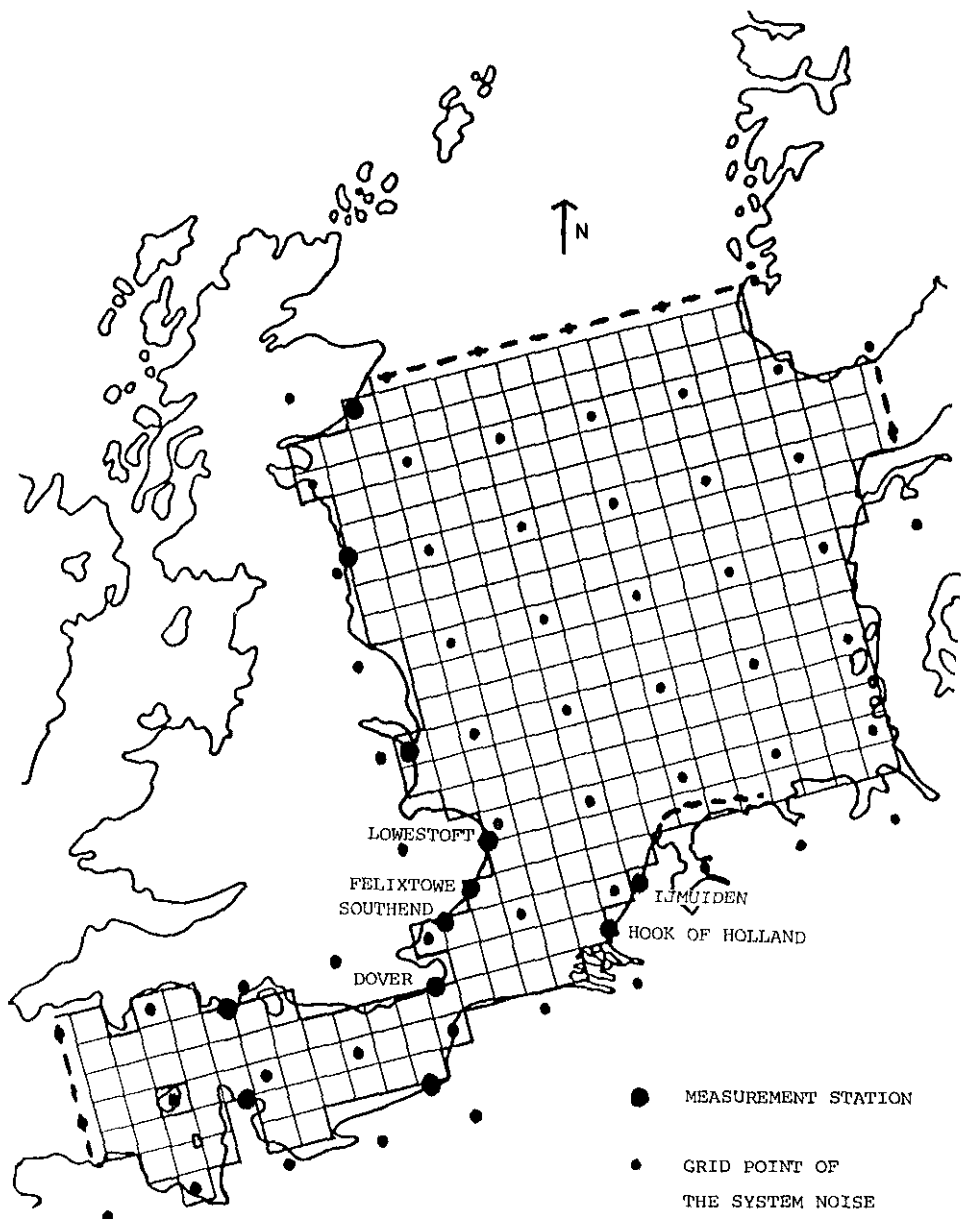


Figure 6.5: The grid G_2 of the system noise and some measurement stations in the North Sea.

6.3.3 The boundary treatment

The uncertainty associated with the open boundary conditions in the model can be introduced in different ways. If the water-level (6.17) at the boundary is prescribed, we may assume (see figure 6.2):

$$H_{i,j}^{k+1} = f_H^{i,j}(t_{k+1}) + W_H^{i,j}(t_{k+1}) \quad (6.30)$$

or, analogously to the one-dimensional case described in Subsection 5.3.3:

$$H_{i,j}^{k+1} = H_{i,j}^k + f_H^{i,j}(t_{k+1}) - f_H^{i,j}(t_k) + W_B^{i,j}(t_{k+1}) \quad (6.31)$$

where the system noise $W_H^{i,j}(t_k)$ or $W_B^{i,j}(t_k)$ represents the uncertain part of the boundary. In non-linear models $f_H^{i,j}(t_k)$ usually is the astronomical tide that has been determined by a harmonic analysis of field data gathered along the boundary. In case of a linear model that is only used to describe the meteorological effect, $f_H^{i,j}(t_k)$ is often assumed to be zero. However, in both cases the most important errors associated with the open boundary are caused by external surges that are created outside the domain of the problem and that propagate across this boundary. Since we know that these external surges propagate approximately like Kelvin waves (see Subsection 5.2.2), we propose a modified boundary condition to exploit this knowledge:

$$H_{i,j}^{k+1} = H_A^k e^{-\zeta i \Delta x} + f_H^{i,j}(t_{k+1}) + W_H^{i,j}(t_{k+1}) \quad (6.32)$$

where ζ is a known constant (see Subsection 5.2.2), x is the coordinate along the boundary and H_A^k is considered to be an additional component of the state vector corrupted by system noise.

Using measurements taken along the boundary, $H_{i,j}^k$ and H_A^k can be estimated by the filter. If there are no observations available in the neighbourhood of the boundary, the filter is not able to estimate these components of the state vector accurately and the erroneous boundary condition propagates into the model. However, as soon as measurements are available the errors caused by the erroneous boundary condition that is prescribed are corrected by filtering these measurements.

As described in Section 6.2 the boundary conditions (6.30), (6.31) and (6.32) are not attractive from the numerical point of view. Another, more stable condition can be obtained similarly as (6.32) if the Riemann invariant is prescribed at the open boundary:

$$H_{i,j}^{k+1} = \mp \sqrt{\frac{D}{g}} V_{i,j}^{k+1} + R_A^k e^{-\zeta i \Delta x} + \sqrt{\frac{D}{g}} f_R^{i,j}(t_{k+1}) + W_R^{i,j}(t_{k+1}) \quad (6.33)$$

Here $W_{R,i}^k(t_k)$ represents the uncertainty associated with this boundary. R_A^k is considered to be an additional component of the state vector. Although Riemann invariants cannot be measured in nature they can be identified by the filter using water-level observations. This is fundamentally different to the deterministic case described in Section 6.2.

Analogously to Stelling (see Section 6.2) we also propose the more general boundary condition:

$$H_{i,j}^{k+1} = f_{H,i}^k(t_{k+1}) \mp \beta \left[V_{i,j}^{k+1} - V_{i,j}^k \pm \sqrt{\frac{g}{D}} (H_{i,j}^{k+1} - H_{i,j}^k) \right] + H_A^k e^{-\xi i \Delta x} + W_{H,i}^k(t_{k+1}) \quad (6.34)$$

For $\beta = 0$ (6.34) reduces to the condition (6.32) while for very large values of β (6.34) approaches the weakly reflective condition (6.15).

The choice of boundary condition in practical situations depends on the numerical stability of the boundary treatment as well as on the accuracy of $f_{H,i}^k(t_k)$ and $f_{R,i}^k(t_k)$. If neither of these functions are known with great precision we prefer condition (6.33). However, if $f_{H,i}^k(t_k)$ is known rather accurately, e.g. if the astronomical tide along the boundary has been analysed, boundary (6.34) is an attractive alternative. In this case β has to be chosen sufficiently small to guarantee that (6.34) is an accurate approximation of (6.32). However, unlike the deterministic case described in Section 6.2, when employing the Kalman filter approach the deviations caused by prescribing the numerically more stable condition (6.34) instead of (6.32), can be corrected by using the measurements available.

6.3.4 The steady-state filter

The model described in Subsections 6.3.2 and 6.3.3 is time-invariant. Since the initial transient period is of no consequence and we are only interested in the steady-state filter, both the original filter equations and the Chandrasekhar-type algorithm can be employed (see Section 4.8). Using the second implementation we are able to exploit the fact that $p \ll n$ and to reduce the number of computations and the computer storage requirements drastically.

To obtain the desired steady-state filter gain K , the recursive equations (4.74) - (4.79) are iterated until

$$\| K(k+1) - K(k) \| < \varepsilon \| K(k) \| \quad (6.35)$$

where ϵ is prespecified and

$$\| \mathbf{M} \| = \max_{i,j} |(\mathbf{M})_{ij}| \quad (6.36)$$

Since the model (6.21) is of the hyperbolic type the number of iterations required depends on the travelling time of the waves in the model and therefore, on the size of the domain of the problem. Using the finite difference approximation (6.1) - (6.3), for very short waves the computed wave-celerity is considerably less than the true wave-celerity (see Section 6.2). As a consequence, the number of iterations required to obtain the steady-state filter gain can be large. However by introducing the smoothing operators (6.8) and (6.9) the very short waves are dissipated and this number becomes considerably less.

The number of iterations required also depends on the choice of the open boundary condition. Choosing the condition (6.34) with $\beta = 0$, the water-level is prescribed and numerical reflections are likely to occur (see Section 6.2). As a consequence, the noise waves generated inside the model can be reflected against the open boundary and if these waves are not dissipated the convergence of the filter equations can be slow. By choosing $\beta \neq 0$ or by prescribing the Riemann invariant (6.33) at the open boundary the short noise waves can travel across this boundary outside the domain of the problem. As a result the convergence of the filter equations is faster.

Finally we note that since numerical errors often manifest themselves as short waves, it is to be expected that by introducing a dissipative mechanism such as the operators (6.8) and (6.9) numerical errors are partly eliminated.

To illustrate the effects described above we have performed some experiments. To allow double precision calculations and to be able to use both the original and the Chandrasekhar-type algorithms we have developed a filter based on a relatively small North Sea model. The grid G_1 and the measurement locations that are assumed to be available are shown in *figure 6.6*. The grid G_2 of the system noise is chosen to coincide with G_1 . The measurements are supposed to be taken each hour. Since only the numerical errors in the filter gain $K(k)$ directly degrades the accuracy of the predictions, we study the behaviour of the error $\delta K(k)$. Using the conventional algorithm, $\delta K(k)$ behaves similarly as $\delta P(k|k)$ that is analysed in Section 4.8. However, using the Chandrasekhar-type implementation we have from equation (4.91):

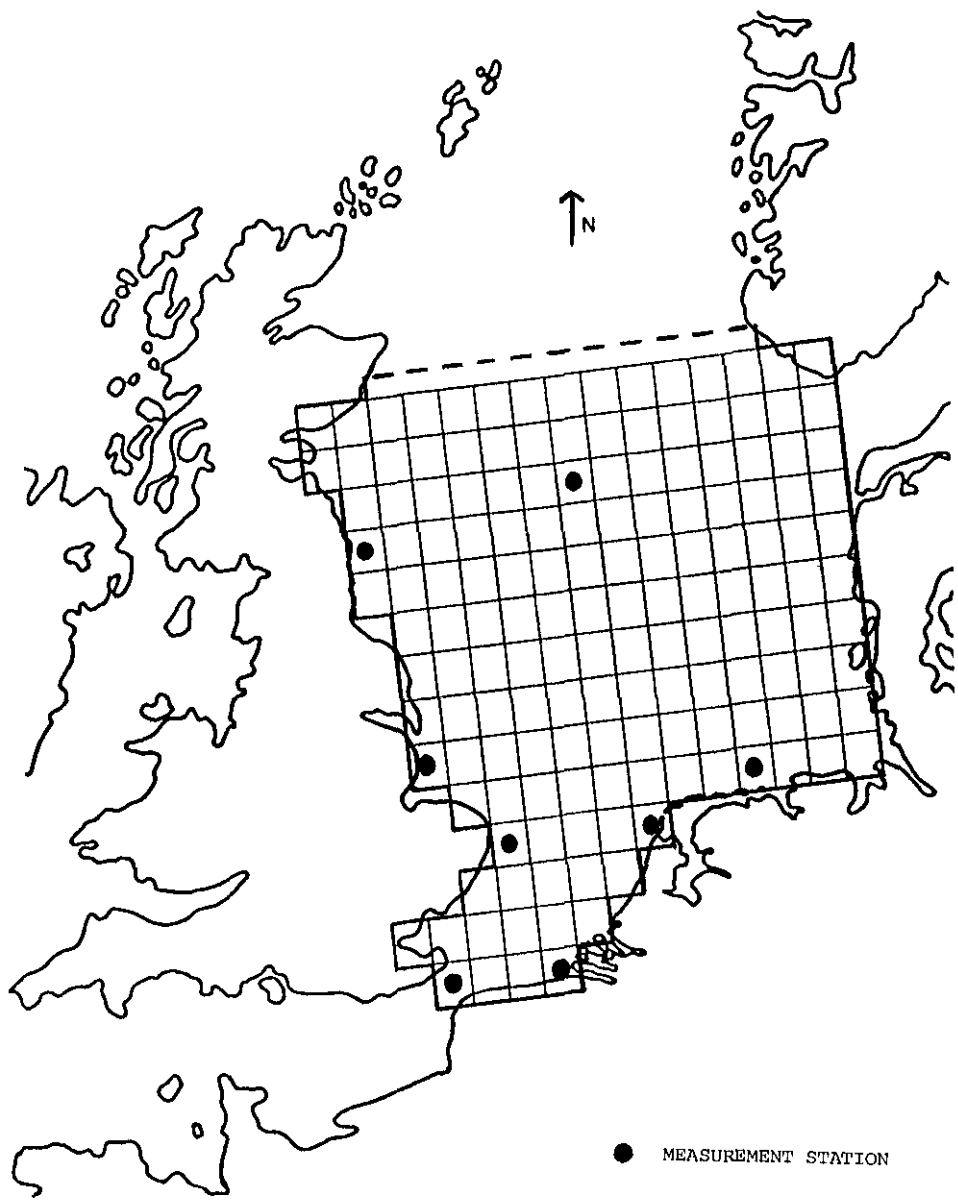


Figure 6.6: The grid of the small North Sea model and the measurement stations that are assumed to be available.

$$\begin{aligned}
\delta K(k+1) &= \delta G(k+1) R(k+1)^{-1} - G(k+1)^{-1} \delta R(k+1) R(k+1)^{-1} \\
&\quad + O(\Delta^2) \\
&= [I - K(k+1)M] \delta G(k+1) R(k+1)^{-1} + O(\Delta^2) \\
&\leq \delta G(k+1) R(k+1)^{-1} + O(\Delta^2)
\end{aligned} \tag{6.37}$$

As was shown in Section 4.8, $\|\delta G(k)\|$ increases with k . However, also $\|R(k+1)\|$ grows in time and as a result $\|\delta K(k)\|$ can either increase or decrease with k .

The results of the experiments are shown in figures 6.7 - 6.9. Here $K_d(k)$ represents the double precision result which can be considered to be perfect. The machine precision is approximately 10^{-8} . The main conclusions which can be drawn from these figures are:

- The total accumulated errors in $K(k)$ decrease with the introduction of the dissipative mechanism with a smoothing factor $c = 0.02$ to the finite difference scheme, although the effect is not dramatical. Note that the difference of the total errors in $K(k)$ and $K(k+1)$, which is mainly caused by the errors performed in iteration $k+1$, is decreased also by choosing $c = 0.02$.

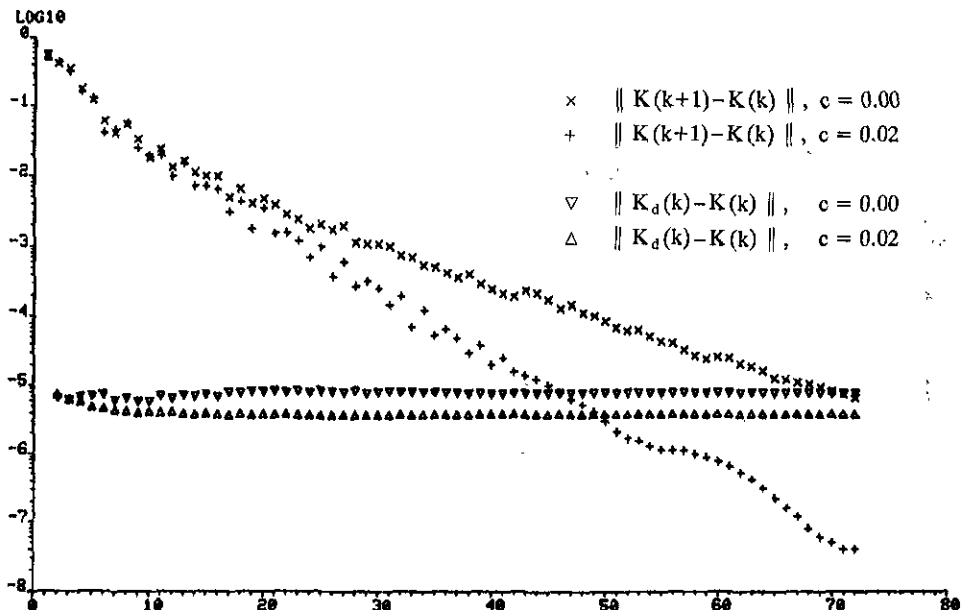


Figure 6.7: The influence of a dissipative mechanism on the numerical properties of the Chandrasekhar-type algorithm.

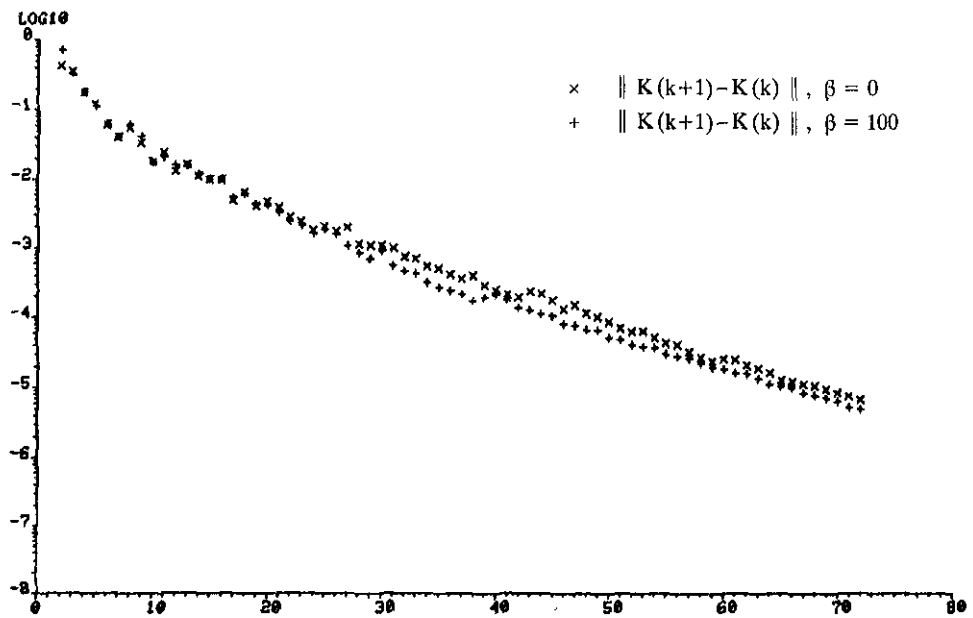


Figure 6.8: The influence of the boundary treatment on the numerical properties of the Chandrasekhar-type algorithm.

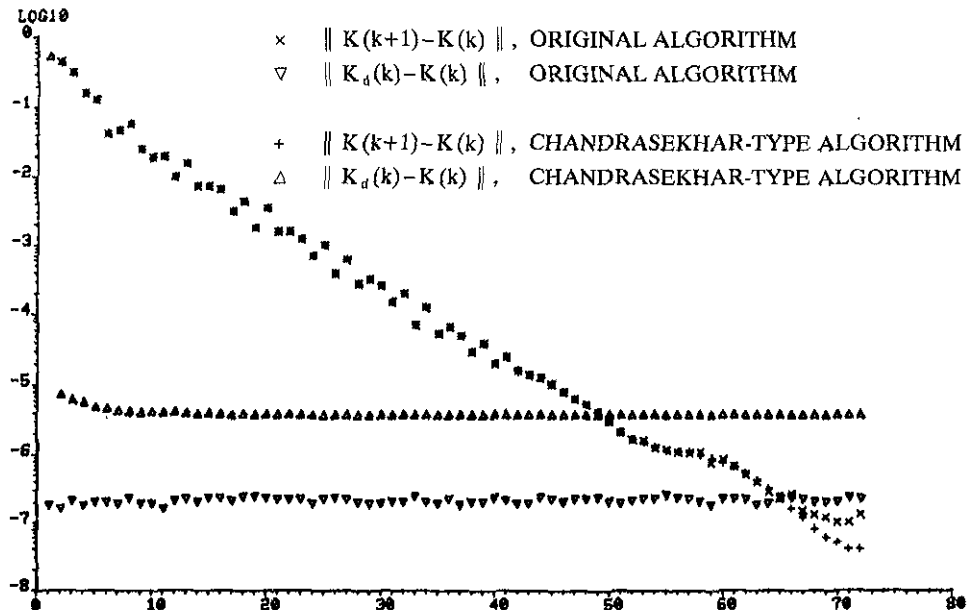


Figure 6.9: The numerical properties of the original algorithm with respect to the Chandrasekhar-type implementation.

- The number of iterations required to obtain the steady-state filter is significantly reduced by the introduction of the smoothing operator. Also by increasing the value of β in the boundary condition (6.34) the convergence of the filter is a little faster. Of course, these effects depend very much on the geometry of the problem.
- The total accumulated errors in $K(k)$ employing the original filter algorithm is very small.
- For the Chandrasekhar-type algorithm the errors performed in iteration k and consequently $\delta K(k+1) - \delta K(k)$ converge to zero. For the original algorithm this is not the case.

The observations just described are completely in agreement with the discussion of the numerical properties of the Kalman filter algorithms in Section 4.8.

The experiments just described have been performed with a relatively crude model to allow double precision calculations. However, we may expect similar results for the larger model described in Section 6.2.

6.4 Implementation of the algorithm on a vector processor

The computer storage and time requirements on the UNIVAC 1100/60 of the Rijkswaterstaat for the computation of the steady-state filter based on the model described in Section 6.2 are approximately:

core memory : 600 Kbytes
 computation time : 28 min. CPU

Here we have assumed that the measurements are available each hour at the nearest grid point of the locations indicated in figure 6.5. Obviously the results depend on the choice of ϵ in equation (6.35), on the numerical viscosity, the open boundary conditions and on the system and measurement noise covariance matrices.

The numerical model described in Section 6.2 consists of approximately 900 active calculation points, i.e. the dimension of the state $n \approx 900$. However, deterministic models of the North Sea and adjoining waters often result in dimensions $n = 5000-10000$. It is clear that combining the filter described in this chapter with such a large model is not feasible on a UNIVAC 1100/60. However, here we recall that our filter approach is time-invariant and, consequently, all the time-consuming second moment calculations can be performed off-line on a large computer. Therefore, in this section we briefly present the basic ideas of a computationally efficient filter algorithm suitable for implementation on a CDC CYBER 205 vector processor. The vectorization of the filter algorithm is a modification of the implementation of a

deterministic model on the CYBER 205 which was carried out by Stelling, Willemse and Rozendaal (1986).

We do not intend to give a detailed introduction to the use of vector processors. The interested reader is referred to SARA (1984). Here we only recall the definition of a vector: a vector is a set of contiguous storage locations in memory. The implication of this definition is that a loop that accesses arrays in a nonsequential manner lacks vector structure and therefore, is not vectorizable. However, on the CYBER 205 two vector instructions are available for the purpose of moving data elements from nonsequential to sequential locations (GATHER) or the reverse (SCATTER). If a loop is vectorizable it is possible to exploit the special architecture of the CYBER 205 and to replace the loop by a single vector instruction. For large vectors with a length of more than, say, 100 elements, this vectorization reduces the CPU-time by one order of magnitude.

The filter algorithm (4.74) - (4.79) consists of two different parts: the time propagation equation (4.74) and the up-date equations (4.75) - (4.79). We first consider the vectorization of the time propagation equation. Here we note that:

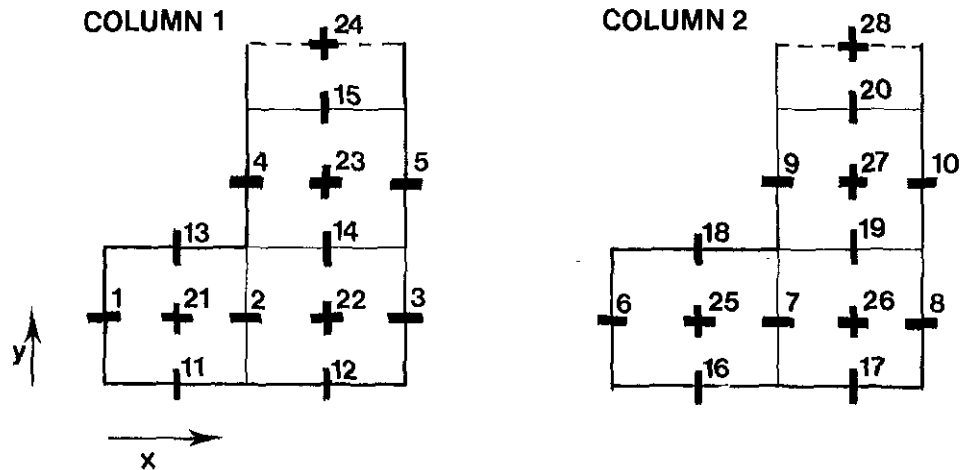
$$(Y(k+1))_j = \Phi(S(k))_j \quad (6.38)$$

where $(M)_j$ is the j^{e} column of a matrix M . As a consequence, the computation of the columns of $Y(k+1)$ can be performed independently of each other. In fact, the deterministic model Φ is employed parallel for p different initial conditions, i.e. the p columns of $S(k)$. In order to store the matrix $S(k)$ efficiently, we number the active calculation points of the p models both in the x -direction and in the y -direction as indicated in *figure 6.10*. Furthermore, we define an index array to rearrange a vector in y -direction if it was stored in x -direction using the GATHER instruction or vice versa using the SCATTER instruction. The elements of $S(k)$ can now be stored either in x -direction or in y -direction, after which the vectorization of the time propagation equation is a rather straightforward procedure. Leaving the boundary treatment out of consideration, for most vector instructions the vector length is approximately $1/3 np$, while for some instructions it is approximately $1/3 n$. The vectorization of the up-date equations (4.75) - (4.79) being full matrix manipulations, is relatively simple. Here the dominant vector length is approximately $1/3 n$.

To show some results of the algorithm, the filter has been implemented on a CYBER 205. We compare the CPU-time to compute the steady-state filter in three different cases. The results are shown in table 6.1. Here, we would add some notes to the results:

- The algorithm can be implemented very efficiently on a vector processor. This is due to the large vectors and to the fact that the boundary conditions can also be

NUMBERING IN X-DIRECTION



NUMBERING IN Y-DIRECTION

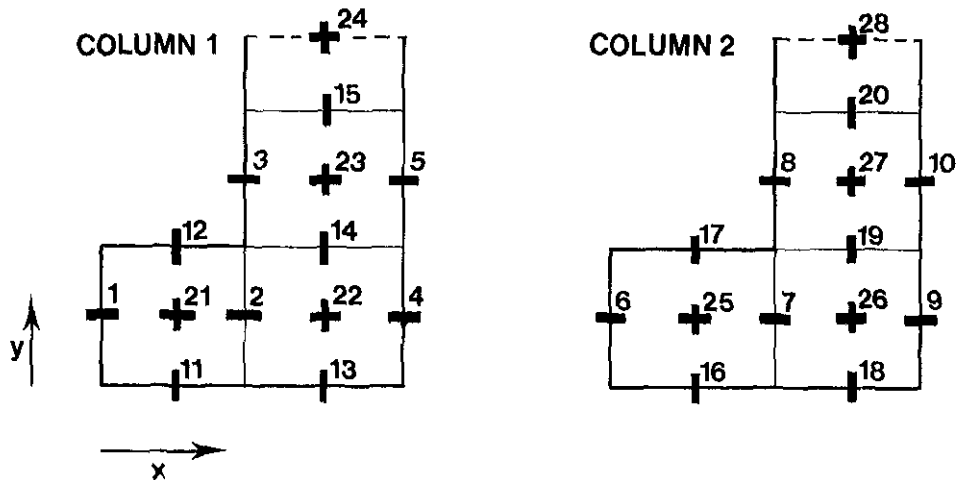


Figure 6.10: Numbering of the elements of $S(k)$ in x-direction (above) and y-direction (below) in case of a very simple model with dimension of the system noise $p = 2$.

vectorized with a vector length of at least p . Implementing a deterministic numerical model on a vector processor, the boundary conditions often cannot be vectorized efficiently.

- The storage requirements of the vector processor implementation are approximately 1200 Kbytes. The increase with respect to the scalar implementation is mainly caused by the introduction of a number of arrays to store intermediate

results. Furthermore, while in the scalar case only the non-zero elements of $S(k)$ are stored, in the vector case the zero elements corresponding to the boundary conditions $u=0$ and $v=0$ also have to be stored to obtain a vector structure of the algorithm (see figure 6.10).

- From the results described above it is to be expected that it is possible to combine the steady-state filter approach with a large deterministic model with, say, 20000 active calculation points.

CPU-time		
UNIVAC 1100/60	:	scalar algorithm 28 min.
CYBER 205	:	scalar algorithm 2.7 min.
CYBER 205	:	vector algorithm 12 sec.

Table 6.1 CPU-time of different implementations of the Kalman filter algorithm.

6.5 Experiments using simulated data

6.5.1 Introduction

Before the filter can be safely applied to prototype situations, it is necessary to demonstrate that it can perform adequately under known conditions. Therefore, analogously to the one-dimensional case, by means of a random generator data sets are created using a truth-model. By employing the filter based on the filter-model that differs from the truth-model it is possible to investigate whether the filter is able to reconstruct the water-levels and velocities using the simulated data, despite the differences between the filter-model and the truth-model. Experiments have revealed that many results of the special one-dimensional filtering problem described in Section 4.5, are also valid in the two-dimensional case.

Since, as was noted before, the most important errors of the filter model are due to the fluctuations in the meteorological input and the uncertain open boundary condition, in this section we concentrate our attention on the capability of the filter to correct these errors. To test the filter, we have performed numerous experiments. As representative examples we briefly describe some of these tests in Subsections 6.5.2 and 6.5.3 dealing respectively with erroneous meteorological inputs and uncertain open boundaries. Other tests can be found in Heemink (1984, 1985).

Measurements are assumed to be available each hour in the grid points indicated in *figure 6.11*. At the open boundaries we prescribe the condition (6.33).

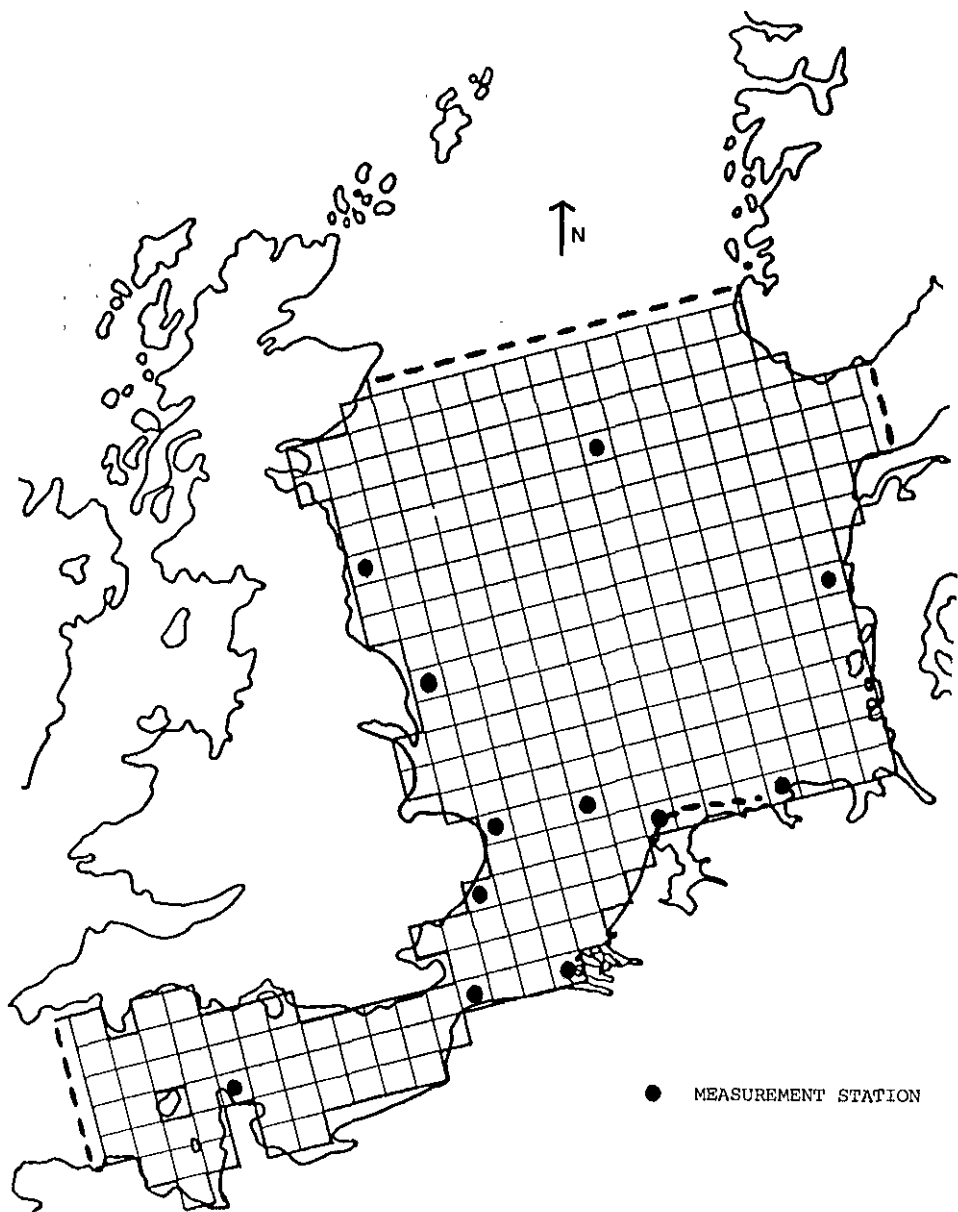


Figure 6.11: The measurement stations that are assumed to be available in the experiments using simulated data.

It is obvious that when using such a limited number of measurements the entire wave motion cannot be reconstructed uniquely, i.e. the system is not observable. The spatial variability of the water movement that can be identified depends on the spatial distribution of the measurement locations. In the southern part of the North Sea the number of tide gauges available is relatively large. As a consequence, the filter is able to produce a detailed picture of the water movement. However, in the remote parts of the model this is not the case. Fortunately, owing to the Coriolis forces, external surges as well as surges created in the northern part of the model propagate approximately like Kelvin waves along the English coast toward the south. From the results of the one-dimensional approach we may expect that by using the measurements available as shown in figure 6.11, this wave motion, which is in essence one-dimensional, can be identified accurately.

6.5.2 Internal surge

Experiment 6.1

Data are generated by means of the truth-model with a homogeneous wind input that varied in time as shown in *figure 6.12*. The standard deviation of the measurement noise is chosen to be 0.05 m. In the filter-model it is assumed that no wind has occurred. Therefore, without using the generated data the estimates computed by the filter-model would be zero. However, by filtering this data water-levels and

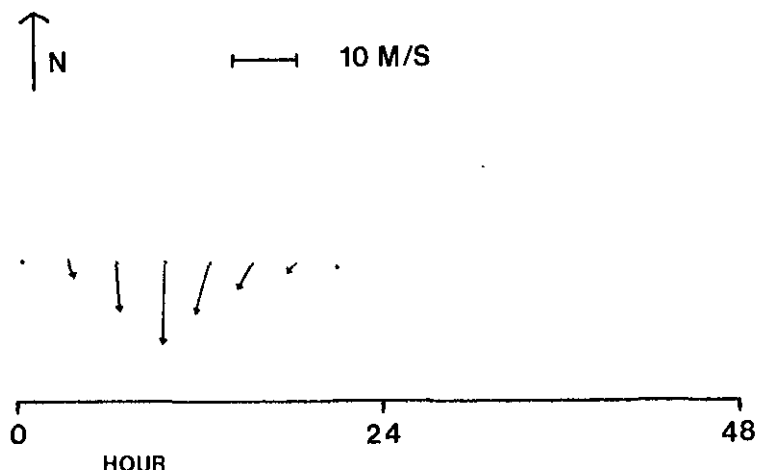


Figure 6.12: Wind velocities used in the experiments 6.1 and 6.2.

velocities can be identified. Here, we note that the filter does not know that the wind input is homogeneous. By choosing $\alpha < 1.0$ in the equations (6.23) and (6.25) the wind input is allowed to vary in space. Therefore, we may expect that the results of this experiment would be similar in case the wind velocities would have been slowly varying in space.

Of course, this experiment describes an extreme situation in which the filter has to reconstruct the entire storm surge. However, such tests are very good to study the performance of the filter under a variety of circumstances.

The variance of the measurement noise in the filter-model is similar to that of the truth-model. The parameters of the system noise are chosen to be: $\sigma^2 = 100$ and $\alpha = 0.95$. The system noise is introduced each measurement time.

In *figure 6.13* the generated and the filtered velocities at time $t = 12$ hours (see *figure 6.12*) are shown. Similar results are presented in *figure 6.14* for $t = 21$ hours.

The experiment shows that the filter is able to reconstruct the velocities accurately. Here we note that the accuracy depends on the location of the measurement stations and, of course, on the accuracy of the measurements. It can be seen from the figures that in the southern part of the North Sea, where most tide gauges are located, the filtered velocities are more accurate than in the remote parts of the model.

In practice we are mainly interested in the water-levels. Therefore, in *figure 6.15* the predictions of the water-levels at Flushing are shown. Here, since in the filter-model of this experiment it is assumed that no wind has occurred, in computing the water-level predictions the future wind input was assumed to be zero. In these figures we also present the predictions computed with perfect knowledge of the water-levels and velocities at the time these predictions are computed. In fact, these predictions indicate the best filter results that can be achieved. The differences between the two predictions are due to the fact that only twelve measurement locations are available and that the measurements are not perfect. These differences can be decreased by increasing the number of measurement locations or improving the accuracy of the measurements. As can be seen from *figure 6.15* the filter results are accurate.

The difference between the best filter results that can be achieved and the simulated water-levels are simply caused by the fact that in the filter-model of this experiment the future wind input is not known and assumed to be zero. Of course, no filter can correct an erroneous prediction of the meteorological input without using future measurements of the water-level.

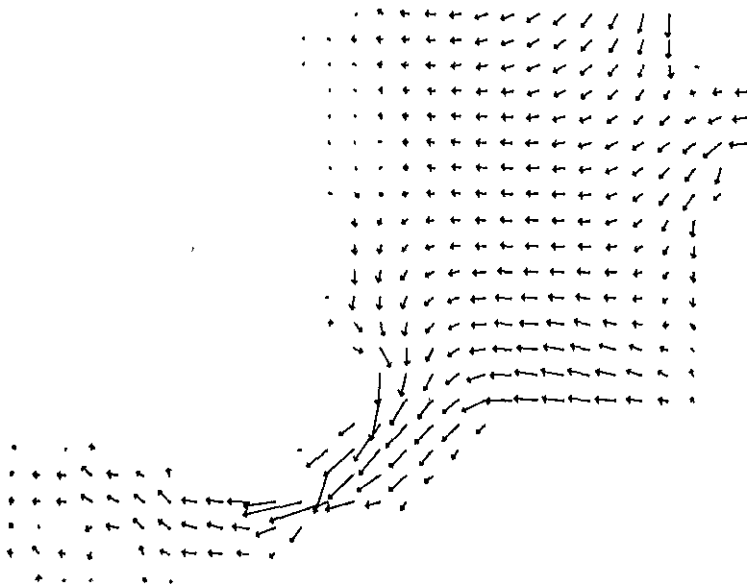
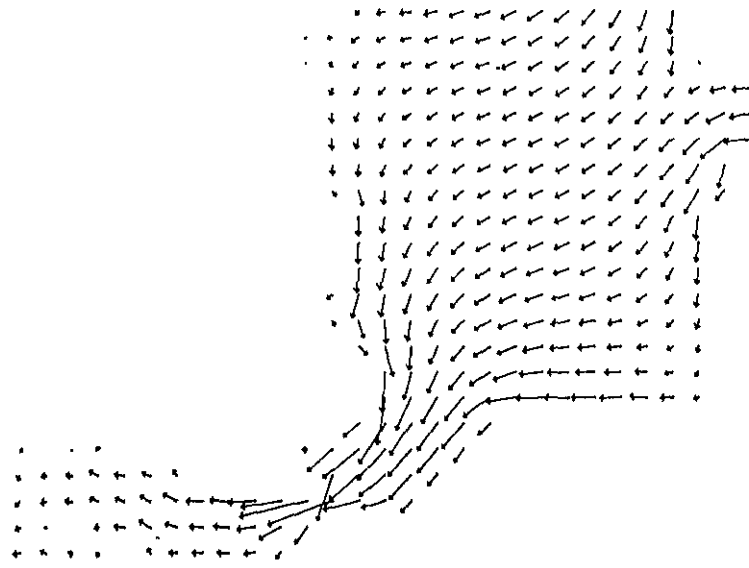


Figure 6.13: Simulated (above) and filtered (below) velocities at time $t = 12$ hours.

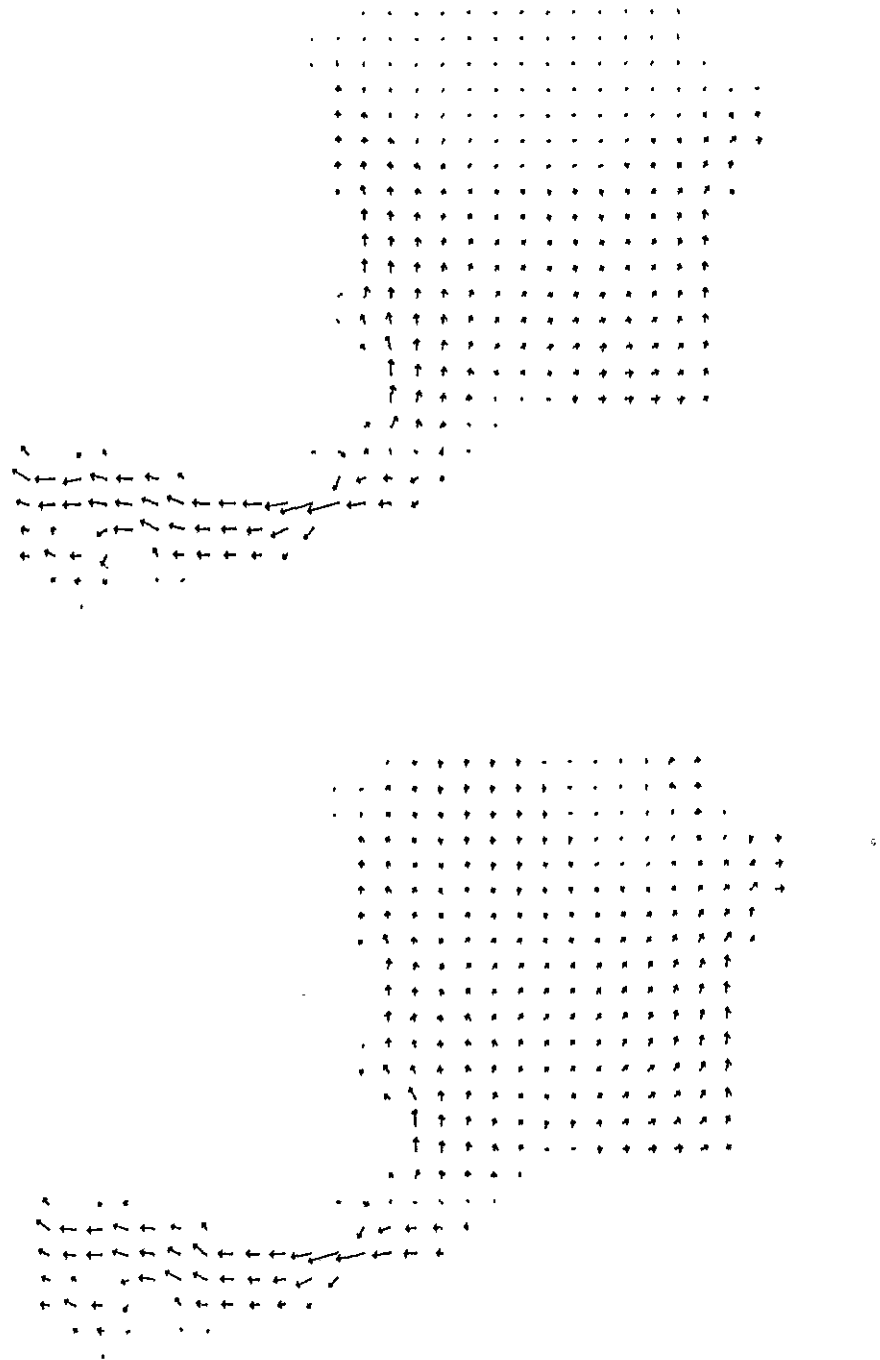


Figure 6.14: Simulated (above) and filtered (below) velocities at time $t = 21$ hours.

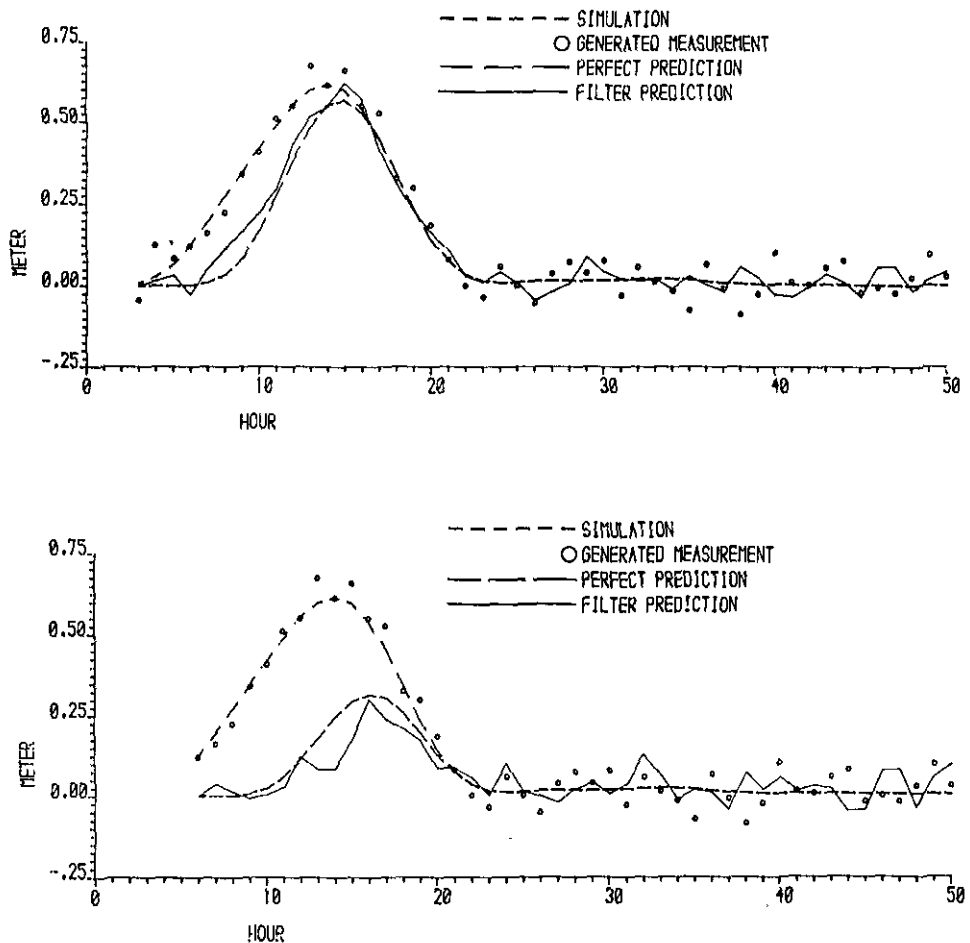


Figure 6.15: Three hours ahead (above) and six hours ahead (below) predictions of the water-level at Flushing.

Experiment 6.2

To study the sensitivity of the results with respect to the uncertain parameter α of the system noise in the filter model (see Subsection 6.3.2), the generated data used in experiment 6.1 are filtered in this experiment with $\alpha = 0.5$. The filtered velocities for time $t = 12$ hours and $t = 21$ hours are shown in figure 6.16. They should be compared with the simulated and filtered ($\alpha = 0.95$) velocities in figures 6.14 and 6.15 respectively.

The figures show that by choosing $\alpha = 0.5$ the filter introduces many wiggles on the grid. This is completely in agreement with the results obtained in Section 4.5.

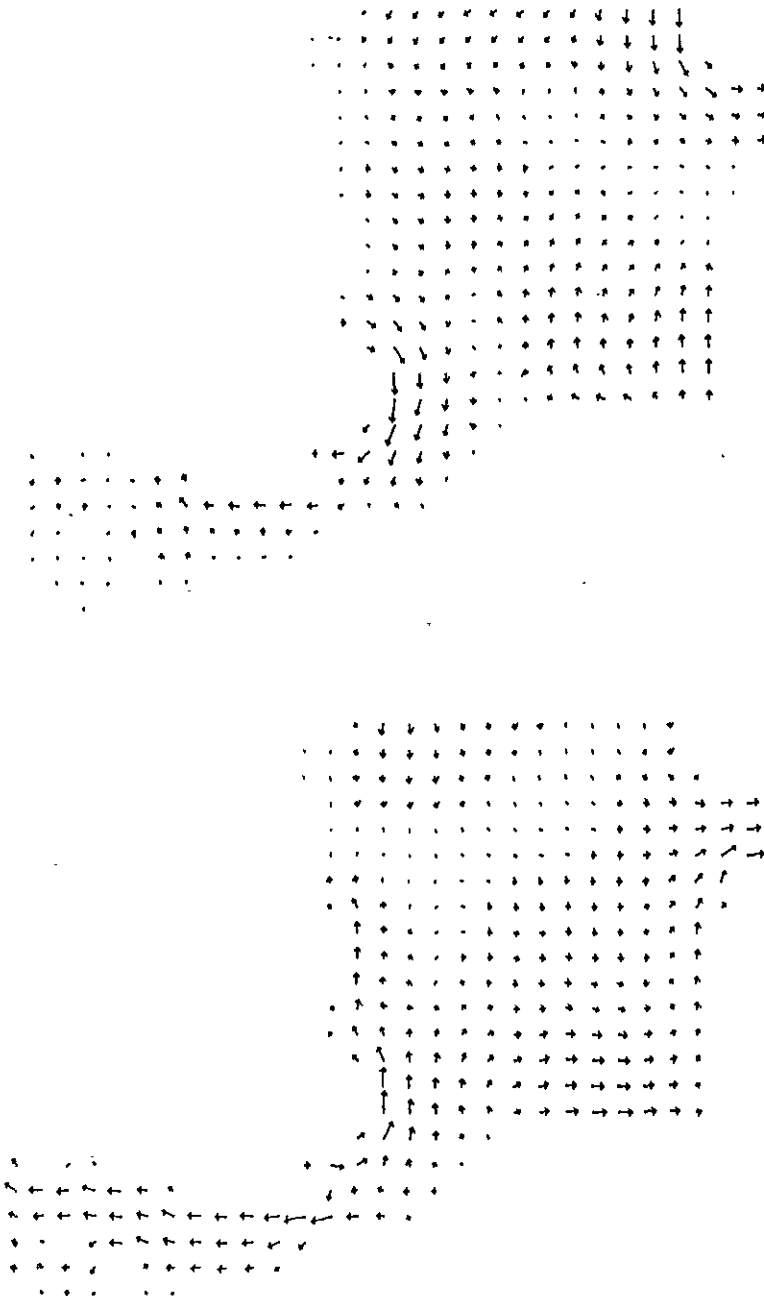


Figure 6.16: Filtered velocities at time $t = 12$ hours (above) and at time $t = 21$ hours (below) in case $\alpha = 0.5$.

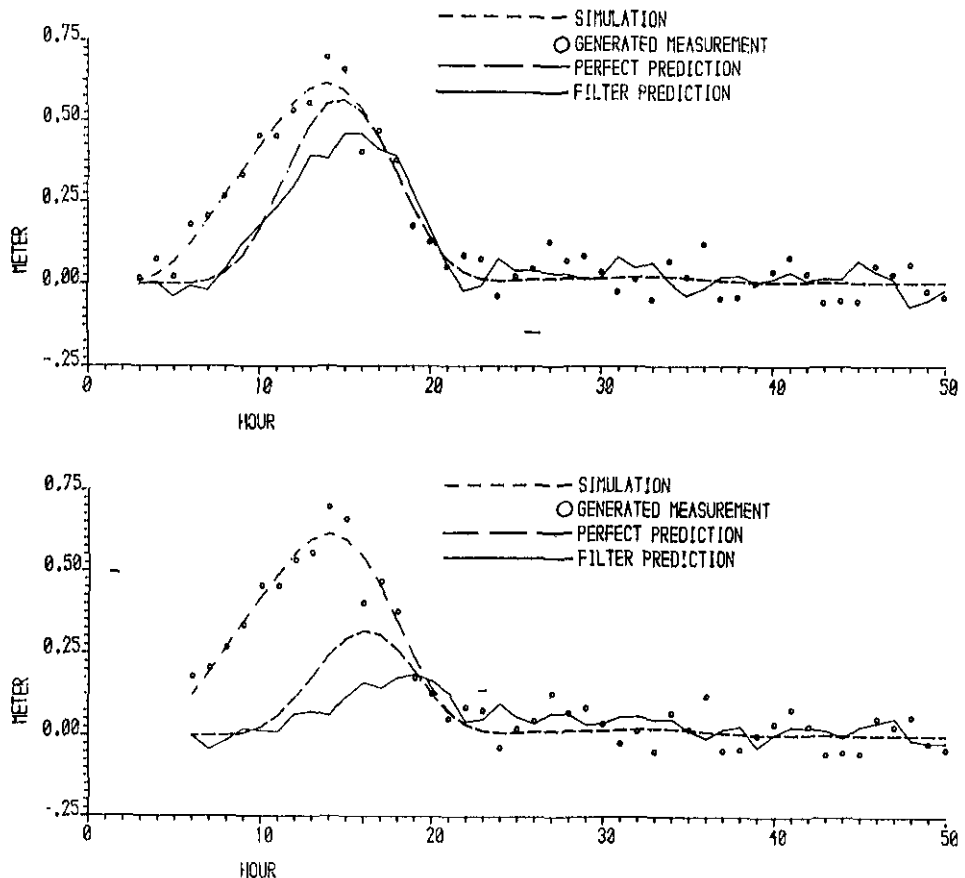


Figure 6.17: Three hours ahead (above) and six hours ahead predictions (below) of the water-level at Flushing in case $\alpha = 0.5$.

In figure 6.17 the water-level predictions produced by the filter ($\alpha = 0.5$) are shown. Although the results are not as accurate as those that were obtained in experiment 6.1 ($\alpha = 0.95$, see figure 6.15) the difference is not dramatically large. This observation shows that the water-level is not very sensitive to variations in the water velocities.

Experiment 6.3

To study filter performance in case of a more realistic wind input, data are generated by means of the truth-model with wind velocities as computed by an atmospheric model of the K.N.M.I. Here, we have chosen the stormy period from



Figure 6.18: Simulated (above) and filtered (below) velocities in case of a realistic wind input.

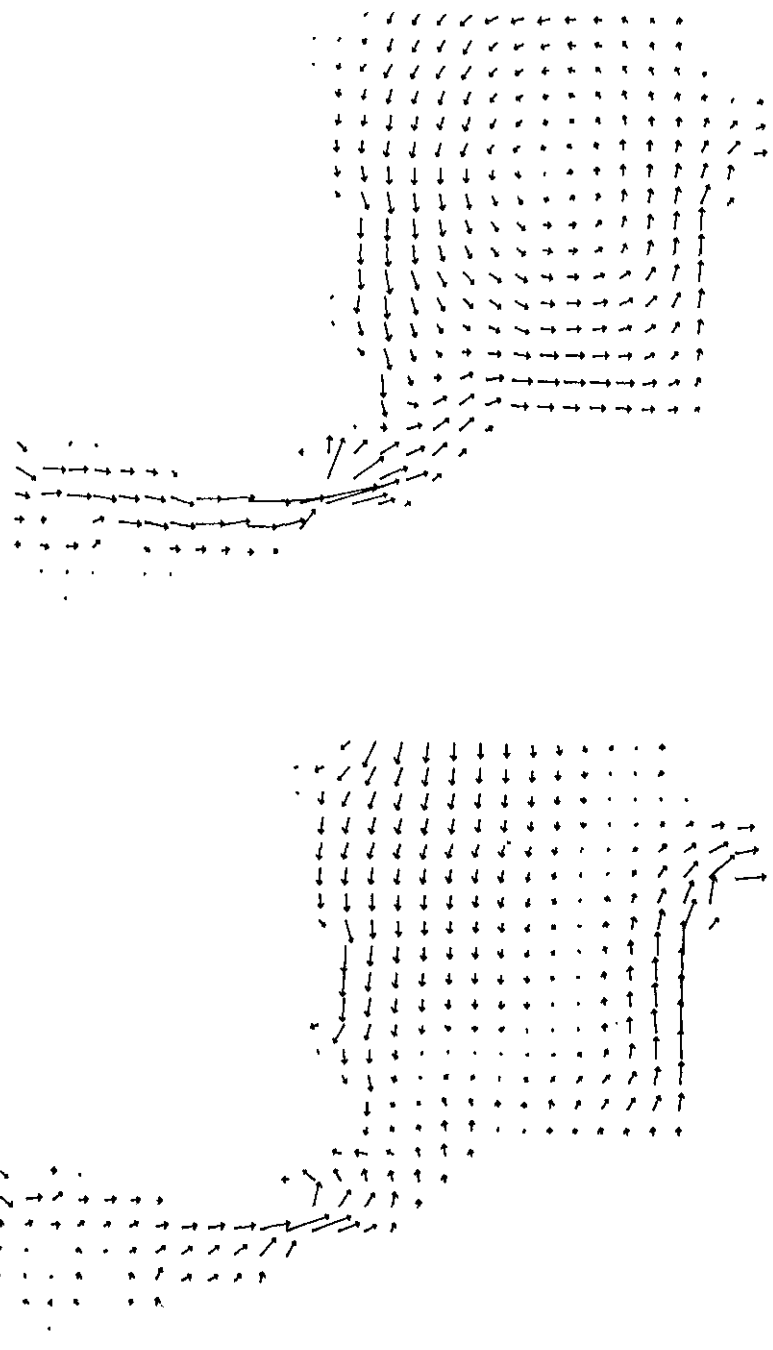


Figure 6.19: Simulated (above) and filtered (below) velocities in case of a realistic wind input.

January 26, 1983 - February 2, 1983. The parameters of the truth and filter-model are chosen as in experiment 6.1. The results can be found in the *figures 6.18* and *6.19* where the simulated and filtered velocities at two different times are presented. The experiment shows that, considering the limited number of measurements available, the filter is able to satisfactorily reconstruct the velocities in case of a realistic spatially variable wind input. Here we note that in the case shown in figure 6.19 the storm depression is located exactly above the North Sea. As a consequence, the spatial variability of the wind velocities in this area is extremely large.

6.5.3 External surge

Experiment 6.4

This experiment deals with the capability of the filter to correct errors associated with the northern open boundary. Measurements are generated using the truth-model in which at this open boundary the in-going Riemann invariant is prescribed. In the filter-model it is assumed that this Riemann invariant is zero. In both models the wind input is not taken into consideration. The parameters of the truth and filter-model are chosen as in experiment 6.1. In the *figures 6.20* and *6.21* at two different times the simulated and filtered velocities are shown. In the northern part of the model the velocities are reconstructed not very accurately since very few measurements are available in this area. However, as the waves propagate southwards more measurements become available and the reconstruction becomes more accurate.

In *figure 6.22* the predictions of the water-level at Flushing are compared with the results of the truth-model. The experiment shows that the filter is capable of correcting an erroneous boundary condition and that it can identify the wave motion along the English coast using the water-level measurements that are available.

6.6 Experiment using field data

In this section we describe an application of the Kalman filter to field data gathered during the stormy period January 26, 1983 - February 2, 1983. The wind velocities and pressure fields have been computed by an atmospheric model of the K.N.M.I. The twelve tide gauges that have been used were shown in figure 6.5. The measurements were available each hour and are assumed to be taken at the nearest grid point of the model. At the open boundaries we prescribe the condition (6.33). Because of the linearity of the model the astronomical tide has been eliminated by means of harmonic analysis. The filter is only used to estimate and predict the meteorological effect that is superimposed on the astronomical tide.

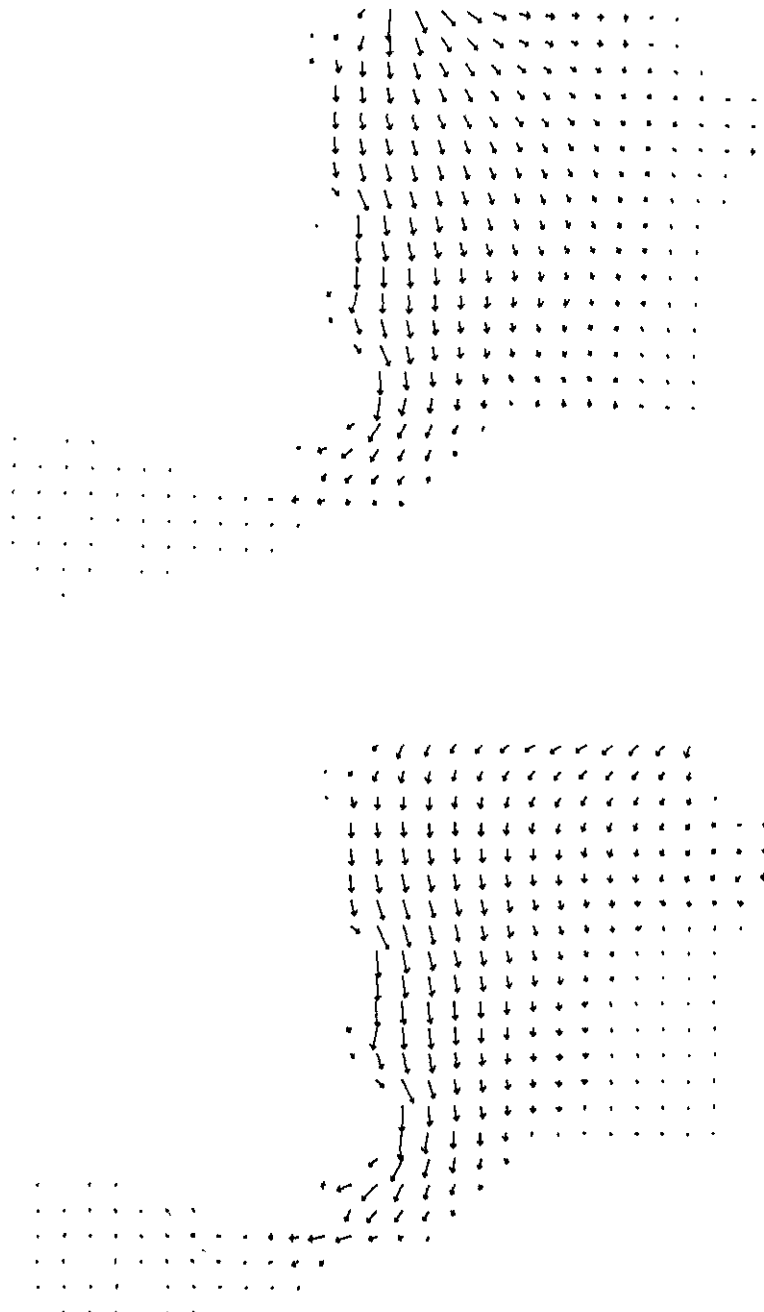


Figure 6.20: Simulated (above) and filtered (below) velocities.

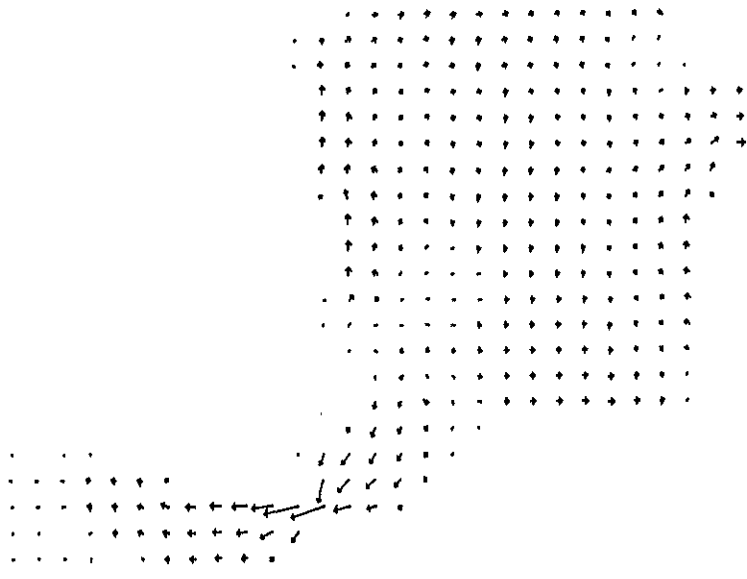


Figure 6.21: Simulated (above) and filtered (below) velocities.

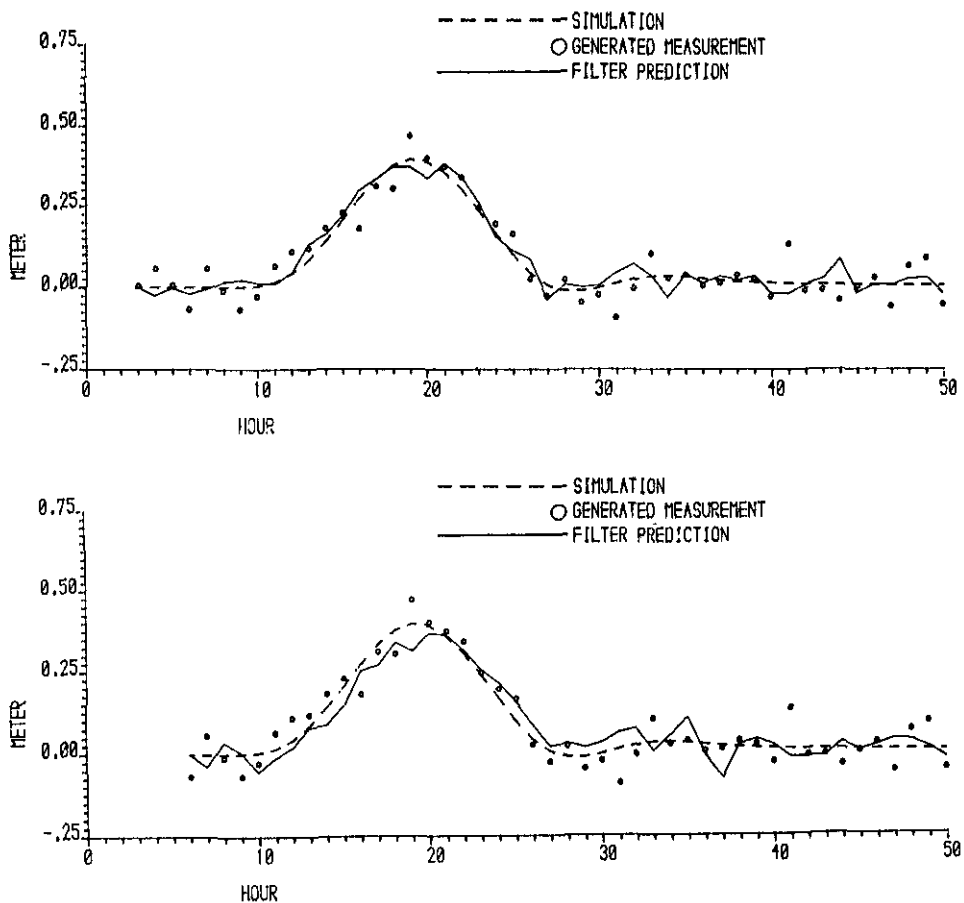


Figure 6.22: Three hours ahead (above) and six hours ahead (below) predictions of the water-level at Flushing.

We have assumed the standard deviation of the measurement noise to be: $r = 0.03$ m. The statistics of the system noise processes have been determined by studying the results of experiment 6.3. The values of σ^2 and α are chosen such that the capability of the filter to reconstruct the water velocities that are created by a realistic wind input is as good as possible, yielding $\sigma^2 = 100$ and $\alpha = 0.90$. The system noise is introduced each measurement time.

The results of the three hours ahead predictions at a number of measurement stations during the period January 26, 00:00 - January 29, 23:00 are shown in figures 6.23 and 6.24. Here the predictions of the deterministic model without using the data and the filter predictions are compared with the observations. During this period two

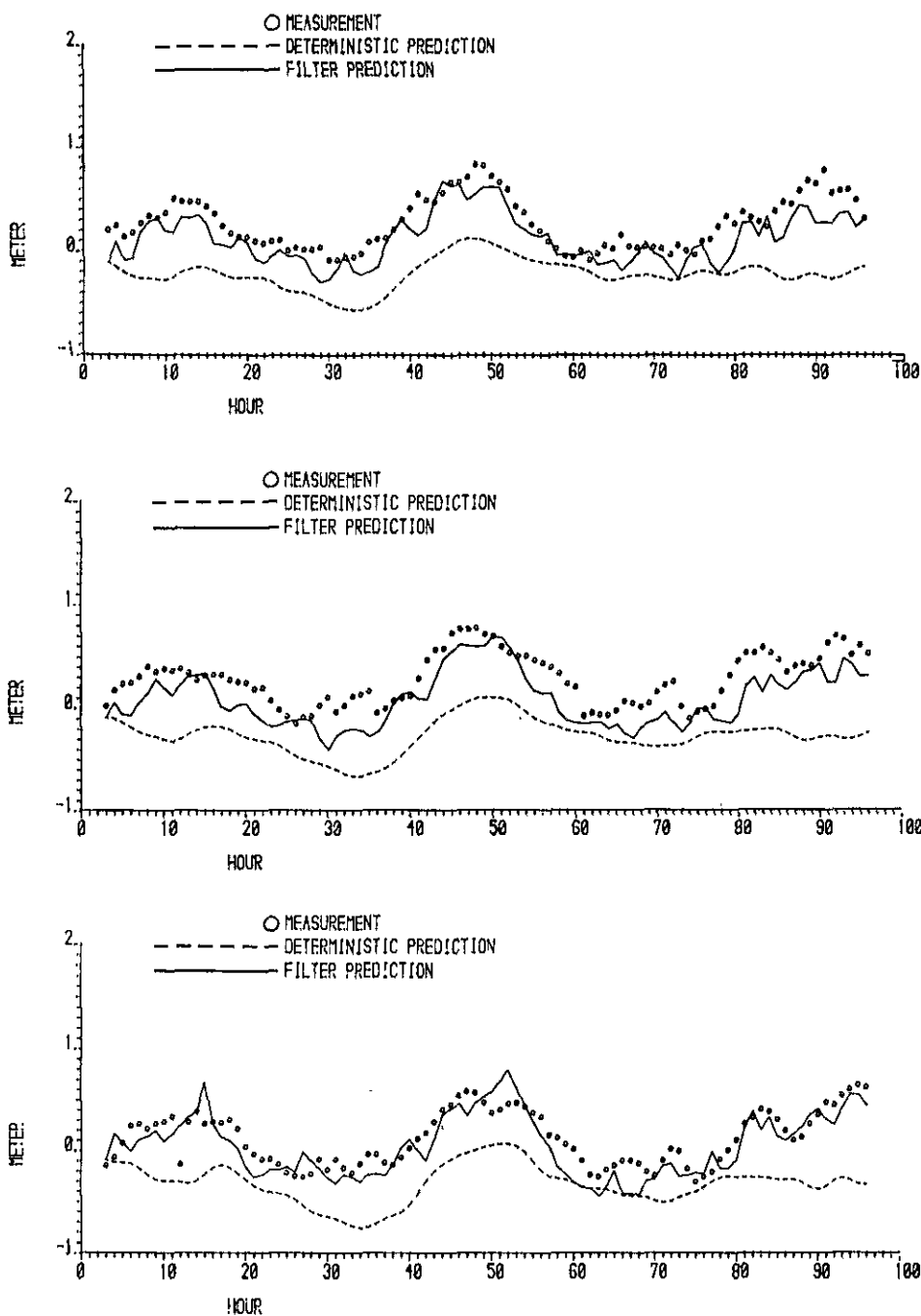


Figure 6.23: Three hours ahead predictions at Lowestoft (above), Felixstowe (middle) and Southend (below).

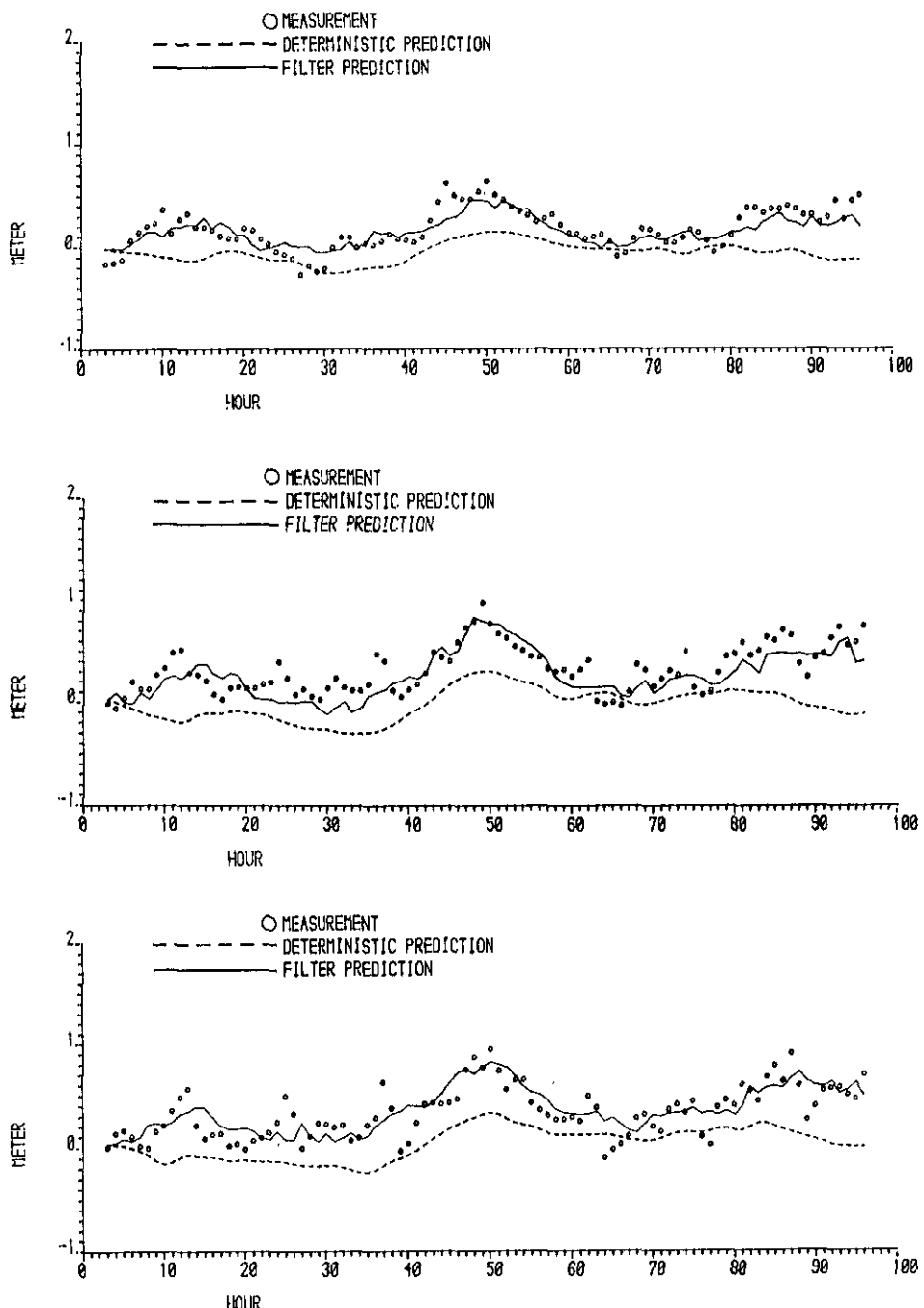


Figure 6.24: Three hours ahead predictions at Dover (above), Hook of Holland (middle) and IJmuiden (below).

	deterministic prediction		filter prediction	
	mean	standard deviation	mean	standard deviation
Dover	-18 cm	17 cm	-1 cm	13 cm
Hook of Holland	-28 cm	18 cm	-15 cm	11 cm
IJmuiden	-20 cm	14 cm	-2 cm	9 cm

Table 6.2. Six hours ahead predictions during January 26 - January 29.

	deterministic predictions		filter prediction	
	mean	standard deviation	mean	standard deviation
Dover	-16 cm	24 cm	-2 cm	18 cm
Hook of Holland	-24 cm	25 cm	-17 cm	17 cm
IJmuiden	-14 cm	19 cm	-2 cm	15 cm

Table 6.3. Six hours ahead predictions during January 30 - February 2.

relatively small surges occurred. The six hours ahead predictions at Dover, Hook of Holland and IJmuiden can be found in *figures 6.25 - 6.27*. Here, since we are mainly interested in the predictions during high and low water, we also present the predictions with the astronomical tide included. Similar results, obtained during January 30, 00:00 - February 2, 23:00, are shown in *figures 6.28 - 6.32*. During this period one small surge and one extremely large surge occurred. To summarize the results we have computed – in tables 6.2 and 6.3 – the mean and standard deviation of the six hours ahead predictions at high and low water.

The results show that, although the deterministic model produces erroneous predictions, the filter is able to predict accurately. Here we note that by increasing the domain of the North Sea model or by using a more detailed, possibly non-linear model, the deterministic predictions can be improved. However, the largest errors of the deterministic model are caused by the erroneous meteorological input and as a consequence, no such model, linear or non-linear, would produce accurate results*. Of course, the filter results also depend on the meteorological input. However, the influence of an erroneous input on the predictions produced by the filter is limited. Only input errors inside the domain of dependence of the predictions degrade the

* This is no criticism of atmospheric models. Predicting meteorological conditions is extremely complicated due to the chaotic behaviour of the atmosphere.

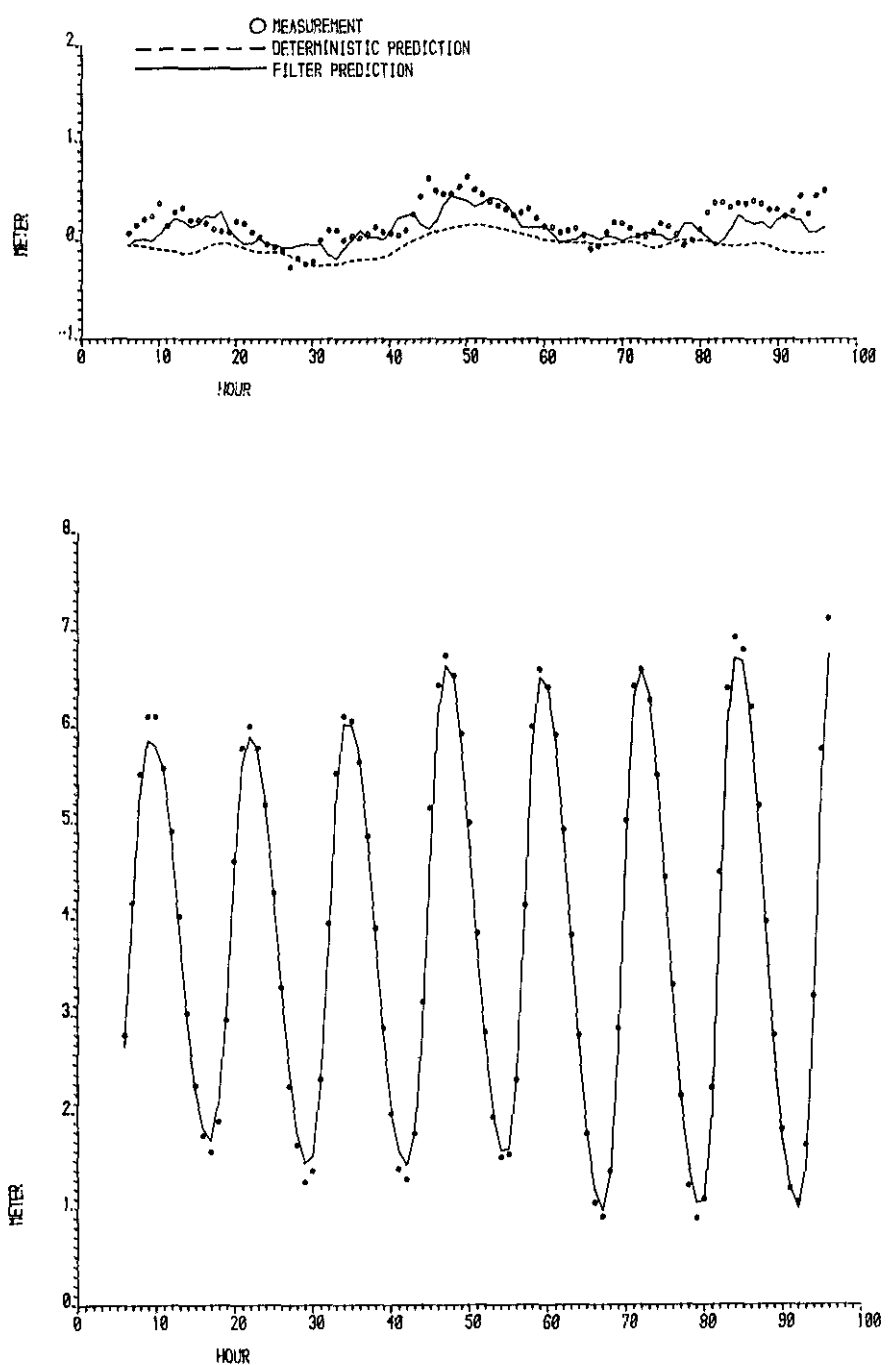


Figure 6.25: Six hours ahead predictions at Dover.

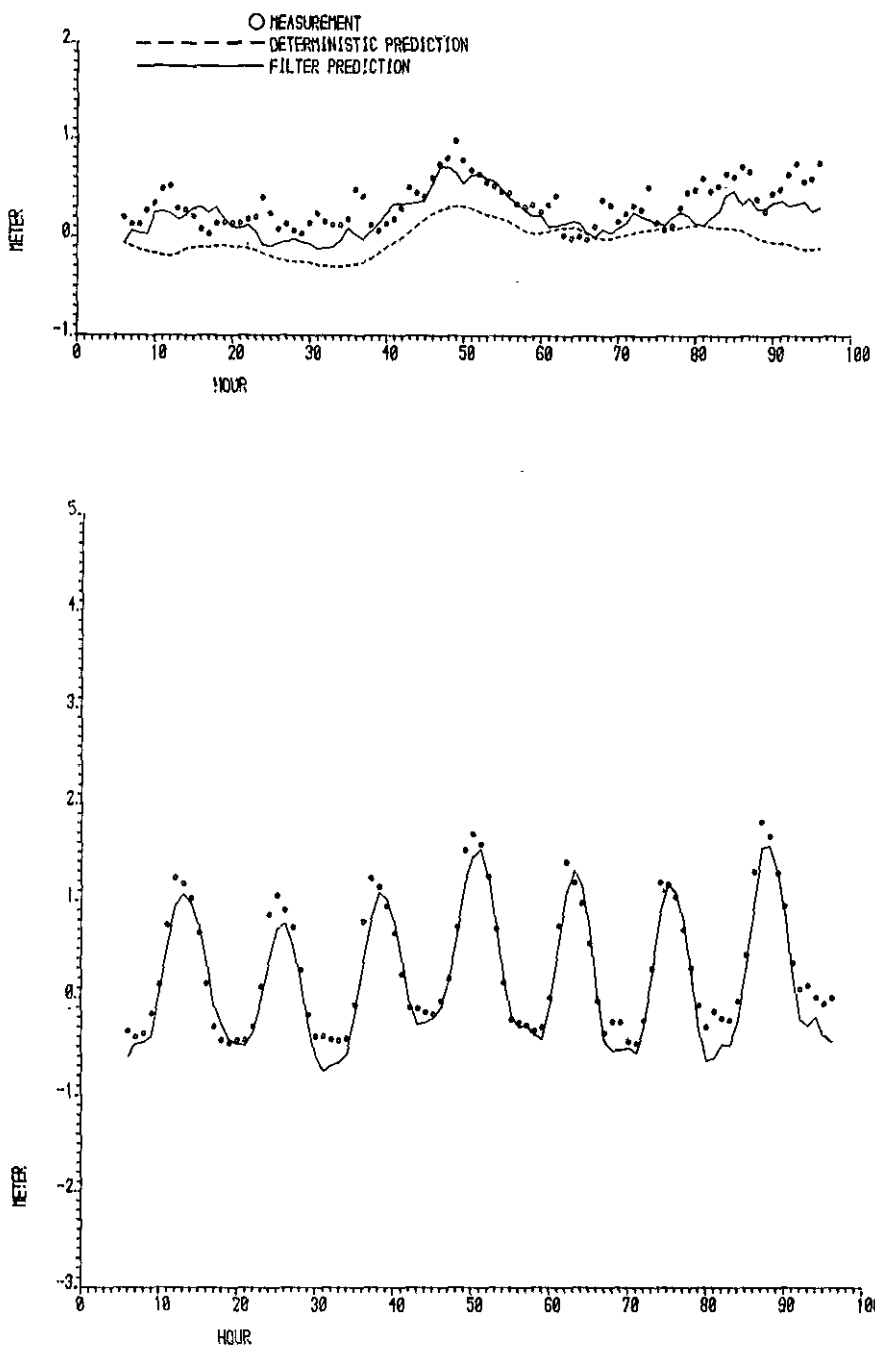


Figure 6.26: Six hours ahead predictions at Hook of Holland.

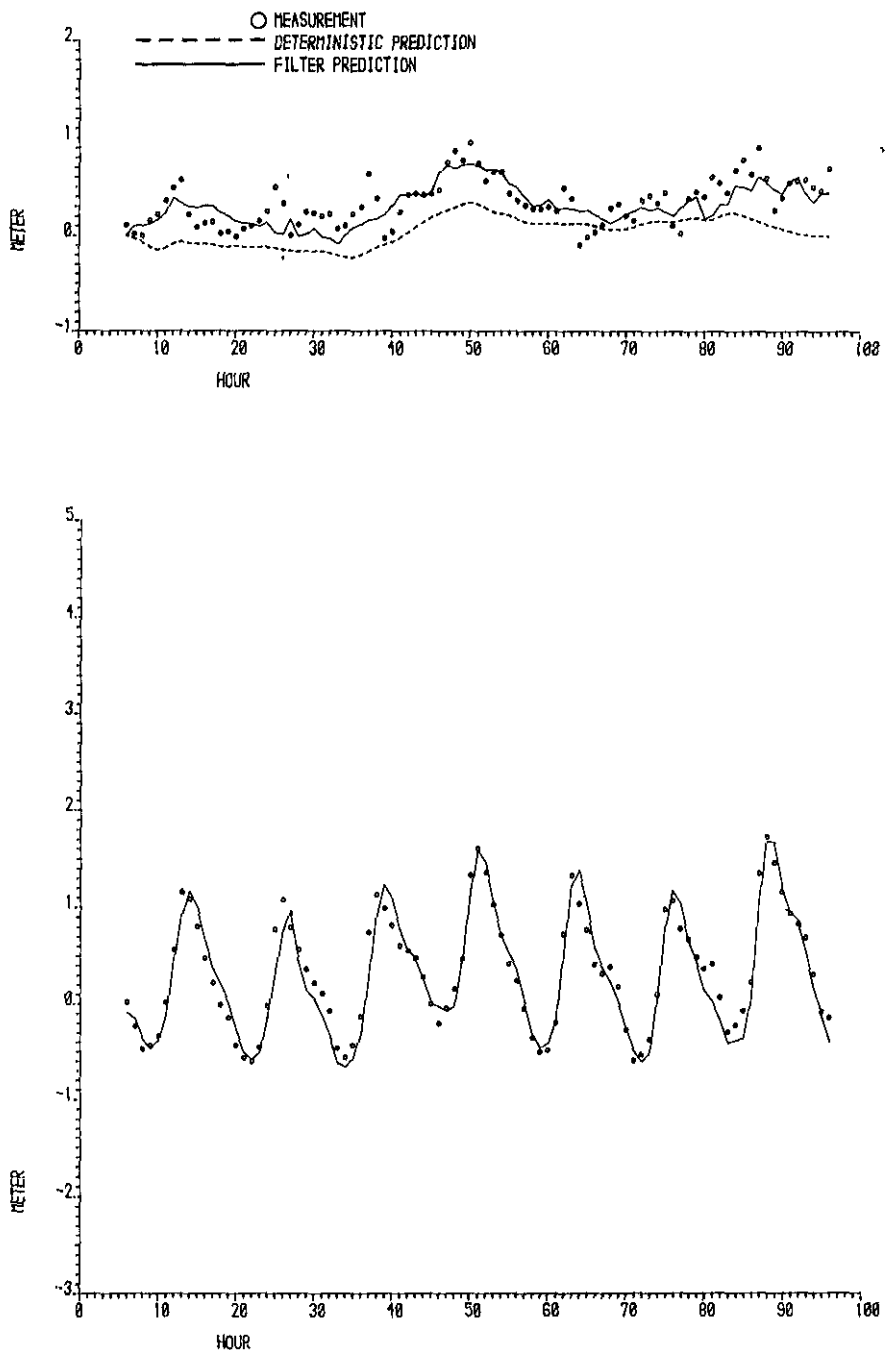


Figure 6.27: Six hours ahead predictions at IJmuiden.

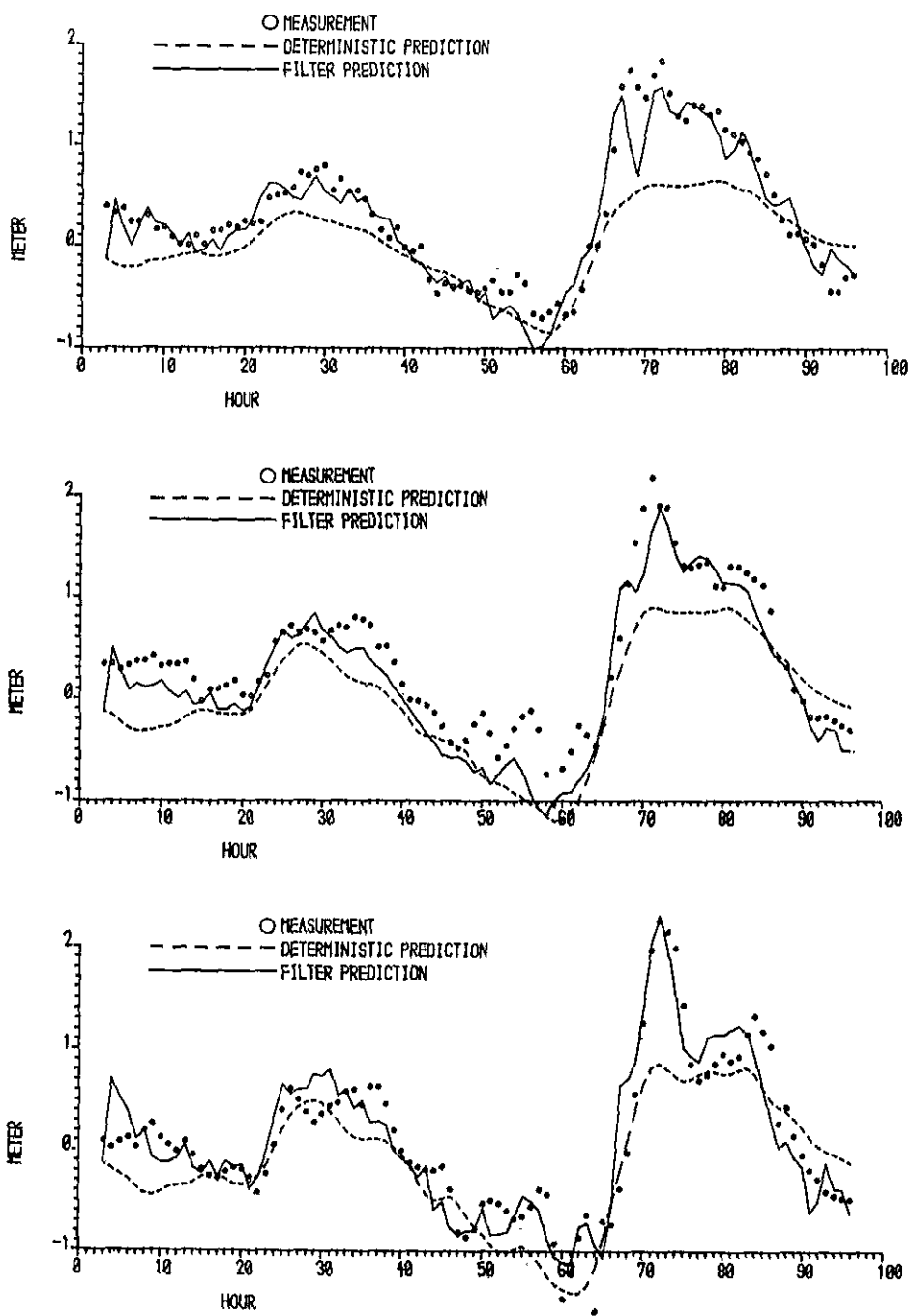


Figure 6.28: Three hours ahead predictions at Lowestoft (above) and Felixstowe (middle) and Southend (below).

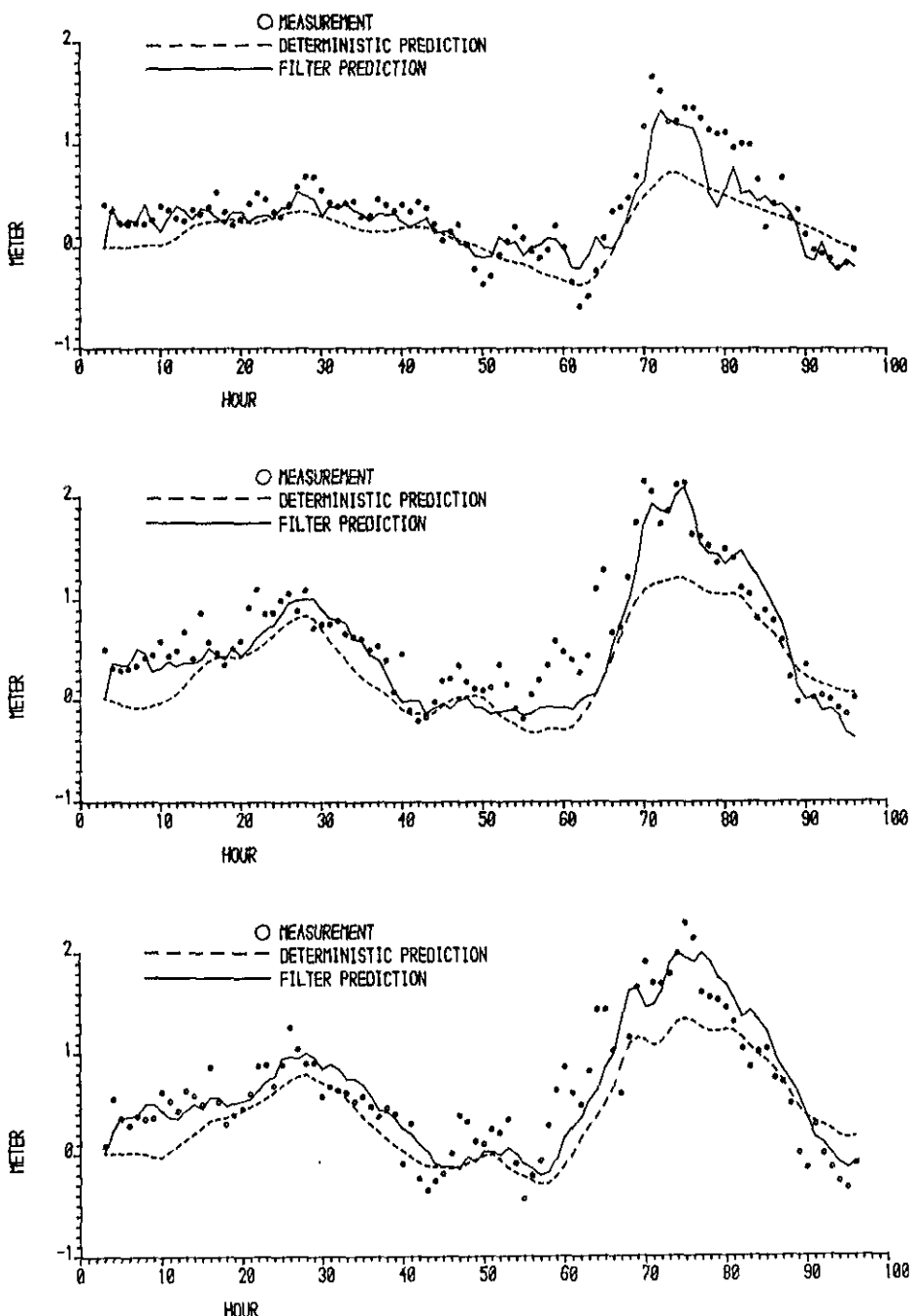


Figure 6.29: Three hours ahead predictions at Dover (above), Hook of Holland (middle) and IJmuiden (below).

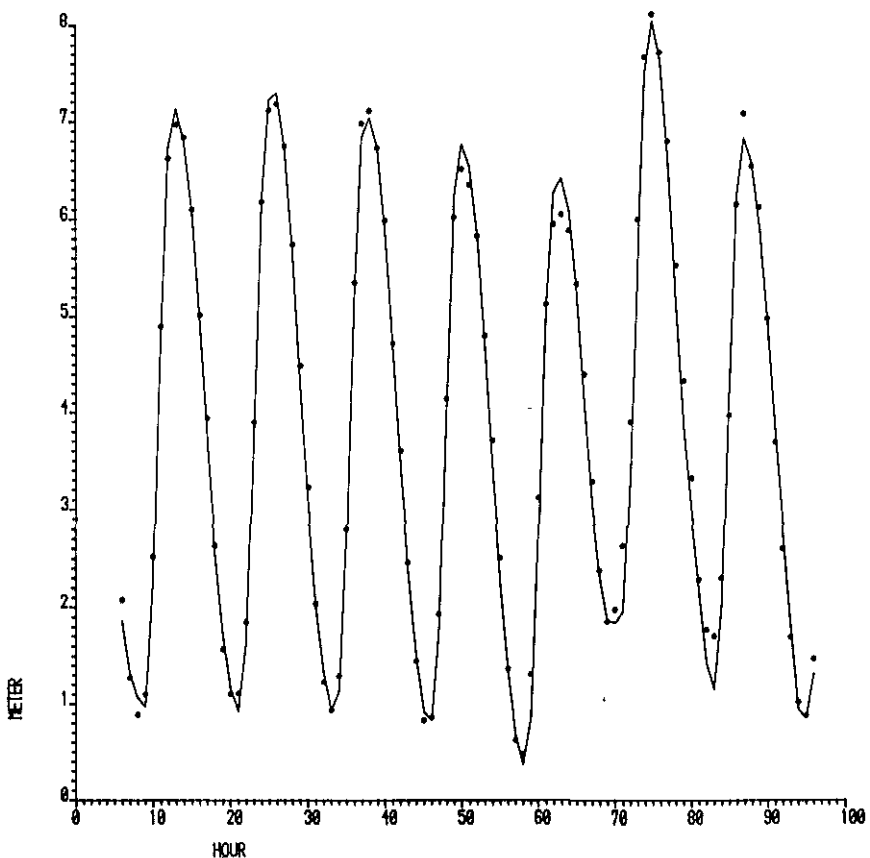
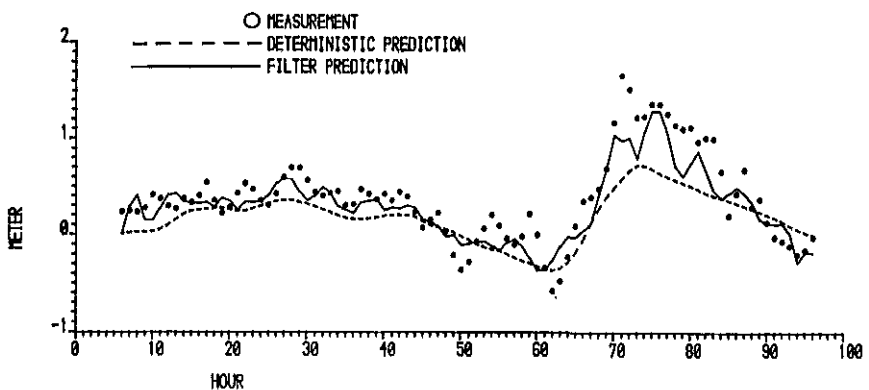


Figure 6.30: Six hours ahead predictions at Dover.

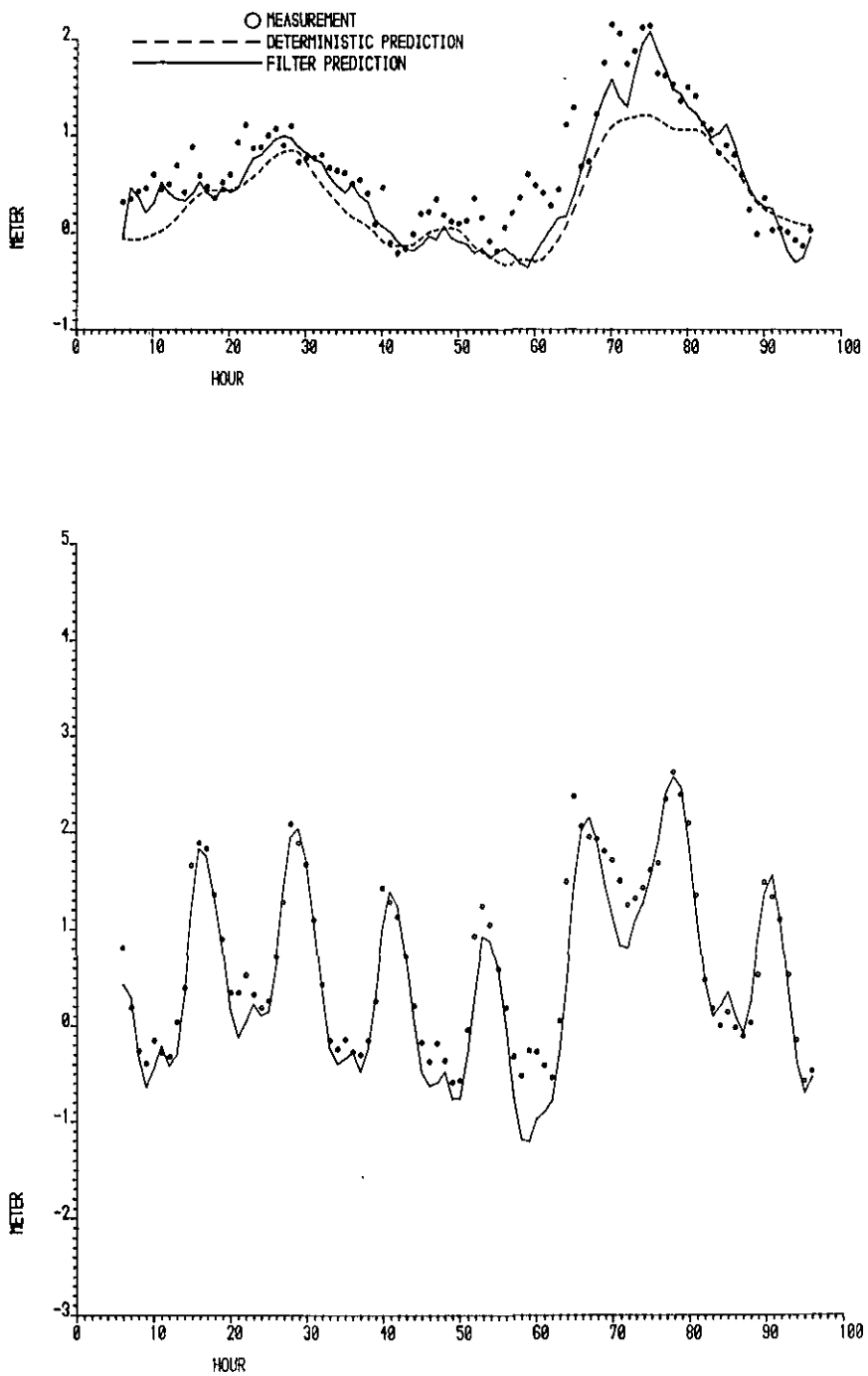


Figure 6.31: Six hours ahead predictions at Hook of Holland.

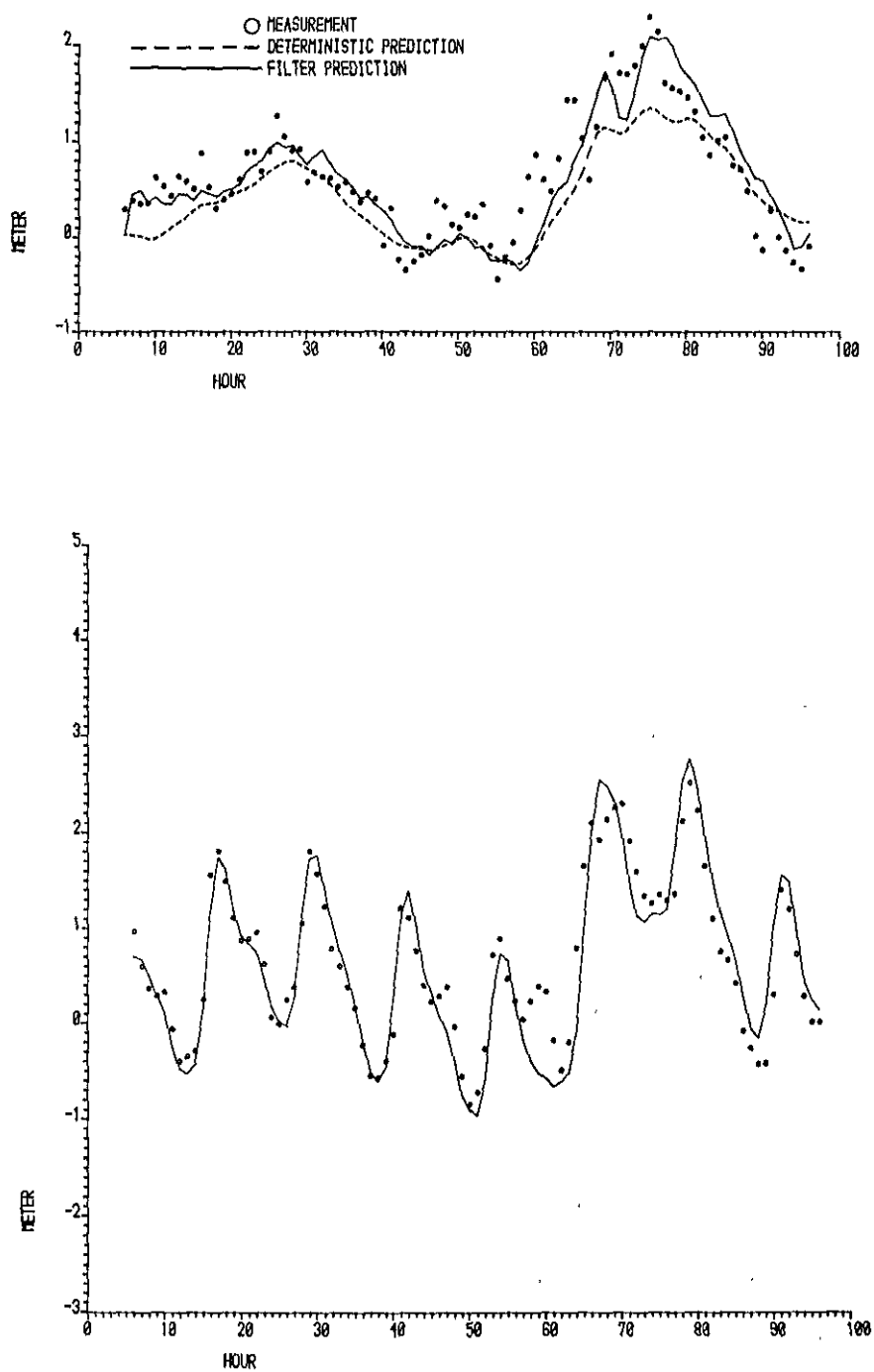


Figure 6.32: Six hours ahead predictions at IJmuiden.

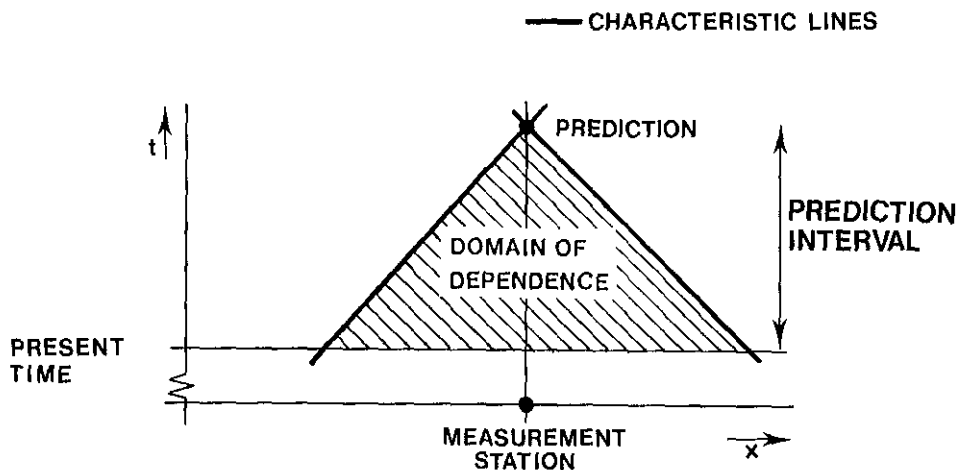


Figure 6.33: Domain of dependence of the predictions in case of one space dimension (in case of two space dimensions we have, instead of two characteristic lines, a characteristic coin).

performance of the filter (see *figure 6.33*). The size of this domain depends on the prediction interval. By increasing this interval the influence of an erroneous meteorological input becomes more important.

To illustrate this discussion we have applied the deterministic model as well as the filter with a wind friction coefficient $\gamma = 2.5 \times 10^{-6}$. In *figure 6.34* and *6.35* respectively the three and six hours ahead predictions at Dover, Hook of Holland and IJmuiden during January 30, 00:00 - February 2, 23:00 are shown. These results should be compared with the predictions that are computed with $\gamma = 3.2 \times 10^{-6}$ and that are presented in *figures 6.28 - 6.32*. While the difference between the two deterministic simulations at certain times is more than 30 cm, the predictions produced by the two filters differ maximal 8 cm for the three hours ahead predictions and 15 cm for the six hours ahead predictions.

Besides the erroneous meteorological input, prediction errors are caused by the fact that we have used a linear model and have neglected the non-linear interaction between tide and surge. However, as in the case of the erroneous meteorological input, only the non-linearities inside the domain of dependence of the predictions degrade filter performance. Unfortunately, the most important non-linear effects are introduced in the southern part of the North Sea and consequently, for the six hours predictions, inside the domain of dependence of these predictions. Therefore, we may expect that the filter predictions can be improved by the use of a non-linear model.

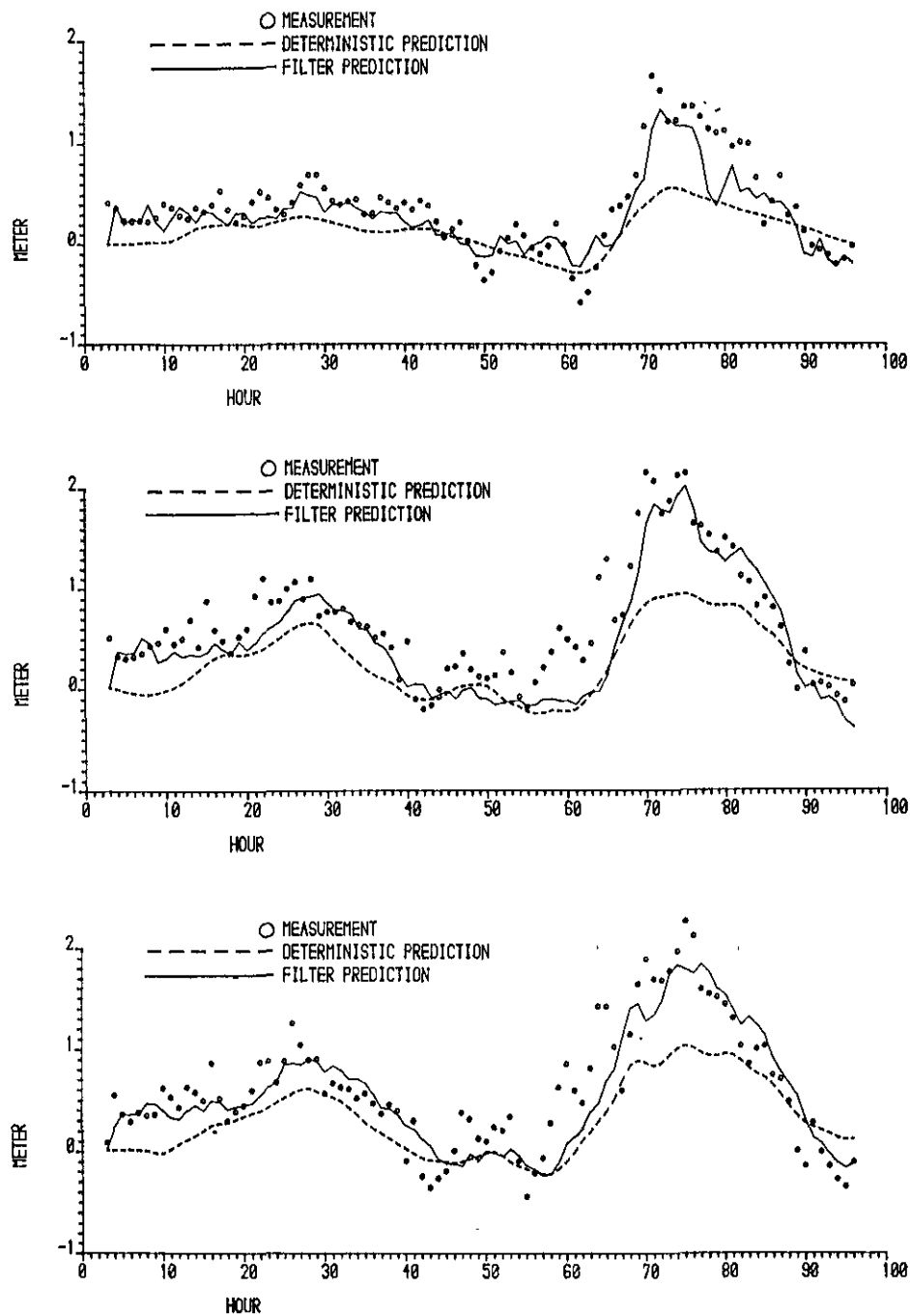


Figure 6.34: Three hours ahead predictions at Dover (above), Hook of Holland (middle) and IJmuiden (below) in case of an erroneous wind friction coefficient.

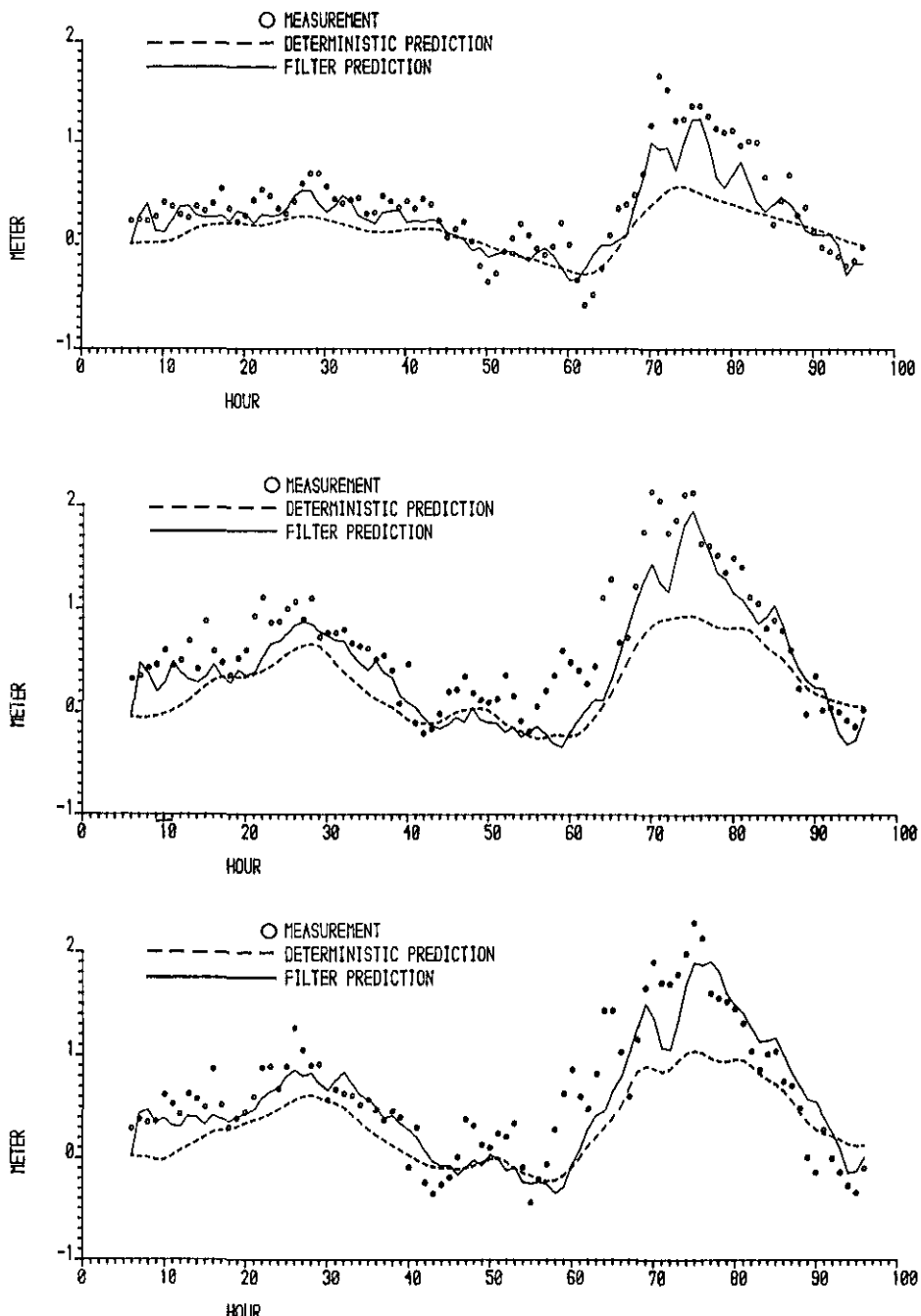


Figure 6.35: Six hours ahead predictions at Dover (above), Hook of Holland (middle) and IJmuiden (below) in case of an erroneous wind friction coefficient.

6.7 Discussion

In this chapter a steady-state Kalman filter based on a two-dimensional model of the North Sea has been described. The deterministic model has been derived by discretising the linearized shallow water equations using a modified Sielecki scheme. By defining the system noise process on a coarse grid and in addition, by employing the Chandrasekhar-type algorithm, a computational attractive implementation of the filter is obtained. Furthermore, we have shown that the algorithm can be vectorized efficiently and that using a CDC CYBER 205 vector processor it is possible to combine the steady-state filter approach with very large deterministic models. Numerical difficulties can be avoided by carefully choosing the finite difference scheme, the boundary treatment and, most important, the system noise process.

The filter has been tested extensively using simulated data and field data. The results show excellent filter performance, especially if we take into account that the number of measurements available (as yet) has been very limited. With respect to the results of the deterministic model without using the water-level measurements available, the improvement obtained by filtering these measurements is substantial.

Since the deterministic North Sea model that has been developed in this chapter is linear, the non-linear interaction between tide and surge has not been taken into account. Therefore, to improve the predictions it is intended to combine the filter with the existing WAQUA system of Rijkswaterstaat for the deterministic computation of two-dimensional shallow water flow. When this general software package for two-dimensional shallow water flow identification becomes available, it will be easy to embed the very recently developed non-linear WAQUA model of the North Sea (Voogt 1985) in a Kalman filter. Since the depth of the North Sea is approximately 20-100 m and consequently, the non-linearities of the model are relatively small, we expect from the results shown in Sections 4.5 and 5.4 that the constant gain extended Kalman filter will produce results that are nearly optimal. Furthermore, since the grid of this non-linear model is very fine with respect to the grid of the atmospheric model and, consequently, of the system noise, we may expect that the introduction of the numerical viscosity to eliminate the short waves is not necessary.

7 Conclusions and recommendations

In this study two Kalman filters have been developed to predict water-levels along the Dutch coast. One approach is based on a non-linear one-dimensional model of the tidal movement. However, since the filter is able to estimate the uncertain parameter in this conceptual model using the measurements available, this model can be continuously adapted to changing circumstances. The filter is shown to produce satisfactory predictions during storm surge conditions. However, the prediction interval is limited since the one-dimensional approximation is only realistic for a small part of the southern North Sea.

Using the results of the one-dimensional approach, WAKFIL, a general software package for one-dimensional tidal filtering, has been developed. It is based on the IMPLIC system of Rijkswaterstaat for the deterministic description of one-dimensional tidal movement. Using WAKFIL it is possible to embed almost any existing IMPLIC model in a Kalman filter. Employing WAKFIL, the one-dimensional approach will be improved by using an existing, more detailed model of the Eastern Scheldt.

Although the WAKFIL system has been developed to predict water-levels in the Eastern Scheldt, it is applicable to a wide range of practical shallow water flow problems. It can be used for instance to predict water-levels in a river since in this case a one-dimensional representation of the water movement is quite adequate. Accurate predictions of the water-level along the Rhine and the Meuse in case of a river flood are of importance in taking precautionary actions to protect the dikes along these rivers.

Another application of WAKFIL is the calibration of one-dimensional models. The accepted practice is that the modeller adjusts the uncertain parameters by means of "trial and error" until the model produces results that resemble the available recorded data. This is a rather subjective process that takes up much time. Furthermore, due to changing topographic flow conditions, the parameters in the model will not be constant over a long period of time and consequently they will have to be adjusted regularly. By employing WAKFIL to estimate the uncertain parameters in the model the calibration process becomes very simple. Moreover, studying the time-dependent behaviour of these parameters may suggest improvements of the empirical parametrizations in the model.

The second Kalman filter approach developed in this study is based on a two-dimensional model of the entire North Sea. To obtain a computationally efficient implementation the Kalman filter is approximated by a time-invariant one. Using field data gathered during a stormy period, the filter has produced accurate predictions despite the fact that the results of the deterministic model without filter has been poor. It is shown that by using a vector processor the filter can be combined with large, possibly non-linear, two-dimensional models.

When a two-dimensional filter based on a large model is used on an operational basis the steady-state filter gain has to be computed on a vector processor. Once this filter gain is available the filter calculations that have to be performed on-line are very limited. Compared with the underlying deterministic model, the additional computational effort required to filter the measurements available and to improve the deterministic results is less than 10%. The additional on-line storage requirement is, say, 100%.

It is intended to combine the two-dimensional filter with the existing WAQUA system of Rijkswaterstaat for the deterministic description of two-dimensional shallow water flow. Since WAQUA is based on an alternating-direction-implicit scheme to approximate the shallow water equations (Stelling 1983) the filter approach will be modified by adopting this finite difference scheme. When this general system for two-dimensional shallow water flow identification becomes available it will be easy to combine the very recently developed WAQUA model of the North Sea (Voogt 1985) with a Kalman filter. Of course, in this case also many other existing WAQUA models can be embedded in a Kalman filter.

The water-level prediction in the Eastern Scheldt can be further improved by combining the one and two-dimensional approaches. The two-dimensional filter produces a realistic prediction of the global water movement in the North Sea, especially in case of spatially varying meteorological conditions. The predictions of the two-dimensional filter can then serve as the boundary conditions for a one-dimensional filter, in which more local effects are taken into account.

Still further investigations on the application of Kalman filtering to tidal prediction problems are required. Besides the improvement of the underlying deterministic models just described, a number of further studies can be recommended.

In the derivation of the filter equations it has been assumed that the system noise is white, i.e. uncorrelated in time. In practice this condition is not likely to be satisfied. Jazwinski (1970) describes a procedure to take into account an exponential autocorrelation of the system noise by augmenting the state vector with the noise components. The system noise is in this case said to be coloured. In case of the one-

dimensional filter, this procedure results in a new state vector that is approximately twice as large as the original one and consequently, an unacceptable increase of the computational effort would be required. However, in the two-dimensional case the introduction of coloured system noise increases the computing time and memory requirements very little. We may expect that by implementing this feature the accuracy of the predictions can be further improved.

In developing the two-dimensional filter attention has been concentrated on the estimation and prediction of the water movement. However, by introducing a small modification, the filter will be able to estimate the wind velocity as well. In this case the water-level observations available can be used to obtain information about the actual wind velocities above the North Sea.

One of the major problems of the application of Kalman filters is that the noise statistics have to be specified. This knowledge is very poor and therefore adaptive filters often have been employed (Jazwinski 1970). Using these filters the residuals are examined to establish whether or not they actually possess their theoretical statistical properties and, if not, the statistics of the noise processes are adopted. However, in our case these filters are not successful. Since the filter results are not very sensitive to the noise statistics, many residuals have to be analysed before a statistically significant conclusion can be drawn. Unfortunately, during stormy periods the conditions change rapidly and consequently the filter is not able to adapt the model in time. In fact, the storm is over before the filter is aware of the fact that there is something wrong with the covariance matrices of the noise processes. A more promising approach to adapt the noise processes to changing conditions would be to develop an empirical expression that describes the relation between the noise statistics and the wind velocity or another relevant parameter. Investigations should be carried out to gain insight into these relations.

Further investigation is also required to generalize the two-dimensional filter to the time-varying case. Such a filter would be important to exploit the knowledge about the time-dependent behaviour of the noise processes. Furthermore, if in future satellites are used to obtain water-level observations, the measurement locations will be time-dependent. Consequently, the steady-state filter developed in this study will have to be modified.

References

- Abbott, M.B., AN INTRODUCTION TO THE METHOD OF CHARACTERISTICS, Elsevier, Amsterdam, 1966.
- Abbott, M.B., COMPUTATIONAL HYDRAULICS, Pitman, London, 1979.
- Anderson, B.D.O., and J.B. Moore, OPTIMAL FILTERING, Prentice-Hall, Englewood Cliffs, New Jersey, 1979.
- Batchelor, G.K., AN INTRODUCTION TO FLUID DYNAMICS, Cambridge University Press, Cambridge, U.K., 1970.
- Bierman, G.J., FACTORIZATION METHODS FOR DISCRETE SEQUENTIAL ESTIMATION, Academic Press, New York, 1977.
- Box, G.E.P., and J.M. Jenkins, TIME SERIES ANALYSIS: FORECASTING AND CONTROL, Holden-Day, San Francisco, 1970.
- Bretschneider, C.L., ENGINEERING ASPECTS OF HURRICANE SURGE, in: ESTUARY AND COASTLINE HYDRODYNAMICS, A.T. Ippen (ed.), McGraw-Hill, New York, 1966.
- Bretschneider, C.L., STORM SURGES, in: ADVANCES IN HYDROSCIENCE, Vol 4, 1967.
- Brummelhuis, P.G.J. ten, WATERHOOGTEVOORSPELLEN IN DE OOSTERSCHELDE MET BEHALF VAN KALMAN FILTERING, M. Sc. Thesis, T.H. Twente, 1984 (in Dutch).
- Brummelhuis, P.G.J. ten; B. de Jong and A.W. Heemink, ON-LINE PREDICTION OF WATER-LEVELS IN AN ESTUARY USING KALMAN FILTERS, Proceedings of the 4th Int. Symp. on Stochastic Hydraulics, Urbana-Champaign, 1984.
- Brummelhuis, P.G.J. ten, B. de Jong and A.W. Heemink, KALMAN FILTERS FOR THE DESCRIPTION AND PREDICTION OF TIDAL MOTION, DIV-report nr. 1985-769, 1985.
- Budgell, W.P., and A. El-Shaarawi, TIME SERIES MODELLING OF STORM SURGES ON A MEDIUM-SIZED LAKE, in: MARINE FORECASTING, J.C.J. Nihoul (ed.), Elsevier, Amsterdam, 1978.
- Budgell, W.P., A STOCHASTIC-DETERMINISTIC MODEL FOR PREDICTING TIDES IN BRANCHED ESTUARIES, Proceedings of the 3rd Int. Sym. on Stochastic Hydraulics, Tokyo, 1980
- Budgell, W.P., A STOCHASTIC-DETERMINISTIC MODEL FOR ESTIMATING TIDES IN BRANCHED ESTUARIES, Report No. 10, Ocean Science and Surveys, Fisheries and Oceans, Burlington, 1981.
- Cartwright, D.E., OCEANIC TIDES, Int. Hydrogr. Rev., 55, 1978.
- Chao-lin Chiu (ed.), APPLICATION OF KALMAN FILTER THEORY TO HYDROLOGY, HYDRAULICS AND WATER RESOURCES, University of Pittsburg, Pittsburg, 1978.
- Chao-lin Chiu and E.O. Isu, KALMAN FILTER IN OPEN CHANNEL FLOW ESTIMATION, Journ. Hydraul. Div., 104, 1978.
- Chavent, G., IDENTIFICATION OF DISTRIBUTED PARAMETER SYSTEMS: ABOUT THE OUTPUT LEAST SQUARES METHOD, ITS IMPLEMENTATION AND IDENTIFICATION AND SYSTEM PARAMETER ESTIMATION, Pergamon Press, Darmstadt, 1979.
- Christianssen, H., W. Siefert, STORM SURGE PREDICTION BY COMBINED WIND AND TIDE DATA, Proceedings of the 16th Coastal Engineering Conf., Hamburg, 1978.
- Cunge, J.A., F.M. Holly and A. Verwey, PRACTICAL ASPECTS OF COMPUTATIONAL RIVER HYDRAULICS, Pitman, Boston, 1980.
- Davies, A.M., APPLICATION OF THE GALERKIN METHOD TO THE FORMULATION OF A THREE-DIMENSIONAL NON-LINEAR HYDRODYNAMIC NUMERICAL SEA MODEL, Appl. Math. Modelling, 4, 1980.
- Desalu, A.A., L.A. Gould and F.C. Schweppe, DYNAMIC ESTIMATION OF AIR POLLUTION, IEEE Trans. Autom. Control, Vol AC19, 1974.
- Dooren, P. van, and M. Verhaegen, THE USE OF CONDENSED FORMS IN LINEAR SYSTEM THEORY, IEEE Workshop on Robust Numerical Software in Control Systems Design, London, 1983.
- Dooren, P. van, and M. Verhaegen, ON THE RELIABILITY AND EFFICIENCY OF DIFFERENT KALMAN FILTER ALGORITHMS. PART I: THEORETICAL RESULTS, IEEE Trans. Autom. Control, 1986, to appear.
- Dronkers, J.J., TIDAL COMPUTATIONS IN RIVERS AND COASTAL WATERS, North Holland Publishing Company, Amsterdam, 1964.

- Dronkers, J.J., TIDAL COMPUTATIONS FOR RIVERS, COASTAL AREAS AND SEAS, Journal of Hydraulics Division, 1969.
- Dronkers, J.J., TIDAL THEORY AND COMPUTATION, in: ADVANCES IN HYDROSCIENCES, Vol 10, Ven Te Chow (ed.), Academic Press, New York, 1975.
- Dun-Christensen, PROVISIONAL EXPERIENCE WITH THE PRACTICAL USE OF AN IIN MODEL FOR CALCULATION OF SEA LEVEL VARIATIONS ALONG THE DANISH NORTH SEA COAST, in: NORTH SEA DYNAMICS, J. Sündermann, and W. Lenz (eds.), Springer-Verlag, Berlin, 1983.
- Eykhoff, P., SYSTEM IDENTIFICATION, New York, Wiley-Interscience, 1974.
- Flather, R.A., TIDAL MODEL OF THE NORTH-WEST EUROPEAN CONTINENTAL SHELF, Mém. Soc. R. Sci. Liège, 10, 1976.
- Flather, R.A. and R. Procter, PREDICTION OF NORTH SEA STORM SURGES USING NUMERICAL MODELS: RECENT DEVELOPMENTS IN U.K., in: NORTH SEA DYNAMICS, J. Sündermann and W. Lenz (eds.), Springer-Verlag, Berlin, 1983.
- Fronza, G., A. Sipriro and A. Tonielli, REAL-TIME FORECAST OF AIR POLLUTION OF EPISODES IN THE VENETIAN REGION, PART 2: THE KALMAN PREDICTOR, Appl. Math. Model., 3, 1979.
- Gerritsen, H., ACCURATE BOUNDARY TREATMENT IN SHALLOW WATER FLOW COMPUTATIONS, Ph. D. Thesis, T.H. Twente, 1982.
- Ghil, M., et al., APPLICATION OF ESTIMATION THEORY TO NUMERICAL WEATHER PREDICTION, in: DYNAMIC METEOROLOGY: DATA ASSIMILATION METHODS, L. Bengtsson, M. Ghil and E. Källén (eds.), Springer-Verlag, New York, 1981.
- Godin, G., THE ANALYSIS OF TIDES, University of Toronto Press, Toronto, 1972.
- Goodson, R.E., and R.E. Klein, DEFINITION AND SOME RESULTS FOR DISTRIBUTED SYSTEM OBSERVABILITY, IEEE Trans. Autom. Control, Vol AC15, 1970.
- Goodson, R.E., and R.E. Klein, AUTHORS REPLY TO: COMMENTS ON A DEFINITION AND SOME RESULTS FOR DISTRIBUTED SYSTEM OBSERVABILITY, IEEE Trans. Autom. Control, Vol AC16, 1971.
- Hahn, W., THEORY AND APPLICATION OF LIAPUNOV'S DIRECT METHOD, Prentice-Hall, Englewood Cliffs, New Jersey, 1963.
- Heaps, N.S., A TWO-DIMENSIONAL NUMERICAL SEA MODEL, Philos. Trans. A, 265, 1969.
- Heemink, A.W., KALMAN FILTERS VOOR DE ÉÉN-DIMENSIONALE ONDIEPWATERVERGELIJKINGEN, DIV-report, No. 1980-698, 1980 (in Dutch).
- Heemink, A.W., EEN KALMAN FILTER VOOR HET VOORSPELLEN VAN DE WATERHOOGTE IN DE MOND VAN DE OOSTERSCHELDE, DIV-report, No. 1981-1632, 1981 (in Dutch).
- Heemink, A.W., KALMAN FILTERS VOOR TWEEDIMENSIONALE GETIJBEREKENINGEN IN DE NOORDZEE, DIV-report, No. 1984-2225, 1984 (in Dutch).
- Heemink, A.W., APPLICATION OF KALMAN FILTERING TO TIDAL FLOW PREDICTION, Proceedings of the IFAC/IFORS Symposium on System Analysis Applied to Water and Related Land Resources, Lisbon, 1985.
- Heemink, A.W., and B. de Jong, THE USE OF KALMAN-BUCY FILTERS IN FORECASTING THE WATER-LEVELS IN THE DUTCH COASTAL AREA, Proceedings of the 4th Int. Conf. on Finite Elements in Water Resources, Springer-Verlag, Berlin, 1982.
- Henriksen, R., A CORRECTION OF A COMMON ERROR IN TRUNCATED SECOND-ORDER NON-LINEAR FILTERS, Modelling Identification and Control, 1, 1980.
- Hornman, J.C., A TIDE PREDICTION METHOD AS USED BY RIJKSWATERSTAAT, DIV-report Nr. 77735, 1977.
- Houwen, P.J. van der, ON THE STABILITY OF A DIFFERENCE SCHEME FOR THE NORTH SEA PROBLEM, Rep. T.W. 100, Mat. Cen., Amsterdam, 1966.
- Houwen, P.J. van der, FINITE DIFFERENCE METHODS FOR SOLVING PARTIAL DIFFERENTIAL EQUATIONS, Mat. Cen. Tracts, 20, Mat. Cen., Amsterdam, 1968.
- Jazwinski, A.H., STOCHASTIC PROCESSES AND FILTERING THEORY, Academic Press, New York, 1970.
- Kalman, R.E., A NEW APPROACH TO LINEAR FILTER AND PREDICTION THEORY, J. Bas. Engng. 82, 1960.
- Kalman, R.E., and R.S. Bucy, NEW RESULTS IN LINEAR FILTERING AND PREDICTION THEORY, J. Bas. Engng 83, 1961.
- Kikkawa, H., and Y. Iwase (eds.), proceedings 3rd Intern. Symp. on Stochastic Hydraulics, Tokyo, 1980.
- Koda, M., and J.H. Seinfeld, ESTIMATION OF URBAN AIR POLLUTION, Automatica, 14, 1978.
- Kwakernaak, H., and R. Sivan, LINEAR OPTIMAL CONTROL SYSTEMS, Wiley-Interscience, 1972.
- Lauwerier, H.A., and B.R. Damste, THE NORTH SEA PROBLEM VII: A NUMERICAL TREATMENT, Proc Kon. Ned. Akad. v. Wetensh. A66, 1963.

- Leendertse, J.J., ASPECTS OF COMPUTATIONAL MODEL FOR LONG PERIOD WATER-WAVE PROPAGATION, Rand Corporation, Memorandum RM-5294-PR, Santa Monica, 1967.
- Liggett, J.A., and J.A. Cunge, NUMERICAL METHODS OF SOLUTION OF THE UNSTEADY FLOW EQUATIONS, in: UNSTEADY FLOW IN OPEN CHANNELS, K. Mahmood and V. Yevjevich (eds.), Water Resources Publications, Fort Collins, 1975.
- Maybeck, P.S., STOCHASTIC MODELS, ESTIMATION AND CONTROL, Vol I, Academic Press, New York, 1979.
- Maybeck, P.S., STOCHASTIC MODELS, ESTIMATION AND CONTROL, Vol II, Academic Press, New York, 1982.
- Miller, R.N., TOWARD THE APPLICATION OF THE KALMAN-BUCY FILTER TO REGIONAL OPEN OCEAN MODELLING, Journal of Physical Oceanography, Vol 16, 1986.
- Morf, M., S.S. Sidhu and T. Kailath, SOME NEW ALGORITHMS FOR RECURSIVE ESTIMATION IN CONSTANT, LINEAR, DISCRETE TIME SYSTEMS, IEEE Trans. Autom. Control, Vol AC19, 1974.
- Munk, W.H., and D.E. Cartwright, TIDAL SPECTROSCOPY AND PREDICTION, Phil. Trans. R. Soc. Ser. A, 259, 1966.
- Munk, W.H., and K.F. Hasselmann, SUPER RESOLUTION OF TIDES, Studies on Oceanography, 1964.
- Polis, M.P., THE DISTRIBUTED SYSTEM PARAMETER IDENTIFICATION PROBLEM: A SURVEY OF RECENT RESULTS, 3rd IFAC Symp. on the Control of Distributed Parameter Systems, Touylouse, 1982.
- Polis, M.P., and R.E. Goodson, PARAMETER IDENTIFICATION IN DISTRIBUTED SYSTEMS: A SYNTHESIZING OVERVIEW, Proceedings IEEE, Vol 64, No 1, 1976.
- Richtmyer, R.W., and K.W. Morton, DIFFERENCE METHODS FOR INITIAL VALUE PROBLEMS, Wiley-Interscience, New York, 1967.
- Rossiter, J.R., RESEARCH ON METHODS OF FORECASTING STORM SURGES ON THE EAST AND SOUTH COASTS OF GREAT BRITAIN, Quart. J. Roy. Met. Soc., 85, 1959.
- Saeijs, H.L.F., CHANGING ESTUARIES, Rijkswaterstaat Communications, The Hague, 1982.
- SARA, CYBER 205 USER'S GUIDE, SARA Publication 33, PART 3: OPTIMIZATION OF FORTRAN PROGRAMS, 1984.
- Safonov, M.G., and M. Athans, ROBUSTNESS AND COMPUTATIONAL ASPECTS OF NON-LINEAR STOCHASTIC ESTIMATORS AND REGULATORS, IEEE Trans. Autom. Control, Vol AC23, 1978.
- Schagen, I.P., INTERPOLATION IN TWO DIMENSIONS - A NEW TECHNIQUE, J. Inst. Maths. Appl., Vol 23, 1979.
- Schalkwijk, W.F., A CONTRIBUTION TO THE STUDY OF STORM SURGES ON THE DUTCH COAST, Thesis, Algemene Landsdrukkerij, Den Haag, 1947.
- Soetje, K.C., and Ch. Brockmann, AN OPERATIONAL NUMERICAL MODEL OF THE NORTH SEA AND THE GERMAN BIGHT, in: NORTH SEA DYNAMICS, J. Sündermann, and W. Lenz (eds.), Springer-Verlag, Berlin, 1983.
- Stelling, G.S., ON THE CONSTRUCTION OF COMPUTATIONAL METHODS FOR SHALLOW WATER FLOW PROBLEMS, Ph. D. Thesis, T.H. Delft, 1983.
- Stelling, G.S., J.B.Th.M. Willemse and A. Rozendaal, A COMPUTATIONAL MODEL FOR SHALLOW WATER FLOW PROBLEMS ON THE CYBER 205, Supercomputer, 11, 1986.
- Timmerman, H., ON THE IMPORTANCE OF ATMOSPHERIC PRESSURE GRADIENTS FOR THE GENERATION OF EXTERNAL SURGES IN THE NORTH SEA, Deutsche Hydro. Z., Bd 28, 1975.
- Timmerman, H., METEOROLOGICAL EFFECTS ON TIDAL HEIGHTS IN THE NORTH SEA, K.N.M.I., Med. en Verh. No. 99, 1975.
- Verboom, G.K., and A. Slob, WEAKLY REFLECTIVE BOUNDARY CONDITIONS FOR TWO-DIMENSIONAL SHALLOW WATER FLOW PROBLEMS, Adv. Water Resources, Vol 7, 1984.
- Verboom, G.K., G.S. Stelling and M.J. Officier, BOUNDARY CONDITIONS FOR THE SHALLOW WATER EQUATIONS, in: M.B. Abbott and J.A. Cunge (eds.), ENGINEERING APPLICATIONS OF COMPUTATIONAL HYDRAULICS, Vol 1, Pitman, Boston, 1982.
- Voogt, L., Unpublished Manuscript, 1984.
- Voogt, L., EEN GETIJMODEL VAN DE NOORDZEE GEBASEERD OP DE JONSDAP-1976 MEETING, rapport WWKZ-84G.006, 1985 (in Dutch).
- Weenink, M.P.H., A THEORY AND METHOD OF CALCULATION OF WIND EFFECTS ON SEA LEVELS IN A PARTLY ENCLOSED SEA, WITH SPECIAL APPLICATION TO THE SOUTHERN COAST OF THE NORTH SEA, K.N.M.I., Med. en Verh. Nr. 73, 1958.
- Wilkinson, J.H., THE ALGEBRAIC EIGENVALUE PROBLEM, Clarendon Press, Oxford, 1965.

Notations

All symbols are explained when they first appear in the text. The following list contains the more globally used symbols. In case of non-uniqueness of symbols, their meaning is clear from the text.

h	= water-level
u, v, w	= water velocities in the x, y and z-directions respectively
A	= amplitude
ϕ	= phase
ω	= frequency
D	= depth of the water
f	= Coriolis parameter
λ	= linear bottom friction coefficient
μ	= non-linear bottom friction coefficient
V	= wind speed
ψ	= wind direction
χ	= wind direction of maximum wind effect
\underline{V}	= wind vector
ρ	= density of a fluid
ρ_a	= density of air
ρ_w	= density of water
p_a	= atmospheric pressure
g	= acceleration of gravity
s	= set up, internal wind effect
a	= coefficient
η	= reflection coefficient
Φ	= system dynamics matrix
$\underline{\Phi}$	= non-linear system
\underline{x}	= deterministic state vector
n	= dimension of \underline{x}
\underline{X}	= stochastic state vector
B	= deterministic input matrix
\underline{W}	= system noise
p	= dimension of \underline{W}
Q	= system noise covariance matrix
Z	= measurement process
m	= dimension of \underline{Z}

M	= measurement matrix
m	= non-linear relation between state and measurements
V	= measurement noise
R	= measurement noise covariance matrix
\hat{X}	= estimate of X
P	= covariance of the estimation error of \hat{X}
K	= filter gain
Ψ	= state transition matrix
$\ \cdot\ $	= matrix norm
Ω	= domain
Γ	= boundary of Ω
Δt	= time step
$\Delta x, \Delta y$	= space steps
τ, T	= time intervals
c_1, c_2, \dots	= constants
i, j, k	= integer indices corresponding to the x, y and time-dimensions respectively
j	= imaginary unit
C_r	= courant number
l	= wave number
$G(l)$	= amplification matrix
$g(l)$	= eigenvalues of $G(l)$
θ	= weighting factor
ϵ	= small constant
δM	= error in a matrix M
Δ	= constant such that $\Delta^2 \ll \Delta$
c	= smoothing factor
σ^2	= variance of the system noise
α	= parameter that measures the spatial variability of the system noise
Λ	= interpolation
β	= parameter of the open boundary condition

Summary

In this study the theory of Kalman filtering has been employed to develop a new method for predicting water-levels along the Dutch coast. The combination of the standard Kalman filter with a non-linear tidal model of the entire North Sea is, from a computational point of view, not (yet) feasible. Therefore, in this investigation two different approaches have been developed. The first is based on the approximation of the tidal movement in the Dutch coastal area by a one-dimensional model. The two-dimensional effects due to the wind and the Coriolis force are taken into account by introducing some additional, empirical equations. The finite difference scheme and the system noise processes, introduced to describe the uncertainty associated with the model, are chosen such that numerical difficulties are avoided. Water-levels and velocities as well as the uncertain parameters in the model are estimated on-line by the Kalman filter. Since the model is continuously being adapted to the changing conditions, even this simple conceptual model gives satisfactory predictions. However, the time interval over which accurate predictions can be produced is limited because the one-dimensional approximation is only realistic for a small part of the southern North Sea.

To increase the prediction interval the second Kalman filter approach that is developed in this investigation is based on a two-dimensional model of the entire North Sea. The extension of the one-dimensional filter to two space dimensions does not give rise to conceptual problems but, as noted before, impose an unacceptably greater computational burden. In order to reduce this burden, the Kalman filter is approximated by a time-invariant one. In this case the time-consuming filter equations do not have to be computed over again as new measurements become available, but need only be solved once. Furthermore, by defining the system noise processes on a coarse grid and by employing a Chandrasekhar-type filter algorithm, a computationally attractive implementation of the filter is obtained. It is shown that the algorithm can be vectorized efficiently and that using a CDC CYBER 205 vector processor it is possible to combine the steady-state filter approach with very large models. Numerical difficulties can be avoided by carefully choosing the finite difference scheme, the boundary treatment and most important, the system noise processes.

The filter has been tested extensively using simulated data as well as field data. The results show excellent filter performance, especially if we take into account that the number of measurements available (as yet) has been very limited. With respect to the results of the deterministic model without using the water-levels measurements available, the improvement obtained by filtering these measurements is substantial.

Samenvatting

In dit onderzoek is een nieuwe methode, gebaseerd op Kalman filtering, ontwikkeld voor het voorspellen van waterstanden langs de Nederlandse kust. Het gebruik van het standaard Kalman filter in combinatie met een niet-lineair getijmodel van de gehele Noordzee is, door het zeer grote geheugengebruik en de lange rekentijden, (nog) niet mogelijk. Daarom zijn in deze studie twee verschillende aanpakken ontwikkeld. De eerste is gebaseerd op het beschrijven van de getijbeweging langs de Nederlandse kust met behulp van een één-dimensionaal model. Twee-dimensionale effecten ten gevolge van de wind en de Coriolis kracht zijn op empirische wijze gemodelleerd. Het eindige differentieschema en de systeemruis, geïntroduceerd om de onzekerheden in het model te beschrijven, zijn zo gekozen dat numerieke problemen geen belangrijke rol spelen. Zowel de waterstanden en -snelheden als de onzekere parameters in het model worden simultaan, on-line, door het Kalman filter geschat. Doordat het eenvoudige conceptuele model voortdurend wordt aangepast aan de zich wijzigende omstandigheden, produceert het bevredigende resultaten. Echter, de voorspeltermijn is beperkt omdat de één-dimensionale benadering alleen toegepast kan worden in een klein deel van de zuidelijke Noordzee.

Om de voorspeltermijn te vergroten is in deze studie tevens een Kalman filter methode gebaseerd op een twee-dimensionaal model van de gehele Noordzee ontwikkeld. De uitbreiding van het één-dimensionale filter naar twee dimensies is in principe eenvoudig, echter, zoals al eerder is opgemerkt, zou resulteren in onaanvaardbaar lange rekentijden. Om deze rekentijden te reduceren, wordt het Kalman filter benaderd door een tijdsonafhankelijk filter. Hierdoor hoeven de filtervergelijkingen slechts éénmaal, off-line, te worden opgelost, en niet iedere keer als er een nieuwe meting beschikbaar komt. Verder is door de systeemruis te definiëren op een grof rooster en door een Chandrasekhar-type filter algoritme te gebruiken een efficiënte implementatie van het filter verkregen. Numerieke problemen kunnen worden voorkomen door het eindige differentieschema, de randbehandeling en vooral de systeemruis zorgvuldig te kiezen. Het algoritme is efficiënt gevektoriseerd en door gebruik te maken van een CDC CYBER 205 supercomputer kan het tijdsonafhankelijke filter worden gecombineerd met zeer grote modellen.

Het filter is uitgebreid getest door gebruik te maken van zowel gesimuleerde data als prototype data. De resultaten tonen aan dat het filter uitstekend functioneert, vooral als in aanmerking wordt genomen dat het aantal beschikbare meetstations (nog) gering is. Ook blijkt dat, in vergelijking met de resultaten van een deterministisch model dat geen gebruik maakt van de beschikbare waterstandsmetingen, de verbetering bereikt door deze metingen te filteren aanzienlijk is.

In the series of Rijkswaterstaat Communications the following numbers have been previously published:

- No. 1. *Tidal Computations in Shallow Water*
Dr. J.J. Dronkers† and prof. dr. ir. J.C. Schönfeld
Report on Hydrostatic Leveling across the Westerschelde
Ir. A. Waalewijn, 1959
- No. 2. *Computations of the Decca Pattern for the Netherlands Delta Works*
Ir. H.Ph. van der Schaaf† and P. Vetterli, Ing. Dipl. E.T.H., 1960
- No. 3. *The Aging of Asphaltic Bitumen*
Ir. A.J.P. van der Burgh, J.P. Bouwman and G.M.A. Steffelaar, 1962
- No. 4. *Mud Distribution and Land Reclamation in the Eastern Wadden Shallows*
Dr. L.F. Kamps†, 1962
- No. 5. *Modern Construction of Wing-Gates*
Ir. J.C. le Nobel, 1964
- No. 6. *A Structure Plan for the Southern IJsselmeerpolders*
Board of the Zuyder Zee Works, 1964
- No. 7. *The Use of Explosives for Clearing Ice*
Ir. J. van der Kley, 1965
- No. 8. *The Design and Construction of the Van Brienenoord Bridge across the River Nieuwe Maas*
Ir. W.J. van der Eb†, 1968
- No. 9. *Electronic Computation of Water Levels in Rivers during High Discharges*
Section River Studies. Directie Bovenrivieren of Rijkswaterstaat, 1969
- No. 10. *The Canalization of the Lower Rhine*
Ir. A.C. de Gaay and ir. P. Blokland†, 1970
- No. 11. *The Haringvliet Sluices*
Ir. H.A. Ferguson, ir. P. Blokland† and ir. drs. H. Kuiper, 1970
- No. 12. *The Application of Piecewise Polynomials to Problems of Curve and Surface Approximation*
Dr. Kurt Kubik, 1971
- No. 13. *Systems for Automatic Computation and Plotting of Position Patterns*
Ir. H.Ph. van der Schaaf†, 1972
- No. 14. *The Realization and Function of the Northern Basin of the Delta Project*
Deltadienst of Rijkswaterstaat, 1973
- No. 15. *Physical-Engineering Model of Reinforced Concrete Frames in Compression*
Ir. J. Blaauwendraad, 1973
- No. 16. *Navigation Locks for Push Tows*
Ir. C. Kooman, 1973
- No. 17. *Pneumatic Barriers to reduce Salt Intrusion through Locks*
Dr. ir. G. Abraham, ir. P. van der Burg and ir. P. de Vos, 1973

- No. 18. *Experiences with Mathematical Models used for Water Quality and Water Problems*
Ir. J. Voogt and dr. ir. C.B. Vreugdenhil, 1974
- No. 19. *Stand Stabilization and Dune Building*
Dr. M.J. Adriani and dr. J.H.J. Terwindt, 1974
- No. 20. *The Road-Picture as a Touchstone for the three dimensional Design of Roads*
Ir. J.F. Springer and ir. K.E. Huizinga (also in German), 1975
- No. 21. *Push Tows in Canals*
Ir. J. Koster, 1975
- No. 22. *Lock Capacity and Traffic Resistance of Locks*
Ir. C. Kooman and P.A. de Bruijn, 1975
- No. 23. *Computer Calculations of a Complex Steel Bridge verified by Model Investigations*
Ir. Th.H. Kayser and ir. J. Brinkhorst, 1975
- No. 24. *The Kreekrak Locks on the Scheldt-Rhine Connection*
Ir. P.A. Kolkman and ir. J.C. Slagter, 1976
- No. 25. *Motorway Tunnels built by the Immersed Tube Method*
Ir. A. Glerum, ir. B.P. Rijter, ir. W.D. Eysink and W.F. Heins, 1976
- No. 26. *Salt Distribution in Estuaries*
Rijkswaterstaat, Delft University of Technology, Delft Hydraulics Laboratory, 1976
- No. 27. *Asphalt Revetment of Dyke Slopes*
Committee on the Compaction of Asphalt Revetments of Dyke Slopes, 1977
- No. 28. *Calculation Methods for Two-dimensional Groundwater Flow*
Dr. ir. P. van der Veer, 1978
- No. 29. *Ten Years of Quality Control in Road Construction in the Netherlands*
Ir. C. van de Fliert and ir. H. Schram, 1979
- No. 30. *Digital Large Scale Restitution and Map Compilation*
J.G. van der Kraan, H. Rietveld, M. Tienstra and W.J.H. IJzereef, 1980
- No. 31. *Policy Analysis for the National Water Management of the Netherlands*
(Netherlands Contribution, related to the PAWN-study, for the ECE-seminar on Economic Instruments for the Rational Utilization of Water Resources – Veldhove, Netherlands – 1980)
- No. 32. *Changing Estuaries*
Dr. H.L.F. Saeijs, 1982
- No. 33. *A Bird's Eye View of the Shipping Traffic on the North Sea*
North Sea directorate, 1982
- No. 34. *Contribution to Remote Sensing: Applications of Thermal Infrared*
H.W. Brunsved van Hulten (ed.), P. Hoogenboom, A.F.G. Jacobs, C. Kraan, G.P. de Loor and L. Wartena, 1984
- No. 35. *On the Construction of Computational Methods for Shallow Water Flow Problems*
Dr. ir. G.S. Stelling, 1984

- No. 36. *Wrong-way Driving*
Ir. G.A. Brevoord, 1984
- No. 37. *The Use of Asphalt in Hydraulic Engineering*
Technical Advisory Committee on Waterdefences, 1985
- No. 38. *Recycling of Road Pavement Materials in the Netherlands*
J.J.A. Gerardus and C.F. Hendriks, 1985
- No. 39. *Groundwater Infiltration with Bored Wells*
National Institute for Water Supply et. al., 1985
- No. 40. *Biological Research Ems-Dollard Estuary*
Biological Study of the Ems-Dollard Estuary (BOEDE), 1985
- No. 41. *Sutrench-Model*
L.C. van Rijn and G.L. Tan, 1985
- No. 42. *Phytoplankton off the dutch coast*
Dr. R.J. Leewus, 1985
- No. 43. *Aspects of sediment- and morphodynamics of subtidal deposits of the Oosterschelde (the Netherlands)*
Dr. J.H. van den Berg, 1986
- No. 44. *Ecotoxicological aspects of dithiocarbamates*
Dr. C.J. van Leeuwen, 1986
- No. 45. *Allocation of priorities for national highway projects in the Netherlands*
W.H.M. Cortenraad, K.J. Moring and J.H. Jonk, 1986